Spring 2020

Investigating the factors impacting the success of immiscible carbon dioxide injection in unconventional shale reservoirs: An experimental study

Sherif M. Fakher

Recommended Citation

INVESTIGATING THE FACTORS IMPACTING THE SUCCESS OF IMMISCIBLE

CARBON DIOXIDE INJECTION IN UNCONVENTIONAL SHALE RESERVOIRS:

AN EXPERIMENTAL STUDY

by

SHERIF MOHAMED HISHAM ABDULAZIZ FAKHER

A DISSERTATION

Presented to the Faculty of the Graduate School of the

MISSOURI UNIVERSITY OF SCIENCE AND TECHNOLOGY

In Partial Fulfillment of the Requirements for the Degree

DOCTOR OF PHILOSOPHY

in

PETROLEUM ENGINEERING

2020

Approved by:

Abdulmohsin Imqam, Advisor
Shari Dunn Norman
David Borrok
Ralph Flori
Mohamed Elgawady

PUBLICATION DISSERTATION OPTION

This dissertation consists of the following ten articles, formatted in the style used by the Missouri University of Science and Technology:

Paper I, found on pages 6–32, has been published in the proceedings of SPE Western Meeting, Bakersfield, CA, USA.

Paper II, found on pages 33-81, has been published in the Journal of Petroleum Exploration and Production Technology.

Paper III, found on pages 82-114, has been submitted to SN-Applied Sciences Journal.

Paper IV, found on pages 115-148, has been published in Journal of Petroleum Exploration and Production Technology.

Paper V, found on pages 149-174, has been published in Fuel Journal.

Paper VI, found on pages 175-196, has been published in SN-Applied Science Journal.

Paper VII, found on pages 197-228, has been published in Journal of Petroleum Exploration and Production Technology.

Paper VIII, found on pages 229-264, has been published in SN-Applied Sciences Journal.

Paper IX, found on pages 265-295, has been published in the International Journal of Greenhouse Gas Control.

Paper X, found on pages 296-324, has been published in Fuel Journal.

ABSTRACT

Unconventional shale reservoirs are currently gaining significant interest due to the huge hydrocarbon volumes that they bear. Enhanced oil recovery (EOR) techniques have been suggested to increase recovery from shale reservoirs. One of the most promising EOR methods is gas EOR (GEOR), most notably carbon dioxide (CO_2). Not only can CO_2 increase oil recovery by interacting with the oil and the shale, but it has also been shown to adsorb to the shale rock and thus is effective in both EOR applications and also carbon storage purposes. This research aims to experimentally investigate several of the interactions that may impact CO_2 injection in shale reservoirs in hopes of defining and quantifying the factors impacting these interactions and how these factors can contribute to an improvement in oil recovery from these reservoirs.

This research begins by undergoing a review and data analysis on immiscible CO_2 injection to investigate its injection methods, mechanisms, governing equations, and factors influencing its applicability. Following this, a mathematical simulation was undergone to investigate the different CO_2 flow regimes that could occur during CO_2 injection in shale reservoirs. The interaction of the CO_2 with the shale rock via adsorption was investigated by undergoing several adsorption experiments. The CO_2 interaction with the oil was also investigated by undergoing oil swelling which is considered the main mechanism by which oil recovery can be increased during immiscible CO_2 injection, and asphaltene experiments to investigate the factors impacting these two interactions. Finally, cyclic CO_2 injection was performed to determine the oil recovery potential of GEOR from shale reservoirs.

ACKNOWLEDGEMENTS

Firstly, I would like to thank Allah (God) for his innumerous blessings, grace and benevolence without which this thesis would not have been possible.

I would also like to thank Missouri University of Science and Technology for providing me with the Chancellor's Distinguished Fellowship with which I have completed this Master's degree and with which I am currently completing my PhD.

I would like to thank my greatest supporters, my parents, sisters, and brother for their continuous support and help through good and tough times.

I would like to thank my advisor Dr. Abdulmohsin Imqam for his help through the duration of my PhD research.

I would also like to thank my committee members Dr. Shari Dunn Norman, Dr. Ralph Flori, Dr. David Borrok, and Dr. Mohamed ElGawady for their help and support during the duration that I spent in the department and for their valuable and highly appreciated feedback.

I would like to thank my friends in USA, Canada, and Egypt for their constructive discussions and their support through their ideas and friendship.

I would also like to extend my gratitude to Wendy Albers, Sharon Lauck, Patricia Robertson, and Janessa Buchely for their help in all department related matters.

A special thanks to Jeff Heniff in the Rock Mechanics Research Center for his help and tips on overcoming numerous obstacles during my research.

TABLE OF CONTENTS

LIST OF ILLUSTRATIONS

LIST OF TABLES

PAPER X

NOMENCLATURE

Symbol	Description
K_n	Knudsen Number
λ	Mean Molecular Free Path, m
L	Representative Physical Length, m
K_b	Boltzmann Constant, J/K
T	Temperature, K
d	Particle Hard Shell Diameter, m
p	Pressure, Pascal, psi
v	Fluid Velocity
μ	Fluid Viscosity, cp
L_t	Tune Length
Ψ	Flow Potential
Z	Compressibility Factor
R	Universal Gas Constant
x	Distance
v_x	Velocity in x Direction
ρ	Fluid Density
β	non-Darcy Flow
K_g	Gas Permeability
q_1	Flow Rate
P_1	Injection Pressure

P_2	Atmospheric Pressure
μ_g	Gas Viscosity
a	Internal Diameter of the Porous Media
G	Geometric Factor
n	Mole Flow Rate
D_{Kn}	Knudsen Diffusion
M	Molecular Weight
N_i	Molar Flux
D_i	Diffusion Coefficient
C_i	Concentration
δ	Asphaltene and Crude Oil Solubility Parameter
ΔH	Enthalpy Change
R	Universal Gas Constant
T	Temperature
v	Volume
$\emptyset$	Volume Fraction
A	Fraction of Asphaltene
f	Fraction
μ_{cAi}	Viscosity
V_{fAi}	Initial Volume Fraction of Asphaltene
N_{sAi}	Segment Number
$\emptyset_r$	Volume Fraction of Resins in the Mixture
v_r	Molar Volume of Resins

v_m	Molar Volume of Mixture
δ_m	Solubility Parameter of Mixture
δ_r	Solubility Parameter of Resins
M_{Ai}	Asphaltene Molecular Weight
V^s	Volume of Solid Phase
F	Distribution Function
C	Correction Term for Asphaltene
S	Ratio of Volume of Injected Solvent to the Weight of Crude Oil
W	Weight Percent
Z	Constant
GOR	Gas Oil Ratio
x	Maltene Solvency Power
δ	Binary interaction parameter
T	Temperature
T_c	Critical Temperature
ω	Acentric factor
R_s	Solution gas
P_s	Saturation Pressure
γ	Specific Gravity
S_{CO2}	CO2 solubility
MW	Molecular weight
S_o	Oil Swelling
V_{so}	Volume of Swelled Oil

V_{uo}	Volume of Unswelled Oil
P	Pressure of CO2
V	Volume Occupied by The Experimental Vessel
z	Compressibility Factor of CO2
n	Number of Moles
R	Universal Gas Constant
T	Temperature at Which The Experiment is Conducted
1	Initial Conditions at The Beginning of The Experiment
2	Final Conditions after The Experiment Was Concluded
IFT	Interfacial Tension
V_{total}	Total volume of the system
V_{solid}	Volume of the shale in the sample cell
V_{gas}	Volume of gas injected
V_{gc}	Total volume of gas in the cell
V_{ads}	Volume of gas adsorbed
V_{void}	Void space volume
P_h	Helium pressure in the pump
ΔV	Change in volume of the helium
P_1	Helium pressure before expansion
P_2	Helium pressure after expansion
z_1	Helium compressibility before expansion
z_2	Helium compressibility after expansion
n_{ads}	Number of moles adsorbed

n_{inj}	Number of moles of adsorbate injected
n_{unads}	Number of moles of adsorbate unadsorbed
n_{Gibbs}	Gibbs adsorption
ρ_{gas}	Gas density
n_{Abs}	Absolute adsorption
cm^3	Cubic centimeter

1. INTRODUCTION

1.1. STATEMENT AND SIGNIFICANCE OF THE PROBLEM

Unconventional shale reservoirs are one of the most important sources of hydrocarbons nowadays. Production from these sources has reached an all time high due to the increased activity and drilling operations that are ongoing in those reservoirs, especially in the United States. A lot of research and development work is currently being conducted to increase recovery from these reservoirs further beyond their current production potential.

The main method of production from shale reservoirs today is by hydraulic fracturing. Although this method has proven efficient, as is clear from the production volume that is currently being recovered, hydraulic fracturing can only recovery an average of 7 to 10% hydrocarbons per well. If a method can be implemented to increase recovery beyond these percentages efficiently, safely, and economically, this can be a huge potential to increase reserves from shale reservoirs beyond their current estimates.

In conventional hydrocarbon reservoirs, the primary recovery mechanisms account for a portion of the recovery. After they have been exhausted, secondary or tertiary mechanisms are usually implemented to increase recovery furthermore. In unconventional shale reservoirs, one can regard hydraulic fracturing as being the primary recovery mechanism. Based on this, it has been proposed to apply EOR to further increase recovery beyond the primary hydraulic fracturing method, and thus increase the total reserves estimated for the unconventional reservoirs, and prolong the life of the producing wells beyond their current life-span.

During its injection into the reservoir, the CO_2 will have many interactions with both the shale rock and the crude oil. Each of these interactions will be impacted by multiple factors, which adds to the complexity of the process. This is one of the main reasons behind the complexity of CO_2 injection in shale reservoirs, which is why it is still ambiguous as to whether this EOR mechanism will be successful in all shale plays. Some of the CO_2 interaction with the shale rock include mineral dissolution, mainly carbonates, and CO_2 adsorption. In terms of its interaction with the crude oil, the CO_2 can be miscible with the crude oil, or immiscible. Each of these states will yield different interactions in its own. Since CO_2 EOR in unconventional shale reservoirs is still considered a novel procedure, several interactions between the CO_2 and the shale and oil need to be investigated in order to be able to determine the factors that can strongly impact this EOR process. By studying these factors, a better understanding of the applicability of CO_2 EOR in shale plays, and its ability to increase oil recovery can be obtained.

1.2. EXPECTED IMPACTS AND CONTRIBUTIONS

By undergoing this research, a better understanding of immiscible cyclic CO_2 injection in unconventionals shale reservoirs could be obtained. This research will help the industry in many ways including, but not limited to, these main points:

- Obtain an overview on the mechanism, governing equations, and factors influencing immiscible CO_2 injection.

- Illustrate the flow regimes that will dominate the CO_2 flow through different features in the shale reservoirs.

- Determine the impact of several factors on CO_2 adsorption to shale rock and the adsorption capacity of the shale.

- Study asphaltene instability in the crude oil during CO_2 injection and its impact on pore plugging in shale reservoirs.

- Investigate the extent to which CO_2 can swell the oil, and the reservoir and operational factors impacting this swelling.

- Show the extent to which cyclic CO_2 injection in shale reservoirs can increase oil recovery and the factors impacting this GEOR method.

1.3. OBJECTIVES

The main objective of this research is to provide a holistic understanding of the main factors that will impact the success of CO_2 EOR in both stimulated and unstimulated unconventional shale reservoirs in order to help define where and how to apply CO_2 in unconventional shale reservoirs. In order to achieve this goal, this research is divided into several tasks, each with its own objectives. The main objective from each task is as follows:

- Study the mechanisms of immiscible CO_2 injection and how it can improve oil recovery from the formation.

- Perform a comprehensive data analysis on immiscible CO_2 injection to determine the conditions under which it has been applied, and the factors that will influence its success in different reservoirs and formations.

- Develop flow regime maps for different pore sizes in shale reservoirs, ranging from 0.2 nanometers, up to micrometer sized pores to provide a guideline to the different flow regimes that will be encountered in different pore sizes during CO_2 injection

- Analyze CO_2 interaction with the shale rock under different conditions to evaluate the CO_2 storage potential in shale reservoirs through adsorption and the factors impacting the adsorption capacity.

- Evaluate immiscible CO_2 interaction with the oil by swelling the oil under different thermodynamic conditions and using different crude oils with different viscosity.

- Study the factors affecting asphaltene stability in the crude oil during CO_2 injection, and investigate asphaltene precipitation and deposition on shale pore plugging.

- Perform cyclic CO_2 injection, also referred to as huff-n-puff, experiments to investigate GEOR potential in increasing oil recovery from shale reservoirs and the factors impacting the oil recovery.

1.4. SCOPE OF WORK

This research will be divided into six main tasks, five of which are experimental, and one of which is a mathematical modeling task. The six tasks conducted in this research are presented in Figure 1.1 below. Initially, a critical review of immiscible CO_2 injection including the methods by which it is applied and how it interacts with the crude oil to increase recovery is done. A data analysis was also performed to determine the most suitable conditions at which immiscible CO_2 injection can be applied. After getting a profound understanding of the immiscible CO_2 injection mechanisms through the review and data analysis, the next step was to study the CO_2 flow mechanism in the shale formations and generate flow regime maps for different pores sizes present in the shale layers. Following that, the CO_2 interaction with the shale rock was investigated by studying and analyzing the main factors that will impact CO_2 adsorption to the shale rock. The next

step was to study how the immiscible CO_2 will interact with the crude oil, and the mechanism by which it will increase oil recovery. The interactions include a negative interaction which will result in asphaltene liberation from the crude oil, and a positive interaction through oil swelling which will improve the mobility of the oil and thus make it easier to produce. The factors affecting asphaltene stability in the crude oil were studied at different conditions and their impact was quantified. Oil swelling was investigated using a novel method and the main factors impacting the interaction were studied. The interaction of the CO_2 with the rock and the oil were studied together by evaluating how cyclic CO_2 injection, also referred to as CO_2 Huff-n-Puff, will increase oil recovery from the shale reservoir.
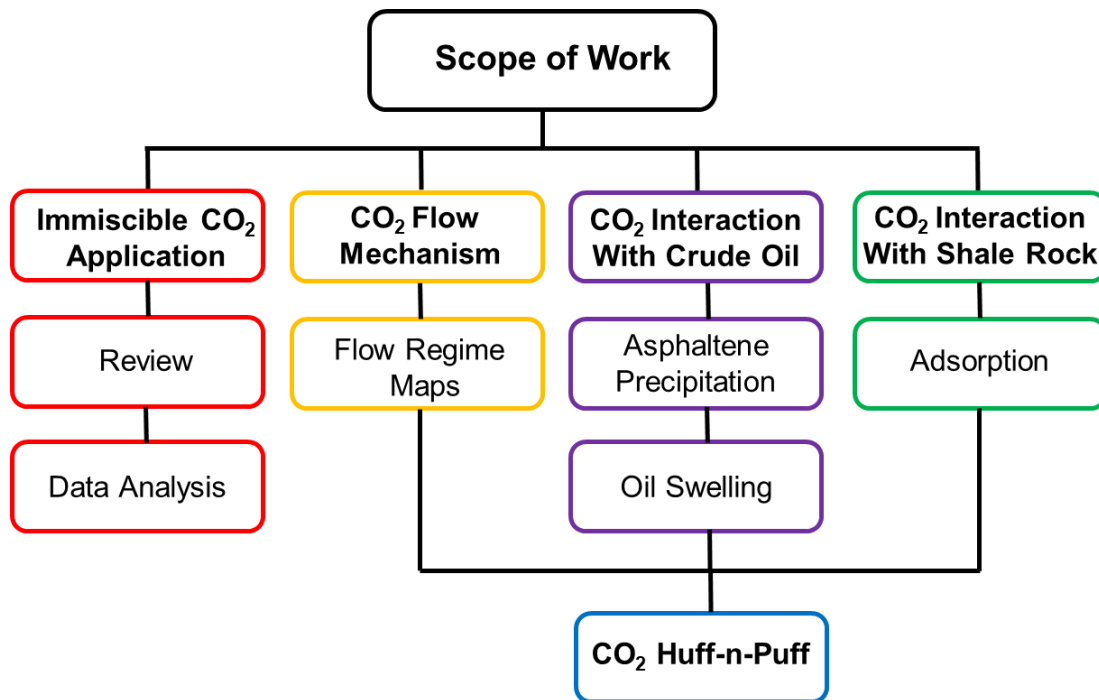
Figure 1.1. PhD Scope of Work

PAPER

I. WHAT ARE THE DOMINANT FLOW REGIMES DURING CARBON DIOXIDE PROPAGATION IN SHALE RESERVOIRS' MATRIX, NATURAL FRACTURES AND HYDRAULIC FRACTURES

ABSTRACT

Carbon dioxide (CO_2) injection in low permeability shale reservoirs has recently gained much attention due to the claims that it has a large recovery factor and can also be used in CO_2 storage operations. This research investigates the different flow regimes that the CO_2 will exhibit during its propagation through the fractures, micropores, and the nanopores in unconventional shale reservoirs to accurately evaluate the mechanism by which CO_2 recovers oil from these reservoirs. One of the most widely used tools to distinguish between different flow regimes is the Knudsen Number. Initially, a mathematical analysis of the different flow regimes that can be observed in pore sizes ranging between 0.2 nanometer and more than 2 micrometers was undergone at different pressure and temperature conditions to distinguish between the different flow regimes that the CO_2 will exhibit in the different pore sizes. Based on the results, several flow regime maps were conducted for different pore sizes. The pore sizes were grouped together in separate maps based on the flow regimes exhibited at different thermodynamic conditions. Based on the results, it was found that Knudsen diffusion dominated the flow regime in nanopores ranging between 0.2 nanometers, up to 1 nanometer. Pore sizes between 2 and 10 nanometers were dominated by both a transition flow, and slip flow. At 25 nanometer,

and up to 100 nanometers, three flow regimes can be observed, including gas slippage flow, transition flow, and viscous flow. When the pore size reached 150 nanometers, Knudsen diffusion and transition flow disappeared, and the slippage and viscous flow regimes were dominant. At pore sizes above one micrometer, the flow was viscous for all thermodynamic conditions. This indicated that in the larger pore sizes the flow will be mainly viscous flow, which is usually modeled using Darcy's law, while in the extremely small pore sizes the dominating flow regime is Knudsen diffusion, which can be modeled using Knudsen's Diffusion law or in cases where surface diffusion is dominant, Fick's law of diffusion can be applied. The mechanism by which the CO2 improves recovery in unconventional shale reservoirs is not fully understood to this date, which is the main reason why this process has proven successful in some shale plays and failed in others. This research studies the flow behavior of the CO2 in the different features that could be present in the shale reservoir to illustrate the mechanism by which oil recovery can be increased.

1. INTRODUCTION

Fluid flow in porous media is one of the most important concepts in the hydrocarbon industry. It describes how the reservoir fluids and the injected fluids will propagate through the pores of the reservoir in order to be able to estimate how much hydrocarbons are recoverable (Fakher, S. et al., 2020a; 2020b; 2020c; Fakher, S. and Imqam, A., 2018; 2019a; Fakher, S. et al., 2019d; 2019e; Fakher, S. 2019a; 2019b). Different pore sizes will exhibit different flow regimes inside the reservoirs, and thus it is important to be able to model flow though different pore sizes accurately to avoid

erroneous calculations and predictions (Patzek, T. et al., 2017; Fakher, S. and Imqam, A., 2020c; 2020d; 2020e;). One of the most widely used tools to determine flow regime in different types of pores is the Knudsen Number (Ning, Y. et al., 2015; Fakher, S. and Imqam, A., 2020a; 2020b; Fakher, S. et al., 2017; 2018; 2019a; 2019b; 2019c). It has been used to describe different flow regimes through various types of pores and for numerous fluids.

The majority of researchers utilized the Knudsen Number to construct mathematical models that can predict flow of gas through nanopores of shale, or other unconventional reservoirs. Shabro, V. et al. (2011;2012) combined a new pore scale model with a reservoir simulation algorithm to develop a model that quantifies macroscopic petrophysical properties of formations using an algorithm of gas transport that simultaneously considers the effects of no-slip and slip flow, Knudsen diffusion, and Langmuir desorption. Gao, C. et al. (2013) generated a theoretical model to illustrate the relationship between the Knudsen Number, which is considered a microscopic parameter, and the shale or tight rock permeability, which is considered a macroscopic parameter, using the pulse-decay permeability measurement method. Niu, C. et al. (2014) proposed a permeability-correlation model for nano-scale flow in highly compacted shale reservoir. Based on the mode, it was observed that increasing the Knudsen Number resulted in a negative effect on shale permeability due to the molecular-accumulation effect. Okamoto, N. et al. (2015;2018) characterized fluid flow using Knudsen Number by applying molecular dynamics simulation. Negara, A. et al. (2016) investigated the effect of Knudsen diffusion on shale gas production behavior. Wu, K. et al. (2016) developed a model for bulk-gas transfer in nanopores dependent on slip flow and Knudsen diffusion. Xu, J. et al.

(2017) studied free gas transport in nanopores of shale rocks through Knudsen diffusion using real gas equation of state and elastics hard-sphere model. Davudov, D. and Moghanloo, R. (2017) divided the shale matrix into accessible and inaccessible pores to characterize pore compressibility values as a function of pressure and to analyze different flow regimes, including Knudsen diffusion. Li, J. et al. (2017) established a gas-slip model for methane transport in nanopores and verified the model's results using laboratory results by varying the Knudsen number and gas relative permeability.

Some researchers coupled the Knudsen Number with other parameters to generalize their mathematical model or to incorporate several other factors within their model. Alharthy, N. et al. (2012) developed two models including a dual-porosity and triple-porosity finite-difference (FD) for single-phase flow of a multicomponent gas which integrate advective, diffusive, and Knudsen flow mechanisms. Shi, J. et al. (2013) developed a novel diffusion-slippage-flow model after investigating the pore size distribution and water distribution in shale matrix pores and the organic content's effect on the Knudsen Number. Li, Y. et al. (2014) investigated the non-Darcy flow mechanism of fluids in unconventional gas reservoirs, and classified the flow character based on the change of pore scale and pressure under adsorption, desorption, slip flow, transition flow, Knudsen diffusion or continuous flow. Singh, H. et al. (2014) proposed a model to describe the apparent permeability in shale reservoirs using a single analytical equation that depends on pore size, pore geometry, temperature, gas properties, and average reservoir pressure, while being valid for a wide range of Knudsen Numbers, including values less than unity. Wu, K. et al. (2015) coupled slip flow and Knudsen diffusion together to describe general gas transport mechanisms including continuous flow, slip flow, transitions flow, and

Knudsen diffusion. Labed, I. et al. (2015) used Knudsen flow to model apparent gas permeability in shale matrix as a function of pressure and pore size distribution. Wang, R. et al. (2016) differentiated between fluid flow in organic and inorganic pores of shale reservoirs by showing the impact of pressure causing stress on the shale layers on fluid flow in shale nanopores using Knudsen Number. He, S. et al. (2016) applied boundary-driven non-equilibrium molecular dynamics simulation to estimate natural gas transport and diffusivity coefficient in organic and non-organic nanopores. It was found that the transport diffusivity coefficients were highly dependent on the mean free path, and thus the Knudsen number played a significant role in the values of these coefficients. Cao, C. et al. (2017) used weighted coefficient to establish a diffusion permeability model that includes the effect of matrix shrinkage, stress sensitivity, and adsorption, by coupling the transition and Knudsen diffusion. Miao, Y. et al. (2018) developed a novel analytical model to accurately estimate the volume of stimulated reservoir volume in shale gas reservoirs by incorporating both Knudsen diffusion of bulk gas and surface diffusion of adsorbed gas directly into the model. Chai, D. et al. (2019) characterized single component gas flow in organic and inorganic nanopores of shale reservoirs. The model includes viscous flow zone, Knudsen diffusion zone, and a surface diffusion zone.

The majority of the researchers that utilized Knudsen number focused on developing mathematical models to be able to model fluid flow through nanopores, or to predict several intrinsic properties of the shale rock. This research focuses on the four main flow regimes including viscous, slip, transition, and Knudsen flow, and aims to identify the presence of each flow regime in different pore sizes, and the conditions at which the flow will transition from one regime to another during CO2 injection in shale reservoirs.

Instead of generating a mathematical model based on assumptions, this research will utilize only the Knudsen Number Equation in order to reduce error, and construct a map to flow regimes within different pore sizes ranging from 0.2 nanometer, up to micrometer sized pores. The research will also illustrate the impact of heterogeneity in pore sizes on the change of flow regime within the different porous media pore sizes.

2. KNUDSEN NUMBER DEFINITION

Unconventional shale reservoirs will have several features within them, each with its own properties and characteristics. Fluid flow through these features must be modelled with the appropriate flow model or equation since generally, not all flow regimes are best modelled using a single equation (Knudsen, M., 1909). The first step in defining which equation to use, is to determine the proper flow regime for the fluid. One of the most applied and accurate tools to study fluid flow regime in different pore sizes is the Knudsen Number. Knudsen Number is a ratio between the mean free path and the representative physical length of the porous media. The general form of the Knudsen Number is presented below:

$$K_n = \frac{\lambda}{L} = \frac{K_b T}{\sqrt{2}\pi d^2 p L}$$

where K_n is the Knudsen number, λ is the mean molecular free path (m), L is the representative physical length which is the pore radius for this work (m), K_b is the Boltzmann constant (1.38065×10^{-23} J/k), T is the temperature (k), d is the particle hard

shell diameter, or the diameter of the CO_2 molecule in this research (2.32×10^{-10} m), p is the pressure (Pa).

As the fluid molecules flows through a tightly bounded space, the pore walls will limit the available space for the fluid molecules to move, and will thus increase the probability of the molecules to interact with themselves and the pore wall (Civan, F., 2000). Based on this, Knudsen Number divided the flow into four regimes, based on the value of the Knudsen Number. These four regimes, shown in Figure 1, include viscous, slip, transition, and Knudsen flow. Each of these flow regimes have unique characteristics and are best characterized using different equations that can accommodate their exact flow mechanism. Each of these flow regimes will be explained in detail.

Viscous Flow	Slip Flow	Transition Flow	Knudsen Flow
• Low Reynolds Number • Immobile Fluid at pore wall • Darcy's Law Applicable	• Gas Molecules Slip at solid interface. • Darcy's Law Applicable with Klinkenberg Correction or Knudsen Modification.	• Both slip and diffusion can occur. • Darcy's law begins to fail and is considered erroneous to use. • Safer to apply Knudsen's Diffusion	• Darcy's law becomes fully inapplicable. • Gas molecules exhibit little or no interaction with neighboring gas molecules. • Apply Diffusion Laws

0   0.01   0.1   10   ∞

Knudsen Number

Figure 1. Knudsen Number Flow Regimes

2.1. VISCOUS FLOW

Viscous flow dominates the flow behavior in conventional hydrocarbon reservoirs. For viscous flow, Darcy's law can be applied safely given that the flow is laminar, which is usually represented by a low Reynolds number, usually close to unity. Viscous flow occurs at a Knudsen number below 0.01. At high pressures, the fluid density becomes high due to the compression of the molecules together in the confined space. When this occurs, the fluid molecules will begin to collide with each other thus increasing the friction with the pore surface. This will result in the fluid molecules sticking to the surface of the pore wall, thus creating a zero velocity, no slip zone on the wall surface. This can be modeled using the Hagen-Poiseuille Equation, shown below (Civan, F., 2000).

$$v = \frac{D^2 \Delta \Psi}{32 \mu L_t}$$

where v is the fluid velocity, L is the average diameter of the interconnect pore space, μ is the viscosity, L_t is the tube length, and Ψ is the flow potential.

The mole flow rate for viscous flow is given by (Civan, F., 2000):

$$n_v = \frac{p \Delta \Psi \pi L^4}{128 \mu Z R T L_t}$$

If the flow becomes turbulent, such as in fractures or extremely high permeability formations or features, Forchheimer's equation becomes more applicable. Forchheimer's equation is shown below (Forchheimer, P., 1901).

$$\frac{dp}{dx} = \frac{-\mu}{k}v_x + \rho\beta v_x{}^2$$

where p is the pressure, x is the distance, v_x is the velocity in x direction, ρ is the fluid density, and β is the non-Darcy flow coefficient of the porous medium.

2.2. SLIP FLOW

During gas flow, the gas molecules will experience to some extent slippage at the pores' interface (Klinkenberg, L.J., 1941; Maxwell J.C., 1867). This slippage becomes more profound as the permeability decreases, until a point where the gas slippage becomes overcome by diffusion in nano-pores. In the presence of gas, the conventional Darcy law can be applied, however a correction must be made to obtain representative values (Knudt and Warburg, 1875; Klinkenberg, L.J., 1941). This correction could either be the Klinkenberg correction, which is usually applied for gas permeability correction during gas slip, or the Knudsen modification. Slip flow occurs for a Knudsen number value between 0.01 and 0.1. The Klinkenberg permeability correction is given by (Klinkenberg, L.J., 1941):

$$K_g = q_1 \mu_g \frac{P_1}{a} G(P_1^2 - P_2^2)^2$$

where K_g is the gas permeability, q_1 the flow rate. P_1 is the injection pressure, P_2 is the atmospheric pressure, μ_g is the gas viscosity, a is the internal diameter of the porous media, and G is the geometric factor.

2.3. TRANSITION FLOW

When the pore throats are decreased further beyond that of the slip flow, a transition flow occurs where both slip, and diffusion flow are present. This occurs for a Knudsen number between 0.1 and 10. Even though Darcy's law has been applied to model flow during this flow regime, it usually produces erroneous results especially as the Knudsen number approaches 10. It is, therefore, safer to apply Knudsen's diffusion equation (Ziarani and Aguilera, 2012). The mole flow rate for both the slip and transition flow regimes can both be modeled using the equation below (Civan, F., 2000).

$$n_s = \frac{\pi^2 D^3 cp\Delta\Psi}{64pZRTL}$$

where zRT are the same variables in the real gas equation of state, representing the compressibility, universal gas constant, and temperature resepectively.

2.4. KNUDSEN FLOW

As the Knudsen number exceeds 10, the flow regime becomes Knudsen's Free Molecular flow. In this flow regime, Darcy's law becomes completely inapplicable, and diffusion based equations, such as Knudsen's diffusion, must be applied. In this type of flow, the gas molecules interact with the pore surface, and reach a point where there is almost no interaction between the gas molecules themselves (Sandler, S., 1972). This will occur mainly in the nano-pores of the unconventional shale reservoirs. Knudsen's diffusion equation is shown below (Knudsen, M., 1909).

$$D_{Kn} = \frac{d_k}{3}\sqrt{\frac{8RT}{\pi M}}$$

where D_{Kn} is the Knudsen diffusion, d_k is the pore throat radius, R is the universal gas constant, M is the molecular weight, and T is the temperature.

During this flow regime, the fluid molecules will diffuse into the matrix of the rock, rather than flow normally within it. The mole flow rate during Knudsen flow regime is given by (Civan, F., 2000):

$$n_k = \frac{p\Delta\Psi\pi cD^3}{12pZRTL}$$

If the pore size is extremely small, surface diffusion will be become predominant (Roque-Malherbe, R.M.A., 2007). Surface diffusion is modeled using Fick's first law.

$$N_i = -D_i\nabla c_i$$

where N_i is the molar flux, D_i is the diffusion coefficient, and c_i is the concentration.

Fick's second law can also be used in some cases. The second law is more complicated however since it is time dependant rather than being instantaneous as is the case in the first law.

3. METHODOLOGY

Unconventional shale reservoirs will have multiple features within their layers. These can include hydraulically induced fractures, natural fractures present due to the nature of the shale, and the shale matrix itself, which will have different pore sizes ranging within the nano-scale. Due to this wide range of pore sizes, it is important to determine the flow regimes that may be observed in each pore size in order to understand the method and mechanism by which the fluid injection will propagate through these different features, and to understand the impact of heterogeneity on fluid flow through the shale porous media.

The pore sizes in this research were divided based on the type of flow that was observed within each range, at different pressure and temperature conditions. A temperature range of 20 to 500 ºC, and a pressure range between 500 to 20000 psi were used in this research. It would be very rare to find temperature and pressure conditions beyond those mentioned in the ranges, and thus these thermodynamic conditions cover an extremely broad range which contains almost all reservoirs. Based on the definition of Knudsen number, and using the diameter of the CO_2 molecule, different values were generated at different pressures and temperatures in order to determine the flow regime at each condition, including more than 10000 values. Based on these values, the pore size ranges were divided into the following:

- **0.2 to 1 Nanometers**: This represents the smallest pore sizes in the shale. It will be part of the shale matrix and is considered the least favorable and the most difficult pore size range for fluid flow, including gas and liquid.

- **2 to 10 Nanometers**: This range represents the intermediate pore size range for unconventional shale matrix. Flow of fluids through this pore size is much easier compared to the previous pore size range.

- **25 to 100 Nanometers**: In this range, the pore size begins to become larger. In fact, some researchers consider the 100 nanometer to be within the micron range since it is equal to 0.1 microns.

- **150 to 1000 Nanometers**: This range is usually associated with much larger sized conduits, and could be present in unstimulated natural fractures found within the shale formation. This range is considered a transition range from nano sized pores to micron sized pores, and thus will also represent a transition in flow regimes.

- **Micrometer Range**: Anything in micron scale or larger present in shale reservoir will represent either a natural fracture, or a hydraulically fractured shale reservoir. In these conduit sizes, the flow is much easier compared to the smaller pore sizes.

3.1. FLOW REGIME MAP FOR 0.2 TO 1 NANO PORES

Of the smallest pores sizes that can be found in the shale matrix, this range includes the majority of these sizes. This section will explain the most commonly observed flow regimes that will be observed in pore sizes ranging between 0.2 to 1 nanometers. Figure 2 shows the map for the different flow regimes noticed in pores sizes ranging from 0.2 to 1 nanometer at different pressures and temperatures. Three pore sizes are present in the figure, including 0.2, 0.5, and 1 nanometer. The lines in the plot represent each pore size. Each line points out the transition moment from one flow to another at a specific pressure and temperature. It was noticed that at the pressure and temperature conditions used in this

research, only Knudsen and Transition flows were observed in this pore size range. This is mainly due to the small pore sizes, that hinder the normal flow of the CO_2 through the pores, and thus the gas has to diffuse through the matrix. Any point below the lines in the figure indicate Knudsen flow, while any point above them indicates Transition flow. From this, it can be deduced that at this pore size range, it is highly likely that only Knudsen Diffusion or Transition flow will be observed, and thus the conventional Darcy equation cannot accurately model the flow in these pore sizes.
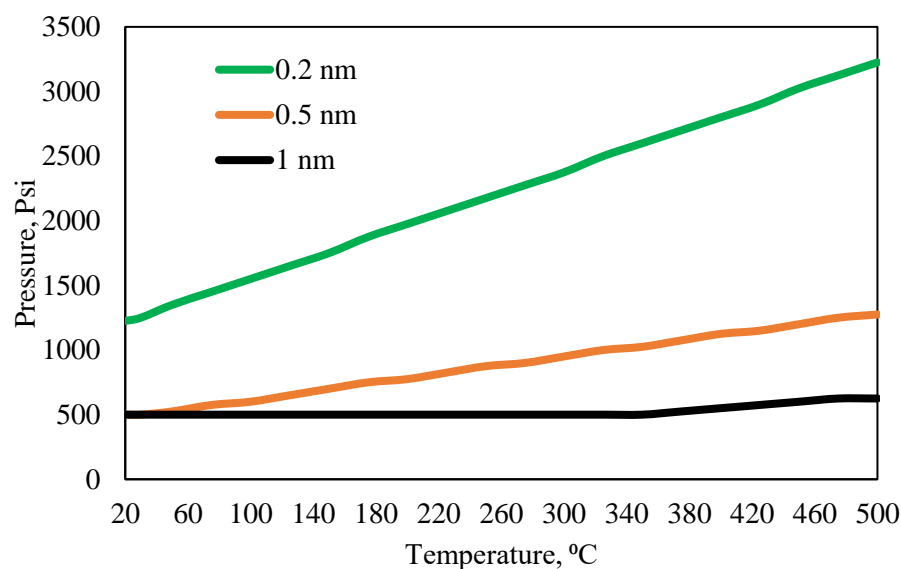
Figure 2. Flow Regime Map for Pores between 0.2 and 1 Nanometers

3.2. FLOW REGIME MAP FOR 2 TO 10 NANO PORES

When the pores size increases beyond 1 nanometer, a different flow regime is noticed at some pressures and temperatures. This section will present the results for the most commonly observed flow regimes in pore sizes ranging from 2 to 10 nanometers. Figure 3 presents the flow regime map for 2, 5, and 10 nanometer pore sizes at different

pressures and temperatures. The first thing of great interest that was noticed was that the Knudsen flow disappeared in this pore size range, at the pressure and temperature conditions specified. This indicates that at pore sizes above 1 nanometer, diffusion will not be the main flow regime for the CO_2, which opposes common belief that fluid flow in any shale matrix will be dominated by diffusion, either Knudsen or surface. The solid lines in the figure indicate the point where the flow regime will transition from Transition flow, beneath the solid lines, to Slip flow, above the solid lines. As the pore size increases, the solid line will move further below in the chart due to the reduction in pressure conditions at which the flow regime will shift from transition to slip. This means that as the pore size increases, the easier flow regime for the CO_2 begins to dominate, until the more severe flow regime disappears, as was the case for the Knudsen flow which disappeared entirely when the pore size increased.
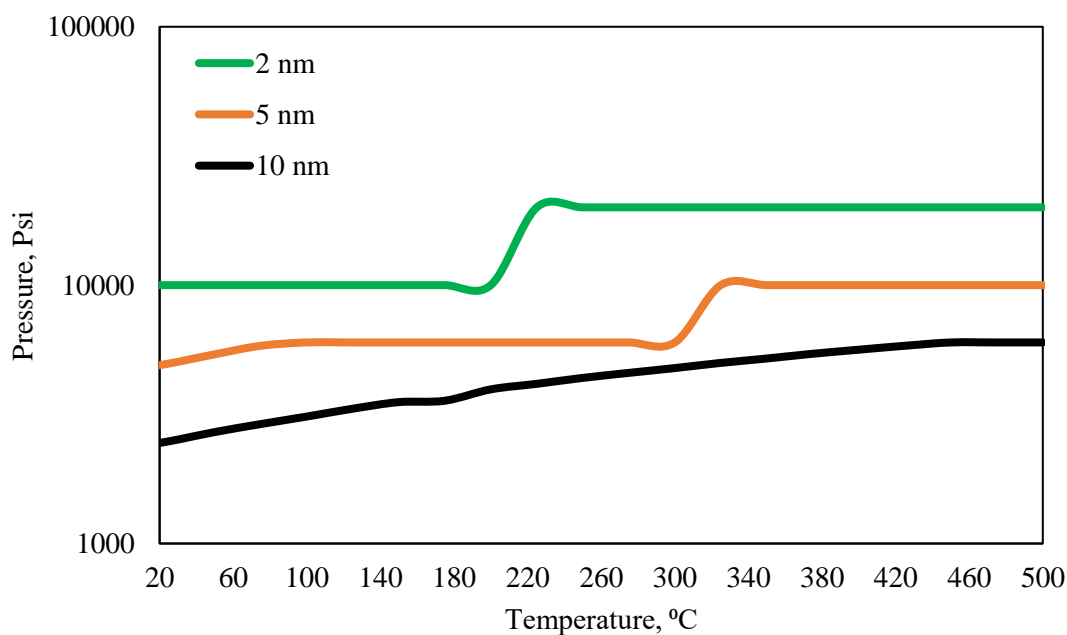
Figure 3. Flow Regime Map for Pores between 2 and 10 Nanometers

3.3. FLOW REGIME MAPS FOR 25 TO 100 NANO PORES

For the range of pore sizes between 25 to 100 nanometers, a unique observation was made. Three different flow regimes can be observed within this range, which is different from all other ranges in this research, which included only one or two flow regimes. This is the main reason why this pore size range can be considered the major transition range for flow regimes from small-pore-diffusion dominated flow to large-pore-Darcy dominated flow. Even though Knudsen diffusion is not present in this pore size range, transition flow is considered more diffusion dominated. Figure 4 presents the flow regime map for CO_2 flow through pore sizes ranging from 25 to 100 nanometers regarding the transition from Transition Flow to Slip Flow only. For the 25 nanometer pore size, it is clear that with the increase in pressure beyond 100 psi for all temperatures, the flow will be slip flow. As the pore size increases however, the transition pressure becomes the minimum pressure used in this research, which is 500 psi, until a temperature of 150 ºC is reached, at which point the larger pores will begin to transition at higher pressures. This clearly shows that as the pore sizes increases beyond 25 nanometer, there will be a point where Transition flow regime will disappear altogether. This is where the major transition in flow regimes can be observed, where the flow is now favoring the normal Darcy flow rather than the Knudsen diffusion flow. When the flow favors the normal Darcy flow, then the overall flow behavior of the fluid is not transitioning towards the normal flow in the conventional reservoirs. Gas slippage may also occur due to the relatively larger pore sizes, however it can be modeled accurately using the Klinkenberg equation, which is generally used in the case of gas slippage in conventional reservoirs.
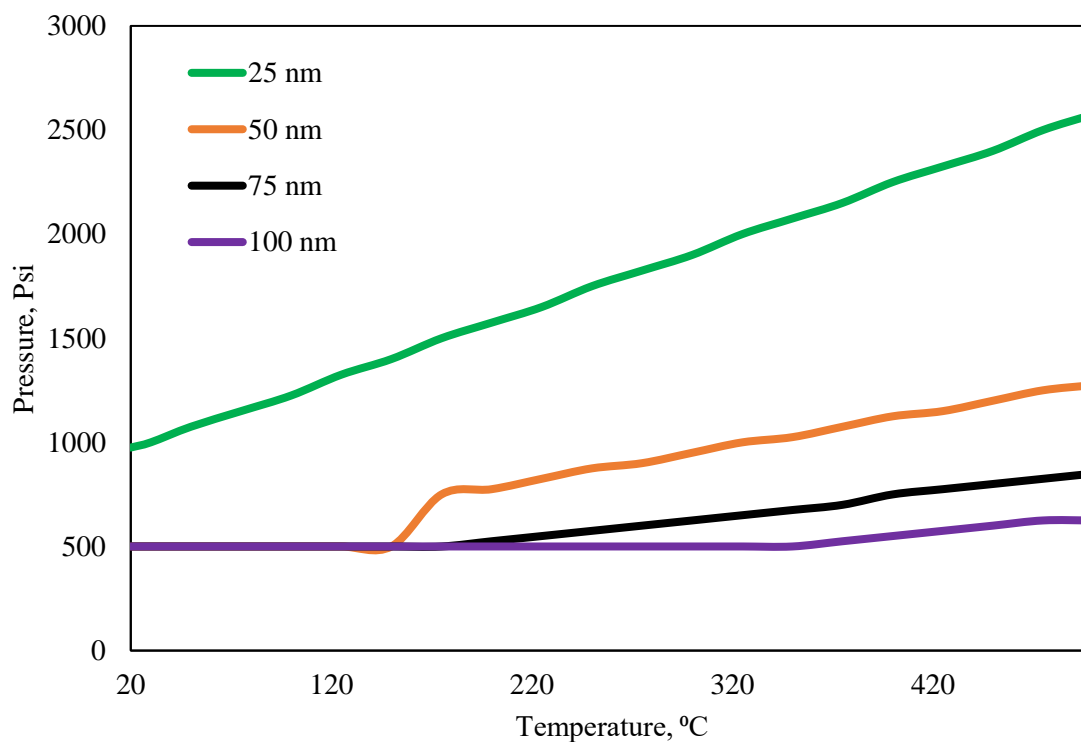
Figure 4. Flow Regime Map for Pores between 25 and 100 Nanometers

As the pressure increases in the 25 to 100 nanometer pore size range, the CO_2 density will increase due to the higher compression at higher pressure, which will result in a high collision rate between the gas molecules and a high friction with the pore walls, and thus a zero velocity at the wall surface will be created. This marks the transition from Slip to Viscous Flow. Figure 5 presents the flow regime map for the 25 to 100 nanometer pore size for the transition between slip and viscous flow. The first observation from this chart is that the pressures are higher than those in Figure 4 which indicates that even though a Viscous Flow regime can be observed in this pore size range, it will be observed at higher pressures. This shows that this pore size range still is within a transition between one flow regime domination to another, which will occur at lower pressures when the pore size

increases further. For the 75 and 100 nanometer pore sizes, the transition from slip flow to viscous flow occurs at relatively lower pressures compared to the 50 and 25 nanometer pore sizes. The zones above the lines in the figure indicate viscous flow, whereas the zones beneath the lines indicate slip flow. The increase in temperature will result in an increase in the pressure required for the transition from one flow regime to another due to the higher energy of the CO_2 molecules at higher temperatures which makes them unstable and thus unlikely to flow through the pores easier.
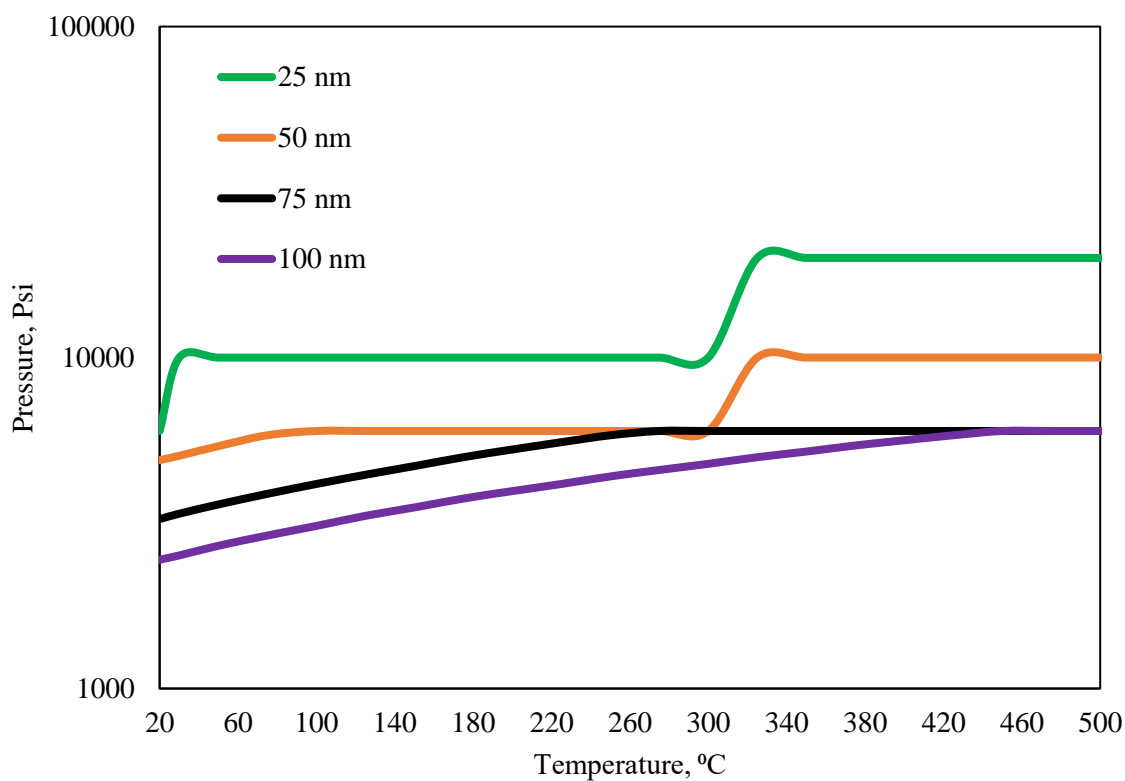
Figure 5. Flow Regime Map for Pores between 25 and 100 Nanometers at High Pressures

3.4. FLOW REGIME MAP FOR 150 TO 1000 NANO PORES

This pore size range is between 150 and 1000 nanometers, which therefore includes both micro and nanometer sized pores. This pores size range represents the final transition in flow regimes, and thus any pore size beyond this will only have one flow regime, which will be mentioned in the following section. Figure 6 shows the flow regime map for the pore size range between 150 and 1000 nanometers at different pressures, ranging between 500 and 4500 psi, and temperatures between 20 and 500 °C. Two flow regimes are present in this map, including slip and viscous flow. Any point above the lines in the figure represents viscous flow, while any point beneath the lines indicates slip flow. For the 1000 nanometer pore size, which is the same as 1 micrometer, the flow regime is entirely within the viscous-Darcy flow, except at the extremely elevated temperatures, which indicates that at this point, the majority of the pores sizes will exhibit viscous flow. As the pore size decreases, until 150 nanometer, the transition will occur at higher pressures. Slip flow will dominate the 150 nanometer pore size, until enough pressure is available to alter the flow regime to viscous flow, and thus at some point the CO_2 molecules will no longer slip, therefore the Klinkenberg effect will not be observed. This is one of the main reasons why the Klinkenberg correction is not needed when the pore sizes are relatively large (Klinkenberg, L.J., 1941), which is even clearer in the 1000 nanometer pore size since it exhibits very little slip at highly elevated temperatures.
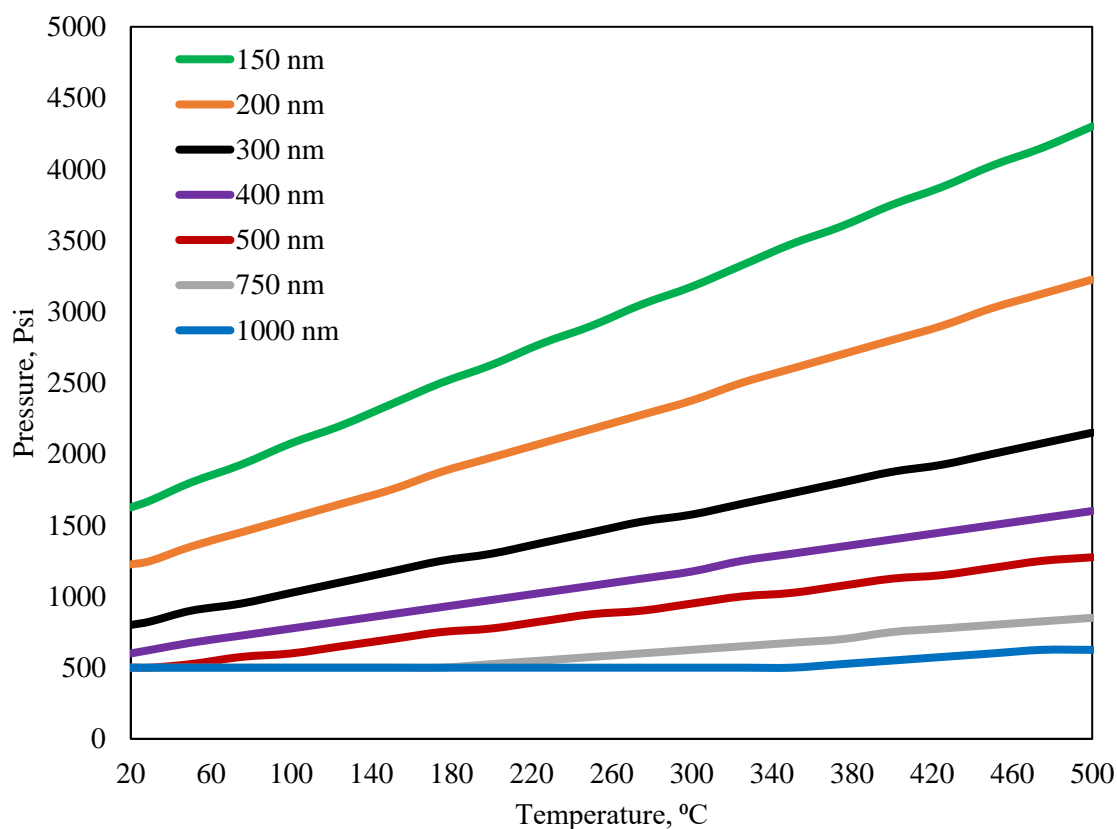
Figure 6. Flow Regime Map for Pores between 150 to 1000 Nanometers

3.5. FLOW REGIME MAP FOR MICRO PORES

This section will cover all the pore sizes above 1 micrometer, which was the largest pore size included in the previous section. It was observed that at all pressures, from 500 psi and up to 20,000 psi, and temperatures ranging from 20 to 500 ℃, the flow remained within the viscous flow regime, presented in Figure 7 below. This shows that under these conditions, the flow regime for the micropores greater than 1 micron will remain viscous flow, which is best represented by Darcy's equation. It is important to note that this conclusion was built based on the temperature and pressure ranges used in this research, and thus different conclusions could be drawn based on the pressure and temperature.
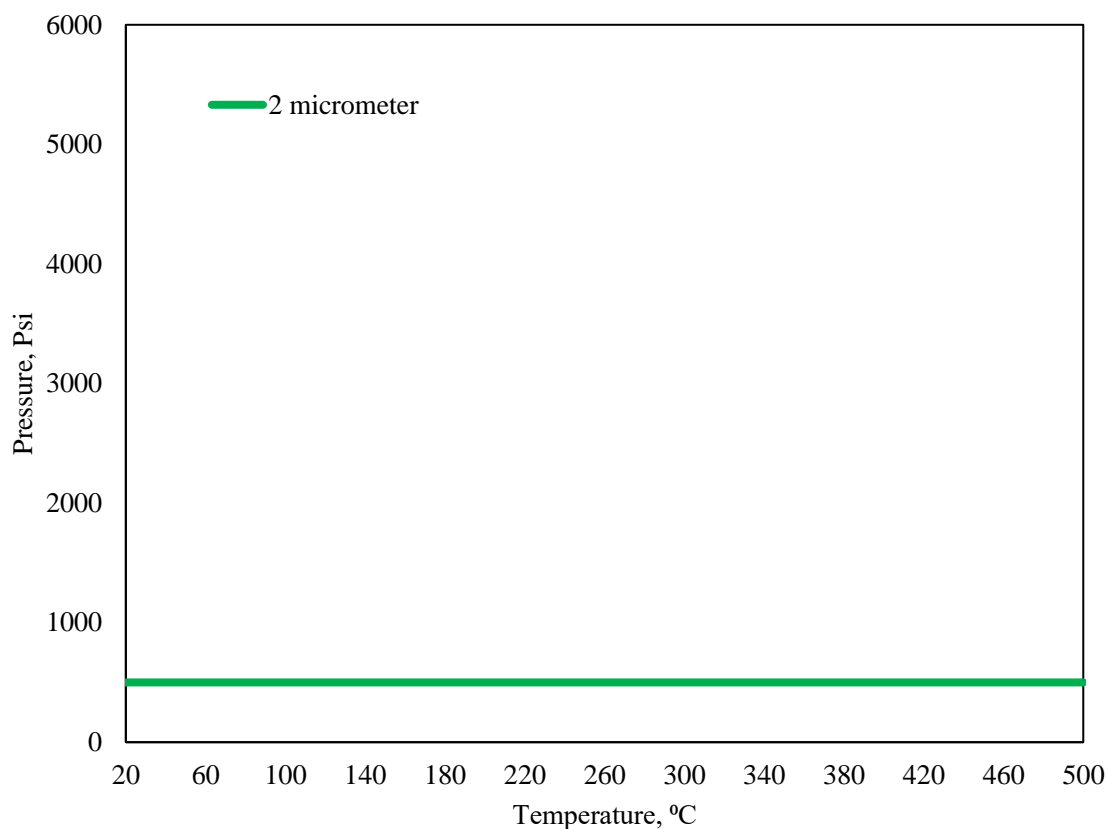
Figure 7. Flow Regime Map for Pores Greater Than 1 Micrometer

3.6. SUMMARY OF FLOW REGIME MAPS

Based on the pore sizes used in this research, different ranges were made, and flow regime maps were constructed for these ranges. Each range was defined based on the flow regimes that were most observed for each pore size. Based on this, five ranges were developed in order to define the flow regime of CO_2 within pore sizes ranging from 0.2 nanometers, up to micro sized pores in order to model all pore sizes within the shale formations including the shale matrix, natural fractures within the formation, and hydraulically induced fractures. Table 1 provides a summary of the pore size ranges defined in this research and the flow regimes present in each pore size range.

Table 1. Pore Size Range and Flow Regimes Present in Each Range

Pore Size Range	Flow Regimes Present
0.2-1 Nanometers	Knudsen and Transition Flow
2-10 Nanometers	Transition and Slip Flow
25-100 Nanometers	Transition, Slip, and Viscous Flow
150-1000 Nanometers	Slip and Viscous Flow
Micro-Sized Pores	Viscous Flow

4. CONCLUSIONS

Due to the presence of multiple features within the shale formations, the flow regime of fluids inside these formations must be well understood in order to increase recovery from shale reservoirs. This research uses the Knudsen Number definition to generate flow regime maps for pore sizes ranging between 0.2 nanometer up to micro sized pores in order to define the dominating flow regimes within each pore size range, and thus define how the CO_2 will flow in each pore size, and the change in the flow regime as the pore size changes in the shale formation. Based on the results obtained, the pore size ranges generated included five major ranges, 0.2 to 1 nanometer, 2 to 10 nanometers, 25 to 100 nanometers, 150 to 1000 nanometers, and micro sized pores. For each pore size range, the flow regimes was defined. The Knudsen diffusion flow regime disappeared when the pore size increased beyond 1 nanometer, while the Transition flow regime disappeared when the pore size increased beyond 100 nanometers.

ACKNOWLEDGEMENTS

REFERENCES

Alharthy, N. et al., 2012. Physics and Modeling of Gas Flow in Shale Reservoirs. Presented at the Abu Dhabi International Petroleum Exhibition & Conference, Abu Dhabi, UAE, 11-14, Nov.

Cao, Cheng, et al., 2017. Multi-field Coupling Permeability Model in Shale Gas Reservoir. Presented at the SPE Middle East Oil & Gas Show and Conference, Manama, Bahrain, 6-9 March.

Chai, D. et al., 2019. A New Unified Gas-Transport Model for Gas Flow in Nanoscale Porous Media. SPE Journal.

Civan, F., 2002. A Triple-Mechanism Fractal Model With Hydraulic Dispersion for Gas Permeation in Tight Reservoirs. Presented at the SPE International Petroleum Conference and Exhibition, Mexico, 10-12 Feb.

Davudov, D. and Moghanloo, R., 2017. Interaction of Non-Darcy Flow Regimes Coupled and Pore Volume Compaction in Shale Gas Formations. Presented at the SPE Annual Technical Conference and Exhibition, San Antonio, Texas, USA, 9-11 Oct.

Fakher, S. and Imqam, A. 2018. Investigating and Mitigating Asphaltene Precipitation and Deposition in Low Permeability Oil Reservoirs During Carbon Dioxide Flooding to Increase Oil Recovery. Society of Petroleum Engineers. doi:10.2118/192558-MS.

Fakher, S. and Imqam, A., 2019a. Asphaltene precipitation and deposition during CO2 injection in nano shale pore structure and its impact on oil recovery. Fuel Journal. https://doi.org/10.1016/j.fuel.2018.10.039.

Fakher, S. and Imqam, A., 2020. A Data Analysis of Immiscible Carbon Dioxide Injection Applications for Enhanced Oil Recovery Based on an Updated Database. doi: 10.1007/s42452-020-2242-1.

Fakher, S. and Imqam, A., 2020. An Experimental Investigation of Immiscible Carbon Dioxide Interactions With Crude Oil: Oil Swelling and Asphaltene Agitation. Fuel Journal.

Fakher, S. and Imqam, A., 2020. High Pressure-High Temperature Carbon Dioxide Adsorption to Shale Rocks Using a Volumetric Method. International Journal of Greenhouse Gas Control.

Fakher, S. and Imqam, A., 2020a. Application of carbon dioxide injection in shale oil reservoirs for increasing oil recovery and carbon dioxide storage. Fuel. https://doi.org/10.1016/j.fuel.2019.116944.

Fakher, S. et al., 2017. Novel Mathematical Models to predict Preformed Particle Gel Placement and Propagation through Fractures. Society of Petroleum Engineers. doi:10.2118/187152-MS.

Fakher, S. et al., 2018. Investigating the Viscosity Reduction of Ultra-Heavy Crude Oil Using Hydrocarbon Soluble Low Molecular Weight Compounds to Improve Oil Production and Transportation. Society of Petroleum Engineers. doi:10.2118/193677-MS.

Fakher, S. et al., 2019a. The Impact of Thermodynamic Conditions on CO2 Adsorption in Unconventional Shale Reservoirs Using the Volumetric Adsorption Method. Carbon Management Technology Conference. doi:10.7122/CMTC-558494-MS.

Fakher, S. et al., 2019b. Carbon Dioxide Injection Pressure and Reservoir Temperature Impact on Oil Recovery from Unconventional Shale Reservoirs During Cyclic CO2 Injection: An Experimental Study. Carbon Management Technology Conference. doi:10.7122/CMTC-558561-MS.

Fakher, S. et al., 2019c. Critical review of asphaltene properties and factors impacting its stability in crude oil. J Petrol Explor Prod Technol (2019) doi:10.1007/s13202-019-00811-5.

Fakher, S. et al., 2020. Carbon Dioxide Sequestration in Unconventional Shale Reservoirs Via Physical Adsorption: An Experimental Investigation. SPE-200537-MS. Presented at the SPE Europec featured at 82nd EAGE Conference and Exhibition.

Fakher, S. et al., 2020. Hydrolyzed polyacrylamide – Fly ash reinforced polymer for chemical enhanced oil recovery: Part 1 – Injectivity experiments. https://doi.org/10.1016/j.fuel.2019.116310.

Fakher, S. et al., 2020. Increasing Oil Recovery from Unconventional Shale Reservoirs Using Cyclic Carbon Dioxide Injection. SPE-200636-MS. Presented at the SPE Europec featured at 82nd EAGE Conference and Exhibition.

Fakher, S., 2019. Investigating Factors that May Impact the Success of Carbon Dioxide Enhanced Oil Recovery in Shale Reservoirs. Society of Petroleum Engineers. doi:10.2118/199781-STU.

Fakher, S., and Imqam, A., 2020b. A review of carbon dioxide adsorption to unconventional shale rocks methodology, measurement, and calculation. SN Appl. Sci. 2, 5. doi:10.1007/s42452-019-1810-8.

Fakher, S.M., 2019. "Asphaltene stability in crude oil during carbon dioxide injection and its impact on oil recovery: A review, data analysis, and experimental study" (2019). Masters Theses. 7881.

Forchheimer, P., 1901. Wasserbewegug durch Boden, Zeits. V. Deutsch. Ing 45, 1782–1788.

Gao, C. et al., 2013. The Shale-Gas Permeability Measurement Considering the Rarefaction Effect on Transport Mechanism in the Nanopores. Presented at the International Petroleum Technology Conference, Beijing, China, 26-28 March.

He, S. et al., 2016. Transport Properties of Natural Gas in Shale Organic and Inorganic Nanopores Using Non-Equilibrium Molecular Dynamics Simulation. Presented at the International Petroleum Technology Conference, Bangkok, Thailand, 14-16 Nov.

Kaviany, M., 1991. Principles of Heat Transfer in Porous Media, Springer-Verlag New York Inc., New York, NY, 626p.

Klinkenberg, L.J., 1941. The permeability of Porous Media to Liquid and Gases. paper presented at the API 11th mid year meeting, Tulsa. API Drilling and Production Practices, New York, pp 200–213.

Knudsen, M., 1909. Die Gesetze der Molukularstrommung und der inneren. Reibungsstrornung der Gase durch Rohren. Ann. der Phys. 28:75–130.

Knudsen, M., 1909. The Laws of Molecular and Viscous Flow of Gases Through Tubes, Ann. Physik, 28, 75-177.

Knudt, A., and Warburg, E., 1875. Übwe Reibung and Wärmelei-tung verdünnter Gase. Poggendrfs Annalen der physic und Chemie. 155:337.

Labed, I. et al., 2015. Hydraulic Fracture Spacing Optimization for Shale Gas-Condensate Reservoirs Development. Presented at the SPE Offshore Europe Conference & Exhibition, Aberdeen, Scotland, UK., Sept.

Li, J. et al., 2017. Methane Transport through Nanoporous Shale with Sub-Irreducible Water Saturation. Presented at the SPE Europec 79th EAGE Conference and Exhibition, Paris, France, 12-15 June.

Li, Y. et al., 2014. A Nano-Pore Scale Gas Flow Model for Shale Gas Reservoir. Presented at the SPE Biennial Energy Resources Conference, Port of Spain, Trinidad, 9-11 June.

Liepmann, H.W., 1961. J.Fluid Mech, 10, 65.

Maxwell, J.C., 1867. On stresses in rarefied gases arising from inequalities of temperature. Phil. Trans. Roy. Soc. Lond. 170, 231–256.

Metz, C.R., 1976. Physical Chemistry, McGraw-Hill, New York, 11. Book 1976, Physical.

Miao, Y. et al., 2018. A Practical Method for Estimating Stimulated Reservoir Volume in Shale Gas Reservoirs: Coupling Knudsen Diffusion and Surface Diffusion. Presented at the SPE Trinidad and Tobago Section Energy Resources Conference, Port of Spain, Trinidad and Tobago, 25-26 June.

Negara, A. et al., 2016. Effects of Multiple Transport Mechanisms on Shale Gas Production Behavior. Presented at the SPE Kingdom of Saudi Arabia Annual Technical Symposium and Exhibition, Dammam, Saudi Arabia, 25-28 April.

Ning, Y. et al., 2015. Simulation of Shale Gas in 3D Complex Nanoscale-Pore Structures Using the Lattice Blotzmann Method. Presented at the SPE Asia Pacific Unconventional Resources Conference and Exhibition, Brisbane, Australia, 9-11 Nov.

Niu, C. et al., 2014. Second-Order Gas-Permeability Correlation of Shale During Slip Flow. SPE Journal.

Okamoto, N. et al., 2015. Slip Velocity and Permeability of Gas Flow in Nanopores for Shale Gas Development. Presented at the SPE Asia Pacific Unconventional Resources Conference and Exhibition, Brisbane, Australia, 9-11 Nov.

Okamoto, N. et al., 2018. Slip Velocity of Methane Flow in Nanopores with Kerogen and Quartz Surfaces. SPE Journal.

Patzek, T. et al., 2017. Knudsen-Like Scaling May Be Inappropriate for Gas Shales. Presented at the SPE Annual Technical Conference and Exhibition, San Antonio, Texas, USA, 9-11, 2017.

Roque-Malherbe, R.M.A., 2007. Adsorption and Diffusion in Nanoporous Materials. CRC Press, Taylor & Francis Group, Boca Raton.

Sandler, S., 1972. Temperature dependence of the Knudsen permeability. Ind. Eng. Chem. Fundam. 11, 424–427.

Shabro, V. et al., 2011. Numerical Simulation of Shale-Gas Production: from Pore-Scale Modeling of Slip-Flow, Knudsen Diffusion, and Langmuir Desorption to Reservoir Modeling of Compressible Fluid. Presented at the SPE North American Unconventional Gas Conference and Exhibition, Woodlands, Texas, USA, 14-16, June.

Shabro, V. et al., 2012. Forecasting Gas Production in Organic Shale with the Combined Numerical Simulation of Gas Diffusion in Kerogen, Langmuir Desorption form Kerogen Surfaces, and Advection in Nanopores. Presented at the 2012 SPE Annual Technical Conference and Exhibition, San Antonio, Texas, USA, 8-10 Oct.

Shi, J. et al., 2013. Diffusion and Flow Mechanisms of Shale Gas through Matrix Pores and Gas Production Forecasting. Presented at the SPE Unconventional Resources Conference, Alberta.

Singh, H. et al., 2014. Nonemperical Apparent Permeability of Shale. SPE Reservoir Evaluation & Engineering.

Wang, R. et al., 2016. Analytical Solution of Matrix Permeability of Organic-Rich Shale. Presented at the International Petroleum Technology Conference, Bangkok, Thailand, 14-16 Nov.

Wu, K. et al., 2015. A Model for Gas Transport in Micro Fractures of Shale and Tight Gas Reservoirs. Presented at the SPE/CSUR Unconventional Resources Conference, Calgary, Alberta, Canada, 20-22 Oct.

Wu, K. et al., 2016. A Unified Model for Gas Transfer in Nanopores of Shale-Gas Reservoirs: Coupling Pore Diffusion and Surface Diffusion. SPE Journal.

Xu, J. et al., 2017. Nanoscale Free Gas Transport in Shale Rocks: A Hard-Sphere Based Model. Presented at the SPE Unconventional Resources Conference, Alberta, Canada, 15-16, Feb.

Ziarani A. S. and Aguilera, R. 2012. Knudsen's Permeability Correction for Tight Porous Media. Transp. Porous Med. 91 (1): 239260. https://doi.org/10.1007/s11242-001-9842-6.

II. CRITICAL REVIEW OF ASPHALTENE PROPERTIES AND FACTORS IMPACTING ITS STABILITY IN CRUDE OIL

ABSTRACT

Asphaltene is a component of crude oil that has been reported to cause severe problems during production and transportation of the oil from the reservoir. It is a solid component of the oil that has different structures and molecular makeup which makes it one of the most complex components of the oil. This research provides a detailed review of asphaltene properties, characteristics, and previous studies to construct a guideline to asphaltene and its impact on oil recovery. The research begins by an explanation of the main components of the crude oil and their relation to asphaltene. The method by which asphaltene is quantified in the crude oil is then explained. Due to its different structures, asphaltene has been modeled using different models all of which are then discussed. All chemical analysis methods that have been used to characterize and study asphaltene are then mentioned and the most commonly used method is shown. Asphaltene will pass through several phases in the reservoir beginning from its stability phase up to its deposition in the pores, wellbore and facilities. All these phases are explained and the reason they may occur is mentioned. Following this, the methods by which asphaltene can damage oil recovery are presented. Asphaltene rheology and flow mechanism in the reservoir is then explained in detail including asphaltene onset pressure determination and significance and the use of micro and nano fluidics to model asphaltene. Finally, the mathematical models, and previous laboratory and field studies conducted to evaluate

asphaltene are discussed. This research will help increase the understanding of asphaltene and provide a guideline to how to properly study and model asphaltene in future studies.

1. INTRODUCTION

Asphaltene was first defined by Boussingault (1837) as the "distillation residue of bitumen insoluble in alcohol and soluble in turpentine." This definition was later modified, however, due to an error in the initial part of the definition, which limited asphaltene presence to bitumen; this was later found to be incorrect (Golkari, A. and Riazi, M., 2017; Salleh, I.K., et al., 2019). Today, asphaltene is defined as "the heaviest component of petroleum fluids that is insoluble in light n-alkanes such as n-pentane or n-heptane, but soluble in aromatics such as toluene" (Goual, L., 2012). Asphaltene is therefore a solid component of crude oil with an extremely high molecular weight (Mozaffari, S. et al., 2015a; 2017a;2017b; 2018; Struchkov, I.A. et al., 2019; Kor, P. et al., 2017; Nwadinigwe, C. et al., 2015). This is the main reason causing it to be extremely problematic, since it can form dense flocculations and deposits in reservoir, wellbores, and transportation pipelines, and thus can cause severe operational and production problems.

Much research has been conducted to study the precipitation and deposition of high molecular weight components, mainly asphaltene, in the pore spaces of conventional oil reservoirs. Zendehboudi, S. et al. (2014) defined precipitation as the formation of the solid phase from the liquid phase and defined deposition as the adherence or adsorption of the solid phase to the reservoir rock, which usually occurs after precipitation. Asphaltene also forms dense clusters referred to as flocculations (Leandra, S. et al., 2018; Liu, F. et al.,

2017; Fakher, S. et al., 2019). The flocculations have a high density and thus tend to deposit and plug the pore throats in the reservoir (Monger, T.G. and Fu, J.C., 1987; Kim, S.T. et al., 1990; Rassamdana, H.B. et al., 1996; Khamehchi, E. et al., 2018; Ihtsham, M. and Ghosh, B., 2015). The most severe of all the high molecular weight components is asphaltene (Thawer, R. et al., 1990). Therefore, many methods have been proposed to detect asphaltene deposition in conventional oil reservoirs, such as the De Boer Plot (De Boer, R.B. et al., 1995), the Asphaltene to Resin Ratio Approach (Jamaluddin, A.K.M. et al., 2000), the Colloidal Instability Index (Yen, A. et al., 2001), Filtration, the Acoustic Resonance Technique, the Light Scattering Technique (Speight, J.G. et al., 1985; Speight, J.G., 1999; Jamaluddin, A.K.M. et al., 2000; Akbarzadeh, K. et al. 2007), Optical Spectroscopy (Kharrat, A. et al., 2013), Nuclear Magnetic Resonance (Wang, S. et al. 2016), and Gas Chromatography coupled with Mass Spectrometry (Fakher, S., et al., 2018; Elkahky, S. et al., 2019; Iraji, S. and Ayatollahi, S., 2019; Ahmadi, M.A., 2011; Gholami, A. et al., 2016; Kargarpour, M.A. and Dandekar, A., 2016).

Extensive experiments have been conducted to model asphaltene deposition during CO_2 injection in conventional oil reservoirs. Soroush S. et al. (2014) showed that below CO_2 minimum miscibility pressure (MMP), an increase in pressure will result in an increase in asphaltene deposition in sandstone, whereas, above CO_2 MMP, an increase in pressure results in a decrease in asphaltene deposition. Thawer et al. (1990) ran laboratory tests to determine the minimum solubility pressure for asphaltene in the Ula reservoir fluids. They also tested several chemical formulations that could dissolve asphaltene and found that the chemicals that could dissolve asphaltene most effectively were pure aromatics such as toluene and xylene. However, pure xylene and toluene were considered

dangerous to use due to their low flash point, and hence the chemical formulations were considered safer and more stable. Thomas et al. (1995) also sought to find a method to dissolve asphaltene that was deposited in the reservoirs and pipelines. By testing several chemicals, they developed three chemical formulations that could effectively dissolve the asphaltene that was present in the oil. Shen and Sheng (2018) studied asphaltene deposition in the Eagle Ford shale reservoir using cyclic gas injection. They used filter membranes of 30 nm, 100 nm, and 200 nm to study asphaltene precipitation and deposition. The experiments they conducted with the filter membranes were conducted at 50 psi and room temperature. Fakher, S. and Imqam, A. (2018a; 2018b) studied asphaltene instability in crude oil during CO_2 injection in nanofilter membranes.

Based on the aforementioned, it is clear that asphaltene is an extremely complex component of crude oil and the methods by which it is studied are abundant and differ significantly. Due to the numerous amounts of methods by which asphaltene has been studied, it becomes tedious to comprehensively understand asphaltene characteristics, factors impacting its stability, and methods by which it can be accurately studied and quantified. This research provides a comprehensive understanding of asphaltene properties, characteristics, flow mechanisms and rheology, modeling and analysis methods, and its impact on oil recovery based on previous field and lab studies. All previous reviews on asphaltene are extremely limited in their contents and cover only one aspect of asphaltene which makes it very difficult to fully understand asphaltene properties and behavior.

2. MAIN COMPONENTS OF CRUDE OIL

Crude oil components can be divided into multiple compounds and subdivisions based on the composition of the crude oil. Normally, crude oil will contain a percentage of dissolved gasses, liquids, and solids. The liquids can be further divided into saturates, aromatics, and resins. Different types of solids may also exist in the crude oil however, the most prominent is solid asphaltene. These components are usually grouped together as Saturate-Aromatic-Resin-Asphaltene, more commonly referred to as SARA analysis. The SARA analysis is performed using chromatography to determine the presence and concentration of the aforementioned components. The exact description of each of these components and their relation to the asphaltene is explained.

2.1. SATURATES

Saturates are the compounds in the hydrocarbon that are saturated, and thus do not contain any double bonds. The carbon atoms are bonded to the maximum allowable hydrogens, and thus no carbon-carbon double bonds are present. Saturated hydrocarbons are generally referred to as alkanes. The simplest alkane compound is methane, followed by ethane and propane (Goel, P. et al., 2017). The structure of all three compounds is shown in Figure 1. As can be seen, no double bonds are present in the compounds. Saturates are one of the main liquids, or gas in regards to methane, components of the hydrocarbon; asphaltene are in solution within these compounds until it becomes unstable and asphaltene begins to precipitate from the solution. Saturates play no significant role in asphaltene stability; however, they are a major component of crude oil.
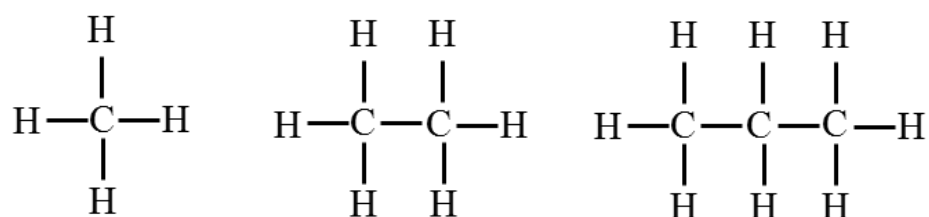
Figure 1. Molecular Structure of Methane, Ethane, and Propane (Garner, W. et al., 1939)

2.2. AROMATICS

Aromatics are the second main component of hydrocarbons. These compounds are slightly more complex in structure than saturates. They are generally nonpolar and are characterized by an unsaturated hydrocarbon ring with multiple carbon-carbon double bonds within the ring configuration (Keshmirizadeh, E.S. et al., 2013; Alshaikh, M. et al., 2019; Punase, A. et al., 2016; Liao, H. et al., 2019; Alskaikh, M. et al., 2018; Prakoso, A.A. et al., 2017). Figure 2 shows the structure of three common aromatics, including toluene, xylene, and phenolic acid. All three compounds have a cyclic hydrocarbon ring attached.
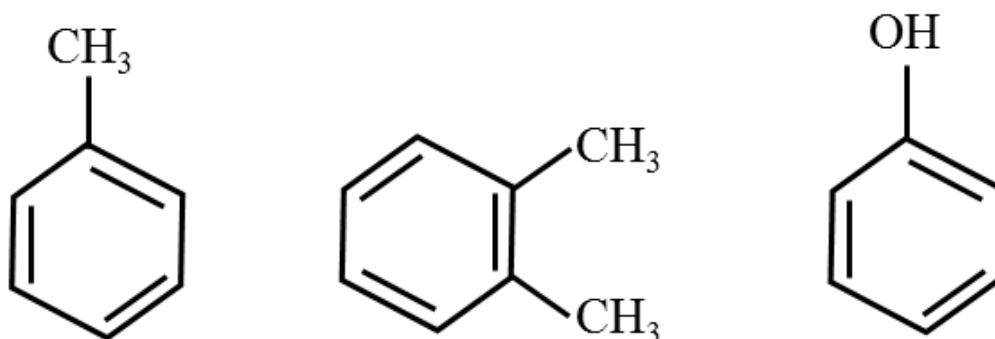
Figure 2. Molecular Structure of Toluene, Xylene, and Phenolic Acid

2.3. RESINS

Resins are considered much more complex in structure compared to saturates and aromatics. They have a higher molecular weight compared to the previous two components as well. Resins play a significant role in the stabilization of the asphaltene in the crude oil (Leon, O. et al., 2002). The crude oil in general is nonpolar, which means it is insoluble in water (Lammoglia, T. and Filho, C.R., 2011). Asphaltene is usually highly polar in nature and thus cannot be homogenized or solubilized in the crude oil on its own, since it is against its nature. Resins are characterized by having both a polar and a nonpolar side and thus function as a bridging material that connects the nonpolar hydrocarbon compounds to the highly polar asphaltene (Miadonye, A., and Evans, L., 2010). Figure 3 shows a typical structure of a resin molecule.
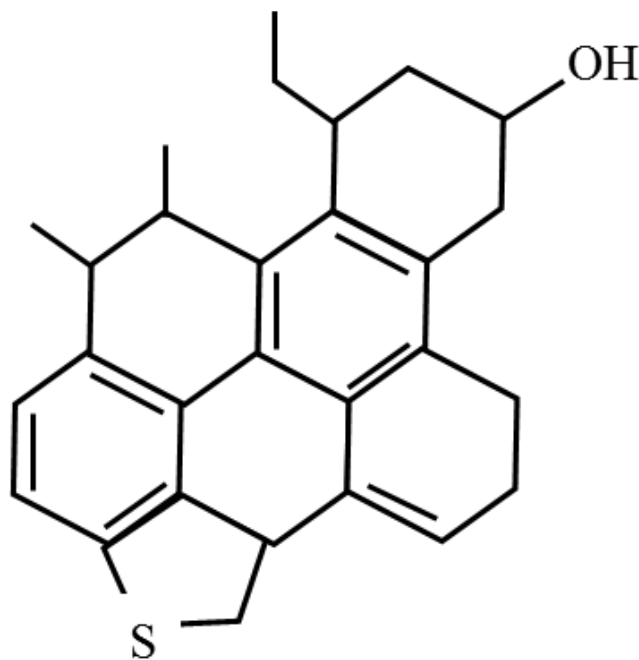
Figure 3. Molecular Structure of Simple Resin Molecule (Abdel-Raouf, M., 2012)

2.4. ASPHALTENE

Asphaltene is considered one of the most complex components of crude oils. It is one of very few components that are solid, shown in Figure 4. Asphaltene complexity comes mainly in the way its structure is defined. All of the three previously explained components have a general structure by which they can be classified. Unfortunately, asphaltene has many different structures, which makes generalizing it into a specific family very difficult (Pazuki, G.R., 2007). Asphaltene is generally classified as a solubility class, since it is characterized as being insoluble in n-alkanes. There are several characteristics that can be used to identify asphaltene, including (Seifried, C. et al., 2013):

- Solid: Asphaltene is a solid phase that is homogenized in the crude oil at reservoir conditions.

- n-Alkane Insoluble: Asphaltene is classified as a solubility class since it has several structures, and thus it is extremely difficult to provide a generalized structure for it. It is therefore defined as the highest molecular weight component in the crude oil that is insoluble in light n-alkanes such as n-pentane or n-heptane, and soluble in aromatics such as toluene or xylene.

- Highly Polar: Asphaltene is one of very few components of crude oil that is highly polar, in contrast to crude oil as a whole, which is considered nonpolar.

- Heteroatoms: Asphaltene is associated with heteroatoms, mainly manifested in nitrogen, oxygen, and sulfur. Also, other heteroatoms may exisit depending on the structure of the asphaltene molecule, its origin, and the conditions at which the kerogen was converted to the hydrocarbon.
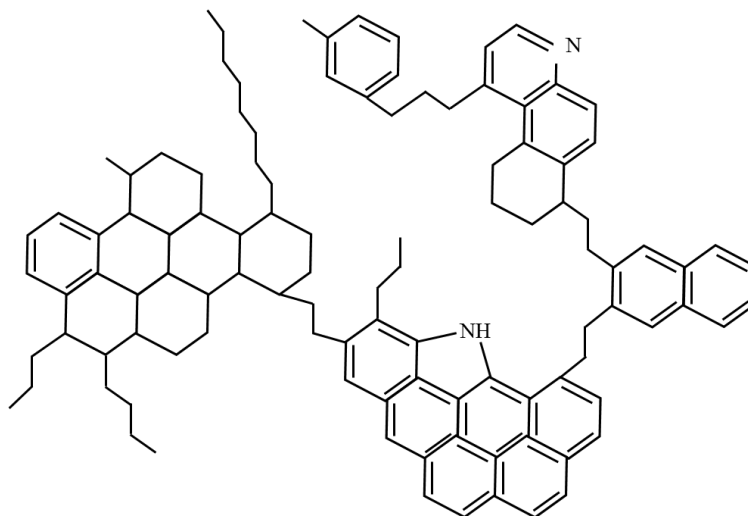
Figure 4. Molecular Structure of an Asphaltene (Groenzin, H. and Mullins, O., 2000)

It is important to be able to differentiate between the different components of the crude oil and isolate each component from the other to both quantify the components, and study each one separately. Based on this, the most common method used to differentiate between saturates, aromatics, resins, and asphaltene, which is referred to as the SARA analysis, will be explained in detail.

3. SARA ANALYSIS

The analysis of the four components, including saturates, aromatics, resins, and asphaltene, is referred to as the SARA analysis. The SARA analysis is conducted based on the Standard Test Method for Separation of Asphalt into Four Fractions, which was created by the American Society for Testing and Materials (ASTM) (D-4124-97-ASTM; Fan, H., 2003; Fan, T. et al., 2002; Jha, N.K. et al., 2014; Theyab, M.A. et al., 2017). The main aim of the SARA analysis is to differentiate between and quantify the four main components

of crude oil (Bissada, K.A. et al., 2016). Figure 5 provides a flowchart of the SARA analysis procedure to differentiate between the different components of crude oil. If a sample of crude oil is added to liquid propane, the aromatics and saturates will be solubilized, whereas the resins and asphaltene will precipitate. This will help isolate the resins and the asphaltene. Several methods can be applied to differentiate between the aromatics and saturates, including gas chromatography. The resin and asphaltene precipitate can then be taken and dissolved in a light n-alkane, most notably n-pentane and n-heptane. The resin will be soluble in the n-alkane, whereas the asphaltene will not and will precipitate. Using this procedure, the asphaltene can be distinguished from the resin. Consequently, all four components of the SARA analysis can be accurately differentiated.
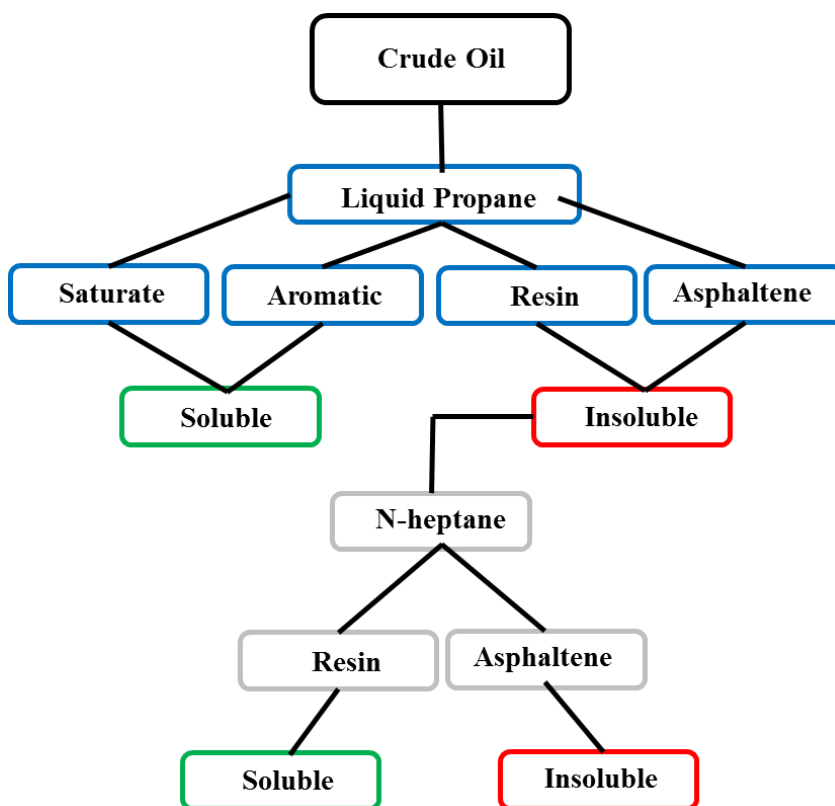
Figure 5. SARA Analysis Flowchart

By isolating the asphaltene from the other components, a detailed study of asphaltene properties can be conducted. Initially, it is important to understand how the asphaltene structure can be modeled, especially due to the complexity of asphaltene composition and its nature of being a solid component in the crude oil. The different models that have arisen to attempt to describe the asphaltene structure will be explained, including the most recent and widely used model, referred to as the Yen-Mullins model.

4. MODELS OF ASPHALTENE STRUCTURE

Asphaltene is extremely complex in nature. Also, it is usually classified as a solubility class rather than a specific structure due to the several varieties of structures available for asphaltene. Several models have been developed in an attempt to provide a standard method that would be able to encompass all the different asphaltene chemical structures and model those structures.

4.1. ARCHIPELAGO MODEL

The archipelago asphaltene model, in accordance with its name, models the asphaltene structure as several aromatic rings connected together though aliphatic chains. An example of an asphaltene molecule that resembles the archipelago model is shown in Figure 6. Several aromatic rings appear as separate groups connected together using several aliphatic chains. However, there is an uncertainty in the model regarding the number of aromatic rings present in the asphaltene molecule. The side chains are believed to have an average length of 5-7 carbons.
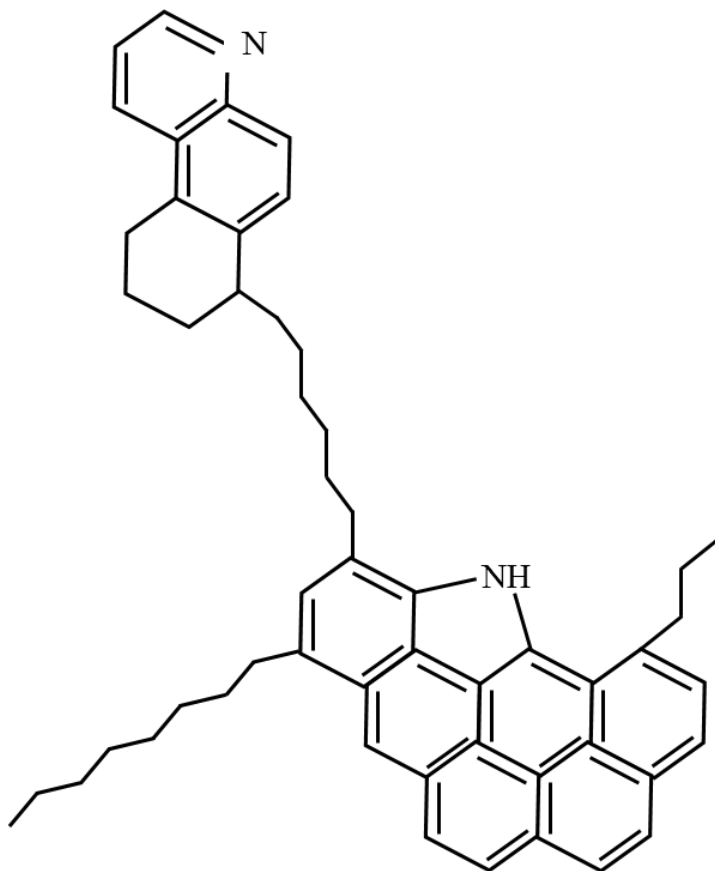
Figure 6. Archipelago Asphaltene Structure (Alvarez, F. and Ruiz-Morales, Y., 2013)

4.2. CONTINENTAL MODEL

The continental model assumed the structure of asphaltene as a large group of aromatic rings in the middle of the asphaltene molecule that are connected to several aliphatic branches. This model is usually associated with lower molecular weight asphaltene, and is hence referred to as the condensed aromatic model. Figure 7 shows an illustration of an asphaltene model that follows the continental model asphaltene structure.
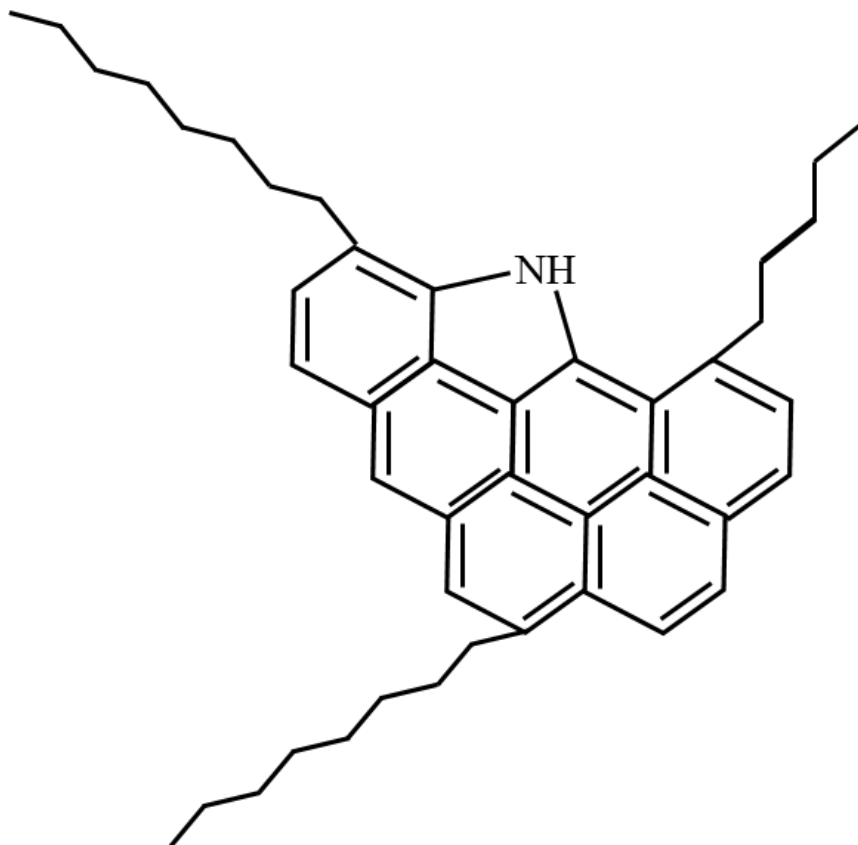
Figure 7. Continental Asphaltene Structure (Kuznicki, T. et al., 2008)

4.3. ANIONIC CONTINENTAL MODEL

The anionic continental model is extremely similar in structure compared the continental model, shown in Figure 8. The major difference lies in a negatively charged group that is attached to one of the aliphatic chains attached to the main structure. This gives the asphaltene structure a negative charge, which adds to the change in potential of the asphaltene and in turn will impact asphaltene stability significantly; this is referred to as the electrokinetic effect and will be explained in detail later on.
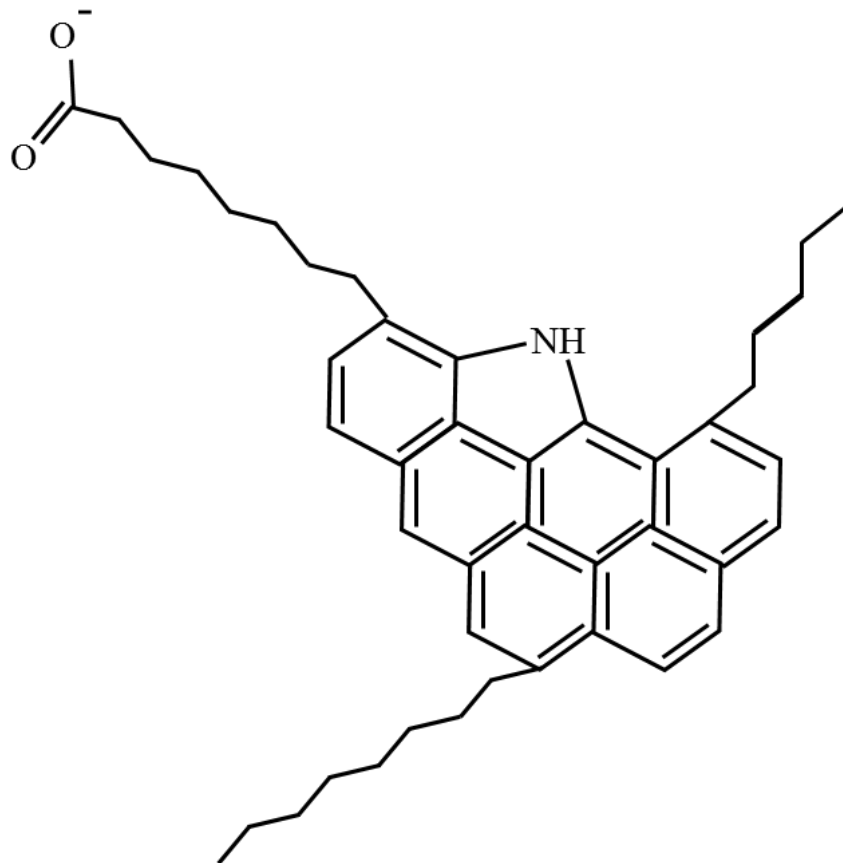
Figure 8. Anionic Continental Asphaltene Structure (Kuznicki, T. et al., 2008)

4.4. YEN – MULLINS MODEL

The Yen-Mullins model is the most widely accepted asphaltene model nowadays, shown in Figure 9 (Mullins, O.C., 2011). This model describes the asphaltene structure based on size and behavior as a function of the crude oil that contains the asphaltene. In light oils, with high API gravity, the asphaltene will be present as small poly-aromatic hydrocarbon molecules with an average diameter of 1.5 nanometers (Forte, E. and Taylor, S.E., 2014; Mishra, V.K. et al., 2012; Seifert, D.J. et al., 2012; Mullins, O.C. et al., 2013). In this case, the asphaltene concentration will be relatively low, and thus the asphaltene

size will not grow. In black oils, with slightly less API gravity, the asphaltene concentration will be higher, and thus the asphaltene will be present in the form of nanoaggregates with an average diameter of 2 nanometers, which is slightly larger than the asphaltene present in light oil. In heavy oils with extremely low API gravity, the asphaltene concentration will be relatively high, and will thus begin to form clusters. These clusters will grow in size and will reach an average diameter of 5 nanometers. The clusters form from the combination of several nanoaggregates. Based on this model, as the asphaltene concentration in the oil increases, the oil will become heavier due to the high molecular weight of asphaltene and its API will decrease, which shows that asphaltene has an overall negative impact on the crude oil.
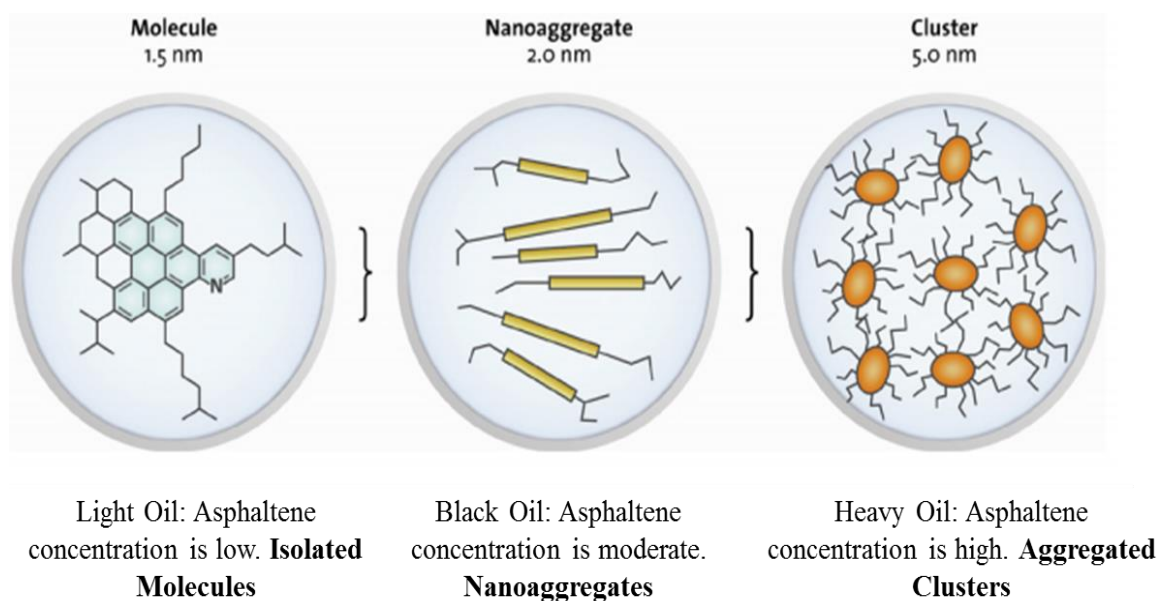
Figure 9. Yen-Mullins Asphaltene Model (Mullins, O.C., 2011)

The Yen-Mullins model provides a means of understanding the size of the asphaltene molecule and the likelihood of its presence in the crude oil. It is also important to understand how to study the chemical aspect of asphaltene and analyze the stability of asphaltene in crude oil. The different methods that have been used over the years to chemically analyze asphaltene will be presented in this research.

5. ASPHALTENE CHEMICAL ANALYSIS

Since asphaltene is extremely complex in structure and varies in composition and size, several methods are used to detect and study asphaltene structure and composition in crude oil. These methods are applied to determine several aspects of the crude oil and vary in terms of accuracy and how they detect asphaltene. Some of these methods can even perform the SARA analysis by determining the different fractions of the crude oil and their compositions. Table 1 summarizes most of the methods used to study asphaltene based on different studies that have been conducted over the years. These methods include methods that are purely chemical and focus on the asphaltene structure and composition, as well as methods that are more concerned with the asphaltene composition in the crude oil, and its stability under different conditions. Also, some of the methods utilized visual setups, whereas others focused on a fractionation approach where the crude oil composition is made based on different factions within the oil, such as chromatography methods. The most common chemical methods include chromatography, where the components of the crude oil are separated based on their composition, and SARA analysis, which is mainly used to

divide the four main fractions of the crude oil. The most novel methods used include the

confocal laser scanning microscope and the optical spectroscopy method.

Table 1. Summary of Chemical Analysis Methods of Asphaltene

Reference	Year	Analysis Technique
Jewell, D.M. et al.	1972	Anion-Cation Exchange Chromatography
Lichaa, P.M. and Herrera, L.	1975	Asphaltene Precipitation Tests
Hernandez, M.E. et al.	1983	SARA Analysis
Pearson, C.D. and Gharfeh, S.G.	1986	Liquid Chromatography with Flame Ionization Detector
Karlsen, D.A. and Larter, S.R.	1991	Thin Layer Chromatography with Flame Ionization Detector
Martinez, M.T. et al.	1997	Thermal Cracking
Kok, M.V. et al.	1998	Oxidation Reaction and SARA Analysis
Groenzin, H. and Mullins, O.C.	2000	Fluorescence Depolarization
Yarranton, H.W. et al.	2000	Vapor Pressure Osmometry
Fan, T. et al.	2002	Clay-Gel Adsorption Chromatography, Thin-Layer Chromatography, and High Pressure Liquid Chromatography Gas Chromatography

Table 1. Summary of Chemical Analysis Methods of Asphaltene (Continued)

Reference	Year	Analysis Technique
Islas-Flores, C.A. et al.	2005	Open Column Chromatography and High Pressure Liquid Chromatography SARA Analysis
Hannisdal, A. et al.	2006	Infrared Analysis
Goual, L and Abudu, A.	2009	Adsorption using Microbalance
Miadonye, A. and Evans, L.	2010	Calorimetry and Filtration
Bahzad, D. et al.	2010	Hydrodematallization
Angle, C.W. and Hua, Y.	2011	Dynamic Light Scattering Microscopy
Cho, Y. et al.	2012	Fourier Transform Ion Cyclotron Resonance Mass Spectrometry with Atmospheric Pressure Photoionization
Keshmirizadeh, E. et al.	2013	Open Column, Thin Layer, and Gas Chromatography Coupled with Flame Ionization Detector
Kharrat, A.M. et al.	2013	Optical Spectroscopy Method
Seifried, C.M. et al.	2013	Confocal Laser-Scanning Microscope
Cendejas, G. et al.	2013	Nuclear Magnetic Resonance
Fakher, S. et al.	2018	SARA Analysis using Chemical Methods
Fakher, S. and Imqam, A.	2018	Filtration based on Heptane
Fakher, S. and Imqam, A.	2018	SARA Analysis and Gas Chromatography

Asphaltene will behave in different ways based on the conditions available in the reservoir. Understanding the asphaltene behavior in the reservoir is important for oil recovery and asphaltene mitigation considerations. This will be explained in detail in this research.

6. ASPHALTENE PRECIPITATION AND DEPOSITION CYCLES

The asphaltene will pass by several phases in the crude oil based on its stability and how well it remains in solution under the thermodynamic and operational conditions at which the oil is being produced (Nghiem, L.X. and Coombe, D.A., 1997). The different phases that the asphaltene can exhibit are shown in Figure 10. Each of these phases will be explained in detail.
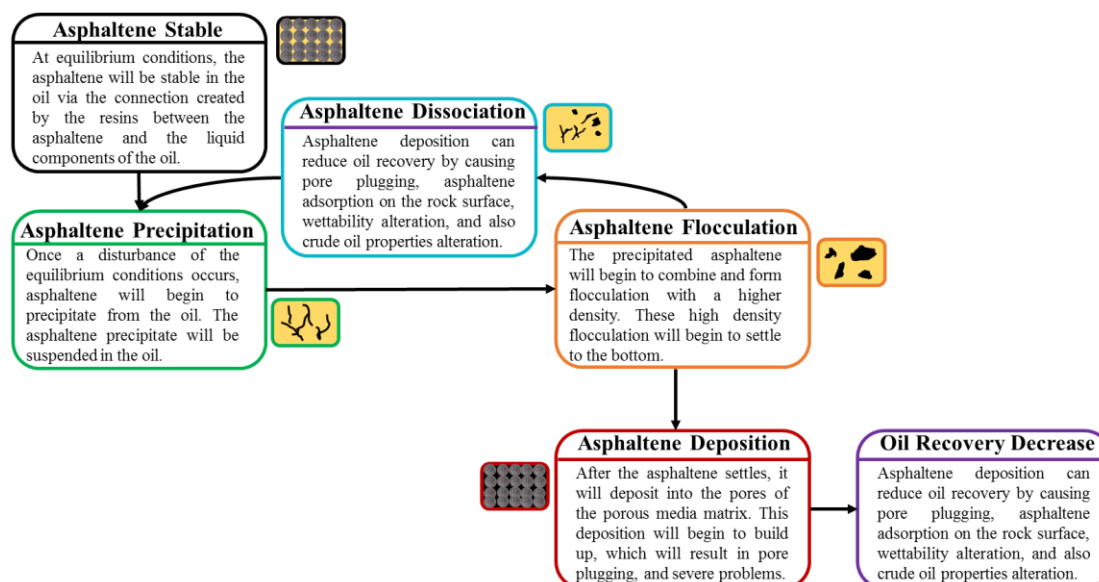
Figure 10. Asphaltene Life Cycle

6.1. ASPHALTENE STABLE

Initially, at reservoir conditions, the asphaltene is soluble in the oil and is stable at the reservoir thermodynamic conditions. The asphaltene will remain stable in the oil until any disturbance to its equilibrium occurs. Following this disturbance, the asphaltene will begin to form solid particles inside the crude oil solution.

6.2. ASPHALTENE PRECIPITATION

At equilibrium conditions, the asphaltene will remain stable in the crude oil. However, once any disturbance, such as production or solvent injection occurs to the oil, the asphaltene will begin to precipitate from the oil solution. Precipitation involves the asphaltene solid coming out of solution and forming visible asphaltene particles that are suspended in the oil. Since the asphaltene is still suspended in the oil, it still does not pose a large threat. The asphaltene will be mobile with the oil, as long as the precipitation does not continue to increase further.

Asphaltene stability in the crude oil can be impacted by many factors (Rogel, E. at al., 1999). These factors can be grouped into operational factors, which are factors that are applied during production from the reservoir, and reservoir factors, which are factors that are originally native to the reservoir but are affected as production or fluid injection commences. The chart presented in Figure 11 shows the main factors that fall under operational and reservoir factors. The reservoir conditions usually involve the reservoir thermodynamics, including pressure and temperature, and the oil properties, including solution gas, oil viscosity, and the oil classification based on its API gravity. The reservoir pressure and temperature usually do not change and are thus uncontrollable. Regarding the

oil properties, these will change depending on the production mechanism, injected fluids inside the reservoir, and pressure changes as the hydrocarbon is mobilized. A solvent is any material that can be solubilized in the crude oil at different conditions based on the solvent and the reservoir properties. Several solvents can be injected into the reservoir, including steam, surfactant, CO_2, nitrogen, methane, and many other solvents that are used to alter the properties of the crude oil. As the solvent begins to interact with the oil, the asphaltene might no longer be stable in the crude oil due to a shift in the equilibrium conditions at which it was initially solubilized in the oil. From its structure, the electrokinetic effect refers to the movements of a substance due to a change in charges. Asphaltene usually carries a charge, and thus during production operations, a drawdown is induced due to the difference in reservoir and wellbore pressure. This drawdown, along with the asphaltene charge, are two of the main reasons behind the electrokinetic effect, which will result in asphaltene instability and eventually asphaltene precipitation. Ashaltene precipitation will be svere based on many factors. These factors include the initial asphaltene concentration in the crude oil, the reservoir thermodynamic conditions including the temperature and pressure, the overall oil composition, the concentration of specific components in the crude oil including the resins for example, the asphaltene properties including its structure and its onset pressure, the fluids present in the reservoir such as water, gas, and crude oil, and the reservoir rock properites including mineralogy, clay content, and total organic content. The number of factors mentioned illustrates the complexity of asphaltene behavior.
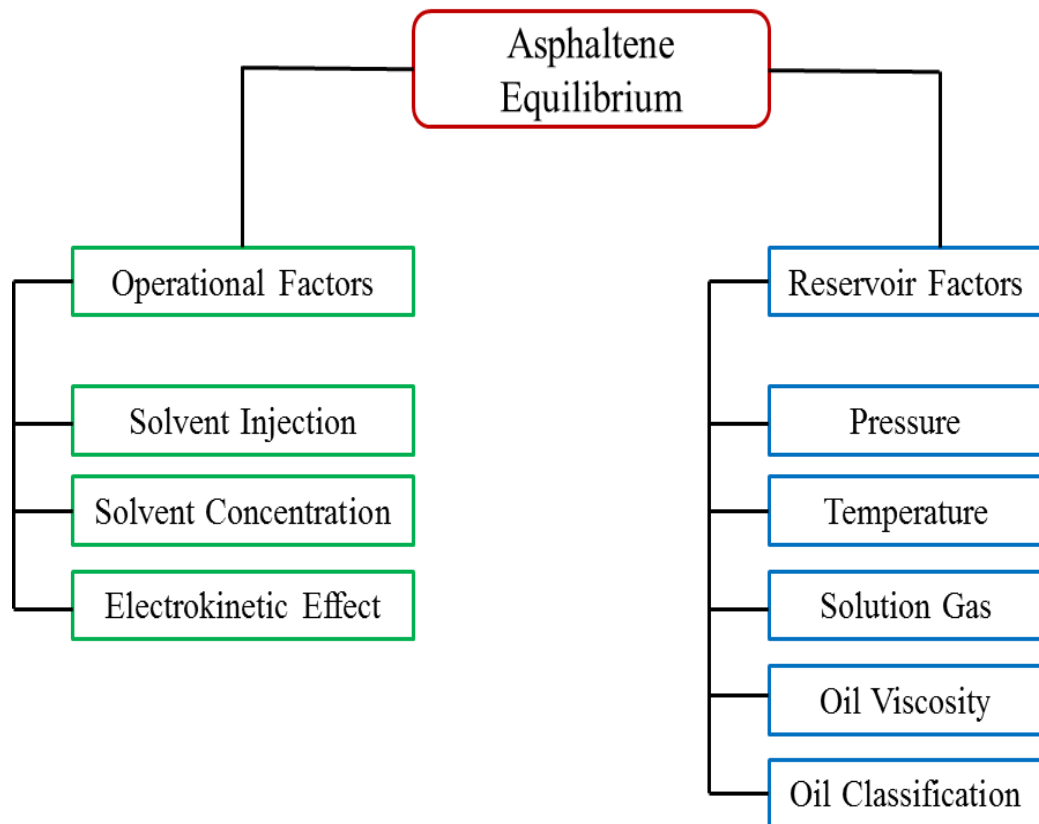
Figure 11. Factors Affecting Asphaltene Equilibrium in Crude Oil

6.3. ASPHALTENE FLOCCULATION

If asphaltene precipitation increases, the asphaltene particles will begin to combine and form larger asphaltene flocculations with a higher density than the previously precipitated particles. These dense flocculations can pose a serious threat since the particles have a large density and thus will begin to deposit in the reservoir pores, wellbores, or pipelines.

6.4. ASPHALTENE DISSOCIATION

If the flocculated asphaltene particles are noticed early, they can be remediated relatively easily. If a proper remedial method is applied, the flocculations can be broken down and dissociated back into the smaller precipitated particles. If this occurs, the precipitated particles can then be homogenized in the crude oil again, usually using a stabilizing chemical reagent.

6.5. ASPHALTENE DEPOSITION

If the asphaltene flocculations are not immediately noticed and are left in the oil, they will begin to deposit. If a large volume of asphaltene is deposited, it will cause severe problems, such as pore plugging in the reservoir, wellbore plugging due to asphaltene buildup, or buildup in the pipeline, which will incontrovertibly result in catastrophic problems if not detected early.

7. ASPHALTENE IMPACT ON OIL RECOVERY

Once asphaltene deposition occurs, it can result in several problems in the reservoir. These problems can include pore plugging, adsorption of the asphaltene to the rock grains, and wettability alternation of the rock from its original wettability to oil wet (Soroush, S. et al., 2014). All of these occurrences will have a strong impact on oil recovery and are considered relatively difficult to mitigate, as is shown in Figure 12.
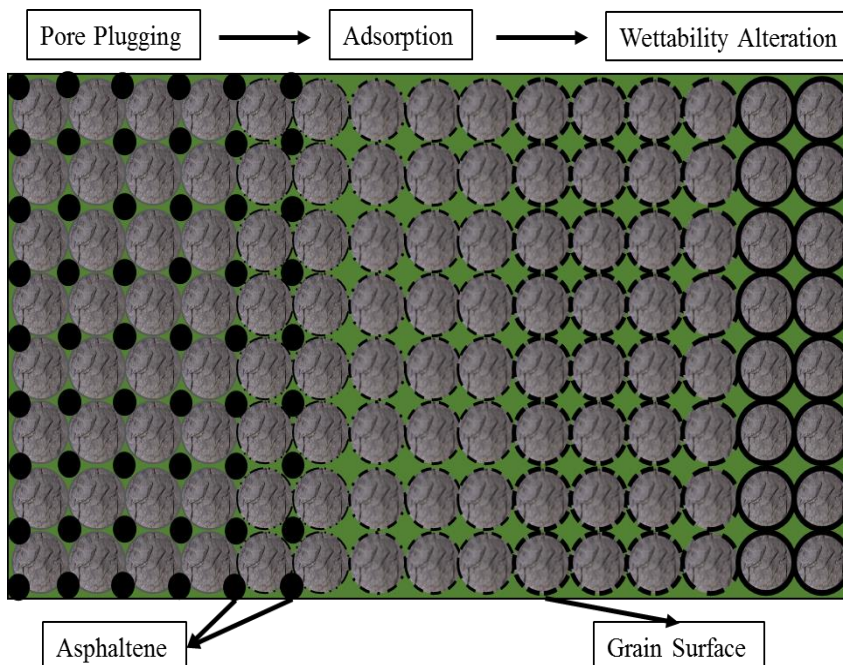
Figure 12. Asphaltene Impacts on Oil Recovery

7.1. PORE PLUGGING

If the asphaltene begins to deposit in the reservoir pores, this deposition will begin to buildup, and eventually it will fill up all the available voids in between the pores. This will result in the pores being plugged. This pore plugging will deter or completely cease the flow of the oil, and will thus significantly affect the oil recovery in a negative manner.

7.2. ASPHALTENE ADSORPTION AND WETTABILITY ALTERATION

If the asphaltene deposition increases to a great length, the asphaltene will begin to adsorb onto the grain surface. This adsorption will result in the grains being surrounded by the asphaltene, which is a component of crude oil, and thus will result in the wettability of the oil becoming strongly oil wet. This will decrease the relative permeability of the oil and decrease oil recovery.

7.3. CRUDE OIL PROPERTIES ALTERATION

The crude oil may undergo alterations due to asphaltene liberation from the oil, which will impact the overall oil properties. If this occurs, the oil will begin to exhibit different characteristics, such as a different flow mechanism or a different relative permeability, which in turn will make it much more difficult to predict how the oil will flow.

Based on the aforementioned problems, asphaltene can be extremely damaging for the reservoir. It is therefore extremely important to understand the rheological properties of asphaltene and how it flows in the reservoir with the crude oil. The rheological properties include the flow behavior of the asphaltene in the reservoir in the presence of the different reservoir fluids, and the behavior of the asphaltene during its propagation through the pores, in the wellbore, and even in the pipelines. All of these locations are viable for asphaltene related problems and thus asphaltene behavior in them should be studied.

8. ASPHALTENE RHEOLOGY AND FLOW BEHAVIOR

As was explained previously, asphaltene is a solid component and thus its flow mechanism and rheology are usually modeled as function of the fluid bearing the asphaltene. This section briefly discusses the rheology of asphaltene through an explanation of the asphaltene onset pressure and the solvent to bitumen ratio. Following this, the asphaltene flow mechanism will be discussed through the previous experiments conducted on asphaltene flow in micro and nano fluidics.

8.1. ASPHALTENE ONSET PRESSURE

Asphaltene onset pressure is the pressure at which asphaltene will begin to separate from the crude oil, or come out of solution (Soleymanzadeh, A. et al., 2018). It is a strong function of many parameters including reservoir temperature, crude oil properties, and asphaltene concentration. There are multiple methods available to measure asphaltene onset pressure; the most prominent methods are explained.

- **Gravimetric Method**: This method involves placing a live crude oil sample in a high pressure PVT cell. The pressure is reduced in stages and oil samples are collected at each stage and analyzed for asphaltene content. Once asphaltene begins to appear, the asphaltene onset pressure is determined at isothermal conditions (Burke, N. et al., 1990; Zendehboudi, S. et al., 2013).

- **Optical Microscopy**: This method utilizes a high-resolution microscope to observe samples of titrated crude oil for asphaltene precipitation (Wang, J. and Buckley, J., 2001).

- **Density Measurement**: When asphaltene precipitates from the crude oil, the oil density will change. This density change can be used as an indication of the asphaltene onset pressure (Ekulu, G. et al., 2004).

- **Light Scattering Method**: This relates light absorbance of different phases to the asphaltene onset pressure. The solid asphaltene will absorb light in a different manner than the liquid crude oil. When there is a disturbance in the light absorbance spectrum, asphaltene precipitation can be observed (Hammami, A. et al., 2000).

- **Refractive Index**: Is a function that depends on the oil density, along with polarizability and oil molecular weight (Castillo, J. et al., 2009).

- **Pressure Method**: Since asphaltene onset pressure is a pressure, it can be measured via pressure release method. This involves gradually decreasing the pressure at constant conditions and then analyzing the crude oil sample for asphaltene presence. This method is usually applied at isothermal conditions since it is not adabiatic.

The asphaltene onset pressure is one of the main parameters that control the asphaltene phase envelope. An example of an asphaltene phase envelope is shown in Figure 13 (Akbarzadeh, K. et al., 2007). This can be used to determine the phase of asphaltene and the pressure and temperature conditions at which asphaltene will begin to precipitate. Different phase envelopes are developed for different crude oils.
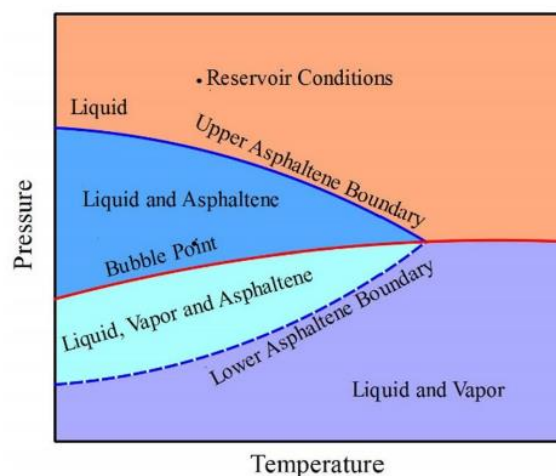
Figure 13. Asphaltene Phase Envelope Example (Akbarzadeh, K. et al., 2007)

8.2. SOLVENT TO BITUMEN RATIO

Solvent injection in crude oil is usually applied to increase the mobility of the oil, especially heavy crudes, and reduce its viscosity. The interaction of the solvent with the oil

can impact asphaltene stability. The Solvent to Bitumen Ratio is an index that can be used to determine asphaltene stability. At some point, there will be a Solvent to Bitumen Ratio at which asphaltene will begin to precipitate (Czarnecki, J. and Moran, K., 2005). Based on the solvent type, this point will differ significantly (Yeung, A. et al., 1999; Xu, Y. et al., 2007). Table 2 shows the point of asphaltene instability using the Solvent to Bitumen Ratio for different solvents that are commonly used in the oil industry (Tchoukov, P. et al., 2010). In the table, FL represents the fluid, while RG represents the rigid interface occurring, which signifies the precipitation of asphaltene from solution.

Table 2. Solvent to Bitumen Ratio at Asphaltene Stability (Tchoukov, P. et al., 2010)

S/B	1	2	3	4	9	19	32.3	99
Bitumen wt.%	50%	33%	25%	20%	10%	5%	3%	1%
Heptane	FL	RG	RG		RG			
Heptol (80:20)	FL	FL	RG	RG	RG	RG		
Heptol (50:50)	FL		FL	FL	FL	FL	RG	RG
Toluene	FL	FL	FL	FL	FL		FL	

8.3. MICRO AND NANO FLUIDICS

Micro and nano fluidics involve the flow in pores or voids that have dimensions less than 100 µm for micro, and less than 100 nm for nano fluidics (Mozaffari, S., 2015). These small channels are usually fabricated from low cost material that is transparent in order to visualize flow in them. The fabrication process includes piranha cleaning and photo lithology of the glass followed by micro/nanochannel etching, and finally glass-bonding to create the channels (Mozaffari, S. et al., 2016). A summary of the previous

studies that have utilized micro and nano fluidics to study the behavior of asphaltene in crude oil is presented in Table 3. The table includes the researcher than conducted each study, and the main observations that were concluded in each study. It is important to note that each of the studies mentioned includes a specific set of experiments or simulations conducted at specific conditions and thus are not necessarily ubiquitous in their application and practice.

Table 3. Summary of Micro and Nano Fluidic Studies Involving Asphaltene

Reference	Study	Main Observations
Mozaffari, S. 2015	Flow of bitumen in nanofluidic tubes	Asphaltene aggregates can limit oil flow and create air pockets
Mozaffari, S. et al., 2016	Heavy crude oil rheology and flow	Solvent of Bitumen Ratio played a strong role in pore plugging
Lin, Y. et al., 2016	Effect of asphaltene solubility on deposition in micro channels	The deposition dynamics of asphaltene varied significantly with solvent (heptane) concentration
Sieben, V. et al., 2016	Used a microfluidic approach for measuring the solubility of asphaltenes in crude oil	The model managed to reduce the required time for analysis of asphaltene solubility
Sieben, V. et al., 2017	Using microfluidics accompanied by a column chromatography	Column chromatography to fractionate the deasphalted oil
Afolabi, R. and Yusuf, E., 2019	Review of using nanotechnology in energy industry	Review of using nanotechnology for asphaltene flow inhibition
Nazemifard, N., 2019	Asphaltene aggregation kinetics	Asphaltene played a significant role on the stability of water-oil emulsions

After understanding the asphaltene rheology and flow behavior, it is important to study the mathematical equations and correlations used to model asphaltene flow. Understanding the mathematical models that are used to study asphaltene behavior and predict asphaltene precipitation and deposition is vital in preventing asphaltene problems in the reservoir. The most common mathematical models used to model asphaltene behavior will be mentioned in this research, along with some of their limitations.

9. ASPHALTENE MATHEMATICAL MODELS

As mentioned previously, asphaltene is extremely complex in structure, and thus no ubiquitous mathematical equation has been developed to model asphaltene behavior in crude oil. The equations provided in this section were developed based on a specific set of experiments, and thus cannot be assuredly applied for all crude oils and all asphaltene structures. Some of these equations attempted to generalize the developed model by using a fitting or scaling parameters, and they are the closest to general model. Two of the most famous equations that have been used as a standard by many researchers over the years include the Hildebrand and the Flory-Huggins models, presented in Table 4 (Flory, P.S., 1941). The Hilderbrand model is mostly known for defining the solubility parameter, which works as an indicator of compatibility. If the solubility parameter of a solution is larger than the asphaltene offset pressure, then the asphaltene is stable. The Flory-Huggins model is mainly used to obtain the chemical potential. Several other equations developed over the years that tried to evaluate asphaltene are presented in Table 5.

Table 4. Hildebrand and Flory-Huggins Models

Correlation	Nomenclature	Description
$\delta^L = \left(\dfrac{\Delta H^L - RT}{v^L}\right)^{1/2}$	- δ^L the solubility parameter of the asphaltene and oil mixture - v volume (m^3 kmol^{-1}) - H enthalpy, L liquid - T temperature (K)	The parameters H^L, v^L and as a result the solubility parameter δ^L are calculated by an equation of state (EOS)
$\emptyset_1^L$ $= exp\left[\left(\dfrac{v_1^L}{v^L - 1}\right)\right.$ $\left.- \left\{\dfrac{A\delta_1^2\left(1 - \dfrac{\delta^L}{\delta_1}\right)^2}{(1 - f\emptyset_2^L)}\right\}\right]$	- μ chemical potential - T temperature (K) - $\emptyset$ volume fraction - r molar volume ratio - L liquid, δ, f solubility parameters - 1 asphaltene, 2 oil mixture	- Lattice system is required - Assumption: The polymer and solvent molecules arrange themselves randomly - Flory-Huggins does not account the volume change upon mixing.

Table 5. Correlations Predicting Asphaltene Properties

Reference	Correlation	Nomenclature	Description
Scott, R.L., and. Magat, M. (1945)	$\dfrac{(\mu_{cAi} - \mu_{cAi}^O)}{RT} = lnV_{fAi} + 1$ $- \left(\dfrac{N_{sAi}}{\hat{N}_{sA}}\right)(1 - V_{fB}) - N_{sAi}V_{fB}$ $+ fN_{sAi}(V_{fb})^2$	- Ai and B"ith" fraction of asphaltene - Ns Segment number - u Chemical potential	- Based on Huggins' theory - More general for heterogeneous polymer/ monomer solutions
Leontaritis, K. and Mansoori, G. A., (1987)	$ln\emptyset_r = \dfrac{v_r}{v_m} - \dfrac{v_r}{RT}(\delta_m - \delta_r)^2 - 1$	- δ_m solubility parameter - v_m molar volume - v_r molar volume of resins, L^3/n	- Asphaltene flocculation prediction - Assumes that asphaltene exists in the oil as solid particles in colloidal suspension
S.Kawanaka (1988)	$V_{fA}^L = \int dV_{fAi}^L$ $= \int_0^\infty \left\langle\dfrac{\left(\dfrac{M_{Ai}}{\hat{M}_A}\right)V_A^C}{(V^L + V^s\exp(-N_{sAi\theta})}\right\rangle F(M_{Ai})dM_{Ai}$	- V_A^C The total volume of asphaltene in crude oil. - V_f Volume fraction	- It can be used to calculate the total volume fraction of asphaltene in the liquid phase in equilibrium with the solid phase

Table 5. Correlations Predicting Asphaltene Properties (Continued)

Reference	Correlation	Nomenclature	Description
de Boer et al. (1995)	$S = \exp\left\{-1 + v_a\left[\frac{1}{v_o} - \frac{(\delta_a - \delta_o)^2}{RT}\right]\right\} * C$	- S Asphaltene solubility, - C correction term for asphaltene polymerization and asphaltene-resin interaction.	- Based on Hildebrand's asphaltene solubility parameter of the oil and asphaltene
Rassamdana et al. (1996)	$X = \dfrac{S}{M^Z} \qquad Y = \dfrac{W}{S^{Z'}}$	M molecular weight solvent - W weight percent - Z Constant	- Conducted asphaltene precipitation experiments with different alkanes - scaling equation on aggregation/gelation based on the design parameters and their properties. This is a generalized equation and thus is highly applicable if the parameters are known.
Ashoori et al. (2003)	$X = \dfrac{S}{T^n M^Z} \qquad Y = \dfrac{W}{S^{Z'}}$	- n Temperature exponent (0.1-0.25)	- Introduced the effect of temperature
Mohammadi, A. H., and Richon, D. (2007)	$x = \dfrac{v_m[(\delta_m - \delta_a)^2] + 2l\delta_m\delta_a}{RT}$	- x maltene solvency power with respect to the asphaltene - δ Solubility parameter	- Does not take into account aggregation
Bagheri et al. (2009)	$X = \dfrac{S * C_t * GOR}{X_{c31} + R_t} \qquad Y = \dfrac{W * S * R_t}{C_t}$	- R_t and C_t are resin and asphaltene contents (wt %)	-

10. PREVIOUS ASPHALTENE STUDIES

In order to better understand asphaltene behavior and problems, previous laboratory and field cases that have both reported asphaltene deposition and have attempted to mitigate asphaltene problems will be presented and explained.

10.1. ASPHALTENE LAB STUDIES

Many lab studies have been conducted to investigate asphaltene pore plugging in different types of formations. The permeability reduction that occurs due to asphaltene precipitation and deposition during normal production and production during solvent injection was investigated as well. A summary of some of the studies and their reported core properties is shown in Table 6. The sand pack and glass bead experiments used extremely high permeability to investigate asphaltene in unconsolidated formations. The lowest permeability that was experienced was from the shale experiment. The shale experiment utilized gas huff-n-puff rather than continuous injection due to the permeability limitation. Some of the methods in the table are purely chemical or for the chemical engineering industrial practice rather than for petroleum engineering. The methods that are purely chemical include thermal cracking. This method is not widely known in the oil industry since it involves a chemical process that occurs at an extremely high temperature and at severe conditions. The slimtube experiment is used mainly for measuring minimum miscibility pressure of a solvent in crude oil. It involves using an extremely long tube, 45 feet in some cases, which a small diameter. The tube is packed with sand or glass beads and then saturated with oil. The solvent is then injected to measure the miscibility value.

Table 6. Core Properties for Asphaltene Pore Plugging Experiments

References	Type	Core Type	Core, in	Core ID, in	Porosity, %	Temp, ⁰C
Martinez, M. T., et al., 1997	Thermal Crack	Sand pack	15.75	0.5	-	425 - 475
Ashoori S., et al., 2006	Slimtube	Glass beads	720	0.244	28	30 - 70
Ferno, M. A., et al., 2010	Core Flooding	Chalk	2.96 - 3.177	1.99 - 2.02	45 - 48	90
Kazempour, M., et al., 2013	Core Flooding	Comp	10.09 - 10.42	1.5	14.87 - 17.7	38 and 52
Wang, S., et al., 2016	Core Flooding	Sand pack	11.81	0.984	28.95 - 35.19	22
Shen, Z., and Sheng, J. J., 2018	Huff n Puff	Shale	1.99 - 2.0	1.49 - 1.5	9.47 - 9.66	21
Alrashidi, H., et al., 2018	Core Flooding	Lime-Stone	6	1.5	14.75 - 16.30	71.11

Some researchers have mentioned asphaltene pore plugging that was observed in their experimental work as a function of permeability reduction. This is extremely significant, since it shows the extent to which asphaltene can have an impact on oil recovery. A summary of the asphaltene permeability reduction percentage observed in some studies is shown in Table 7. The permeability reduction is extremely high in some cases, reaching up to 96%. The extent to which asphaltene can reduce permeability is a function of many parameters, however, which is why it is important to investigate the exact value for each case. The factors that may impact asphaltene-induced permeability reduction include core properties such as porosity, permeability, and mineralogy, and the oil properties, most importantly including the asphaltene concentration and stability in crude

oil at different conditions. Another factor that may impact permeability reduction is the oil production rate and the injected solvent type, concentration, phase, and extent to which it interacts with the crude oil. Based on all of this, it is important to note that asphaltene permeability reduction is an extremely complex issue that requires extensive study and investigation.

Table 7. Asphaltene Permeability Reduction Values for Different Studies

References	Type	Core Type	Core (in)	Core ID (in)	K (mD)	K Reduction (%)
Lichaa, P. M., and Herrera, L., 1975	Core Flooding	Sand pack	12.2	2.87	-	33 - 96
Shedid, S. A., and Zekri, A. Y., 2006	Core Flooding	Carbonate	2.3 - 2.6	1.5 - 1.7	4.97 - 20.03	4.29 - 53.52
Cruz, J. L. M., et al., 2009	Core Flooding	Limestone	2	1.5	20.9 - 22.6	24 - 48
Behbahani, T. J., et al., 2012	Core Flooding	Sandstone	11.81	1.575	1.4	9.25 - 12.8
Kord, S., et al., 2012	Core Flooding	Carbonate	3.374 - 3.516	1.45 - 1.5	1.23 - 18	50
Soroush, A., et al., 2014	Core Flooding	Sand pack	15.748	1.5	850 - 1520	8.2 - 80

10.2. ASPHALTENE FIELD CASES

Several field studies have reported asphaltene plugging during production, which caused several problems on the rig. Table 8 provides a list of some of these cases and their

reported thermodynamic conditions. None of the field cases involve unconventional reservoirs due to lack of investigation of asphaltene in unconventionals, especially for field cases. Most of the reservoirs are at high temperatures and moderately high pressures, which are two parameters that greatly impact asphaltene stability.

Table 8. Thermodynamic Conditions for Some Field Cases Reporting Asphaltene

References	Field Name	Field Location	Formation Type (lithology)	Depth (ft)	Temp (C)	P (psi)
Thawer, R., et al., 1990	Ula	Norway	Sandstone	10974.4	143	7114.68
Thomas, D. C. et al., 1995	-	Mexico	Sandstone	19600	200	-
Jamaluuddin, A. K. M., et al., 2000	Sahil	UAE	-	8860	123.89	4425
Kalantari-Dahaghi A., et al., 2006	Kupal	Iran	Carbonate	-	71.11	6000
Yonebayashi, H., et al., 2011	Arabian Gulf	UAE	Carbonate	-	104.44	-

As has been reported in the lab studies, asphaltene pore plugging has also been reported to cause severe permeability reduction and oil recovery reduction in many field studies worldwide. A summary of some of these case studies is presented in Table 9. Based on the permeability reduction for these fields, it is clear that asphaltene pore plugging is an extremely severe matter and understanding how to prevent asphaltene plugging and how to mitigate asphaltene problems is important both in saving additional costs and time.

Table 9. Summary of Some Field Cases Involving Asphaltene

References	Field Name	Field Location	Formation Type	K (md)	K Red. (%)	Outcome
Thomas, D. C. et al., 1995	-	Mexico	Sandstone	-	-	Production decreased from 4700 to 436 BPD
Thomas, D. C. et al., 1995	-	Louisiana	-	-	-	Production decreased from 406 to 53 BPD
Thomas, D. C. et al., 1995	-	Mexico	-	-	-	Plugged completely
Kalantari-Dahaghi A., et al., 2006	Kupal	Iran	Carbonate	-	45 - 90	-
Al-Ghazi, A. S., and Lawson, J. 2007	Ghawar	Saudi Arabia	Limestone	617	-	Complete flow restriction
Uetani, T., 2014	-	Japan	-	-	-	Wettability alteration.

Asphaltene mitigation is extremely complex since many of the chemicals used to remedy asphaltene problems have several severe drawbacks, such as being incompatible with the reservoir fluids, high in cost, environmentally unfriendly, or unstable at reservoir conditions. Several researchers have therefore developed different formulations that were deemed more stable than the pure chemicals. The main drawback is that the exact formulation for these chemicals is usually not reported, and thus they will be given code names in the table based on how the original researchers referred to them. Table 10 presents the field mitigation methods after asphaltene problems arose and the outcomes obtained

from each method, including the oil recovery increase and the overall success of the mitigation process.

Table 10. Asphaltene Treatment Methods and Their Outcomes

References	Field Location	Treatment Type	Treatment Method	Outcome
Schantz, S.S., and Stephenson, W. K., 1991	ND	Chemical	Xylene	Production increased from 42 to 60 BPD
Schantz, S.S., and Stephenson, W. K., 1991	Wyoming	Chemical	Dispersant	Oil recovery increased by 33%
Thomas, D. C. et al., 1995	Mexico	Chemical	Xylene	Production increased from 436 to 4800 BPD
Thomas, D. C. et al., 1995	Louisiana	Chemical	Xylene	Xylene increased it decreased to 66 BPD.
Yen,, and Yin, Y. R., 2001	West Texas	Chemical	-	Production increased from 40 BPD to slightly more
Al-Ghazi, and Lawson, J. 2007	Saudi Arabia	-	bull heading	First method was unsuccessful.
Uetani, T., 2014	Japan	Chemical	Xylene	Productivity recovered

11. CONCLUSION

This research presents a review of asphaltene in crude oil and the factors that have the strongest impact on asphaltene stability in crude oil. The different models attempting to describe the asphaltene structure were explained, and the most recent and widely accepted model, Yen-Mullins, was described. Asphaltene phases in the crude oil were also mentioned and explained in detail, including asphaltene precipitation, flocculation, dissociation, and deposition. The main factors impacting asphaltene instability were

mentioned as well, including operational and reservoir factors. Also, the main chemical methods used to analyze asphaltene structure and composition were mentioned, along with the different experiments conducted to investigate asphaltene permeability reduction and pore plugging. Finally, several field studies that encountered asphaltene problems were mentioned, and the methods by which they attempted to mitigate the asphaltene problem was mentioned, along with outcome of each method.

ACKNOWLEDGEMENT

REFERENCES

Abdel-Raouf, M. 2012. Factors Affecting the Stability of Crude Oil Emulsions. Crude Oil Emulsions – Composition Stability and Characterization. Book Chapter. 183-204.

Afolabi, R. and Yusuf, E., 2019. Nanotechnology and global energy demand: challenges and prospects for a paradigm shift in the oil and gas industry. Journal of Petroleum Exploration and Production Technology (2019) 9:1423–1441. https://doi.org/10.1007/s13202-018-0538-0.

Ahmadi, M.A. Prediction of asphaltene precipitation using artificial neural network optimized by imperialist competitive algorithm. J Petrol Explor Prod Technol (2011) 1: 99. https://doi.org/10.1007/s13202-011-0013-7.

Akbarzadeh, K. et al., 2007. Asphaltenes -Problematic but rich in potential. Oilfield Review 19 (2), 22–43.

Al-Ghazi, S., & Lawson, J., 2007. Asphaltene Cleanout Using VibraBlaster Tool. Society of Petroleum Engineers. doi:10.2118/110972-MS.

Alrashidi, H., Farid Ibrahim, A., & Nasr-El-Din, H. (2018, June 22). Bio-Oil Dispersants Effectiveness on AsphalteneSludge During Carbonate Acidizing Treatment. Society of Petroleum Engineers. doi:10.2118/191165-MS

Alshaikh, M. et al., 2018. An Innovative Dielectric Constant Measurement Method to Determine the Ideal Surfactant Candidate to Enhance Heavy Oil Recovery. Society of Petroleum Engineers. doi:10.2118/189752-MS.

Alshaikh, M. et al., 2019. Anionic Surfactant and Heavy Oil Interaction during Surfactant-Steam Process. Society of Petroleum Engineers. doi:10.2118/195254-MS.

Alvarez-Ramirez, F. and Ruiz-Morales, Y., 2003. Island versus Archipelago Architecture for Asphaltenes: Polycyclic Aromatic Hydrocarbon Dimer Theoretical Studies. Energy Fuels 2013, 27, 4, 1791-1808. https://doi.org/10.1021/ef301522m.

Angle, C. W., & Hua, Y. (2012). Dilational Interfacial Rheology for Increasingly Deasphalted Bitumens and n-C5 Asphaltenes in Toluene/NaHCO3 Solution. Energy & Fuels, 26(10), 6228-6239. doi:10.1021/ef300846z

Ashoori S, Jamialahmadi M, Müller Steinhagen H, Ahmadi K. Investigation of reversibility of asphaltene precipitation and deposition for an Iranian crude oil. Iran. J. Chem. Chem. Eng. (IJCCE) 2006; 25(3): 41–47.

Bagheri, M. B., Mirzabozorg, A., Kharrat, R., Dastkhan, Z., and Ghotbi, C., "Developing a New Scaling Equation for Modelling of Asphaltene Precipitation," Canadian International Petroleum Conference (CIPC), Calgary, 16–18 June 2009.

Bahzad, D., Al-Fadhli, J., Al-Dhafeeri, A., Abdal A., (2010) "Assessment of selected apparent kinetic parameters of the HDM and HDS reactions of two kuwaiti RESIDUAL oils, using two types of commercial ARDS catalysts" Energy Fuels, 24: 1495-1501

Behbahani, T. J., Ghotbi, C., Taghikhani, V., & Shahrabadi, A. (2012). Investigation on Asphaltene Deposition Mechanisms during CO2 Flooding Processes in Porous Media: A Novel Experimental Study and a Modified Model Based on Multilayer Theory for Asphaltene Adsorption. Energy & Fuels, 26(8), 5080-5091. doi:10.1021/ef300647f

Bissada, K.A. et al., 2016. Group-type characterization of crude oil and bitumen. Part II: Efficient separation and quantification of normal-paraffins iso-paraffins and naphthenes (PIN). Fuel. 173: p. 217-221.

Boussingault JB. Mémoire sur la composition des bitumes. Ann Chim Phys1837;64:141–51.

Burke, N. et al., 1990. Measurement and modeling of asphaltene precipitation (includes associated paper 23831). J Pet Technol 42(11):1440–1446.

Castillo, J. et al., (2009. Measurement of the refractive index of crude oil and asphaltene solutions: onset flocculation determination. Energy Fuels 24(1):492–495.

Cendejasa G, Arreguina A, Laura Castroa V, Floresa Eugenio A, Vazqueza F.Demulsifying super-heavy crude oil with bifunctionalized block copolymers.Fuel 2013;103:356–63.

Cho, Y., Na, J.-G., Nho, N.-S., Kim, S., Kim S., (2012) "Application of saturates, aromatics, resins, and asphaltenes crude oil fractionation for detailed chemical characterization of heavy crude oils by Fourier transform ion cyclotron resonance mass spectrometry equipped with atmospheric pressure photoionization" Energy Fuels, 26: 2558-2565

Cruz, J. L., 2009. Argüelles-Vivas, F. J., Matías-Pérez, V., Durán-Valencia, C. D., & López-Ramírez, S. (2009). Asphaltene-Induced Precipitation and Deposition During Pressure Depletion on a Porous Medium: An Experimental Investigation and Modeling Approach. Energy & Fuels, 23(11), 5611-5625. doi:10.1021/ef9006142

Czarnecki, J. and Moran, K., 2005. On the Stabilization Mechanism of Water-in-Oil Emulsions in Petroleum Systems. Energy Fuels 2005, 19, 5, 2074-2079. https://doi.org/10.1021/ef0501400.

D-4124-97, ASTM. Standard Test Methods for Separation of Asphalt into Four Fractions. Updated 2019.

De Boer, R.B. et al., 1995. Screening of crude oils for asphalt precipitation: theory, practice, and the selection of inhibitors. SPE Prod. Facil. 10 (1), 55–61.

Ekulu, G. et al., 2004. Scanning aggregation phenomena in crude oils with density measurements. J Dispers Sci Technol 25(3):321–331.

Elkahky, S., et al. A comparative study of density estimation of asphaltene structures using group contribution methods and molecular dynamic simulations for an Australian oil field. J Petrol Explor Prod Technol (2019) 9: 2699. https://doi.org/10.1007/s13202-019-0641-x.

Fakher, S., & Imqam, A. (2018a, October 29). Investigating and Mitigating Asphaltene Precipitation and Deposition in Low Permeability Oil Reservoirs During Carbon Dioxide Flooding to Increase Oil Recovery. Society of Petroleum Engineers. doi:10.2118/192558-MS

Fakher, S., et al. An experimental investigation of asphaltene stability in heavy crude oil during carbon dioxide injection. J Petrol Explor Prod Technol (2019). https://doi.org/10.1007/s13202-019-00782-7.

Fakher, S., Imqam, A., & Wanas, E. (2018, December 10). Investigating the Viscosity Reduction of Ultra-Heavy Crude Oil Using Hydrocarbon Soluble Low Molecular Weight Compounds to Improve Oil Production and Transportation. Society of Petroleum Engineers. doi:10.2118/193677-MS

Fakher, S., Imqam, A., 2018b. Asphaltene precipitation and deposition during CO2 injection in nano shale pore structure and its impact on oil recovery, Fuel, 237, 1029-1039, https://doi.org/10.1016/j.fuel.2018.10.039.

Fan, H., 2003. The Effects of Reservoir Minerals on the Composition Changes of Heavy Oil During Steam Stimulation. Journal of Canadian Petroleum Technology, 42 (3).

Fan, T. et al., 2002. Evaluating Crude Oils by SARA Analysis. Presented at the SPE/DOE Improved Oil Recovery Symposium, Tulsa, Oklahoma, 13-17 April. SPE-75228-MS.

Fernø, M. A., Torsvik, M., Haugland, S., & Graue, A. (2010). Dynamic Laboratory Wettability Alteration. Energy & Fuels, 24(7), 3950-3958. doi:10.1021/ef1001716

Flory, PJ.: J. Chern. Phys. (1941) 9, 660, J. Chern. Phys., 10,52.

Forte, E. and Taylor, S.E., 2014. Thermodynamic Modelling of Asphaltene Precipitation and Related Phenomena. Advances in Colloid and Interface Science, 217, 1-12.

Garner, W. and Ham, J., 1939. The Combustion of Methane. The Royal Society A. https://doi.org/10.1098/rspa.1939.0019.

Gholami, A., et al. Improving the estimation accuracy of titration-based asphaltene precipitation through power-law committee machine (PLCM) model with alternating conditional expectation (ACE) and support vector regression (SVR) elements. J Petrol Explor Prod Technol (2016) 6: 265. https://doi.org/10.1007/s13202-015-0189-3.

Goel, P. et al., 2017. Prediction of °API Values of Crude Oils by Use of Saturates/Aromatics/Resins/Asphaltenes Analysis: Computational-Intelligence-Based Models. Society of Petroleum Engineers Journal. 817- 853, doi:10.2118/184391-PA.

Golkari, A. and Riazi, M. Experimental investigation of miscibility conditions of dead and live asphaltenic crude oil–CO2 systems. J Petrol Explor Prod Technol (2017) 7: 597. https://doi.org/10.1007/s13202-016-0280-4.

Goual L, Abudu A. 2009. Predicting the Adsorption of Asphaltenes from Their Electrical Conductivity. Energy Fuel 24: 469–474.

Goual, L., 2012. Petroleum Asphaltenes, Crude Oil Emulsions- Composition Stability and Characterization, (Ed.), ISBN: 978-953-51-0220-5.

Groenzin, H. and O.C. Mullins, 2000. Molecular size and structure of asphaltenes from various sources. Energy and Fuels. 14(3): p. 677-684.

Hammami, A., et al., 2000. Asphaltene precipitation from live oils: an experimental investigation of onset conditions and reversibility. Energy Fuels 14(1):14–18.

Hannisdal, A., Ese, M.H., Hemmingsen, P.V., and Sjoblom, J., Particle-stabilizedemulsions: effect of heavy crude oil components pre-adsorbed onto stabilizing solids, Colloids Surfaces A—Physicochem. Eng. Aspects 276 (2006)45–58.

Hernandez, M. E., M. T. Vives, and J. Pasquali, 1983, Relationships among viscosity, composition, and temperature for two groups of heavy crudes from the eastern Venezuelan basin: Organic Geochemistry, v. 4, p.173–178.

Ihtsham, M. and Ghosh, B. Dynamic asphaltene deposition control in pipe flow through the application of DC potential J. Petrol Explor Prod Technol (2015) 5: 99. https://doi.org/10.1007/s13202-014-0113-2.

Iraji, S. and Ayatollahi, S. Experimental investigation on asphaltene biodegradability using microorganism: cell surface properties' approach. J Petrol Explor Prod Technol (2019) 9: 1413. https://doi.org/10.1007/s13202-018-0537-1.

Islas-Flores, C. A., E. Buenrostro-Gonzalez, et al. (2005). "Comparisons between open column chromatography and HPLC SARA fractionations in petroleum." Energy & Fuels 19(5): 2080-2088.

Jamaluddin, A.K.M. et al., 2000. Experimental and theoretical assessment of the asphaltene precipitation characteristics of the Sahil field under a proposed gas injection scheme. In: Paper SPE # 87292 presented at the SPE Conf. and Exh., 15–18October 2000, Abu Dhabi, UAE.

Jewell, D. et al., 1972. Ion-exchange, coordination, and adsorption chromatographic separation of heavy-end petroleum distillates. Analytical Chemistry. 44(8): p. 1391-1395.

Jha, N.K. et al., 2014. Characterization of Crude Oil of Upper Assam Field for Flow Assurance. Presented at the SPE Saudi Arabia Section Annual Technical Symposium and Exhibition, Al-Khobar, Saudi Arabia, 21-24 April. SPE-172226-MS.

Kalantari-Dahagi, A. et al., 2006, Formation Damage due to Asphaltene Precipitation Resulting from CO2 Gas Injection in Iranian Carbonate Reservoirs. Society of Petroleum Engineers. doi:10.2118/99631-MS.

Kargarpour, M.A. and Dandekar, A. Analysis of asphaltene deposition in Marrat oil well string: a new approach J Petrol Explor Prod Technol (2016) 6: 845. https://doi.org/10.1007/s13202-015-0221-7.

Karlsen, D.A. and S.R. Larter, 1991. Analysis of petroleum fractions by TLC-FID: applications to petroleum reservoir description. Organic Geochemistry. 17(5): p. 603-617.

Kawanaka S, Park SJ, Mansooori GA. The role of asphaltene deposition in EOR gas flooding: a predictive technique. Soc Pet Eng DOE 1988l (SPE17376).

Kazempour, M., Manrique, E. J., Alvarado, V., Zhang, J., & Lantz, M. (2013). Role of active clays on alkaline–surfactant–polymer formulation performance in sandstone formations. Fuel, 104, 593-606. doi:10.1016/j.fuel.2012.04.034

Keshmiri, K. et al., 2016. Using Microfluidic Device to Study Rheological Properties of Heavy Oil. 16th AIChE Annual Meeting, San Francisco, CA, USA.

Keshmirizadeh, E., S. Shobeirian, and M. Memariani, 2013. Determination of saturates, aromatics, resins and asphaltenes (SARA) fractions in Iran crude oil sample with chromatography methods: study of the geochemical parameters. Journal of Applied Chemical Research. 7(4): p. 15-24.

Khamehchi, E., Shakiba, M. and Ardakani, M.S. A novel approach to oil production optimization considering asphaltene precipitation: a case study on one of the Iranian south oil wells. J Petrol Explor Prod Technol (2018) 8: 1303. https://doi.org/10.1007/s13202-017-0409-0.

Kharrat, A. et al., 2013, Asphaltene Content Measurement Using an Optical Spectroscopy Technique, Energy & Fuels 2013 27 (5), 2452-2457. DOI: 10.1021/ef400050y.

Kim, S.T. et al., 1990. The role of asphaltene in wettability reversal. In: SPE Paper presented at the SPE Ann. Tech. Conf. and Exh., 1990, New Orleans, Louisiana.

Kok, M.V., Karacan, O., and Pamir, R., Kinetic analysis of oxidation behaviour of crude oil SARA constituents, Energy & Fuels 12–3 (1998) 580–588.

Kor, P., et al. Comparison and evaluation of several models in prediction of asphaltene deposition profile along an oil well: a case study. J Petrol Explor Prod Technol (2017) 7: 497. https://doi.org/10.1007/s13202-016-0269-z.

Kord, S., Miri, R., Ayatollahi, S., & Escrochi, M. (2012). Asphaltene Deposition in Carbonate Rocks: Experimental Investigation and Numerical Simulation. Energy & Fuels, 26(10), 6186-6199. doi:10.1021/ef300692e

Kuznicki, T. et al., 2008. Molecular Dynamics Study of Model Molecules Resembling Asphaltene-Like Structures in Aqueous Organic Solvent Systems. Energy Fuels 2008, 22, 4, 2379-2389. https://doi.org/10.1021/ef800057n.

Lammoglia, T., & Filho, C. R. d. S. (2011). Spectroscopic characterization of oils yieldedfrom Brazilian offshore basins: Potential applications of remote sensing.RemoteSensing of Environment,115, 2525–2535.

Leandra, S. et al., 2018. Stress relaxation in quasi-two-dimensional self-assembled nanoparticle monolayers. Physical Review E, 96(5), p.052803. https://doi.org/10.1103/PhysRevE.97.052803.

Leon, O., Contreras, E., Rogel, E., Dambakli, G., Acevedo, S.,Carbognani, L., Espidel, J., 2002. Adsorption of native resinson asphaltene particles: A correlation between adsorption andactivity. Langmuir 18, 5106–5112.

Leontaritis, K. and Mansoori, G.A., 1987. Asphaltene flocculation during oil production and processing: A thermodynamic collodial model. in SPE International Symposium on Oilfield Chemistry. Society of Petroleum Engineers.

Liao, H. et al., 2019. Effect of Crude Oil Composition on Microwave Absorption of Heavy Oils. Society of Petroleum Engineers. doi:10.2118/195263-MS.

Lichaa, P.M. and Herrera, L., 1975. Electrical and other effects related to the formation and prevention of asphaltene deposition problem in Venezuelan crudes. in SPE oilfield chemistry symposium. Society of Petroleum Engineers.

Lin, Y. et al., 2016. Examining Asphaltene Solubility on Deposition in Model Porous Media. Langmuir 2016, 32, 34, 8729-8734. https://doi.org/10.1021/acs.langmuir.6b02376.

Liu, F. et al., 2017. Mixture Effect on the Dilatation Rheology of Asphaltenes-Laden Interfaces. Langmuir 33.8 (2017). https://doi.org/10.1021/acs.langmuir.6b03958.

Martinez, M.T., Benito, A.M. and Callejas, M.A., 1997. Thermal cracking of coal residues: kinetics of asphaltene decomposition. Fuel. 76(9): p. 871-877.

Miadonye A., and Evans L., 2010. The Solubility of Asphaltenes in Different Hydrocarbon Liquids. Petroleum Science and Technology Journal. https://doi.org/10.1080/10916460902936960.

Mishra, V.K. et al., 2012. Downhole Fluid Analysis and Asphaltene Nanoscience Coupled with VIT for Risk Reduction in Black Oil Production. Presented at the SPE Annual Technical Conference and Exhibition, San Antonio, USA, 8-10.

Mohammadi, A.H. and D. Richon, 2007. A monodisperse thermodynamic model for estimating asphaltene precipitation. AIChE journal. 53(11): p. 2940-2947.

Monger, T.G. and Fu, J.C., 1987. The nature of CO2-induced organic deposition. In: SPE Paper # 16713 presented at the SPE Ann. Tech. Conf. and Exh., Houston, TX.

Mozaffari, S. et al., 2015a. Effect of Asphaltene Aggregation on Rheological Properties of Diluted Athabasca Bitumen. Energy & Fuels, 29(9), pp.5595-5599. https://doi.org/10.1021/acs.energyfuels.5b00918.

Mozaffari, S. et al., 2016. Capillary driven flow in nanochannels – Application to heavy oil rheology studies. Colloids and Surfaces A: Physicochemical and Engineering Aspects. 513 (5), 178-187. https://doi.org/10.1016/j.colsurfa.2016.10.038.

Mozaffari, S. et al., 2017a. Capillary driven flow in nanochannels – Application to heavy oil rheology studies. Colloids and Surfaces A: Physicochemical and Engineering Aspects, 513, pp.178-187. https://doi.org/10.1016/j.colsurfa.2016.10.038.

Mozaffari, S. et al., 2017b. Colloidal nanoparticle size control: experimental and kinetic modeling investigation of the ligand–metal binding role in controlling the nucleation and growth kinetics. Nanoscale, 9(36), 13772-13785. https://doi.org/10.1039/C7NR04101B.

Mozaffari, S. et al., 2018. Ligand-Mediated Nucleation and Growth of Palladium Metal Nanoparticles. J. Vis. Exp. (136), e57667, doi:10.3791/57667.

Mozaffari, S., 2015. Rheology of Bitumen at the Onset of Asphaltene Aggregation and its Effects on the Stability of Water-in-Oil Emulsion. Masters Thesis, University of Alberta, Canada.

Mullins, O.C. et al., 2013. Asphaltene Nanoscience and Reservoir Fluid Gradients, Tar Mat Formation, and the Oil-Water Interface. Presented at the SPE Annual Technical Conference and Exhibition, Louisiana, USA, 30 Sept- 2 Oct.

Mullins, O.C., 2011. The modified yen model. Energy and Fuels, 2010. 24(4): p. 2179-2207. Mullins, O.C., The asphaltenes. Annual Review of Analytical Chemistry. 4: p. 393-418.

Nazemifard, N., 2019. Application of Micro/Nanofluidics in Energy. Fluids at Brown, Division of Applied Mathematics, Fluids and Thermal Sciences, School of Engineering, Joint Seminar Series.

Nghiem, L.X., and D.A. Coombe, 1997. Modelling asphaltene precipitation during primary depletion. SPE Journal. 2(02): p. 170-176.

Nwadinigwe, C. et al. Studies on precipitation performance of n-heptane and n-pentane/n-heptane on C7 and C5/C7 asphaltenes and maltenes from 350 °C atmospheric residuum of three Nigerian light crudes. J Petrol Explor Prod Technol (2015) 5: 403. https://doi.org/10.1007/s13202-014-0150-x.

Pazuki, G.R., 2007. Application of a new cubic equation of state to computation of phase behavior of fluids and asphaltene precipitation in crude oil. Fluid Phase Equilibria. 254(1): p. 42-48.

Pearson, C.D. and S.G. Gharfeh, 1986. Automated high-performance liquid chromatography determination of hydrocarbon types in crude oil residues using a flame ionization detector. Analytical Chemistry. 58(2): p. 307-311.

Prakoso, A. A. et al., 2017. A Mechanistic Understanding of Asphaltenes Precipitation From Varying-Saturate-Concentration Perspectives. Society of Petroleum Engineers. doi:10.2118/177280-PA.

Punase, A. et al., 2016. The Polarity of Crude Oil Fractions Affects the Asphaltenes Stability. Society of Petroleum Engineers. doi:10.2118/180423-MS.

Rassamdana, H. and Sahimi, M., 1996. Asphalt flocculation and deposition: II. Formation and growth of fractal aggregates. AIChE journal. 42(12): p. 3318-3332.

Rassamdana, H.B. et al., 1996. Asphaltene flocculation and deposition: I. The onset of precipitation. AIChE J. 42 (1), 10–22.

Rogel, E. et al., 1999. Asphaltene Stability in Crude Oils. Society of Petroleum Engineers. doi:10.2118/53998-MS.

Salleh, I.K., et al. Micro-emulsion-based dissolver for removal of mixed scale deposition. J Petrol Explor Prod Technol (2019) 9: 2635. https://doi.org/10.1007/s13202-019-0643-8.

Schantz, S., and Stephenson, W., 1991. Asphaltene Deposition: Development and Application of Polymeric Asphaltene Dispersants. Society of Petroleum Engineers. doi:10.2118/22783-MS.

Scott RL, Magat M. The thermodynamics of high-polymer solutions: the free energy of mixing of solvents and polymers of heterogeneous distribution. J Chem Phys. 1945;13/5:172–177.

Seifert, D.J. et al., 2012. Black Oil, Heavy Oil, and Tar in One Oil Column Understood by Simple Asphaltene Nanoscience. Presented at the Abu Dhabi International Petroleum Exhibition & Conference, UAE, 11-14 November.

Seifried, C. et al., 2013. Kinetics of Asphaltene Aggregation in Crude Oil Studied by Confocal Laser-Scanning Microscopy. Energy & Fuels, 27, 1865-1872.

Shedid and Zekri, 2006, Formation Damage Caused by Simultaneous Sulfur and Asphaltene Deposition. Society of Petroleum Engineers. doi:10.2118/86553-PA.

Shen and Sheng, 2018, Experimental and numerical study of permeability reduction caused by asphaltene precipitation and deposition during CO2 huff and puff injection in Eagle Ford shale, Fuel, 211, 432-445, https://doi.org/10.1016/j.fuel.2017.09.047.

Sieben, V. et al., 2016. Microfluidic Approach for Evaluating the Solubility of Crude Oil Asphaltenes. Energy Fuels 2016, 30, 3, 1933-1946. https://doi.org/10.1021/acs.energyfuels.5b02216.

Sieben, V. et al., 2017. Optical Measurement of Saturates, Aromatics, Resins, And Asphaltenes in Crude Oil. Energy Fuels 2017, 31, 4, 3684-3697. https://doi.org/10.1021/acs.energyfuels.6b03274.

Soleymanzadeh, A. et al., 2018. A review on methods of determining onset of asphaltene precipitation. Journal of Petroleum Exploration and Production Technology (2019) 9:1375–1396. https://doi.org/10.1007/s13202-018-0533-5.

Soroush, S. et al., 2014. A Comparison of Asphaltene Deposition in Miscible and Immiscible Carbon Dioxide Flooding in Porous Media. Society of Petroleum Engineers. doi:10.2118/169657-MS.

Speight, J.G. et al., 1985. Molecular weight and association of asphaltenes: a critical review. Revue De L'Institut FrancaisDu Petrole 40 (1), 51–61.

Speight, J.G., 1999. The chemical and physical structure of petroleum: effect on recovery operations. J. Pet. Sci. Eng. 22, 3–15.

Struchkov, I.A., et al. Laboratory investigation of asphaltene-induced formation damage. J Petrol Explor Prod Tech (2019) 9: 1443. https://doi.org/10.1007/s13202-018-0539-z.

Tchoukov, P. et al., 2010. Study of water-in-oil thin liquid films: Implications for the stability of petroleum emulsions. Colloids and Surfaces A: Physicochemical and Engineering Aspects. 372 1, 3,15-21. https://doi.org/10.1016/j.colsurfa.2010.09.007.

Thawer, R. et al., 1990. Asphaltene Deposition in Production Facilities. Society of Petroleum Engineers. doi:10.2118/18473-PA.

Theyab, M.A. et al., 2017. Study of Fluid Flow Assurance in Hydrocarbon Production – Investigation Wax Mechanisms. PhD Thesis, London South Bank University.

Thomas, D. et al., 1995. Controlling Asphaltene Deposition in Oil Wells. Society of Petroleum Engineers. doi:10.2118/25483-PA.

Uetani, T. (2014, November 10). Wettability Alteration by Asphaltene Deposition: A Field Example. Society of Petroleum Engineers. doi:10.2118/171788-MS

Wang, J. and Buckley, J., 2001. A two-component solubility model of the onset of asphaltene flocculation in crude oils. Energy Fuels. 15(5):1004–1012.

Wang, S. et al., 2016. Characterization of Produced and Residual Oils in the CO2 Flooding Process, Energy & Fuels 2016 30 (1), 54-62, DOI: 10.1021/acs.energyfuels.5b01828.

Xu, Y. et al., 2007. Destabilization Of Water In Bitumen Emulsion By Washing With Water. Journal of Petroleum Science and Technology. 17 9, 1051-1070. https://doi.org/10.1080/10916469908949765.

Yarranton, H.W., Alboudwarej, H., and Jakher, R., 2000. Investigation of asphaltene association with vapor pressure osmometry and interfacial tension measurements. Industrial and engineering chemistry research. 39(8): p. 2916-2924.

Yen, A. et al., 2001. Evaluating asphaltene inhibitors: laboratory tests and field studies. In: Paper SPE -65376-MS presented at the SPE Int. Symp. Oilfield Chem. 2001,Houston, Texas.

Yeung, A. et al., 1999. On the interfacial properties of micrometre–sized water droplets in crude oil. Royal Society A. https://doi.org/10.1098/rspa.1999.0473.

Yonebayashi, H. et al., 2011. Dynamic Asphaltene Behavior for Gas-Injection Risk Analysis. Society of Petroleum Engineers Reservoir Evaluation and Engineering Journal. 513- 524, doi:10.2118/146102-PA.

Zendehboudi, S. et al., 2013. Thermodynamic investigation of asphaltene precipitation during primary oil production: laboratory and smart technique. Ind Eng Chem Res 52(17):6009–6031.

Zendehboudi, S. et al., 2014. Asphaltene precipitation and deposition in oil reservoirs – Technical aspects, experimental and hybrid neural network predictive tools, Chemical Engineering Research and Design, 92 (5), 857-875.

III. FLOW OF CARBON DIOXIDE IN MICRO AND NANO PORES AND ITS INTERACTION WITH CRUDE OIL TO INDUCE ASPHALTENE INSTABILITY

ABSTRACT

Carbon dioxide (CO_2) flow in different pore sizes will impact the mechanism by which it propagates through the porous media significantly. Also, during its flow, CO_2 will interact with the crude oil and will be impacted by the pore size in the porous media as well. During this interaction, asphaltene, one of the most damaging components of the crude oil, may precipitate from solution thus causing severe operational problems. This research investigates the flow mechanism of CO_2 through nano and micro pores and the impact of this flow on oil mobilization and asphaltene instability in the crude oil. The flow mechanism of CO_2 was determined using numerical modeling through the Knudsen number to determine the flow regimes under different thermodynamic conditions. Following this, the oil production and asphaltene stability was studied using a filtration vessel supplemented with nano and micron sized filter membranes. The effect of varying CO_2 injection pressure, oil viscosity, porous media pore size, and porous media thickness on oil mobilization and asphaltene stability was studied. Regarding the flow regimes, it was found that four distinct flows were observed during CO_2 injection in the nano and micro pores. These flow regimes included diffusion, transition, slippage, and viscous flow. As the pore size increased, the flow became viscous dominated. Increasing the CO_2 injection pressure increase oil production and decreased the asphaltene concentration in the bypassed crude oil, which is the oil remaining in the filtration vessel and could not be produced. The lower oil viscosity was associated with a lower asphaltene concentration

and thus yielded an overall higher oil viscosity as well. By undergoing this research, a better understanding of how the CO_2 flows through nano and micro pores can be achieved, and oil mobilization and asphaltene instability with time can also be understood.

1. INTRODUCTION

During its injection in oil reservoirs, the CO_2 will propagate through the pores of the formation and interact with the crude oil in order to mobilize the oil and facilitate its production. Understanding the flow regimes by which CO_2 flows in the pores of the formation is extremely important in order to determine how and where the CO_2 is most likely to go in the formation and thus determine the CO_2 oil production potential [1-5]. CO_2 can result in asphaltene instability which may impact oil mobilization negatively along with causing severe problems in facilities and pipelines. It is extremely important to understand the effect that CO_2 has on asphaltene instability and how that may impact oil filtration.

Different methods have been used to model CO_2 flow in the reservoir and the flow regimes that may arise during its propagation through the pores. Shabro, V. et al. [6] combined a new pore scale model with a reservoir simulation algorithm to model fluid flow while incorporating the effects of no-slip and slip flow, Knudsen diffusion, and Langmuir desorption. Okamoto, N. et al. [7,8] modeled fluids displacement mechanisms using Knudsen Number via molecular simulation. Negara, A. et al. [9] investigated the effect of Knudsen diffusion on shale gas production behavior. Wu, K. et al. [10] developed a model for bulk-gas transfer in nanopores dependent on slip flow and Knudsen diffusion. Xu, J. et

al. [11] studied free gas transport in nanopores of shale rocks through Knudsen diffusion using real gas equation of state and elastics hard-sphere model. Jin et al. [12] used the definition of the Knudsen Number to prove that the CO_2 flow in the nano-pores of the shale mainly falls under the Free Molecular Flow behavior and is hence mainly governed by diffusion. Li, J. et al. [13] established a gas-slip model for fluid movement in nanopores and determined the accuracy of the model using laboratory results by varying the Knudsen number and gas relative permeability.

Asphaltene instability in different formations and lithologies has been studied by many researchers using different experimental and modeling techniques. Zendehboudi, S. et al [14] differentiated between precipitation, coming out of solution, and deposition, adhesion of the asphaltene to the rock. This helped provide a method by which to analyze asphaltene stages including precipitation, deposition, and flocculation [15-19]. Rassamdani, H.B. et al. [20] observed another stage of asphaltene, referred to as asphaltene flocculation, where the asphaltene particles began forming clusters and aggregates of a large diameter size. Soroush, S. et al. [21] studied asphaltene stability during CO_2 injection and determined that the state of asphaltene can actually impact asphaltene stability. Kalantari-Dahagi, A. et al. [22] conducted one of the few studies that investigated asphaltene problems in carbonate reservoirs and found asphaltene to be extremely problematic at the bubble point. Shedid and Zekri [23] showed that with the increase in the rock permeability and average pore size, the asphaltene problems decreased significantly. This shows that studying the impact of pore size on asphaltene stability becomes extremely important. Tavakkoli, M. et al. [24] attempted to model asphaltene precipitation using computer modeling and compared the results to those of the experimental results to

investigate its accuracy. Yonebayashi, H. et al. [25,26] studied asphaltene instability using dynamic experiments in order to incorporate the electro-kinetic effect on asphaltene precipitation and deposition. Moradi et al. [27] investigated asphaltene instability in small micro pores using filter membranes with 0.2 µm pore size using nitrogen injection. Struchkov, et al. [28] performed a detailed study formation damage due to asphaltene deposition in pores. The methodology utilized actual core plugs instead of filter membranes which makes their study extremely valuable. Results showed that asphaltene deposition will decrease the core permeability and thus may limit oil mobility and reduce the overall oil recovery. Shen and Sheng [29] researched asphaltene problems in shale reservoirs using Eagle Ford cores and nano filter membranes. Their research did not include the mechanism of asphaltene instability. Fakher, S. and Imqam, A. [30, 31] performed an extensive study of asphaltene behavior in nano pores and methods by which asphaltene can be mitigated. Mohammed et al. [32] conducted one of very few numerical modeling studies of asphaltene instability in small pore sized and attempted to reduce asphaltene damage without the use of chemical agents by relying on the injected fluid properties and the production method and schedule.

Understanding the mechanism by which CO_2 flows in oil reservoirs and studying the impact of CO_2 flow on asphaltene instability is extremely important both when modeling CO_2 flow and to avoid asphaltene operational problems during production. Even though several researchers have studied both topic using multiple methods, very few researchers have evaluated the effect of CO_2 flow regimes on asphaltene instability in both micro and nano pores together. This research extends the previous work conducted by Fakher, S. et al. [19] which studied asphaltene instability visually and using some filtration

studies. This research investigates CO_2 flow mechanisms, oil filtration, asphaltene buildup, and asphaltene content in both micro pores and nano pores in both the produced and the bypassed oil, which is the oil that was not produced, in order to provide a holistic view on the impact of some factors on CO_2 flow regimes, oil mobilization, and asphaltene instability in these pore sizes.

2. EXPERIMENTAL MATERIAL

2.1. FILTRATION VESSEL

A stainless steel high pressure filtration vessel was used to conduct all the experiments. The vessel housed both the crude oil and the CO_2.

2.2. CARBON DIOXIDE

CO_2 was supplied using a high pressure CO_2 cylinder. The flow of CO_2 was regulated using a pressure regulator attached to the cylinder.

2.3. FILTER MEMBRANES

Filter membranes with 2.7 µm, 100 nm, 10 nm, and 0.2 nm pore size were used to conduct the filtration experiments and to study the flow regime. These sizes were used in order to incorporate a wide size distribution.

2.4. TEST TUBES

Glass test tubes were used to collect the produced crude oil. Glass was used since plastic was found to interact with some of the components of the crude oil and the heptane used for the asphaltene quantification.

2.5. CRUDE OIL

Crude oil with viscosity 469, 260.7, 119, and 63.7 cp were used to conduct the experiments. The crude oil was obtained from Kirk lease in Kansas. The 469 cp oil had an initial asphaltene concentration of 5.73 wt%. The crude oil was obtained from the separator with an initial viscosity of 469 cp. The viscosity was then reduced using different weight percent kerosene mixing. The kerosene was highly soluble in the crude oil. Other chemicals can also be used to reduce the viscosity of the crude oil such as xylene or naphtha, however, kerosene was used in this study due to avalibility.

3. EXPERIMENTAL SETUP

The experimental setup used to conduct the asphaltene stability experiments is shown in Figure 1. The setup includes the CO_2 cylinder connected to a pressure regulator to control the flow from the cylinder and control the pressure value. The main filtration vessel includes the filter membrane, crude oil and CO_2. An O-ring is placed to prevent any leakages during the experiment. Also, a 60-micron mesh screen is added to prevent the filter membrane from rupturing at high pressure. The produced oil is collected at the outlet in a glass test tube for further analysis. The oil that remained in the filtration vessel and

could not be produced was referred to as the bypassed oil and was also collected for analysis. The filtration vessel used differs slightly from the one used in our previous study [33]. The vessel used in this setup acquires a seal using a high vacuum rubber, while the other one is sealed using steel bolts.
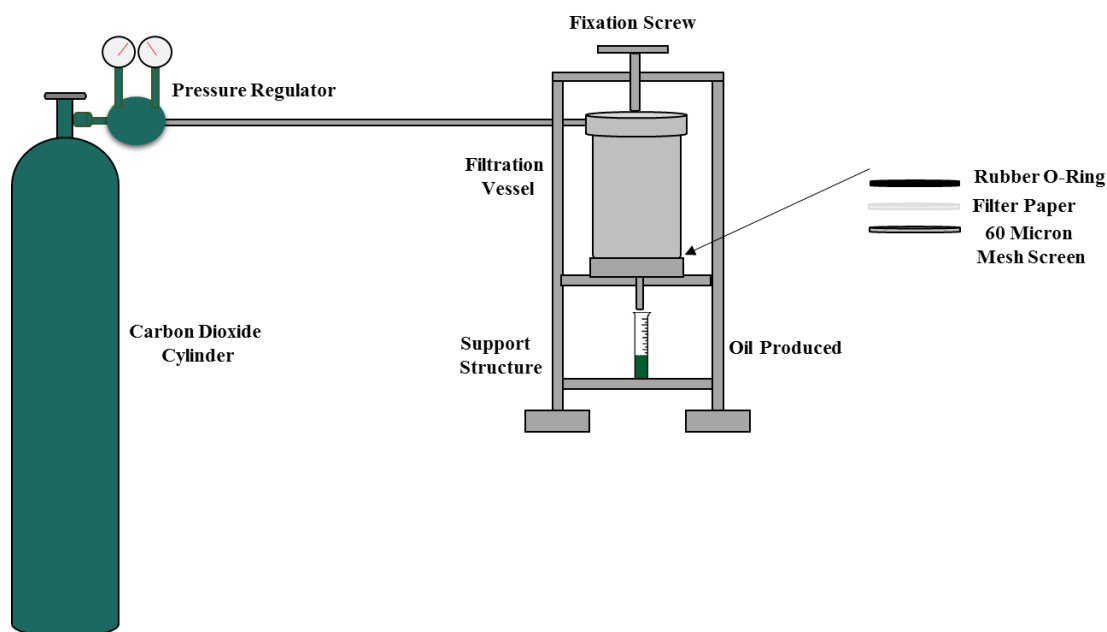
Figure 1. Specially Modified Filtration Setup

4. EXPERIMENTAL PROCEDURE

The experimental procedure was based on initially preparing the crude oil sample to be tested, and then conduct the experiment. The procedure followed to conduct all the experiments is as follows:

- To prepare the filtration vessel, the bottom cap was detached, and then the 60 micron mesh screen was inserted into it. The mesh screen is a vital component of

the setup since it provides a support base for the filter paper, and prevent is from rupturing during the experiment, while causing no hindrance to the flow since its pore size is much larger than that of the filter paper. The filter paper is then placed on top of the mesh screen, and then a rubber O-ring is placed on top of the filter paper. The O-ring ensures that a perfect seal is attained between the bottom cap assembly and the filtration vessel to avoid any potential for leaks during the experiment.

- After connecting the bottom cap, 100 ml of the specific viscosity oil used to run the experiment is poured into the filtration vessel. The top cap of the filtration vessel is then attached to the CO_2 cylinder, and fixed to the filtration vessel using the fixation screw on the top.

- The CO_2 cylinder is then opened, and the regulator is used to adjust the pressure to that of the experiment. The recording of the time commences as soon as the pressure regulator allows the release of the CO_2 to the setup.

- The oil production is recorded every 30 seconds for the first hour, and then every minute for the remaining duration of the experiment. The oil production flow rate is then calculated based on the produced volume and the time. The oil produced is collected for further analysis following the conclusion of the experiment.

- The CO_2 injection is maintained until CO_2 breakthrough occurs and no further oil production is observed.

- The bypassed oil, unproduced oil, is the collected from the vessel and stored for further analysis. The filter paper is also collected and stored in vacuum for further analysis.

- The asphaltene wt% in the produced oil and the bypassed oil is then calculated for each experiment to study the extent to which the asphaltene will plug the pores.

- The filter cake thickness and the area of asphaltene plugging on the filter paper is also calculated for each filter paper.

- In order to measure the weight of the asphaltene, the filter membrane bearing the asphaltene had to be dried initially. This was done by placing the filter membrane in a vessel with temperature of 80 °C. The membrane was maintained in the vessel for three days.

- Following this, the membrane was analyzed to ensure that it was completely dry and had no heptane in it. The filter membrane was then weighed in a scale with an accuracy of a 1000th of a gram.

5. ASPHALTENE DETECTION TEST

Asphaltenes are defined as the heavy components of the crude oil that are insoluble in n-alkanes, such as n-heptane or n-pentane, but soluble in aromatics such as toluene or xylene [34]. It is important to determine if the crude oil used in this study has a percentage of asphaltene, and it is also crucial to quantify this asphaltene since it is a main operational problem during CO_2 flooding; the asphaltene detection and quantification test was run using the standard test for determination of asphaltenes (heptane insolubles) in crude petroleum (IP 143) [35]. It should be noted that the 0.45μm membrane may bypass some of the asphaltene, especially for the smaller pore size experiment such as the 100, 10, and 0.2 nm experiments.

The procedure followed for the asphaltene detection test involved dissolving 0.1 ml of crude oil in 10 ml of n-heptane. The test tube is stirred vigorously for twenty seconds to ensure that the oil has been totally dissolved. The test tube is then set in an upright position for 48 hours. Precipitation of the asphaltene will begin to become visible approximately one hour after the oil is dissolved, however the test tube must be left for at least 48 hours to ensure that all the asphaltene has deposited from the solution. The asphaltene is then filtered from the solution using a 0.45 µm filter paper, and then the weight percent is calculated. The weight percent of the asphaltene was calculated using the equation below:

$$Asphaltene\ wt\% = \frac{wt\ of\ asphaltene}{total\ wt\ of\ oil} \times 100$$

6. RESULTS AND DISCUSSION

Both the CO_2 flow mechanism in nano and micro pores and the asphaltene deposition and precipitation will be discussed in this section. The CO_2 flow mechanism will include the CO_2 flow regimes identified using the Knudsen Number, the effect of varying CO_2 injection pressure, oil viscosity, pore size of the filter membrane, and filter membrane thickness. The asphaltene deposition and precipitation will include the asphaltene weight percent in both the produced oil and the unproduced oil and its effect on oil production.

6.1. CO₂ FLOW MECHANISM IN NANO AND MICRO PORES

It is important to differentiate between the flow of CO_2 in conventional reservoirs and the flow of CO_2 in unconventional reservoirs. To be able to establish this differentiation, an understanding of the different flow regimes that could arise must be presented. The Knudsen number is considered one of the most applied and accurate indications of the type of flow that is occurring in the porous media [36-41]. The general form of the Knudsen number is presented.

$$K_n = \frac{\lambda}{L} = (\frac{K_b T}{\sqrt{2}\pi d^2 p})/L$$

where K_n is the Knudsen number, λ is the mean molecular free path (m), L is the representative physical length which is the pore radius for this work (m), K_b is the Boltzmann constant (1.38065×10^{-23} J/k), T is the temperature (k), d is the particle hard shell diameter, or the diameter of the CO_2 molecule in this research (2.32×10^{-10} m), p is the pressure (Pa).

By using the Knudsen number, the flow regime for each pore size filter membrane can be identified for each of the CO_2 injection pressures used. Ziarani and Aguilera [36] defined four distinct flow regimes based on the value of the Knudsen number. These regions are defined in Figure 2. It is important to note that other flow regime diagrams for the Knudsen number may be available with more flow regimes, however this diagram was used in this study mainly since it contains the four main flow regimes that are of great interest to this study. Also, the four regimes defined may contain other transition regimes, however they were not included in the diagram.

Viscous Flow	Slip Flow	Transition Flow	Knudsen Flow
• Low Reynolds Number • Immobile Fluid at pore wall • Darcy's Law Applicable	• Gas Molecules Slip at solid interface. • Darcy's Law Applicable with Klinkenberg Correction or Knudsen Modification.	• Both slip and diffusion can occur. • Darcy's law begins to fail and is considered erroneous to use. • Safer to apply Knudsen's Diffusion	• Darcy's law becomes fully inapplicable. • Gas molecules exhibit little or no interaction with neighboring gas molecules. • Apply Diffusion Laws

```
0            0.01              0.1               10            ∞
```

Knudsen Number

Figure 2. Different Flow Regimes Identified Using Knudsen Number

Viscous flow dominates the flow behavior in conventional hydrocarbon reservoirs. For viscous flow, Darcy's law can be applied safely given that the flow is laminar, which is usually represented by a low Reynolds number, usually close to unity. Viscous flow occurs at a Knudsen number below 0.01. If the flow becomes turbulent, such as in fractures or extremely high permeability formations or features, Forchheimer's equation becomes more applicable. Forchheimer's equation is shown [42].

$$\frac{dp}{dx} = \frac{-\mu}{k} v_x + \rho \beta v_x{}^2$$

where p is the pressure, x is the distance, v_x is the velocity in x direction, ρ is the fluid density, and β is the non-Darcy flow coefficient of the porous medium.

During gas flow, the gas molecules will experience to some extent slippage at the pores' interface [43, 44]. This slippage becomes more profound as the permeability

decreases, until a point where the gas slippage becomes overcome by diffusion in nano-pores. In the presence of gas, the conventional Darcy law can be applied, however a correction must be made to obtain representative values [43, 45]. This correction could either be the Klinkenberg correction or the Knudsen modification. Slip flow occurs for a Knudsen number value between 0.01 and 0.1.

When the pore throats are decreased further beyond that of the slip flow, a transition flow occurs where both slip and diffusion flow occur. This occurs for a Knudsen number between 0.1 and 10. Even though Darcy's law has been applied to model flow during this flow regime, it usually produces erroneous results especially as the Knudsen number approaches 10. It is, therefore, safer to apply Knudsen's diffusion equation [36].

As the Knudsen number exceeds 10, the flow regime becomes Knudsen's Free Molecular flow. In this flow regime, Darcy's law becomes completely inapplicable, and diffusion based equations, such as Knudsen's diffusion, must be applied. In this type of flow, the gas molecules interact with the pore surface, and reach a point where there is almost no interaction between the gas molecules themselves [46]. This will occur mainly in the nano-pores of the unconventional shale reservoirs. Knudsen's diffusion equation is shown [38].

$$D_{Kn} = \frac{d_k}{3} \sqrt{\frac{8R_g T}{\pi M}}$$

where D_{Kn} is the Knudsen diffusion, d_k is the pore throat radius, R_g is the universal gas constant, M is the molecular weight, and T is the temperature.

If the pore size is extremely small, surface diffusion will be become predominant [47]. Surface diffusion is modeled using Fick's first law, shown.

$$N_i = -D_i \nabla c_i$$

where N_i is the molar flux, D_i is the diffusion coefficient, and c_i is the concentration.

The Knudsen number was calculated for all the pore sizes used in this research at different pressures. Table 1 shows the Knudsen number values. All values were calculated using the form of Knudesn equation presented before. It is important to note that other forms of Knudsen equation are present. Each form has a different usage and also has different assumptions and boundary conditions.

Based on these results, it is clear that the flow for all the experiments conducted using the 2.7 µm filter membranes is governed mainly using Darcy's law, with Klinkenberg correction in slip flow. When the filter membrane pore size decreases to the nano-meter scale, the flow becomes governed mainly by diffusion, modeled using Knudsen's diffusion or Fick's first law. This shows that the flow regime in the nano pores differs significantly form that of the micro pores, and hence there is a significant difference between the CO_2 flow behavior in unconventional and conventional reservoirs. The flow regimes in the different nano pore sizes also vary significantly. This shows that the flow regime in the unconventional reservoirs will not always be diffusion dominated. As the nano pores increase in size the flow regime will beign to be transition flow dominated, followed by slip flow dominated. When the slip flow begins to dominate as the main flow regime, this is an indication that the normal Darcy law can be used.

Table 1. Knudsen Number Value and Equivalent Flow Regime for Experiments

Pore Size (L)	**Pressure, Psi**	**Mean Free Path (λ), m**	**Knudsen Number (λ/L)**	**Flow Regime**	**Recommended Equation**
2.7 µm	25	9.84867×10^{-8}	0.03648	Slip Flow	Darcy, with Klinkenberg
2.7 µm	50	4.92434×10^{-8}	0.01824	Slip Flow	Darcy with Klinkenberg
2.7 µm	100	2.46217×10^{-8}	0.00912	Viscous Flow	Darcy's Law
100 nm	300	8.20893×10^{-9}	0.082084	Slip Flow	Darcy with Klinkenberg
10 nm	300	8.20893×10^{-9}	0.82084	Transition Flow	Knudsen's Diffusion
0.2 nm	600	4.10347×10^{-9}	20.5174	Knudsen Flow	Knudsen's Diffusion or Fick's Law

The flow mechanism study in this research has a specific applicability range based on the material used and the definition of the Knudsen number. The limitations of the flow mechanism study must therefore be mentioned and considered to avoid confusion. The main limitations of the flow mechanism methodology are as follow:

- The method does not consider heterogeneity or tortuosity.

- Since filter membranes are used, a longer porous media can such as cores can yield different results.

- The values used are for pure CO_2 and do not take into consideration other gases or mixtures.

Three CO_2 injection pressures were used, including 25, 50, and 100 psi to study the effect of CO_2 injection pressure on the oil filtration, and the asphaltene deposition. The CO_2 when injected at different pressure will interact with the oil and flow through the pore spaces in a different manner. This difference in interaction and flow behavior results in both an effect on oil filtration, and oil flow, which was explained using the Knudsen number.

The effect of CO_2 injection pressure is shown in Figure 3. Regardless of the oil viscosity, it is evident that as the CO_2 injection pressure increases, the oil production increases, and the CO_2 breakthrough time through the oil bank decreases. For example, regarding the 260.7 cp oil in Figure 3b, the CO_2 breakthrough time for the 100 psi pressure was 480 seconds, or 8 minutes, with an oil production of 93% while the CO_2 breakthrough for the 25 psi was 2220 seconds, or 37 minutes, with an oil production of 91.5%.; even though this increment in oil production is not significant, in a real reservoir, compared to the filter membrane, the increment will be much higher. The oil production increase with the increase in CO_2 injection pressure was observed by several researchers and is mainly attributed to the higher displacement of the oil due to the higher pressure [21-23].

The CO_2 could not produce all of the oil in the filtration vessel mainly due to its inability to mobilize the higher molecular weight components since they require larger pressure differentials to force them through the filter membranes. Even though there was a possibility to mobilize these components and force them through the micro-sized filter membranes, this possibility is eliminated in the nano-sized filter membranes.
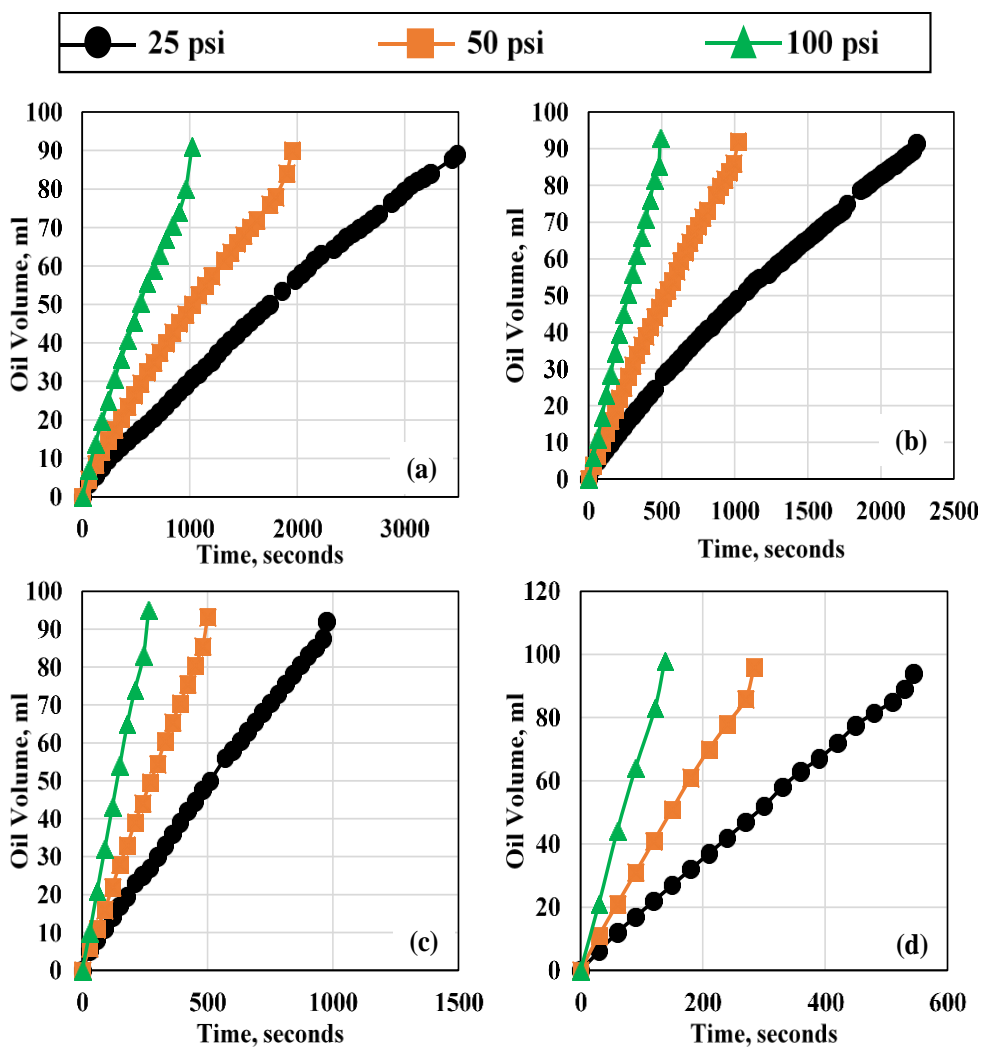
Figure 3. Impact of Varying CO_2 Injection Pressure on Oil Filtration for Oil Viscosities (a) 469 cp, (b) 260.7 cp, (c) 119 cp, (d) 63.7 cp

The CO_2 breakthrough time is another significant parameter that was affected by the CO_2 injection pressure. From Figure 3, the CO_2 breakthrough time is decreased significantly as the pressure increases. This shows that the CO_2 will produce all the oil that it is capable of mobilizing in a shorter duration compared to the lower CO_2 injection pressure. The CO_2 breakthrough time can be observed in the plots in Figure 3 above as the data point before the last. The last data point shows a sudden increase in the oil filtration

compared to the somewhat linear trend that the plots are following. This last data point is the oil filtration following CO_2 breakthrough. The sudden increase is due to the CO_2 mobilizing the last few milliliters of oil that it can after it has broken through. Due to the simultaneous production of the two fluids, including oil and CO_2, following this breakthrough, a more that usual oil volume is produced for a few seconds before production ceases. Other researchers also reported an increase in oil production after CO_2 breakthrough. The oil viscosity is one of the main contributors to the oil filtration, and also one of the main factors that will impact asphaltene equilibrium in the oil and their precipitation and deposition. It was therefore paramount to investigate the viscosity's effect on oil filtration and asphaltene deposition. For the 2.7µm filter membrane, four different viscosities were used in this study, including 469 cp, 260.7 cp, 119 cp, 63.7 cp. Four experiments were conducted for three different CO_2 injection pressures to study the impact of oil viscosity at different CO_2 injection pressures. Figure 4 shows the results for all the oil viscosities at different CO_2 injection pressures.
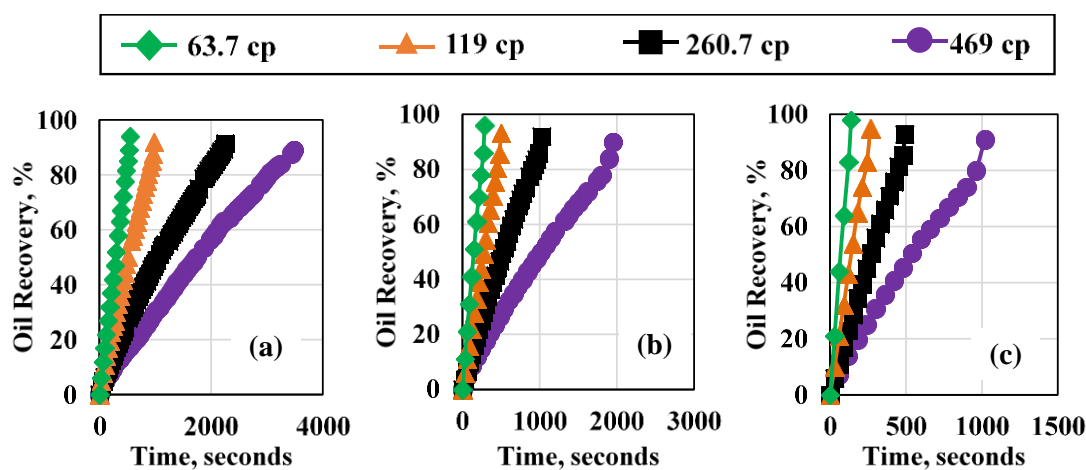
Figure 4. Impact of varying Oil Viscosity on Production Using (a) CO_2 Injection Pressure 25 psi, (b) CO_2 Injection Pressure 50 psi, (c) and CO_2 Injection 100 psi

When the oil viscosity was reduced for all the CO_2 injection pressures, the oil production increased. This is due to two main reasons. The first is that the decrease in oil viscosity makes it more prone to be mobilized by the CO_2, even at lower pressures. This in turn results in both a higher, and more rapid oil production, which can also be seen in Figure 4. Lower viscosity oils required less time to produce the oil compared to the higher viscosity oils. The second reason is related to the asphaltene in the oil. As the viscosity of the oil is reduced, the overall asphaltene weight percent in the oil is also reduced, and therefore a smaller amount of oil is left behind, as will be clearly shown in the asphaltene weight percentages section. For example, in Figure 4a, the oil production for the 469 cp oil took 3485 seconds, or 58 minutes to produce, whereas the 63.7 cp oil only took 530 seconds, or 8.8 minutes to produce. The asphaltene wt% for the 469 cp oil was found to be 5.73%, compared to 3.22% in the 63.7 cp oil. It is also important to point out that the values for the oil production are extremely high in all the experiments mainly due to the use of the filter membranes rather than a long porous media.

Four pore sizes were used in this research, including 2.7 µm, 100 nm, 10 nm, and 0.2 nm. It was identified earlier, using Knudsen Number, that the flow regime was different for different pore sizes. This section compares different pore sizes in terms of oil production, and oil production rate to further emphasize the difference between CO_2 flow in different pore sizes.

A comparison between the oil production, and the oil production flow rate for the 10 nm, and 100 nm is shown in Figure 5. The 2.7 µm was not included in the comparison since the experiments were run at a different pressure. Also, the 0.2 nm will be explained separately since its results were different.
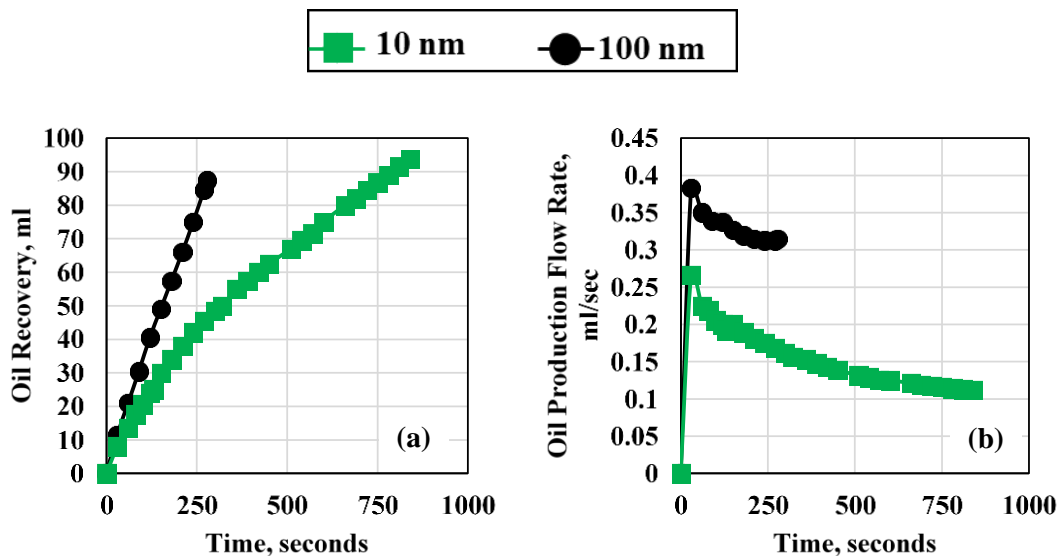
Figure 5. Comparing 100nm and 10nm (a) Oil Production with Time, and (b) Oil Production Flow Rate with Time

Both the 10 nm and the 100 nm experiments were conducted at 300 psi using a 100 ml initial volume. The total time until gas breakthrough was much longer for the 10 nm pore size membrane compared to the 100 nm membrane due to fluid being much more difficult to pass through the smaller pore size. The oil production for the 10 nm membrane appears to be larger compared to the 100 nm membrane. At the experimental conditions, crude oil will not be impacted significantly by CO_2 dissolution. This was studied in detail by Lobanov et al. [48] who showed experimentally that when CO_2 completely dissolved in the crude oil at 10wt% CO_2, the crude oil hardly swelled at all. The asphaltene many have played a role in varying the crude oil production however no conclusive reason can be reached with only the oil recovery data.
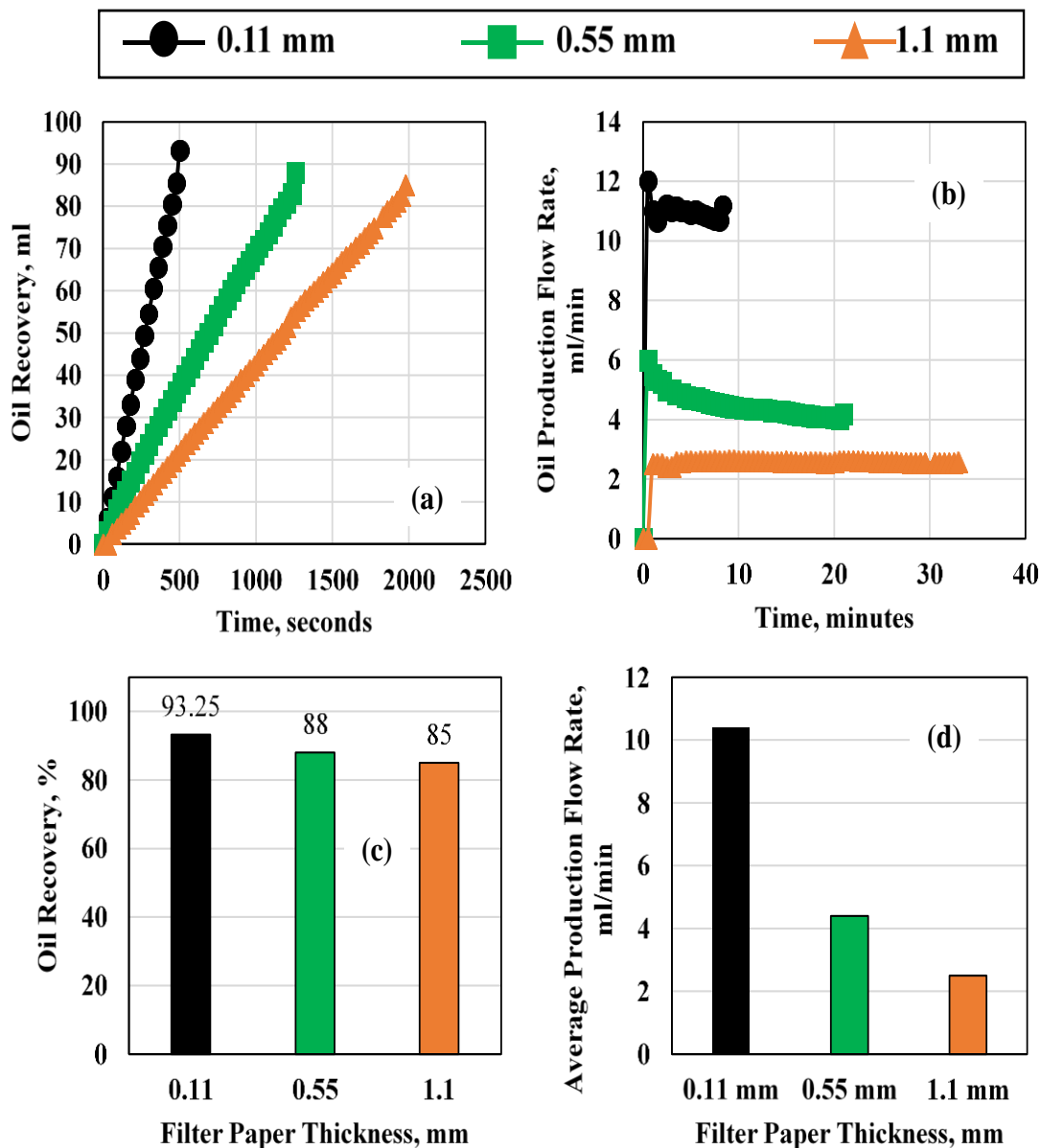
Figure 6. Filter Paper Thickness Effect on (a) Gas Breakthrough Time, (b) Oil Production Flow Rate, (c) Oil Production, and (d) Average Production Flow Rate

The experiments were repeated two more times with the overall trend being the same. Also, when compared to the 2.7 µm filter membrane results, the oil production from the nano-membranes was reduced mainly due to the difference in the flow regime, and the

inability to mobilize the majority of the asphaltene and heavy molecular weight components. The oil production flow rate indicated a longer time until stable flow rate for the 10 nm compared to the 100 nm which gives an indication of a larger filter cake thickness formation time for the smaller pore size. All in all, both the 100 nm and the 10 nm follow the same trend with a difference in oil production and oil flow rate stability time due to the difference in pores size. This same trend is related to both pore sizes exhibiting the same flow regime based on their calculated Knudsen number, shown in Table 3.

All of the experiments in this research were conducted using a uniform thickness filter membrane. As the thickness of the membrane increases, it become more difficult for the CO_2 to mobilize the oil, and also the oil begins adsorbing to the filter membrane surface, and thus production decreases, and the flow behavior changes. Three different filter paper thicknesses were used in this study, including 0.11 mm, 0.55 mm, and 1.1 mm. The experiments were conducted using 50 psi injection pressure, and 119 cp oil viscosity. Figure 6 shows all the results obtained using the three different filter paper thicknesses.

The increase in the filter paper thickness resulted in a decrease in the oil production and an increase in the gas breakthrough time. The average oil production flow rate also decreased significantly with the increase in filter paper thickness. When the filter membrane was recovered, a relatively large volume of the oil was found to have adsorbed to the pores of the membrane, which is one of the main reasons behind the decrease in the oil production. The oil that was adsorbed to the filter paper was composed of a high percentage of asphaltenes which indicates that the asphaltene will result in a high plugging of the pore space of the porous media.

6.2. ASPHALTENE PRECIPITATION AND DEPOSITION

This section will elaborate on both the CO_2 production mechanism in the 2.7 µm filter membrane experiments, explained above, and will also show the significance of the precipitation and deposition of asphaltene, and the impact that both the CO_2 injection pressure and oil viscosity have on both the production mechanism and the asphaltene deposition.

The oil production flow rate was calculated by dividing the recovered volume by the time. Two major things can be derived from the flow rate curves. The first main finding is stability of the production flow rate for each oil viscosity and each CO_2 injection pressure. This can be seen in Figure 7. The initial flow rate for all the plots is extremely high compared to the other flow rates; this is the time at which the CO_2 began mobilizing the oil and hence the largest flow rate is observed; following this point, the flow rate then begins to reach stabilization. The longer the duration of the production, the more time the flow had time to stabilize. The plots for the 63.7 cp, for example, appear to be unstable compared to the plots for the other oil viscosities that took a longer duration to produce. It is important to note that the experiments were conducted using filter membranes, which are not representative of an actual core plug or a real field case. The results obtained therefore have to be verified using an actual core plug in order to ensure that the obtained trends are actually representative of a porous media. This is clear based on the oil recovery results which reached an extremely large value, reaching up to 98% in some cases, which is almost non-existant in any field case, and also has been reported in very high permeability core samples or in unconsolidated sand experiments.
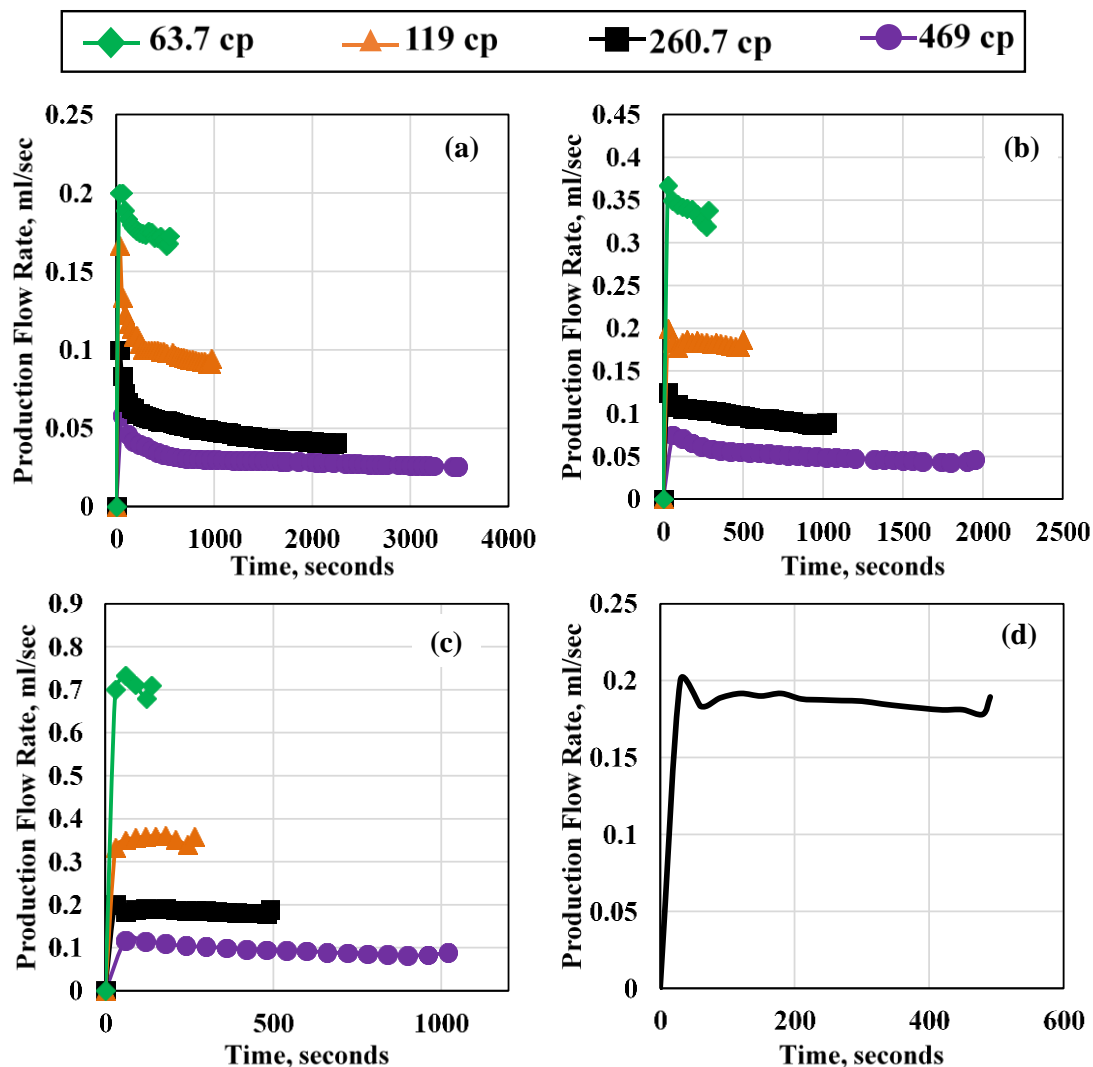
Figure 7. Oil Production Flowrates for CO_2 Injection Pressures of (a) 25 psi, (b) 50 psi, (c) 100 psi, (d) 100 psi, 260.7 cp

A relationship between the average oil production flow rate, the overall oil production, and the CO_2 breakthrough pressure is shown in Table 2. As the CO_2 breakthrough time decreases, the oil production increases for each oil viscosity. Also, the decrease in CO_2 breakthrough time results in a larger average oil flow rate for the same viscosity oil. This shows that as the overall time for production decreases there is a higher

average flow rate which in turn does not allow for the formation of a thick filter cake. This decrease in time occurs either with the increase in CO_2 injection pressure or decrease in oil viscosity; the former has an effect on the oil production behavior, while the latter has an effect on the reduction in asphaltene concentration.

Table 2. Values for Experiments Using 2.7 µm Filter Paper

Oil Viscosity, cp	CO₂ Pressure, psi	Oil Production, %	CO₂ Breakthrough Time, sec	Average Production Flow Rate, ml/min
469	25	89	3340	1.79
469	50	90	1900	3.02
469	100	91	961	5.42
260.7	25	91.5	2220	2.94
260.7	50	92	990	5.71
260.7	100	93	480	10.58
119	25	92	960	5.97
119	50	93.25	480	10.39
119	100	95	244	19.02
63.7	25	94	530	10.11
63.7	50	96	270	18.53
63.7	100	98	122	35.35

The wt% of asphaltene was measured for all the experiments conducted. For each experiment, an oil sample was taken from the produced oil, and the filter cake, and the asphaltene weight percent was calculated using the Asphaltene Detection Test, explained before. The asphaltene weight percent for the original crude oil before running the filtration experiments is shown in Table 3 for reference.

Table 3. Asphaltene Wt% for All The Oil Viscosities

Oil Viscosity, cp	Asphaltene Weight Percent, %
469	5.73
260.7	4.63
119	4.01
63.7	3.22

Table 4 shows the asphaltene weight percent for the filtered oil and the filter cake samples for different viscosity oils, different pressures, and different pore sizes. For the 469 cp oil, increasing the pressure resulted in an increase in the asphaltene wt% in the filtered oil due to the oil being forced through the pores. With the decrease in viscosity, the asphaltene wt% also decrease. This is due to the initial asphaltene wt% being less in the less viscosity oil, as shown in Table 3. When the pore size was decreased, the filtered oil had a lower asphaltene wt%, which indicates that the asphaltene was harder to extrude through the smaller pore, even at a higher CO_2 injection pressure. For all the experiments, as the asphaltene wt% decreases in the filtered oil, it increases in the filter cake, since the concentration of asphaltene becomes higher due to a lower percentage passing though the filter membrane. These results validate the results obtained for the filter cake thickness above, with the highest filter cake thickness showing the highest asphaltene filter cake wt%.

Table 4. Asphaltene Wt% for The Filtered Oil and The Filter Cake

Oil Viscosity, cp	Pressure, psi	Pore Size	Filtered Oil Asphaltene wt%	Filter Cake Asphaltene wt%
469	25	2.7 μm	4.2	16
469	50	2.7 μm	4.4	14
469	100	2.7 μm	4.6	12
260.7	50	2.7 μm	3.8	12
119	50	2.7 μm	3.6	10
63.7	50	2.7 μm	2	6
469	300	100 nm	2.2	18
469	300	10 nm	1.3	23

7. CONCLUSIONS

This research aimed to study the CO_2 flow mechanism in micro and nano pores of oil reservoirs. The research also showed how CO_2 can result in asphaltene instability and the main factors impacting this instability. The main conclusions obtained from this research are summarized below.

- The asphaltene detection test successfully identified the presence of a high weight percent of asphaltene in the crude oil and was calculated to be 5.73 wt%.

- For the 2.7 µm increasing the oil viscosity resulted in an increase in the oil production time, and an increase in asphaltene instability compared to the lighter crude oil.

- The CO_2 breakthrough time was decreased significantly when the oil viscosity was decreased due to the CO_2 being able to mobilize the lighter crude oil much easier than the heavy crude oil.

- The Knudsen number was calculated for all the experiments conducted and it was found that all four flow regimes were covered in this study including viscous, slippage, transition, and Knudsen flows.

- The 10 nm filter paper did not permit the flow of oil until the pressure was raised to 300 psi, which indicates that a high pressure is required in order to allow the CO_2 to move in the nano-pores of the shale. It was also observed that some of the CO_2 dissolved in the oil.

- The 100 nm filter paper experiment was conducted at 300 psi to compare it to the 10 nm experiment. The 100 nm filter paper permitted the flow of oil much faster than the 10 nm, however the duration was still longer than the 2.7 µm even though the pressure was six times higher.

- Based on the Knudsen number calculations, it was evident that the flow in the nano-pores is diffusion dominated, whereas the flow in the micro-pores is viscous, with some slippage effect.

ACKNOWLEGDEMENTS

REFERENCES

Beskok, A., and Karniadakis, G.E., 1999. A model for flows in channels, pipes, and ducts at micro and nano scales. Nanoscale Microscale Thermophys. Eng. 3, 43–77.

Eide, Ø., 2016. Visualization of Carbon Dioxide Enhanced Oil Recovery by Diffusion in Fractured Chalk. Society of Petroleum Engineers. doi:10.2118/170920-PA.

Fakher, S. and Imqam, A., 2018. Investigating and Mitigating Asphaltene Precipitation and Deposition in Low Permeability Oil Reservoirs During Carbon Dioxide Flooding to Increase Oil Recovery. Society of Petroleum Engineers. doi:10.2118/192558-MS.

Fakher, S. and Imqam, A., 2019. Asphaltene precipitation and deposition during CO2 injection in nano shale pore structure and its impact on oil recovery. https://doi.org/10.1016/j.fuel.2018.10.039.

Fakher, S. and Imqam, A., 2020a. Application of carbon dioxide injection in shale oil reservoirs for increasing oil recovery and carbon dioxide storage. Fuel. https://doi.org/10.1016/j.fuel.2019.116944.

Fakher, S. et al., 2018. Investigating the Viscosity Reduction of Ultra-Heavy Crude Oil Using Hydrocarbon Soluble Low Molecular Weight Compounds to Improve Oil Production and Transportation. Society of Petroleum Engineers. doi:10.2118/193677-MS.

Fakher, S. et al., 2019. A characterization of different alkali chemical agents for alkaline flooding enhanced oil recovery operations: an experimental investigation. SN Appl. Sci. 1, 1622 (2019). https://doi.org/10.1007/s42452-019-1662-2.

Fakher, S. et al., 2019. An experimental investigation of asphaltene stability in heavy crude oil during carbon dioxide injection. Journal of Petroleum Exploration and Production Technology. https://doi.org/10.1007/s13202-019-00782-7.

Fakher, S. et al., 2019b. Carbon Dioxide Injection Pressure and Reservoir Temperature Impact on Oil Recovery from Unconventional Shale Reservoirs During Cyclic CO2 Injection: An Experimental Study. Carbon Management Technology Conference. doi:10.7122/CMTC-558561-MS.

Fakher, S. et al., 2019c. Critical review of asphaltene properties and factors impacting its stability in crude oil. J Petrol Explor Prod Technol (2019) doi:10.1007/s13202-019-00811-5.

Fakher, S. et al., 2020. Hydrolyzed polyacrylamide – Fly ash reinforced polymer for chemical enhanced oil recovery: Part 1 – Injectivity experiments. https://doi.org/10.1016/j.fuel.2019.116310.

Fakher, S., 2019a. Investigating Factors that May Impact the Success of Carbon Dioxide Enhanced Oil Recovery in Shale Reservoirs. Society of Petroleum Engineers. doi:10.2118/199781-STU.

Fakher, S., 2019b. Asphaltene stability in crude oil during carbon dioxide injection and its impact on oil recovery: A review, data analysis, and experimental study. Masters Theses. 7881.

Fakher, S., and Imqam, A., 2020b. A review of carbon dioxide adsorption to unconventional shale rocks methodology, measurement, and calculation. SN Appl. Sci. 2, 5. doi:10.1007/s42452-019-1810-8.

Fakher, S., et al., 2019. The Effect of Unconventional Oil Reservoirs’ Nano Pore Size on the Stability of Asphaltene During Carbon Dioxide Injection. Carbon Management Technology Conference. doi:10.7122/CMTC-558486-MS.

Forchheimer, P., 1901. Wasserbewegug durch Boden, Zeits. V. Deutsch. Ing 45, 1782–1788.

Goual, L., 2012. Petroleum Asphaltenes, Crude Oil Emulsions- Composition Stability and Characterization, (Ed.), ISBN: 978-953-51-0220-5.

Jin, L. et al., 2017. Improving Oil Recovery by Use of Carbon Dioxide in the Bakken Unconventional System: A Laboratory Investigation. Society of Petroleum Engineers. doi:10.2118/178948-PA.

Kalantari-Dahagi, A. et al., 2006, Formation Damage due to Asphaltene Precipitation Resulting from CO2 Gas Injection in Iranian Carbonate Reservoirs. Society of Petroleum Engineers. doi:10.2118/99631-MS.

Karniadakis, G., 2005. Microflows and Nanoflows: Fundamentals and Simulation. Springer, New York.

Klinkenberg, L.J., 1941. The permeability of Porous Media to Liquid and Gases. paper presented at the API 11th mid year meeting, Tulsa. API Drilling and Production Practices, New York, pp 200–213.

Knudsen, M., 1909. Die Gesetze der Molukularstrommung und der inneren. Reibungsstrornung der Gase durch Rohren. Ann. der Phys. 28:75–130.

Knudt, A., and Warburg, E., 1875. Übwe Reibung and Wärmelei-tung verdünnter Gase. Poggendrfs Annalen der physic und Chemie. 155:337.

Li, J. et al., 2017. Methane Transport through Nanoporous Shale with Sub-Irreducible Water Saturation. Presented at the SPE Europec 79th EAGE Conference and Exhibition, Paris, France, 12-15 June.

Lobanov et al. "Swelling/extraction test of Russian reservoir heavy oil by liquid carbon dioxide", 2018, doi.org/10.1016/S1876-3804(18)30095-8.

Maxwell, J.C., 1867. On stresses in rarefied gases arising from inequalities of temperature. Phil. Trans. Roy. Soc. Lond. 170, 231–256.

Mohammed, R. et al., 2017, Simulation Study of Asphaltene Deposition and Solubility of CO2 in the Brine During Cyclic CO2 Injection Process in Unconventional Tight Reservoirs, International Journal of Geological and Environmental Engineering, 11 **(6)** 485- 500.

Moradi, S. et al., 2012. Investigation of asphaltene precipitation in miscible gas injection processes: experimental study and modeling. Braz. J. Chem. Eng., São Paulo, v. 29, n. 3, p. 665-676.

Negara, A. et al., 2016. Effects of Multiple Transport Mechanisms on Shale Gas Production Behavior. Presented at the SPE Kingdom of Saudi Arabia Annual Technical Symposium and Exhibition, Dammam, Saudi Arabia, 25-28 April.

Okamoto, N. et al., 2015. Slip Velocity and Permeability of Gas Flow in Nanopores for Shale Gas Development. Presented at the SPE Asia Pacific Unconventional Resources Conference and Exhibition, Brisbane, Australia, 9-11 Nov.

Okamoto, N. et al., 2018. Slip Velocity of Methane Flow in Nanopores with Kerogen and Quartz Surfaces. SPE Journal.

Rassamdana, H.B. et al., 1996. Asphaltene flocculation and deposition: I. The onset of precipitation. AIChE J. 42 (1), 10–22.

Roque-Malherbe, R.M.A., 2007. Adsorption and Diffusion in Nanoporous Materials. CRC Press, Taylor & Francis Group, Boca Raton.

Roy, S., et al., 2003. Modeling gas flow through microchannels and nanopores. J. Appl. Phys. 93, 4870–4879.

Sandler, S., 1972. Temperature dependence of the Knudsen permeability. Ind. Eng. Chem. Fundam. 11, 424–427.

Shabro, V. et al., 2012. Forecasting Gas Production in Organic Shale with the Combined Numerical Simulation of Gas Diffusion in Kerogen, Langmuir Desorption form Kerogen Surfaces, and Advection in Nanopores. Presented at the 2012 SPE Annual Technical Conference and Exhibition, San Antonio, Texas, USA, 8-10 Oct.

Shahriar M, The aggregation of asphaltene molecules as a function of carbon dioxide concentration (PhD Dissertation). Texas Tech University, 2014.

Shedid and Zekri, 2006, Formation Damage Caused by Simultaneous Sulfur and Asphaltene Deposition. Society of Petroleum Engineers. doi:10.2118/86553-PA.

Shen and Sheng, 2018, Experimental and numerical study of permeability reduction caused by asphaltene precipitation and deposition during CO2 huff and puff injection in Eagle Ford shale, Fuel, 211, 432-445, https://doi.org/10.1016/j.fuel.2017.09.047.

Soroush, S. et al., 2014. A Comparison of Asphaltene Deposition in Miscible and Immiscible Carbon Dioxide Flooding in Porous Media. Society of Petroleum Engineers. doi:10.2118/169657-MS.

Struchkov et al. "Laboratory investigation of asphaltene-induced formation damage", 2019, doi.org/10.1007/s13202-018-0539-z.

Tavakkoli, M. et al., 2011. Prediction of Asphaltene Precipitation During Solvent/CO2 Injection Conditions: A Comparative Study on Thermodynamic Micellization Model With a Different Characterization Approach and Solid Model. Society of Petroleum Engineers, Journal of Canadian Petroleum Technology. 65-74, doi:10.2118/145638-PA.

Wu, K. et al., 2016. A Unified Model for Gas Transfer in Nanopores of Shale-Gas Reservoirs: Coupling Pore Diffusion and Surface Diffusion. SPE Journal.

Xu, J. et al., 2017. Nanoscale Free Gas Transport in Shale Rocks: A Hard-Sphere Based Model. Presented at the SPE Unconventional Resources Conference, Alberta, Canada, 15-16, Feb.

Yonebayashi, H. et al., 2011. Dynamic Asphaltene Behavior for Gas-Injection Risk Analysis. Society of Petroleum Engineers Reservoir Evaluation and Engineering Journal. 513- 524, doi:10.2118/146102-PA.

Yonebayashi, H. et al., 2018. Determination of Asphaltene-Onset Pressure Using Multiple Techniques in Parallel. Society of Petroleum Engineers Production and Operations Journal. 1-12, doi:10.2118/181278-PA.

Zendehboudi, S. et al., 2014. Asphaltene precipitation and deposition in oil reservoirs – Technical aspects, experimental and hybrid neural network predictive tools, Chemical Engineering Research and Design, 92 **(5)**, 857-875.

Ziarani A. S. and Aguilera, R. 2012. Knudsen's Permeability Correction for Tight Porous Media. *Transp. Porous Med.* **91** (1): 239260. https://doi.org/10.1007/s11242-001-9842-6.

IV. AN EXPERIMENTAL INVESTIGATION OF ASPHALTENE STABILITY IN CRUDE OIL DURING CARBON DIOXIDE INJECTION

ABSTRACT

Carbon Dioxide (CO_2) injection is one of the most applied enhanced oil recovery (EOR) methods in the hydrocarbon industry, since it has the potential to increase oil recovery significantly and can help reduce greenhouse gases through carbon storage in hydrocarbon reservoirs. Carbon dioxide injection has a severe drawback, however, since it induces asphaltene precipitation by disrupting the asphaltene stability in crude oil that bears even the slightest asphaltene concentration. This can result in severe operational problems, such as reservoir pore plugging and wellbore plugging. This research investigates some of the main factors that impact asphaltene stability in crude oil during CO_2 injection. Initially, asphaltene precipitation, flocculation, and deposition were tested using visual tests without CO_2 in order to evaluate the effect of oil viscosity and temperature on asphaltene stability and content in the crude oil. The results obtained from the visualization experiments were correlated to the Yen-Mullins Asphaltene Model and were used to select the proper chemical to alter the oil's viscosity without strongly affecting asphaltene stability. After performing the visual asphaltene tests, a specially designed filtration vessel was used to perform the oil filtration experiments using filter membranes with a micron and nanometer pore size. The effect of varying CO_2 injection pressure, oil viscosity, filter membrane pore size, and filter membrane thickness on asphaltene stability in crude oil was investigated. The results were then correlated with the Yen-Mullins Asphaltene Model to characterize the asphaltene size within the oil as well. Results showed that as the oil viscosity increased,

the asphaltene concentration in the oil also increased. Also, the asphaltene concentration and filter cake thickness increased with the decrease in filter membrane pore size, since the asphaltene particles either plugged up the smaller pores, or the asphaltene nanoaggregates were larger than the pore sizes, and thus the majority of them could not pass. This research studies asphaltene instability in crude oil during CO_2 injection in different pore sizes and correlates the results to the principle of the Yen-Mullins model for asphaltenes. The results from this research can help emphasize the factors that will impact asphaltene stability during CO_2 injection in different pore sizes in order to help reduce asphaltene-related problems that arise during CO_2 injection in hydrocarbon reservoirs.

1. INTRODUCTION

CO_2 has had significant success in increasing oil recovery from conventional oil reservoirs (Fakher, S. et al., 2017; 2018b; 2019). It has been noted that high molecular weight components in the reservoir oil, such as asphaltene and resins, are not mobilized by the CO_2 during flooding, and hence the components precipitate from the oil phase and deposit into the pore spaces, which in turn results in pore plugging and a lower-than-expected oil recovery (Wang, S. et al., 2016; Al-Ghazi, S. and Lawson, J., 2007; Forte, E. and Taylor, S.E., 2014; Goual, L. and Abudu, A., 2009; Jose, L. et al., 2009; Escobedo, J. and Mansoori, G.A., 1997). The main reason behind the inability of the CO_2 to mobilize the asphaltene is linked to its stability conditions in the crude oil at the reservoir pressure and temperature (Kalantari-Dahagi, A. et al., 2006; Goual, L., 2012; Kord, S. et al., 2012; Lichaa, P.M. and Herrera, L., 1975; Miadonye, A. and Evans, L., 2010). Asphaltenes are

present in the crude oil as micelles, which are stabilized by resins, and maltenes, which surround the asphaltene molecules, while their aliphatic tails are comingled in the oil phase (Thomas, D. et al., 1995; Groenzin, H. and Mullins, O.C., 2000; Hernandez, M.E., 1983; Leontaritis, K. and Mansoori, G.A., 1987; Punase, A. et al., 2016; Mannistu, K. D. et al., 1997). A change in the reservoir conditions that alters or disrupts the equilibrium conditions such as a change in temperature, pressure, or introduction of a foreign agent such as CO_2 in the reservoir causes the precipitation and eventually the deposition of asphaltene in the pores (Zendehboudi, S. et al., 2014; Kalantari-Dahagi, A. et al., 2006; Kariznovi, M. et al., 2012; Mansoori, G.A., 1996; Uetani, T., 2014; Rogel, E. et al., 1999; Rassamdana, H.B. et al., 1996). Asphaltene instability can also result due to reservoir rock properties such as lithology and pore size (Kordestany, A., 2019; Shedid and Zekri, 2006; Mishra, V.K. et al., 2012; Hannisdal, A. et al., 2006; Jha, N.K. et al., 2014)

Much research has been conducted to study the precipitation and deposition of high molecular weight components, mainly asphaltene, in the pore spaces of conventional oil reservoirs. Zendehboudi, S. et al. (2014) showed the difference between phase precipitation and phase deposition by defining precipitation as the formation of the solid phase from the liquid phase, and deposition as the adherence or adsorption of the solid phase to the reservoir rock, which usually occurs after precipitation. Asphaltene can also form flocculations on the rock surface. The flocculations can break up during the process of dissociation and plug the pore throats in the reservoir (Kim, S.T. et al., 1990; Monger, T.G. and Fu, J.C., 1987; Rassamdana, H.B. et al., 1996). Soroush S. et al. (2014) showed that below CO_2 minimum miscibility pressure (MMP), the pore plugging damage will be much lower compared to above the MMP. This is due to the resins that stabilize the asphaltene

being much more unstable above CO_2 MMP. Kalantari-Dahagi, A. et al. (2006) reported that the amount of asphaltene deposition in carbonate cores reached the maximum at the oil bubble point. Asphaltene has also been shown to be much more severe as the oil viscosity increases due to the higher concentration of high molecular weight components (Fakher, S. and Imqam, A. 2018; 2019; Fakher, S. et al., 2018a; Fakher, S.M., 2019). Many methods have therefore been proposed to detect asphaltene deposition in conventional oil reservoirs, such as the De Boer Plot (De Boer, R.B. et al., 1995), Asphaltene Resin Ratio Approach (Jamaluddin, A.K.M. et al., 2000), Colloidal Instability Index (Yen, A. et al., 2001), Filtration, Acoustic Resonance Technique, Light Scattering Technique (Akbarzadeh, K. et al. 2007; Jamaluddin, A.K.M. et al., 2000; Speight, J.G., 1999; Speight, J.G. et al., 1985), Optical Spectroscopy (Kharrat, A. et al., 2013), Nuclear Magnetic Resonance (Wang, S. et al. 2016), SARA Analysis (Fan, T. et al., 2002; Goel, P. et al., 2017; D-4124-97, 2019), and Chromatography (Jewell, D. et al., 1972; Islas-Flores, C. A. et al., 2005; Keshmirizadeh, E.S. et al., 2013).

Recently, CO_2 flooding has been conducted to increase oil recovery from unconventional shale reservoirs. However, very little research work has been conducted to study and evaluate how the asphaltene in the crude oil will behave in micro and nano pores during CO_2 injection. Moradi et al. (2012) ran experiments using a 0.2 µm pore size filter membrane using nitrogen and methane and concluded that asphaltene deposition was much more severe in methane than in to nitrogen. They did not use CO_2 in their study. Mohammed et al. (2017) performed a simulation study to model asphaltene deposition in the low permeability reservoirs during CO_2 flooding and sought to optimize CO_2 injection by suggesting cyclic CO_2 flooding with brine. Shen and Sheng (2018) studied asphaltene

deposition in Eagle Ford shale reservoir using cyclic gas injection. They used filter membranes of 30 nm, 100 nm, and 200 nm to study asphaltene precipitation and deposition. The experiments they conducted with the filter membranes were conducted at 50 psi and room temperature. They did not, however, report the mechanism by which the asphaltene precipitates, deposits, and plugs the nano-pores of the shale. Sun, H., et al. (2019) investigated CO_2 and nitrogen competitive adsorption to asphaltene in nanopores in an attempt to investigate the feasibility of using asphaltene as a means of carbon capture in nanopores during CO_2 injection.

Based on the aforementioned literature review, very little research has been conducted to evaluate asphaltene instability in the crude oil during CO_2 injection in unconventional reservoirs with nanopores. This research performs several asphaltene visualization experiments, to investigate the impact of temperature and oil viscosity on asphaltene precipitation and deposition with time, and then undergoes oil filtration experiments during CO_2 injection using nano-filter membranes to evaluate asphaltene instability when the oil is mobilized through the nanopores. This research can help shed light not only on the factors that impact asphaltene instability in the crude oil during CO_2 injection, but also quantify the impact of each factor through asphaltene concentration measurements. This in turn can help predict asphaltene damage and reduce its overall impact in the oil industry. It can also help determine the main factors that may impact asphaltene and thus undergo better planning to reduce asphaltene damage if asphaltene is determined to be present in the crude oil for the field operation and production or even for ordinary Coreflooding experiments in the lab.

2. YEN – MULLINS ASPHALTENE MODEL

The Yen-Mullins model is currently the most widely accepted asphaltene model, shown in Figure 1 (Mullins, O.C., 2011). This model describes the Yen-Mullins asphaltene structure based on size and behavior as a function of the crude oil that bears the asphaltene. In light oils with high API gravity, the asphaltenes will be present as small poly-aromatic hydrocarbon molecules with an average diameter of 1.5 nanometers. In this case, the asphaltene concentration will be relatively low, and thus the asphaltene size will not grow. In black oils with slightly less API gravity, the asphaltene concentration will be higher and thus the asphaltene will be present in the form of nanoaggregates with an average diameter of 2 nanometers, which is slightly larger than the asphaltene present in the light oil. In heavy oils with extremely low API gravity, the asphaltene concentration will be relatively high, and will thus begin to form clusters. These clusters will grow in size and will reach an average diameter of 5 nanometers. The clusters form from the combination of several nanoaggregates together. Based on this model, as the asphaltene concentration in the oil increases, the oil will become heavier due to the high molecular weight of asphaltenes and thus its API will decrease, which shows that asphaltenes have an overall negative impact. The Yen-Mullins asphaltene model will be used to describe the results for the asphaltene visualization tests in order to illustrate the impact of oil viscosity on the asphaltene concentration in the crude oil.
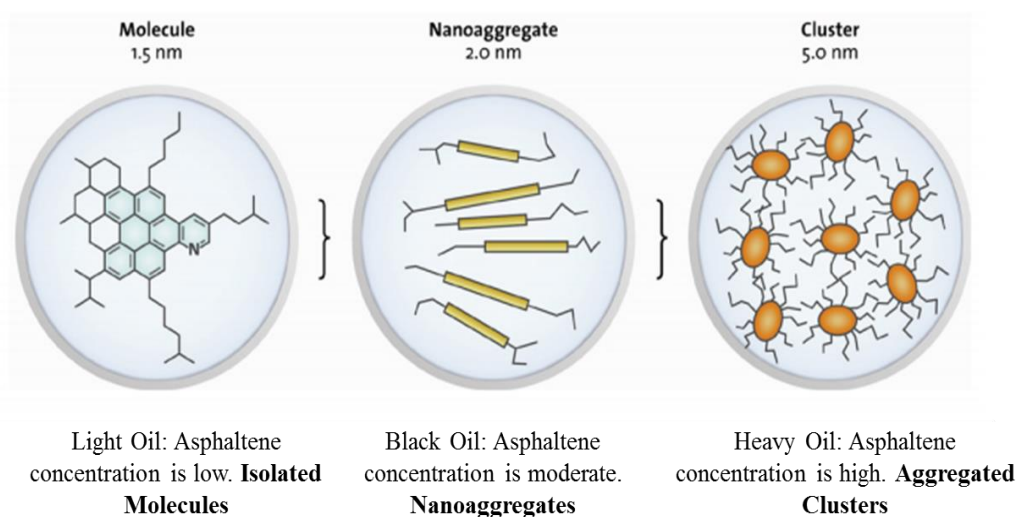
Figure 1. Yen-Mullins Asphaltene Model (Mullins, O.C., 2011)

3. EXPERIMENTAL MATERIAL

3.1. CRUDE OIL

Crude oil with viscosities 469, 260.7, 119, and 63.7 cp were used to run the experiments that were conducted. The exact composition is shown in Table 1.

Table 1. Crude Oil Composition and Asphaltene Concentration

Component	Weight Percentage, %
C_1-C_5	9.37
C_6-C_{10}	14.74
C_{10}-C_{15}	18.89
C_{16}-C_{20}	19.31
C_{20}-C_{30}	11.63
C_{30+}	26.06
Total	100
Asphaltene (Component of C_{30+})	5.73
Asphaltene Precipitant	Heptane (10 ml per 0.1 ml Oil)

3.2. CARBON DIOXIDE

A high pressure CO_2 cylinder with purity 99.99% was connected to the filtration setup directly and used for CO_2 injection.

3.3. FILTER MEMBRANE

Filter membranes with pore sizes of 2.7 µm, 100 nm, 10 nm, and 0.2 nm were used in this study to cover a broad range of pore sizes.

3.4. SPECIALLY DESIGNED LPLT FILTRATION VESSEL

A filtration vessel was used to be able to accommodate the nano-filter membranes, the crude oil, and the CO_2 with no leakages.

3.5. RHEOMETER

A rheometer was used to measure the viscosity of the different crude oils that were used to conduct the experiments.

4. EXPERIMENTAL SETUP

Figure 2 illustrates the setup used to conduct the experiments. It is comprised of a high purity CO_2 cylinder for CO_2 injection, a pressure regulator attached to the cylinder to control the pressure provided by the cylinder, a filtration vessel, that contains the crude oil, a rubber O-ring to prevent leakages, the filter membrane, and a 60 micron mesh screen used to support the filter membrane and prevent it from being punctured during the experiment due to high pressure without constricting the flow of oil. The support structure

was used to fix the filtration vessel at a sufficient height in order to leave space for the test tube used to collect the oil produced from the effluent. The fixation screw helped tightly fix the top cover of the filtration vessel tightly to prevent leakages. The oil that was produced during the experiment will be referred to as the filtrate, while the oil that was not produced will be referred to as the filtride.
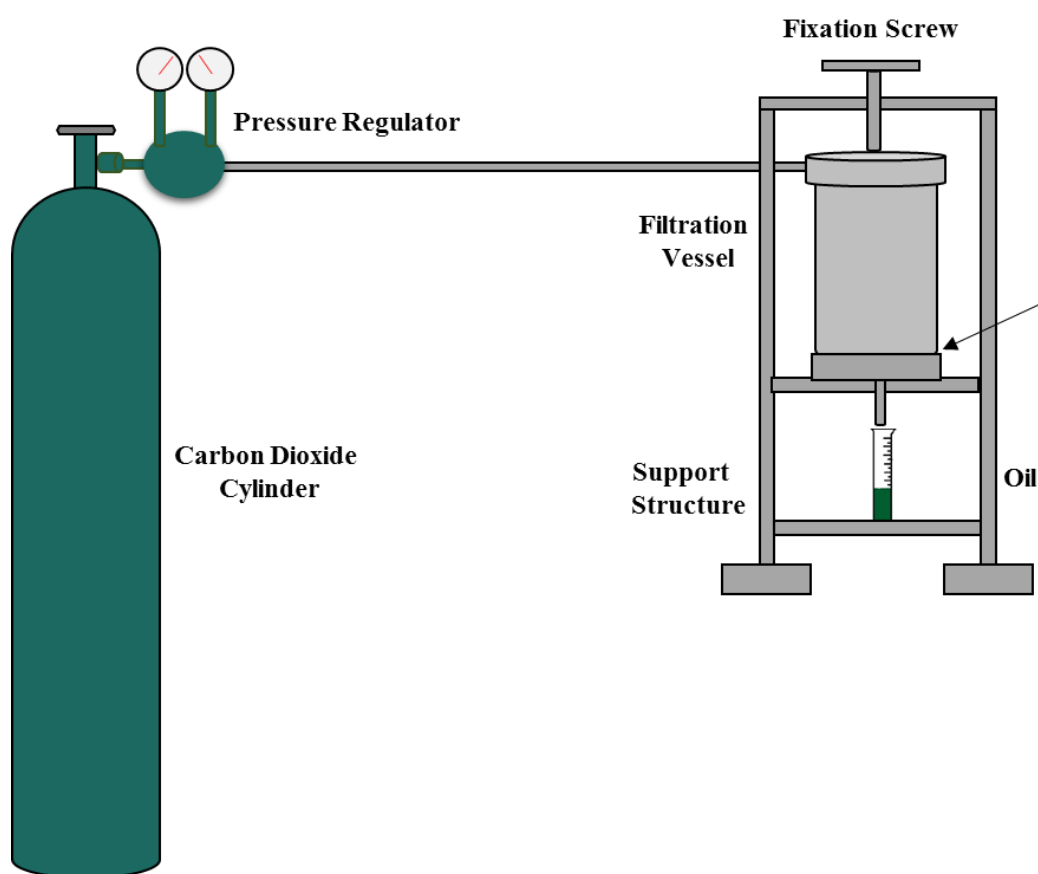
Figure 2. Specially Modified Filtration Setup

5. EXPERIMENTAL PROCEDURE

Two sets of experiments were conducted in this research. These include the asphaltene visualization experiments, and the asphaltene filtration experiments. The experimental procedure for each experiment is explained in this section.

5.1. ASPHALTENE VISUALIZATION EXPERIMENTS

The asphaltene visualization experiments were conducted using the following procedure:

1. 0.1 ml of crude oil was added to the test tube. The volume was measured using a high accuracy needle and a balance to ensure that all samples were the same.

2. 10 ml of heptane was then added to the crude oil in the test tube. The test tube was then shaken vigorously to dissolve the oil in the heptane. The heptane is highly solube in the crude oil and thus was dissolved very quickly. The test tube cap was sealed tightly to avoid evaporation of any fluids during the interaction of the heptane with the crude oil. This was to assure repeatability and accuracy.

3. The tube was sealed using an o-ring and a threaded cap to ensure that no heptane would evaporate and leave the test tube, especially at high temperatures.

4. The test tube was placed in an isothermal water bath and was removed when the pictures were taken and then placed immediately in the water bath again.

5.2. ASPHALTENE FILTRATION EXPERIMENTS

The following procedure was followed to conduct the asphaltene filtration experiments:

1. The filtration vessel was prepared by placing a mesh screen, filter membrane, and rubber o-ring on the bottom cap in the order mentioned. The bottom cap assembly was then attached to the filtration vessel.

2. 100 ml of crude oil was then poured in the filtration vessel. The top cap was then placed and sealed using a fixation screw.

3. CO_2 was injected into the vessel and oil production was recorded with time. The experiment is stopped when no oil production is observed for at least five consecutive minutes.

4. The produced and remaining oil are then collected for asphaltene analysis. The filter membrane is also collected and stored in a vacuum seal for analysis.

6. RESULTS AND DISCUSSION

The results for all the experiments will be discussed in this section. Initially, the asphaltene visualization tests will be discussed, including the oil viscosity and the temperature effects on asphaltene instability in the crude oil. Following this, the filtration experiments results will be discussed, and the asphaltene concentration from different experiments will be provided.

6.1. ASPHALTENE VISUALIZATION EXPERIMENTS

Before conducting the actual filtration experiments, asphaltene visualization tests were conducted to visually investigate the impact of crude oil viscosity and temperature on asphaltene stability in the crude oil. Asphaltene visualization tests can prove to be a very significant tool since the test can show how the asphaltene behaves in terms of precipitation and deposition at different conditions. For each experiment, 0.1 ml of crude oil and 10 ml of heptane were mixed. These amounts were used to ensure that the solution was clear enough to accurately visualize the asphaltene precipitation, flocculation, and deposition. It is important to note that in all the images, there is a dark line at the top of the test tube. This line was created when the images were taken due to the reflections and does not represent anything significant.

Based on the Yen-Mullins model, which was explained previously, as the oil becomes lighter, the percentage of asphaltene in the oil it will decrease. This was visually observed when conducting the asphaltene precipitation and deposition experiments to investigate the impact of oil viscosity on asphaltene stability in the crude oil. The results for crude oil with 178 cp viscosity are shown in Figure 3. Initially, the asphaltene cannot be seen in the sample due to its partial stability in the crude oil. After one hour, however, the asphaltene can be seen in the image as it begins to precipitate from the solution. The asphaltene is still suspended in the sample, however, and has not yet deposited. As time progresses, two significant observations can be made. More asphaltene can be observed in the bottom of the test tube, which signifies asphaltene deposition. The asphaltene begins to form dense flocculations that then deposit to the bottom of the tube. The second important observation is that as the asphaltene deposits, the sample becomes lighter in color in all the

sections, while the bottommost section becomes extremely dark in color due to the high concentration of asphaltene in this section. This shows that asphaltene precipitation and flocculation will not occur immediately, but rather occur with time. This is extremely important for field application since it shows that asphaltene precipitation is a stage-wise process. If precipitation is detected early, it can be mitigated before flocculation takes place.

| 0 hrs. | 1 hrs. | 2 hrs. | 5 hrs. | 24 hrs. |
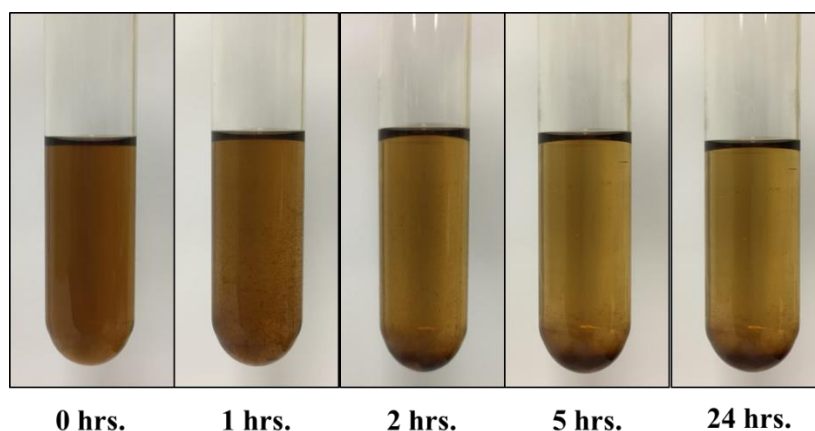
Figure 3. Asphaltene Precipitation and Deposition Using 178 cp Oil

A lighter crude oil with a viscosity of 75 cp was also investigated, shown in Figure 4. The same observations that were made in the heavier crude oil, shown in Fig. 3, were observed. However, the main difference was in the overall color of the sample and the asphaltene concentration present. The lower viscosity crude oil has a lighter color at all times and was also found to have a lower asphaltene concentration compared to the higher viscosity crude oil, which agrees with the Yen-Mullins asphaltene model, which was explained previously. This indicates that even low viscosity crude oils may suffer from asphaltene instability problems. The lower viscosity crude oil had a lower asphaltene

concentration; however, flocculation and deposition still occurred. It is therefore important to undergo asphaltene stability analysis in any crude oil in order to anticipate and avoid asphaltene-related problems.
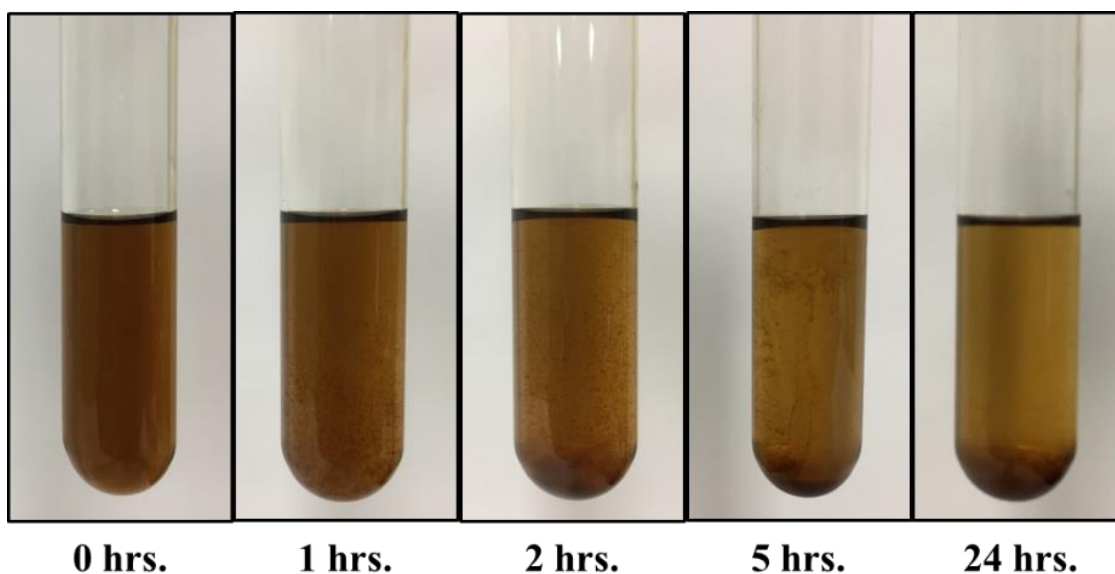
Figure 4. Asphaltene Precipitation and Deposition Using 75 cp Oil

Temperature can have a strong impact on the stability of the asphaltene in the crude oil. As the temperature increases the oil becomes lighter, thus leading to a higher asphaltene deposition. A comparison of the same sample of crude oil was performed at different temperatures to investigate the impact of temperature on asphaltene stability in the crude oil. Figure 5 shows the results for the oil sample at 40 ºC for 24 hours. Initially, no asphaltene can be observed, and the sample color appears to be the same all over. However, as the time progresses, the asphaltene begins to become visual, and the color of the sample begins to become lighter at the top of the test tube and darker at the bottom due to the asphaltene flocculation and deposition. Finally, after 24 hours, almost all of the asphaltene

has deposited and the sample becomes much lighter in color compared to the initial sample at time zero. Temperature had two main effects on the crude oil. Temperature will decrease the viscosity of the crude oil and thus will reduce its tendency to bear asphaltene. Increasing the temperature will result in a rapid severance of the bond between the resin and asphaltene, which will promote asphaltene precipitation. As the temperature increases, the rate at which this bond is severed will be higher, and thus the asphaltene will begin to precipitate faster. However, the asphaltene concentration will be lower since the oil viscosity is decreased.

0 hrs   1 hr   2 hrs   5 hrs   24 hrs
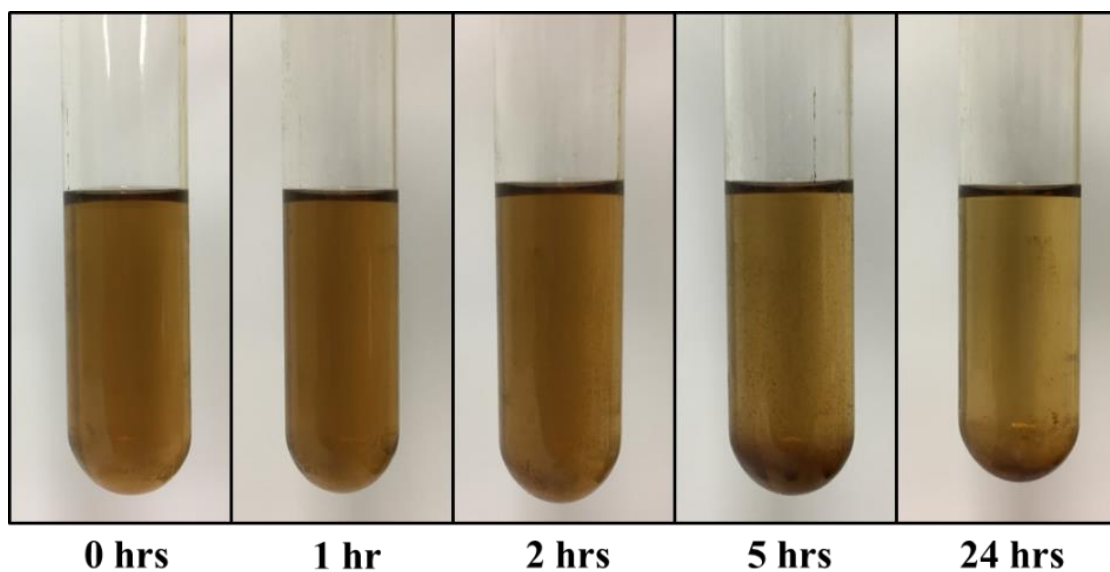
Figure 5. Asphaltene Precipitation and Deposition at 40 ⁰C

At 60 ⁰C, shown in Fig. 6, the oil viscosity becomes lower, which in turn results in a lower asphaltene concentration and an overall lighter color for the sample compared to the same sample at 40 ⁰C. This shows that at the higher temperature the asphaltene concentration was impacted, which is evident from the asphaltene shown in Figure 6 along

with the final color of the sample. An important observation to be made is that the color of the samples becomes clearer earlier than the samples used in the 40 ⁰C experiment. This is due to the rapidity with which the bond between the asphaltene and resin breaks, and the decrease in asphaltene concentration at the higher temperature.
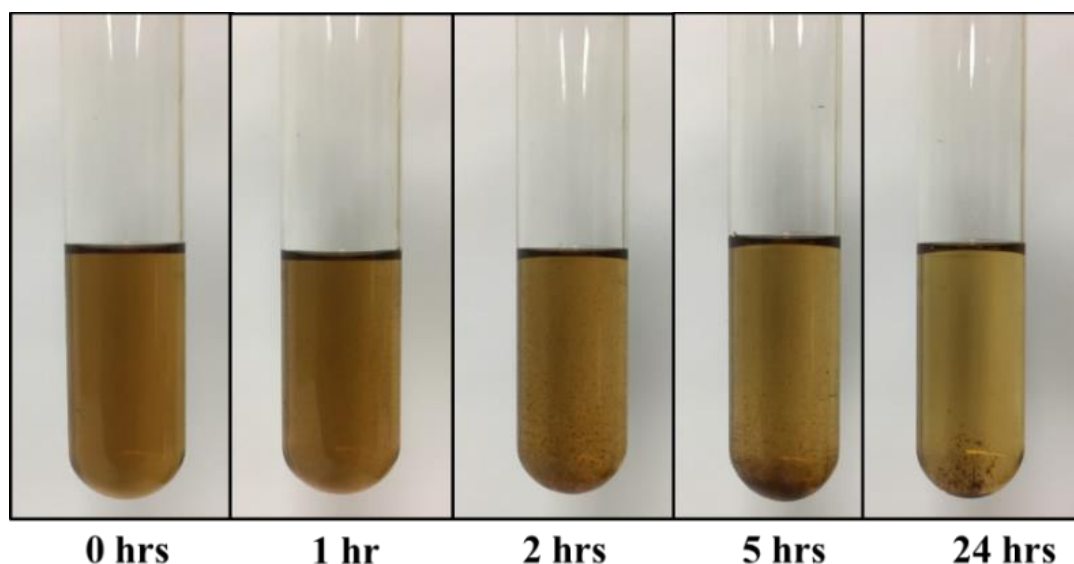
Figure 6. Asphaltene Precipitation and Deposition at 60 ⁰C

When the sample was tested at 80 ⁰C, as is shown in Figure 7, the color became even lighter, which is highly evident after 24 hours, and the asphaltene concentration also changed compared to the 60 and 40 ⁰C samples shown in the previous figures. As was observed in the 60 ⁰C experiment, the sample becomes lighter in color earlier, due to a faster asphaltene precipitation and a lower asphaltene concentration. The decrease in lightnesss is depednant on the original crude oil color, the heptane concentration, and the asphaltene concentration in the original crude oil sample used to conduct the asphaltene behavior and stability experiments.
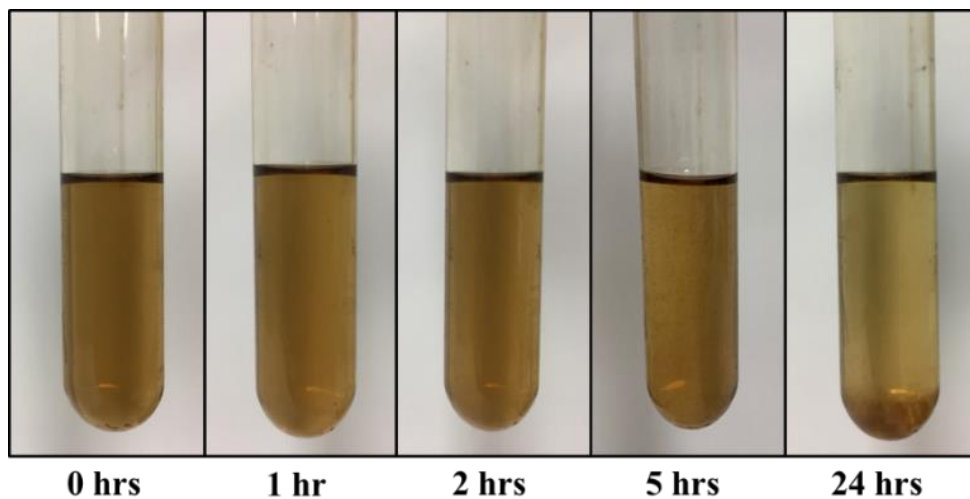
Figure 7. Asphaltene Precipitation and Deposition at 80 ⁰C

In order to provide a clear comparison between the samples at different temperatures. Figure 8 shows the different samples at different temperatures. The images were all taken after two hours. As the temperature increased, the color of the sample became lighter due to the change in asphaltene concentration, as was explained previously.
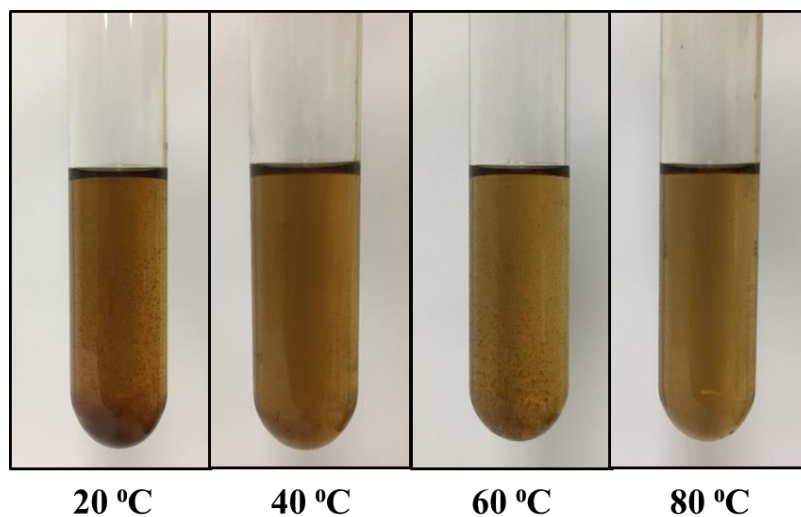
Figure 8. Asphaltene Precipitation and Deposition at Different Temperatures

6.2. ASPHALTENE FILTRATION EXPERIMENTS

Experiments were conducted to study the effect of varying the oil viscosity, CO_2 injection pressure, filter membrane thickness, and filter membrane pore size on asphaltene concentration, filter cake thickness, and filter membrane areal filtrate displacement. Table 2 shows the all the experiments conducted in this research and their significant parameters.

Table 2. Description of All Experiments Conducted in The Research

Experiment	Oil Viscosity, cp	CO₂ Injection Pressure, psi	Filter Pore Size	Filter Thickness, mm
1	469	25	2.7 µm	0.11
2	260.7	25	2.7 µm	0.11
3	119	25	2.7 µm	0.11
4	63.7	25	2.7 µm	0.11
5	469	50	2.7 µm	0.11
6	260.7	50	2.7 µm	0.11
7	119	50	2.7 µm	0.11
8	63.7	50	2.7 µm	0.11
9	469	100	2.7 µm	0.11
10	260.7	100	2.7 µm	0.11
11	119	100	2.7 µm	0.11
12	63.7	100	2.7 µm	0.11
13	119	50	2.7 µm	0.55
14	119	50	2.7 µm	1.1
15	119	50	10 nm	0.11
16	119	50	100 nm	0.11
17	119	600	0.2 nm	0.11

Before running the filtration experiments, the asphaltene concentration in the crude oil samples with different viscosity values was determined. This is an extremely important step since it will help in the comparison between the asphaltene concentration in the filtrate and the filtride following the filtration experiments with the crude oil that was not used to conduct any experiments. The asphaltene concentration in the crude oil before running the experiments therefore serves as a reference to signify the change that occurred after conducting the filtration experiments. The asphaltene weight percentage for the different viscosity oils before running the filtration experiments is shown in Figure 9. As the oil viscosity decreased, the asphaltene weight percentage also decreased, which is supplementary to the Yen-Mullins model. The highest asphaltene weight percentage that was recorded was 5.73% for the 460 cp oil, whereas the lowest asphaltene weight percent was 3.22% for the 63.7 cp.
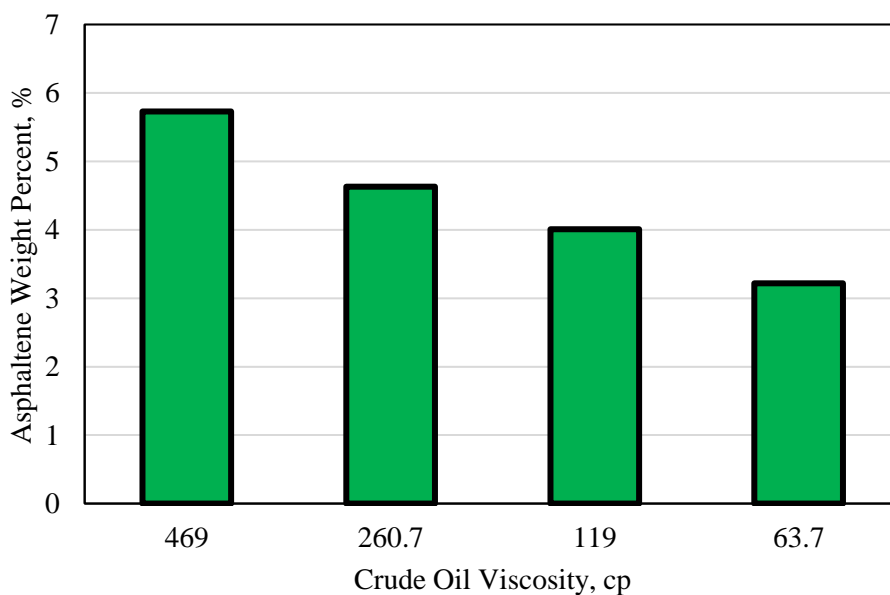
Figure 9. Asphaltene Weight Percent in Normal Crude Oil

The asphaltene weight percentage using different CO_2 injection pressures for both the filtrate, which is the produced oil, and the filtride, which is the unproduced oil, is shown in Figure 10. All experiments were conducted using the 469 cp oil and the 2.7 μm pore size filter membrane. As the CO_2 injection pressure increased, the asphaltene weight percentage in the filtrate increased, and the asphaltene weight percentage in the filtride decreased. This is mainly due to the oil being forced through the filter membrane at the higher pressures. Since a higher percentage of the oil is mobilized through the membrane at the higher pressure, the asphaltene that manages to pass through the membrane becomes higher as well, which in turn results in a larger asphaltene weight percentage in the filtrate at higher pressures compared to the lower ones. Since the asphaltene weight percentage increased in the filtrate at higher pressures, it is expected that the asphaltene weight percent in the filtride will be less in the higher pressures experiments than in the lower pressures.
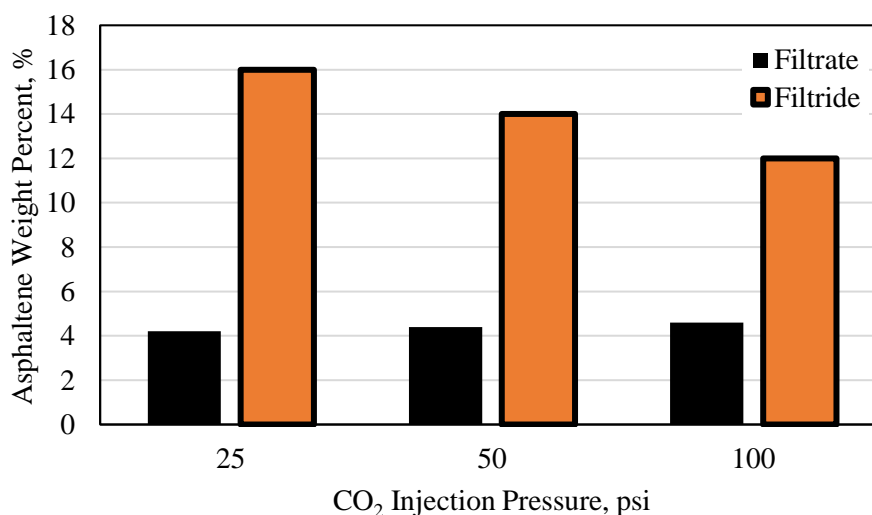
Figure 10. Asphaltene Weight Percent at Different CO_2 Injection Pressures

The effect of changing oil viscosity on the asphaltene weight percentage in both the filtrate and the filtride is shown in Figure 11. All experiments were conducted at 100 psi CO_2 injection pressure using the 2.7 μm pore size filter membrane. Decreasing the oil viscosity resulted in a decrease in the asphaltene weight percentage in both the filtrate and the filtride. This is mainly due to the decrease in the overall asphaltene weight percentage in the crude oil as the viscosity decreases, which was shown in the crude oil that was analyzed before running the filtration experiments in Figure 9. The asphaltene concentration in the filtride was higher for all experiments than the asphaltene weight percentage in the filtrate. This is mainly due to the percentage of asphaltene that managed to be mobilized through the filter membrane. This is a strong indication that asphaltene instability may occur in many types of crude oils, regardless of the viscosity of the crude oil.
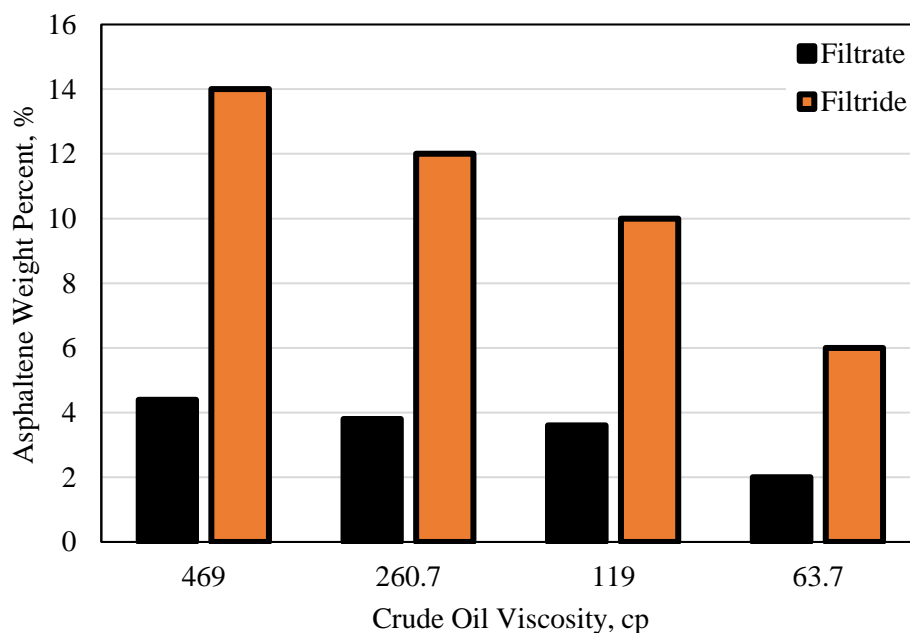
Figure 11. Asphaltene Weight Percentage Using Different Crude Oil Viscosity Values

The effect of varying the asphaltene weight percent was investigated using 2700, 100, 10, and 0.2 nanometers filter membrane pore sizes. The asphaltene weight percentage for the filtrate and the filtride for all the pore sizes is shown in Figure 12. All the experiments were conducted using 100 psi CO_2 injection pressure initially and 469 cp crude oil. For the 100 and 10 nm filter membranes, the oil could not extrude through the filter membranes at that pressure, and thus the pressure was increased in 50 psi increments until it reached 300 psi where the oil began to produce. The results for the 0.2 nm filter membrane will be explained later on. According to the Yen-Mullins asphaltene model, as the oil becomes heavier, the asphaltene in the oil becomes larger in diameter, reaching more than 5 nm in size per cluster. This will impact the ability of the asphaltene to extrude through the filter membrane. This can be observed clearly in the results obtained for the different pore sizes. As the filter membrane pore size decreased, the asphaltene weight percentage in the filtrate decreased as well, while the asphaltene weight percentage in the filtride increased. This is mainly due to the smaller pore sizes restricting the flow of the asphaltene due to the asphaltene diameter being very close to the pore size of the filter membrane, or perhaps even larger than it is. Some of the asphaltene particles that have not formed dense clusters tend to pass through the filter membranes, while the majority of the asphaltene concentration remains. Due to the increase in the asphaltene present in the filtride compared to the crude oil itself, the asphaltene concentration will become extremely high in the filtride, reaching values much higher than the original asphaltene concentration in the crude oil, which was 5.73% for 469 cp oil. Based on the results, asphaltene instability will be much more severe in the smaller nanopores compared to the larger pores.
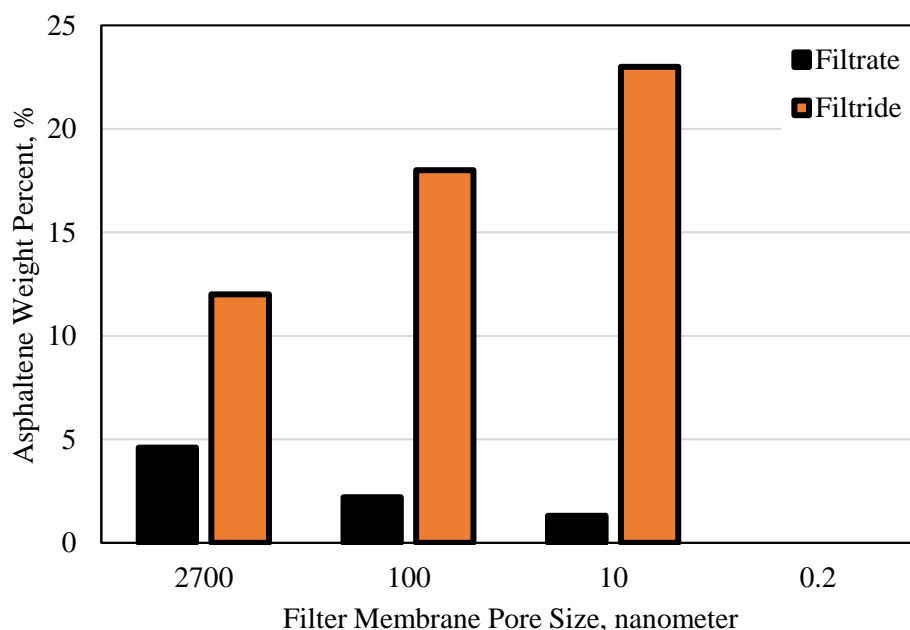
Figure 12. Asphaltene Weight Percent Using Different Filter Membrane Pore Sizes

When the pore size is too small, the oil will propagate through the pores at a lower rate and with more difficulty. This will result in asphaltene instability and will promote asphaltene precipitation and flocculation. The main factors impacting asphaltene instability in the smaller pores are the inability of the oil to propagate through the pores easily and the longer interaction of the CO_2 with the crude oil when the pores are too small. As the asphaltene flocculates, it begins to form large clusters. When the clusters deposit, the size of the pores will influence the ability of the asphaltene to pass through it. If the pore size is too small, only a low percentage of asphaltene will be able to extrude through it, while the remaining percentage will begin to deposit in the pores and create asphaltene buildups. The larger the pore size, the lower the severity of asphaltene buildups due to the ability of the asphaltene cluster to pass through the larger pores.

When undergoing the experiment using the 0.2 nm filter membrane shown in Fig. 12, 100 psi was used initially to displace the crude oil. No oil was produced from the membrane, however, due to the extremely small pore size. The pressure was maintained at 100 psi for two hours with no oil recovery. The pressure was then increased using 50 psi increments up to 600 psi. For each pressure increment, the CO_2 injection was undergone for thirty minutes. The 600 psi pressure was maintained for four hours; however, a pressure reduction was observed after 30 minutes of injection at 600 psi until the pressure reached 500 psi after four hours. The filtration apparatus was tested for leakages using a high accuracy pressure gauge, and no leakages were observed. The test was concluded after no oil production was obtained. When the filtration vessel was opened to obtain the crude oil, it was observed that the oil volume had increased significantly, and bubbles could be seen forming in the oil. Figure 13 shows the bubble formed in the oil when it was retrieved from the filtration vessel after concluding the test.

Figure 13. CO_2 Dissolved in The Crude Oil Being Liberated

At the higher pressure, the oil swelled due to CO_2 becoming soluble in the oil. This resulted in a decrease in the CO_2 pressure applied. Once the pressure was relieved, the CO_2 began liberating from the oil, and finally, the oil volume returned to its original amount. No oil was produced from the 0.2 nm experiments, however, due to the extremely small pore sizes.

Based on the experiments conducted, the asphaltene could not propagate through the 0.2 nm pore size. Also, a high percentage of asphaltene could not extrude through the 10 nm pores. This indicates that the majority of asphaltene clusters ranged in size between 0.2 nm to greater than 10 nm. When the asphaltene deposits on the filter membrane, it begins to build up, and thus it increases in size. This is the main reason behind an increase in asphaltene concentration, even in the largest pore size.

7. ASPHALTENE FILTERCAKE FORMATION AND THICKNESS

The filter cake is the part of the oil that will not pass through the filtration membrane and thus will not be produced; it partially represents the asphaltene, along with other high molecular weight components, that will not be mobilized by the CO_2. As the filter cake begins to form, the flow rate will decrease until it reaches stabilization, where the filter cake has been created, and then either increases slightly, or ceases to increase further. The time for the filter cake formation can be defined as the time starting from the initial decline in the flow rate after the first data point until the flow reached stabilization. Measurement of the filter cake thickness was conducted using both a high accuracy needle apparatus and a high accuracy caliper. The filter cake was measured immediately after concluding the

experiment to avoid movement of the asphaltene or contamination of the filter membrane due to exposure to the atmosphere. Measurements were recorded for different sections of the filter membrane, and the largest value recorded was taken as the filter cake thickness for each experiment. After the filter cake thickness was recorded, a high resolution image of the filter membrane was taken for further analysis, and the filter membrane was vacuum sealed for long-term storage.
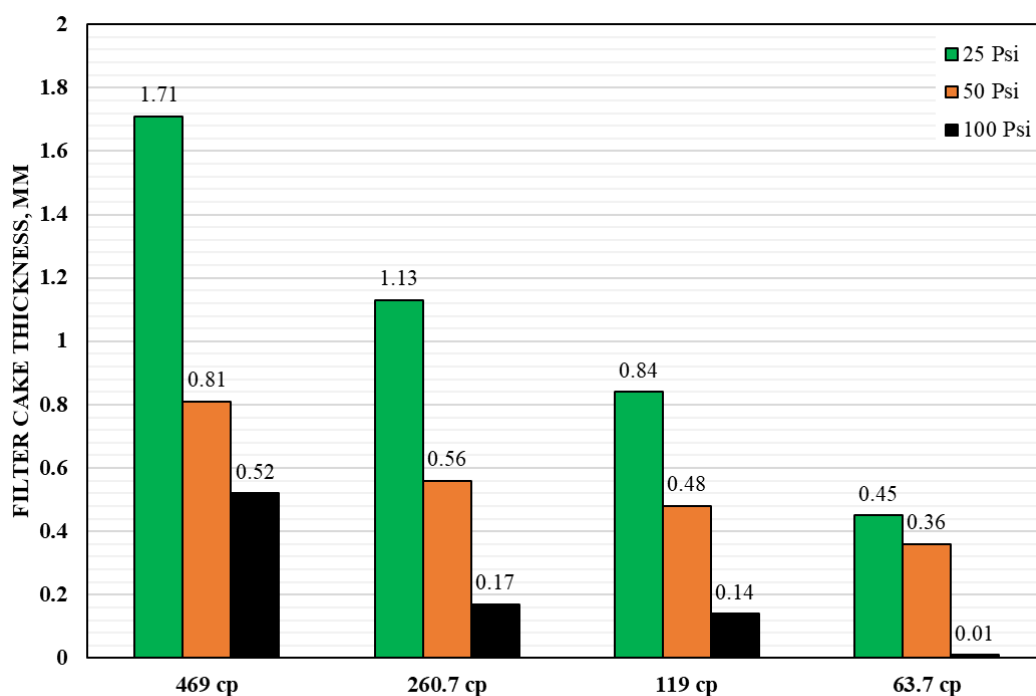
Figure 14. Filter Cake Thickness for Different Oil Viscosities at Different CO_2 Injection Pressures

Figure 14 shows the results for the filter cake thickness. The filter cake represents asphaltene buildup. This buildup is one of the major asphaltene problems in the field and can cause severe operational and production drawbacks during oil recovery. The highest

thickness was obtained for the highest viscosity oil at the lowest CO_2 injection pressure. The filter cake thickness decreased with the increase in CO_2 injection pressure and with the decrease in oil viscosity. This is mainly due to the higher asphaltene concentration found in the highest viscosity oil, which resulted in a thicker filter cake formation on the filter membrane. When correlating the filter cake buildup to the asphaltene visualization experiments, it is clear that a common trend can be observed. This indicates that the asphaltene visualization experiments can be a strong tool to indicate asphaltene problems.
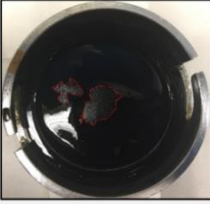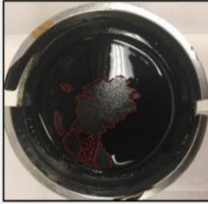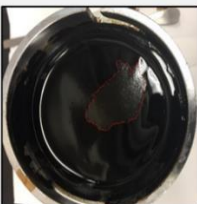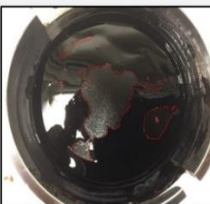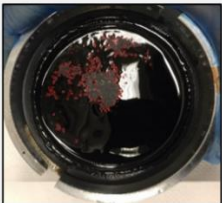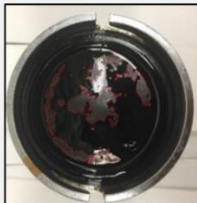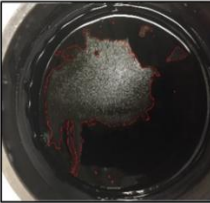
Figure 15. Filtrate Breakthrough Areas and Overall Breakthrough Percentages

After conducting each experiment, high resolution images of each of the filter membranes were taken and analyzed to calculate the area of the filter membrane that had no oil in it. The pictures were taken immediately after the experiment was done to avoid oil movement that would affect the integrity of the results. The area was calculated as both a value in cm^2 and also as a percentage of the overall area of the filter membranes. Figure 15 shows the images for all the filter membranes, and the breakthrough areas outlined in red. As the oil viscosity decreased, the breakthrough area increased, and also as the CO_2 injection pressure increased, the area increased.

8. CONCLUSIONS

This research undergoes two sets of experiments, including asphaltene visualization and asphaltene filtration experiments, to investigate asphaltene stability in crude oil under different conditions. The main conclusions obtained from this research are as follows:

- Asphaltene plugging in nanopores was found to be extremely severe, which was evident from the asphaltene concentration in the filtride. This is mainly due to the size of the pores becoming closer to the size of asphaltene clusters, which made it difficult for the asphaltene to extrude through the pores.

- Asphaltene deposition was found to be a stage-wise process, which begins with asphaltene precipitation then flocculation and finally ends with deposition. Different conditions will impact the severity and rate of these three stages.

- Asphaltene buildup was observed in all experiments, even the experiments using the 2.7 micron filter membrane. This shows that asphaltene buildup and pore

plugging can be a severe problem in both conventional reservoirs with large pores and unconventional reservoirs with nanopores.

- Asphaltene buildup was observed even for the lightest crude oil, 63.7 cp. This shows that asphaltene problems can arise even in light crude oils and will not be limited only to heavy oils. As the oil viscosity increased, the asphaltene concentration also increased. This impacted the rate of asphaltene precipitation, flocculation, and deposition. This also had a strong impact on asphaltene buildup on the filter membrane surface, which in turn will impact asphaltene buildup in the reservoir pores and in the wellbore.

ACKNOWLEDGEMENTS

REFERENCES

Akbarzadeh, K. et al., 2007. Asphaltenes -Problematic but rich in potential. Oilfield Review 19 (2), 22–43.

Al-Ghazi, S., & Lawson, J., 2007. Asphaltene Cleanout Using VibraBlaster Tool. Society of Petroleum Engineers. doi:10.2118/110972-MS.

D-4124-97, ASTM. Standard Test Methods for Separation of Asphalt into Four Fractions. Updated 2019.

De Boer, R.B. et al., 1995. Screening of crude oils for asphalt precipitation: theory, practice, and the selection of inhibitors. SPE Prod. Facil. 10 (1), 55–61.

Escobedo, J. and Mansoori, G.A. 1997. Viscometric principles of onsets of colloidal asphaltene flocculation in paraffinic oils and asphaltene micellization in aromatics. SPE Production & Facilities 12 (2): 116-122.

Fakher, S. and Imqam, A., 2018. Investigating and Mitigating Asphaltene Precipitation and Deposition in Low Permeability Oil Reservoirs During Carbon Dioxide Flooding to Increase Oil Recovery. Society of Petroleum Engineers. doi:10.2118/192558-MS.

Fakher, S. and Imqam, A., 2019. Asphaltene precipitation and deposition during CO2 injection in nano shale pore structure and its impact on oil recovery. Fuel Journal, 273. (1029-1039. https://doi.org/10.1016/j.fuel.2018.10.039.

Fakher, S. et al., 2017. Novel Mathematical Models to predict Preformed Particle Gel Placement and Propagation through Fractures. Society of Petroleum Engineers. doi:10.2118/187152-MS.

Fakher, S. et al., 2018a. Investigating the Viscosity Reduction of Ultra-Heavy Crude Oil Using Hydrocarbon Soluble Low Molecular Weight Compounds to Improve Oil Production and Transportation. Society of Petroleum Engineers. doi:10.2118/193677-MS.

Fakher, S. et al., 2018b. Increasing Production Flow Rate and Overall Recovery from Gas Hydrate Reservoirs Using a Combined Steam Flooding-Thermodynamic Inhibitor Technique. Society of Petroleum Engineers. doi:10.2118/191179-MS.

Fakher, S. et al., 2019. A Comprehensive Review on Gas Hydrate Reservoirs: Formation and Dissociation Thermodynamics and Rock and Fluid Properties. International Petroleum Technology Conference. doi:10.2523/19373-MS.

Fakher, S. M., 2019. "Asphaltene stability in crude oil during carbon dioxide injection and its impact on oil recovery: A review, data analysis, and experimental study". Masters Theses. 7881.

Fan, T. et al., 2002. Evaluating Crude Oils by SARA Analysis. Presented at the SPE/DOE Improved Oil Recovery Symposium, Tulsa, Oklahoma, 13-17 April. SPE-75228-MS.

Forte, E. and Taylor, S.E., 2014. Thermodynamic Modelling of Asphaltene Precipitation and Related Phenomena. Advances in Colloid and Interface Science, 217, 1-12.

Goel, P. et al., 2017. Prediction of °API Values of Crude Oils by Use of Saturates/Aromatics/Resins/Asphaltenes Analysis: Computational-Intelligence-Based Models. Society of Petroleum Engineers Journal. 817- 853, doi:10.2118/184391-PA.

Goual L, Abudu A. 2009. Predicting the Adsorption of Asphaltenes from Their Electrical Conductivity. Energy Fuel 24: 469–474.

Goual, L., 2012. Petroleum Asphaltenes, Crude Oil Emulsions- Composition Stability and Characterization, (Ed.), ISBN: 978-953-51-0220-5.

Groenzin, H. and O.C. Mullins, 2000. Molecular size and structure of asphaltenes from various sources. Energy and Fuels. 14(3): p. 677-684.

Hannisdal, A., Ese, M.H., Hemmingsen, P.V., and Sjoblom, J., Particle-stabilizedemulsions: effect of heavy crude oil components pre-adsorbed onto stabilizing solids, Colloids Surfaces A—Physicochem. Eng. Aspects 276 (2006)45–58.

Hernandez, M. E., M. T. Vives, and J. Pasquali, 1983, Relationships among viscosity, composition, and temperature for two groups of heavy crudes from the eastern Venezuelan basin: Organic Geochemistry, v. 4, p.173–178.

Islas-Flores, C. A., E. Buenrostro-Gonzalez, et al. (2005). "Comparisons between open column chromatography and HPLC SARA fractionations in petroleum." Energy & Fuels 19(5): 2080-2088.

Jamaluddin, A.K.M. et al., 2000. Experimental and theoretical assessment of the asphaltene precipitation characteristics of the Sahil field under a proposed gas injection scheme. In: Paper SPE # 87292 presented at the SPE Conf. and Exh., 15–18October 2000, Abu Dhabi, UAE.

Jewell, D. et al., 1972. Ion-exchange, coordination, and adsorption chromatographic separation of heavy-end petroleum distillates. Analytical Chemistry. 44(8): p. 1391-1395.

Jha, N.K. et al., 2014. Characterization of Crude Oil of Upper Assam Field for Flow Assurance. Presented at the SPE Saudi Arabia Section Annual Technical Symposium and Exhibition, Al-Khobar, Saudi Arabia, 21-24 April. SPE-172226-MS.

José L. Mendoza De La Cruz, Argüelles-Vivas, F. J., Matías-Pérez, V., Durán-Valencia, C. D., & López-Ramírez, S. (2009). Asphaltene-Induced Precipitation and Deposition During Pressure Depletion on a Porous Medium: An Experimental Investigation and Modeling Approach. Energy & Fuels, 23(11), 5611-5625. doi:10.1021/ef9006142

Kalantari-Dahagi, A. et al., 2006, Formation Damage due to Asphaltene Precipitation Resulting from CO2 Gas Injection in Iranian Carbonate Reservoirs. Society of Petroleum Engineers. doi:10.2118/99631-MS.

Kariznovi, M., Nourozieh, H., Abedi, J., Jamialahmadi, M. and Shahrabadi, A. 2012. Experimental, Modeling, and Optimization of Asphaltene Deposition and Adsorption in Porous Media. Canadian Journal of Chemical Engineering, 90, 1356.

Keshmirizadeh, E., S. Shobeirian, and M. Memariani, 2013. Determination of saturates, aromatics, resins and asphaltenes (SARA) fractions in Iran crude oil sample with chromatography methods: study of the geochemical parameters. Journal of Applied Chemical Research. 7(4): p. 15-24.

Kharrat, A. et al., 2013, Asphaltene Content Measurement Using an Optical Spectroscopy Technique, Energy & Fuels 2013 27 (5), 2452-2457. DOI: 10.1021/ef400050y.

Kim, S.T. et al., 1990. The role of asphaltene in wettability reversal. In: SPE Paper presented at the SPE Ann. Tech. Conf. and Exh., 1990, New Orleans, Louisiana.

Kord, S., Miri, R., Ayatollahi, S., & Escrochi, M. (2012). Asphaltene Deposition in Carbonate Rocks: Experimental Investigation and Numerical Simulation. Energy & Fuels, 26(10), 6186-6199. doi:10.1021/ef300692e

Kordestany, A., Hassanzadeh, H. and Abedi, J., 2019. An experimental approach to investigating permeability reduction caused by solvent-induced asphaltene deposition in porous media. The Canadian Journal of Chemical Engineering, 97(1), pp.361-371.

Leontaritis, K. and Mansoori, G.A., 1987. Asphaltene flocculation during oil production and processing: A thermodynamic collodial model. in SPE International Symposium on Oilfield Chemistry. Society of Petroleum Engineers.

Lichaa, P.M. and Herrera, L., 1975. Electrical and other effects related to the formation and prevention of asphaltene deposition problem in Venezuelan crudes. in SPE oilfield chemistry symposium. Society of Petroleum Engineers.

Mannistu, K.D., Yarranton, H.W., and Masliyah, J.H. 1997. Solubility modeling of asphaltenes in organic solvents. Energy & Fuels 11 (3): 615-622.

Mansoori, G.A. 1996. Asphaltene, resin, and wax deposition from petroleum fluids: Mechanisms and modeling. Arabian Journal for Science and Engineering 21 (4 B): 707-723.

Miadonye A., and Evans L., 2010. The Solubility of Asphaltenes in Different Hydrocarbon Liquids. Petroleum Science and Technology Journal. https://doi.org/10.1080/10916460902936960.

Mishra, V.K. et al., 2012. Downhole Fluid Analysis and Asphaltene Nanoscience Coupled with VIT for Risk Reduction in Black Oil Production. Presented at the SPE Annual Technical Conference and Exhibition, San Antonio, USA, 8-10.

Mohammed, R. et al., 2017, Simulation Study of Asphaltene Deposition and Solubility of CO2 in the Brine During Cyclic CO2 Injection Process in Unconventional Tight Reservoirs, International Journal of Geological and Environmental Engineering, 11 (6) 485- 500.

Monger, T.G. and Fu, J.C., 1987. The nature of CO2-induced organic deposition. In: SPE Paper # 16713 presented at the SPE Ann. Tech. Conf. and Exh., Houston, TX.

Moradi, S. et al., 2012. Investigation of asphaltene precipitation in miscible gas injection processes: experimental study and modeling. Braz. J. Chem. Eng., São Paulo, v. 29, n. 3, p. 665-676.

Mullins, O.C., 2011. The modified yen model. Energy and Fuels, 2010. 24(4): p. 2179-2207.

Punase, A. et al., 2016. The Polarity of Crude Oil Fractions Affects the Asphaltenes Stability. Society of Petroleum Engineers. doi:10.2118/180423-MS.

Rassamdana, H.B. et al., 1996. Asphaltene flocculation and deposition: I. The onset of precipitation. AIChE J. 42 (1), 10–22.

Rassamdana, H.B. et al., 1996. Asphaltene flocculation and deposition: I. The onset of precipitation. AIChE J. 42 (1), 10–22.

Rogel, E. et al., 1999. Asphaltene Stability in Crude Oils. Society of Petroleum Engineers. doi:10.2118/53998-MS.

Shedid and Zekri, 2006, Formation Damage Caused by Simultaneous Sulfur and Asphaltene Deposition. Society of Petroleum Engineers. doi:10.2118/86553-PA.

Shen and Sheng, 2018, Experimental and numerical study of permeability reduction caused by asphaltene precipitation and deposition during CO2 huff and puff injection in Eagle Ford shale, Fuel, 211, 432-445, https://doi.org/10.1016/j.fuel.2017.09.047.

Soroush, S. et al., 2014. A Comparison of Asphaltene Deposition in Miscible and Immiscible Carbon Dioxide Flooding in Porous Media. Society of Petroleum Engineers. doi:10.2118/169657-MS.

Speight, J.G. et al., 1985. Molecular weight and association of asphaltenes: a critical review. Revue De L'Institut FrancaisDu Petrole 40 (1), 51–61.

Speight, J.G., 1999. The chemical and physical structure of petroleum: effect on recovery operations. J. Pet. Sci. Eng. 22,3–15.

Sun, H. et al., 2019. Competitive Adsorption of CO_2 over N_2 in Asphaltene Slit Nanopores Studied by Molecular Simulation. Energy and Fuels Journal. DOI: 10.1021/acs.energyfuels.7b02656.

Thomas, D. et al., 1995. Controlling Asphaltene Deposition in Oil Wells. Society of Petroleum Engineers. doi:10.2118/25483-PA.

Uetani, T. (2014, November 10). Wettability Alteration by Asphaltene Deposition: A Field Example. Society of Petroleum Engineers. doi:10.2118/171788-MS

Wang, S. et al., 2016. Characterization of Produced and Residual Oils in the CO2 Flooding Process, Energy & Fuels 2016 30 (1), 54-62, DOI: 10.1021/acs.energyfuels.5b01828.

Yen, A. et al., 2001. Evaluating asphaltene inhibitors: laboratory tests and field studies. In: Paper SPE -65376-MS presented at the SPE Int. Symp. Oilfield Chem. 2001,Houston, Texas.

Zendehboudi, S. et al., 2014. Asphaltene precipitation and deposition in oil reservoirs – Technical aspects, experimental and hybrid neural network predictive tools, Chemical Engineering Research and Design, 92 **(5)**, 857-875.

V. AN EXPERIMENTAL INVESTIGATION OF IMMISCIBLE CARBON DIOXIDE INTERACTIONS WITH CRUDE OIL: OIL SWELLING AND ASPHALTENE AGITATION

ABSTRACT

Immiscible carbon dioxide (CO_2) injection is a method used to increase oil recovery from oil reservoirs. Several interactions will occur between the CO_2 and the crude oil during immiscible CO_2 injection. While some of these interactions may be favorable, others can actually deter oil recovery and cause serious damage to the producing formations and facilities. This research studies the main factors impacting oil swelling, which is the main favorable mechanism that increases oil recovery during immiscible CO_2 injection in oil reservoirs. The research also investigates the impact of the studied factors on asphaltene instability and deposition and its impact on oil recovery reduction. The impact of varying CO_2 injection pressure, temperature, and crude oil viscosity on oil swelling, asphaltene instability, and oil recovery is studied. Crude oil with viscosity of 460, 267, and 67 cp was used in this study. Based on the experiments, results showed that oil swelling increased with the increase in pressure and decrease in oil viscosity, however, it also decreased with the increase in temperature. When testing the effect of these factors on asphaltene stability in the crude oil it was found that asphaltene damage decreased with the increase in pressure and decrease in oil viscosity and increased with the increase in temperature. Based on this, high pressure and low viscosity oils are more favorable for immiscible CO_2 injection to increase oil recovery and also avoid severe asphaltene damage. At higher temperature, precautionary measures should be taken during CO_2 injection to avoid asphaltene damage.

1. INTRODUCTION

During immiscible CO_2 injection in oil reservoirs, the CO_2 will interact with the crude oil in different methods [1-6]. Some of the interactions are favorable for oil recovery while others can be damaging to both oil recovery and reservoir pore structure [7-14]. One of the main interactions that is extremely favorable for oil recovery during immiscible CO_2 injection is oil swelling [15-18]. This interaction can reduce oil viscosity and improve its mobility significantly. During the dissolution of the CO_2 in the crude oil, a disturbance to the equilibrium of the components in the crude oil may also occur, which may induce asphaltene instability and deposition [19-21]. This can result in a significant decrease in oil recovery through pore plugging and can also damage equipment downhole and facilities and equipment on the surface as well [22-24]. Studying both the oil swelling and asphaltene instability together can help provide insight not only on the favorable interaction of immiscible CO_2 injection, but also how this method can actually reduce oil recovery through the negative interaction of asphaltene instability.

Oil swelling is the increase in crude oil volume due to the partial dissolution of CO_2 in the crude oil [25]. It is impacted by several factors mostly related to reservoir thermodynamics and crude oil properties [26]. Oil swelling is the main mechanism by which oil recovery increase is achieved during immiscible CO_2 injection in oil reservoirs [27]. Through this mechanism, several benefits can be obtained including oil viscosity reduction, solution gas drive, increase in oil relative permeability due to increase in oil volume, and increase in oil mobility [28-31]. Oil swelling has been measured by many methods however the most widely used are the pendant drop method and the modified

pendant drop method [32]. These methods are considered highly accurate and can be used for a wide range of crude oil samples. Several researchers have investigated oil swelling of crude oil. Svrcek, W.Y. and Mehrotra, A.K. [33] studied the ability of CO_2 injection to decrease bitumen viscosity and density via dissolution and oil swelling. Holm, L.W. and Josendal, V.A. [34] provided an overview of the main differences between miscible and immiscible CO_2 injection. Yang, C. and Gu, Y. [35] developed a modified Dynamic Pendant Drop Volume Analysis Method to measure diffusion of different agents in crude oil. Sugai, Y. et al. [36] used a modified Pendant Drop Method setup to study oil swelling using CO_2 and its impact on capillary and interfacial tension. Silva, M.K. and Orr Jr., F.M. [37] studied the impact of crude oil molecular weight on CO_2 dissolution. Bahralolom, I. M. and Orr Jr., F.M. [38] investigated the solubility of both CO_2 and nitrogen in crude oil using flow visualization experiments. All of these researches either focused on the experimental setup or the crude oil properties, with very little focus on the reservoir conditions.

Asphaltene is a solid component of the crude oil that is stabilized as a nano-colloid in the crude oil during equilibrium conditions [39-41]. Altering the equilibrium conditions through several means including CO_2 injection can result in asphaltene instability and eventually asphaltene deposition [42-45, 55, 57]. If asphaltene deposition occurs, it can result in pore plugging in the reservoir and thus a reduction in oil mobility and recovery [46-48]. Several researchers have investigated asphaltene instability in crude oil and the factors that may impact this stability. Zendehboudi, S. et al [49] differentiated between precipitation, coming out of solution, and deposition, adhesion of the asphaltene to the rock. This helped provide a method by which to analyze asphaltene stages. Rassamdani,

H.B. et al [50] observed another stage of asphaltene, referred to as asphaltene flocculation, where the asphaltene particles began forming clusters and aggregates of a large diameter size. Soroush, S. et al [51] studied asphaltene stability during CO_2 injection and determined that the state of asphaltene can actually impact asphaltene stability. Kalantari-Dahagi, A. et al [52] conducted one of the few studies that investigated asphaltene problems in carbonate reservoirs and found asphaltene to be extremely problematic at the bubble point. Shedid and Zekri [53] showed that with the increase in the rock permeability and average pore size, the asphaltene problems decreased significantly. Thawer et al. [54] ran laboratory tests to determine the minimum solubility pressure for asphaltenes in the Ula reservoir fluids. Thomas et al. [56] also sought to find a method to dissolve asphaltenes deposited in the reservoirs and pipelines. Fakher, S. et al. [10-13] performed a detailed study of asphaltene properties and behavior in micro and nano pores. All of the mentioned studies investigated asphaltene with no connection to oil swelling, which is the main interaction between the CO_2 and the crude oil during immiscible CO_2 injection.

Even though oil swelling has been researched previously in several studies, most of these studies have focused on either modeling or predicting oil swelling with very little studies attempting to investigate the main factors impacting oil swelling and quantify these impacts. Furthermore, almost no previous research has attempted to tie oil swelling as a mechanism in immiscible CO_2 injection to asphaltene stability in the crude oil. This research performs an analysis of the factors impacting oil swelling capacity during immiscible CO_2 injection in crude oil and quantifies the impact of these factors to reveal their effect. The research then ties these factors to asphaltene stability and oil recovery by illustrating their impact on asphaltene deposition and oil recovery reduction. By

undergoing this research, both the positive and negative aspects of immiscible CO_2 interaction with crude oil are revealed and understood in order to provide a complete understanding of both aspects during immiscible CO_2 injection.

2. EXPERIMENTAL DESCRIPTION

The experimental material, setups, and procedures used to conduct the experiments will be mentioned and explained in this section.

2.1. EXPERIMENTAL MATERIAL

The experimental material used to conduct the oil swelling and asphaltene stability experiments are as follows.

- **Crude Oil.** Crude oil from Kirk lease in Kansas USA was used to conduct all the experiments. The oil viscosity was varied using kerosene. Table 1 shows the oil viscosity values and the equivalent kerosene saturation. The kerosene was added to the crude oil gradually as a weight percentage of the original weight of the solution. This ensured that the kerosene concentration was consistent.

Table 1. Crude Oil Viscosity and The Equivalent Kerosene Weight Percent

Crude Oil Viscosity, cp	Kerosene Weight Percent, wt%
460	0
267	5
67	20

- **Carbon Dioxide.** The CO_2 used was supplied via a high-pressure CO_2 cylinder with a purity of 99.99%.

- **Distilled Water.** Distilled water was used to displace fluids via the pump and also to pressurize the CO_2.

- **Thermometer.** A thermometer was used to record the temperature of the water bath to ensure that there is no temperature change.

- **Water Bath.** A water bath was used to heat the setup and maintain an isothermal temperature for the duration of the experiment.

- **Filter Membranes.** Filter membranes with pore size of 0.2, 10, and 100 nm were used to conduct the asphaltene stability experiments.

- **Heptane.** The heptane used was commercially available. It was used for the asphaltene concentration quantification tests. Heptane was used since asphaltene is insoluble in it and thus will precipitate. Heptane is one of the most widely used chemicals for asphaltene quantification and detection tests.

2.2. EXPERIMENTAL SETUPS

Two different experimental setups were used to conduct the experiments in this research. Both the oil swelling and asphaltene stability setups are explained.

An illustration of the setup used to conduct the oil swelling experiments is shown in Figure 1. The setup is composed of a syringe pump used for pressurization of the CO_2. The CO_2 is initially injected in the accumulator where it is pressurized and injected into the system. Two high pressure vessels are used to conduct the experiments and are placed in a water bath for temperature control. The high pressure vessels used were not transparent

and thus the crude oil could not be visualized. Pressure transducers record the pressure values real-time and save it to a computer for processing after the experiment is concluded.
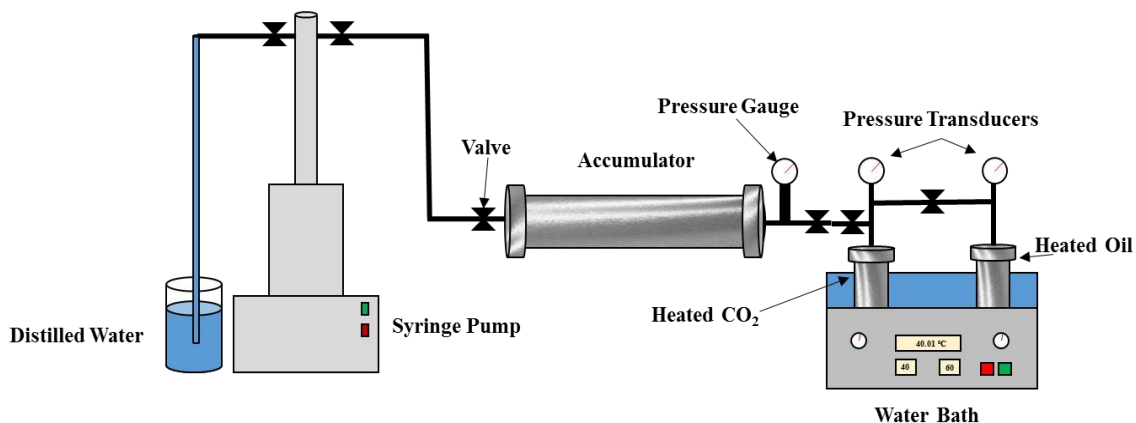
Figure 1. Oil Swelling Experimental Setup

The setup used to conduct the asphaltene stability experiments is shown in Figure 2. The setup is composed of a CO_2 source which is controlled via a pressure regulator. The filtration vessel used to study CO_2 interaction with the oil and its impact on asphaltene stability and oil recovery houses the crude oil and a filter membrane for asphaltene study. A support screen is used to prevent rupturing of the filter membrane during the high pressure experiments. A test tube is used to collect the produced crude oil, referred to as the filtrate, for further analysis. The filtration vessel is heated via a temperature regulator which controls the temperature of the vessel for the duration of the experiments. For all experiments, the filtration vessel was vertical, and the CO_2 was injected from the top of the vessel in order to interact with the crude oil initially before filtration took place. A valve was placed at the outlet to control the flow of the crude oil from the vessel following the

interaction time. The production was mainly via the CO_2 pressure which is similar to a gas cap with solution gas drive mechanisms in an oil field.
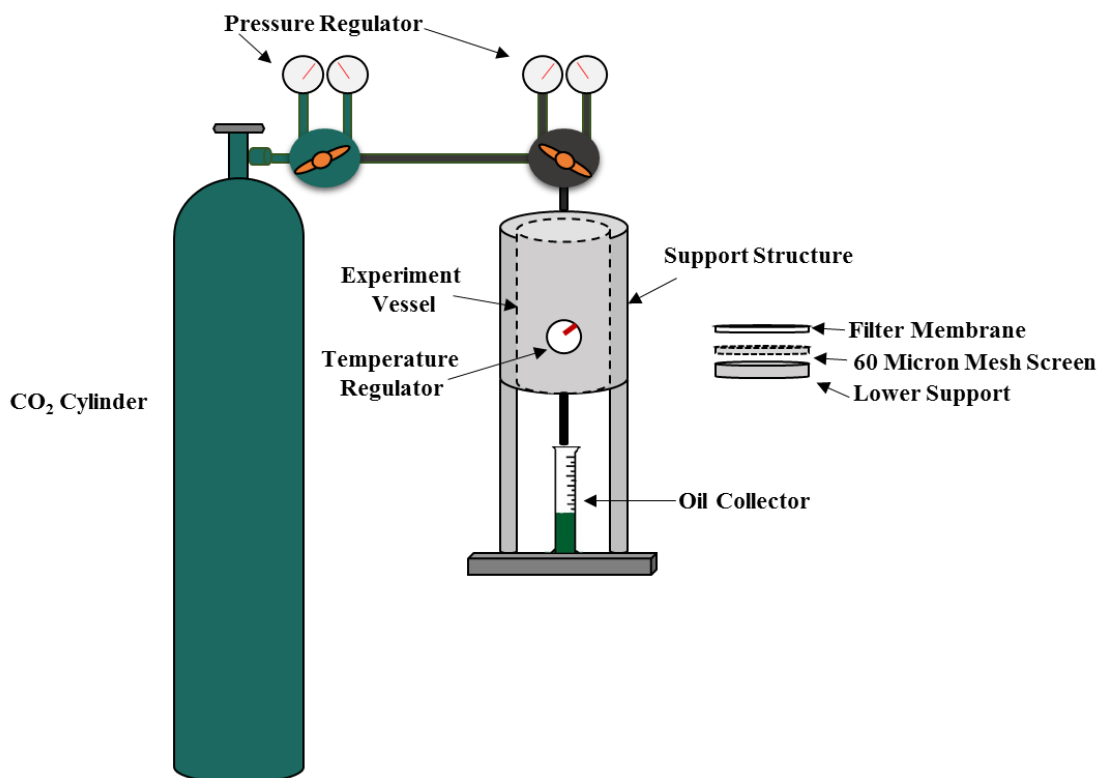
Figure 2. Asphaltene Stability Experimental Setup

2.3. EXPERIMENTAL PROCEDURE

The procedure used to conduct the oil swelling and the asphaltene stability experiments will be explained in detail in this section.

The oil swelling experiments were conducted using pressure change method (pressure decay method) in a closed vessel. The pressure change was then altered to volume using the equation of state. The exact procedure is as follows.

1. The oil swelling vessel was vacuumed for six hours. One milliliter of crude oil was then placed in the oil swelling vessel. The vessel was then placed in the water bath and heated for 12 hours.

2. The heated CO_2 is injected into the oil swelling vessel using the predetermined design pressure. The pressure is then recorded every second until no pressure change is observed for at least two hours. The stable pressure takes up to three weeks to be reached in some cases.

3. The stable pressure value is then recorded and using the real gas equation of state, the swelled oil volume is calculated.

4. Since the experimental vessel was opaque, the oil swelling could not be determined visually. Pressure transducers were used to measure the pressure change in the vessel and then the pressure was converted to volume change. In order to perform the conversion, the following equation was used.

$$\frac{P_1 V_1}{z_1 n_1 R T_1} = \frac{P_2 V_2}{z_2 n_2 R T_2}$$

where 1 and 2 represent the initial and final conditions respectively. P is the pressure, V is the volume, z is the compressibility factor of the gas, n is the number of moles, R is the universal gas constant, and T is the temperature.

5. Since the gas equation of state is used for gas, the variables within it were for the CO_2. By determining the change in volume for the CO_2, the dissolution could be determined. This is then used to measure the oil swelling.

The asphaltene stability experiments were conducted using a combination of the filtration experiments and then asphaltene analysis using heptane precipitation. The exact procedure is as follows:

1. The filter membranes were placed in the filtration vessel. Following this, 30 ml of crude oil were poured on top of the filter membrane. The filtration vessel was occupied by the crude oil only with no porous media to study the interaction of the oil with the CO_2 alone. The filtration vessel was then sealed using six bolts to avoid any leakage during the experiments.

2. The vessel is then heated to the design temperature for six hours. Heated CO_2 is then injected into the vessel and is left to interact with the crude oil for two hours.

3. For all experiments, the crude oil was static with no stirring. The CO_2 interacted with the crude oil via dissolution and thus was in contact with all the oil the vessel for the duration of the experiments.

4. After the two hours, the production valve is opened, and oil recovery commences. Oil recovery is recorded every minute until no recovery is observed for thirty consecutive minutes and CO_2 breakthrough is achieved.

5. The oil remaining inside the filtration vessel is then collected and analyzed for asphaltene concentration. This will resemble the asphaltene pore plugging in the formation and is referred to as the filtride in this study.

6. Asphaltene analysis is conducted by dissolving 0.1 ml of crude oil in 10 ml of heptane. The asphaltene precipitate is the collected and weighed to determine the asphaltene wt%.

7. After dissolving the crude oil in the heptane, the test tube is sealed and shaken vigorously for five minutes. Following this the test tube is left to rest.

8. During the resting period, the asphaltene will begin to liberate from solution and precipitate. After 24-48 hours, the majority of the asphaltene will have deposited at the bottom of the test tube.

9. A filter membrane of $0.47\mu m$ pore size was then used to filter the asphaltene from the remaining oil-heptane mixture. The filtration process takes from 8-12 hours depending on the asphaltene concentration.

10. The filter membrane is then weighed and using the weight difference and density of asphaltene, the asphaltene concentration can be determined.

3. RESULTS AND ANALYSIS

All the results obtained from this research will be mentioned an explained in this section. The factors affecting oil swelling will initially be discussed, followed by the asphaltene instability tests' results.

3.1. OIL SWELLING

The impact of varying CO_2 injection pressure, temperature, and oil viscosity on oil swelling was investigated in this research. All the results obtained from the experiments are presented in this section. Figure 3 shows an image of the crude oil sample before and after swelling. The bubbles observed in the image are the CO_2 being liberated from the crude oil sample immediately following depressurization.
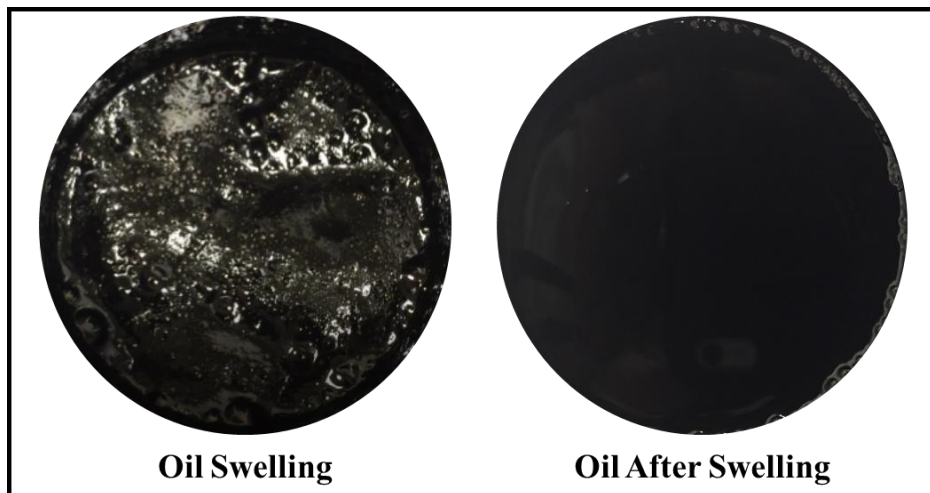
Figure 3. Crude Oil Sample Before and After Swelling

Oil swelling is greatly affected by pressure since it is a strong function of solubility. Since there is still interfacial tension between the CO_2 and the crude oil during immiscible CO_2 injection, the higher the injection pressure, the higher the CO_2 solubility and hence the higher the oil swelling value. Three injection pressures have been studied in this research including 500, 1000, and 1500 psi. Figure 4 shows the oil swelling results for all three pressures. All experiments were conducted at 40 °C using 460 cp crude oil. Increasing the CO_2 injection pressure resulted in an increase in the oil swelling due to the decrease in the interfacial tension between the CO_2 and the oil at higher pressure. The increase from 500 psi to 1000 psi is much more significant compared to the increase from 1000 psi to 1500 psi, which is apparent from the green line in the plot. This could be due to two reasons, the first being the CO_2, where three phases are observed in the plot including gas, liquid, and supercritical at 500, 1000, and 1500 psi respectively. With the change in phase, the CO_2 properties will change which may alter its ability to dissolve in the crude oil. Secondly, as the pressure increases, the interfacial tension will decrease until

a point at which miscibility is reached. The low increase in oil swelling could be an indication that miscibility was near or the conditions at that point were very close to reaching miscibility between the CO_2 and the crude oil.
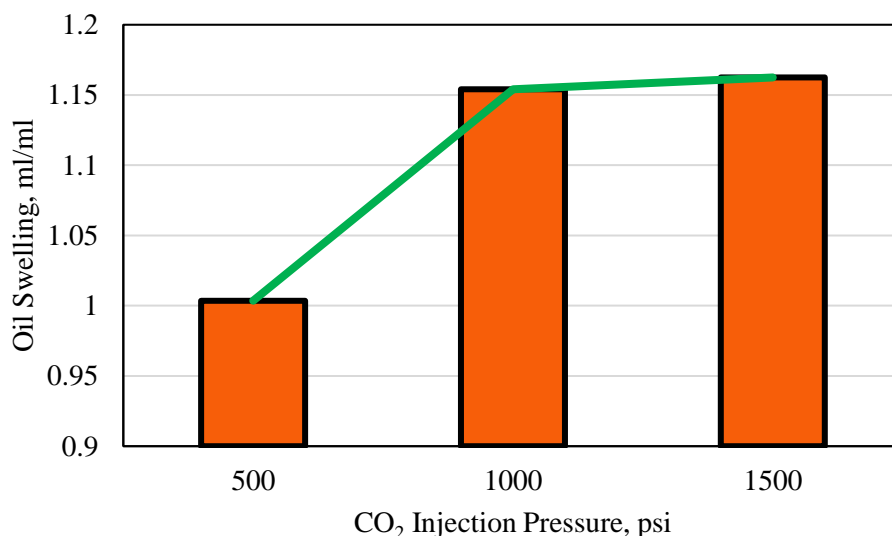
Figure 4. Effect of CO_2 Injection Pressure on Oil Swelling

Increasing the temperature will have two different effects on the CO_2 and crude oil. The temperature increase will reduce the crude oil viscosity. This will reduce the interfacial tension between the CO_2 and the crude oil and thus will allow for more oil swelling. On the contrary, increasing temperature will reduce CO_2 solubility in the crude oil by providing the CO_2 with more energy which will make it less likely to dissolve in the oil. This will result in a reduction in the overall oil swelling. Based on this, the impact of temperature is one of the most important to understand and will also vary from one situation to the other. Based on the initial properties of the crude oil and the overall temperature increase, one of the two aforementioned interactions will become predominant and thus the

overall oil swelling will either increase or decrease. The effect of three temperatures on oil swelling were studied in this research, including 25, 40, and 60 °C. Figure 5 shows the oil swelling results at all temperature. Experiments were conducted using 460 cp crude oil at 1500 psi. Increasing the temperature resulted in a decrease in the oil swelling. The decrease is almost constant as is shown from the green trendline. This indicates that the reduction in CO_2 solubility was the predominant effect in this case and thus the overall oil swelling value decreased with the increase in temperature.
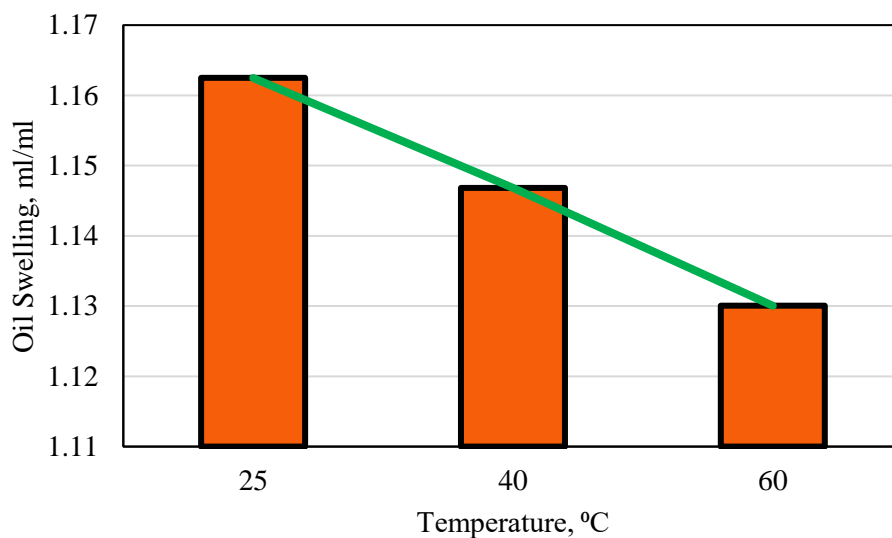
Figure 5. Effect of Temperature on Oil Swelling

Even though the impact of oil viscosity change on oil swelling was part of the temperature change effect, isolating this effect and studying it separately is extremely important in understanding its impact on oil swelling potential. Three crude oil viscosity values were studied in this research, including 460, 267, and 67 cp. The impact of varying the crude oil viscosity on oil swelling is shown in Figure 6. Decreasing the crude oil

viscosity resulted in a near-constant increase in oil swelling. This is mainly due to the reduction in the interfacial tension between the crude oil and the CO_2 as the viscosity decreases, and thus CO_2 solubility increases. This is one of the main reasons behind why miscibility is easier to achieve at lower pressures when the crude oil has a lower viscosity.
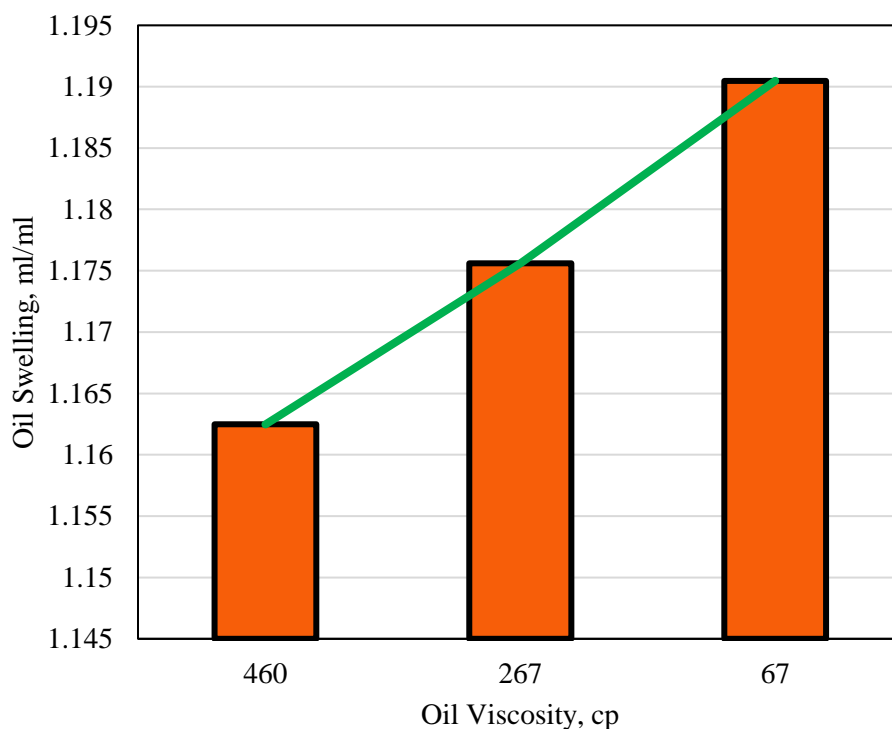
Figure 6. Effect of Oil Viscosity on Oil Swelling

3.2. ASPHALTENE STABILITY

CO_2 dissolution in the crude oil during oil swelling can result in the disturbance of the homogeneity of the components of the crude oil and thus may result in some of the components liberating from solution. One of the problematic components of crude oil that may liberate and cause severe oil recovery and operational problems during CO_2

dissolution is asphaltene. The second part of this research therefore studies the impact of all of the factors investigated for oil swelling, including CO_2 injection pressure, temperature, and oil viscosity, on asphaltene stability in the crude oil and its impact on oil recovery. Figure 7 shows asphaltene from this study during its quantification process on the filter membrane.
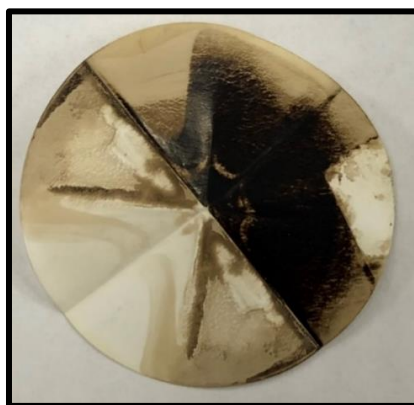
Figure 7. Image of Asphaltene on Filter Membrane During Asphaltene Quantification

The asphaltene concentration for all three crude oils was determined in order to function as a reference value for the experimental results. Table 2 shows all the asphaltene concentrations for the crude oils.

Table 2. Initial Asphaltene Concentrations for All Crude Oils Before Filtration

Crude Oil Viscosity, cp	Asphaltene Concentration, wt%
470	5.73
267	4.63
67	3.22

The impact of increasing CO_2 injection pressure using 200, 400, and 700 psi on oil recovery and asphaltene wt% in the filtride is shown in Figure 8. All experiments were conducted using 460 cp crude oil and 100 °C. Increasing the CO_2 injection pressure resulted in an increase in oil recovery through the filter membrane due to the interaction of the CO_2 with the crude oil, through oil swelling, and also due to the crude oil being forced through the membrane at higher pressures. The asphaltene concentration in the filtride, inside the vessel, also decreased with the increase in pressure. This is mainly due to the smaller asphaltene particles being forced through the filter membrane at higher pressure and thus they could not form large aggregations in time. Based on this, higher pressure shows better overall oil swelling, oil recovery, and asphaltene stability.
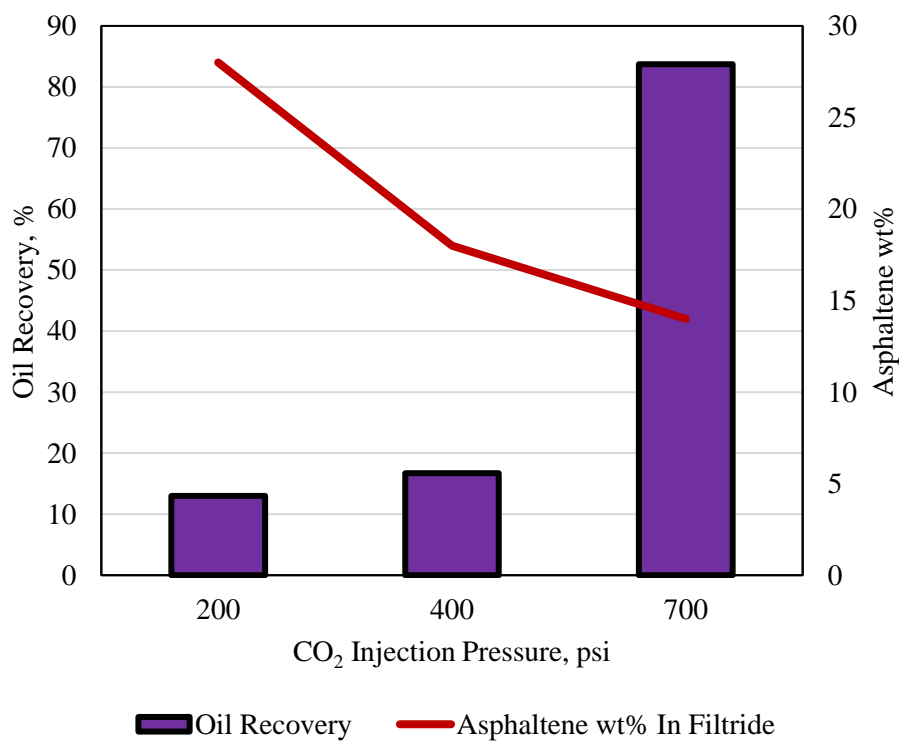
Figure 8. Effect of CO_2 Injection Pressure on Oil Recovery and Asphaltene Stability

The impact of temperature on asphaltene stability in the crude oil was studied using three temperatures including 60, 100, and 130 °C. The asphaltene concentration and oil recovery results for all three temperatures are shown in Figure 9. All experiments were conducted using 460 cp crude oil and 400 psi. Increasing the temperature resulted in an increase in oil recovery. This is due to the reduction in oil viscosity and increase in oil swelling, as was discussed earlier. Increasing the temperature also resulted in an increase in the asphaltene concentration due to the decrease in asphaltene stability in the crude oil at elevated temperatures. This shows that even though elevated temperatures may be favorable for oil recovery, it can also cause asphaltene problems which may result in severe operational problems.
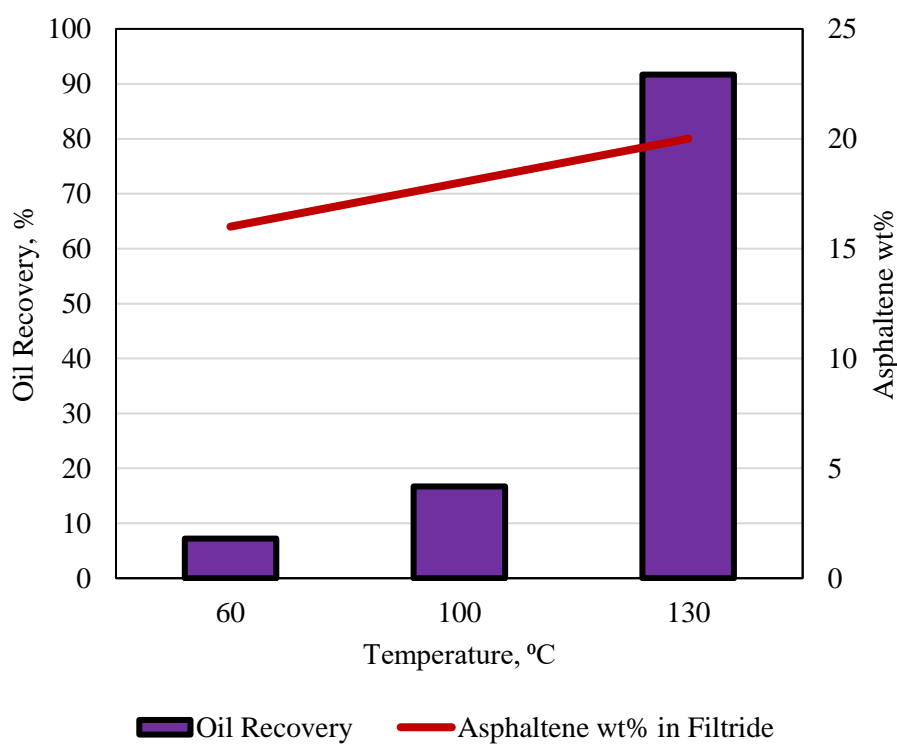
Figure 9. Effect of Temperature on Oil Recovery and Asphaltene Stability

Altering the oil viscosity impacted the oil swelling value which will have an impact on the oil recovery potential. The impact of varying the oil viscosity on asphaltene stability and oil recovery was also investigated in this research using three different viscosity values including 460, 267, and 67 cp. Figure 10 shows the impact of oil viscosity on oil recovery and asphaltene concentration. Decreasing the oil viscosity resulted in a decrease in the asphaltene concentration and an increase in oil recovery. This is mainly due to the overall lower asphaltene content in the low viscosity crude oil compared to the higher viscosity crude oil and the higher mobility of the lower viscosity crude oil. This shows that overall, a lower oil viscosity is more favorable for production compared to the higher oil viscosity since it exhibited higher oil swelling value, higher oil recovery, and lower asphaltene concentration.
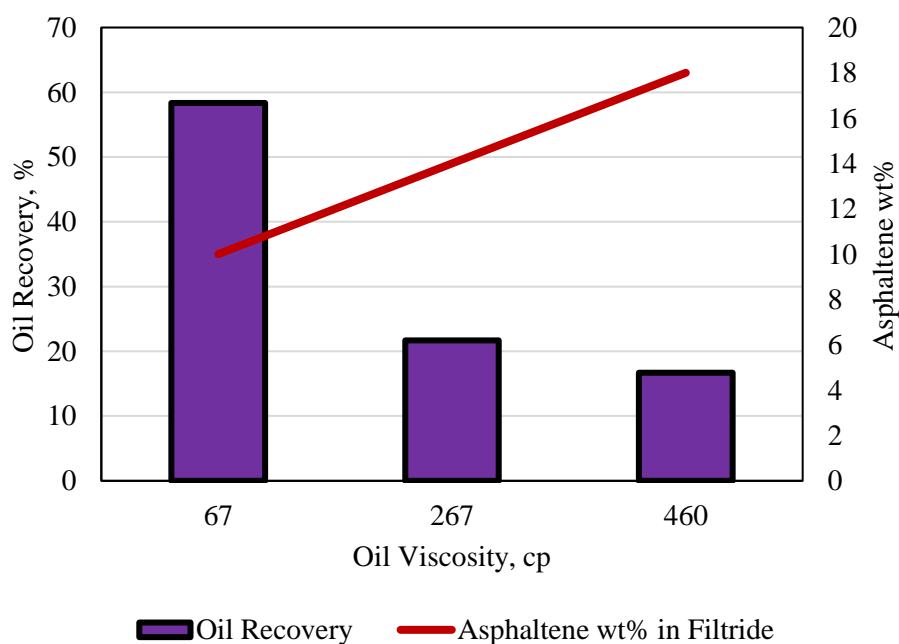
Figure 10. Effect of Oil Viscosity on Oil Recovery and Asphaltene Stability

4. DISCUSSION

Based on the experimental results, it was observed that the CO_2 will interact with the crude oil in different manners and different methods based on the fluid properties and the thermodynamic properties at which the fluids are at. Since oil swelling is an advantageous interaction, while asphaltene instability is a negative interaction, in is important to compare the impact of the factors studied on both interactions in order to assess the overall benefit-damage that will occur in an asphaltene-bearing crude oil during CO_2 injection. A summary of the impact of the factors on oil swelling and asphaltene stability is summarized in Table 3.

Table 3. Impact of Different Factors on Oil Swelling and Asphaltene Stability

Interaction	Factor	Effect
Oil Swelling	Pressure	Increasing the pressure resulted in an increase in oil swelling.
	Temperature	Increasing the temperature reduces the CO_2 solubility.
	Oil Viscosity	Decreasing the oil viscosity lessens the interfacial tension between the CO_2 and the crude oil.
Asphaltene Stability	Pressure	Increasing the pressure resulted in a decrease in the asphaltene concentration.
	Temperature	Increasing the temperature resulted in a decrease in asphaltene stability and thus increased the asphaltene content in the filtride.
	Oil Viscosity	Decreasing the oil viscosity decreased the asphaltene concentration.

5. CONCLUSIONS

This research studied immiscible CO_2 injection interactions with crude oil by investigating oil swelling and asphaltene stability. The main factors impacting oil swelling and asphaltene stability were investigated and quantified. The main conclusions obtained from this research are as follows.

- Immiscible CO_2 injection was found to induce oil swelling and was impacted by CO_2 injection pressure, temperature and oil viscosity.

- CO_2 interaction with the crude oil caused asphaltene agitation which had an impact on oil recovery negatively and thus is considered an overall damaging interaction.

- Increasing the CO_2 pressure resulted in an increase in the oil swelling value and also decreased the asphaltene concentration. Also, increasing the pressure resulted in an increase in the oil recovery.

- Higher temperatures resulted in a lower oil swelling value and a higher asphaltene content. The oil recovery was higher at higher temperatures.

- A lower oil viscosity is more favorable for production compared to the higher oil viscosity since it exhibited higher oil swelling value, higher oil recovery, and lower asphaltene concentration.

ACKNOWLEDGEMENT

REFERENCES

Akbarzadeh, K. et al., 2007. Asphaltenes -Problematic but rich in potential. Oilfield Review 19 (2), 22–43.

Al-Jarba, M. and Al-Anazi, B. D., 2009. A Comparison Study of the CO_2-Oil Physical Properties Literature Correlation Accuracy Using Visual Basic Modelling Technique. NAFTA Journal, **60** (5), 287-291.

Al-Murayri, M. T., Harding, T. G., and Maini, B.B., 2011. Solubility of Methane, Nitrogen, and Carbon Dioxide in Bitumen and Water for SAGD Modelling. Journal of Canadian Petroleum Technology, Society of Petroleum Engineers. doi:10.2118/148630-PA.

Bahralolom, I. M., and Orr, F., 1988. Solubility and Extraction in Multiple Contact Miscible Displacements: Comparison of N_2 and CO_2 Flow Visualization Experiments. SPE Reservoir Engineering, Society of Petroleum Engineers. doi:10.2118/15079-PA.

Barclay, T., and Mishra, S., 2016. New Correlations for CO_2-Oil Solubility and Viscosity Reduction for Light Oils, Journal of Petroleum Production Technology, Springer. DOI 10.1007/s13202-016-0233-y.

De Boer, R.B. et al., 1995. Screening of crude oils for asphalt precipitation: theory, practice, and the selection of inhibitors. SPE Prod. Facil. 10 (1), 55–61.

DeRuiter, R.A., Nash, LJ., and Singletary, M.S., 1994. Solubility and Displacement Behavior of a Viscous Crude With CO_2 and Hydrocarbon Gases. SPE Reservoir Engineering, Society of Petroleum Engineers. doi:10.2118/20523-PA.

Du, F. An Experimental Study of Carbon Dioxide Dissolution Into a Light Crude Oil, 2016. Masters Thesis, Petroleum Systems Engineering, University of Regina.

Fakher, S. and Imqam, A., 2018. Investigating and Mitigating Asphaltene Precipitation and Deposition in Low Permeability Oil Reservoirs During Carbon Dioxide Flooding to Increase Oil Recovery. Society of Petroleum Engineers. doi:10.2118/192558-MS.

Fakher, S. and Imqam, A., 2019. Asphaltene precipitation and deposition during CO2 injection in nano shale pore structure and its impact on oil recovery. Fuel Journal, 273. (1029-1039. https://doi.org/10.1016/j.fuel.2018.10.039.

Fakher, S. et al. 2019. Critical review of asphaltene properties and factors impacting its stability in crude oil. J Petrol Explor Prod Technol (2019). https://doi.org/10.1007/s13202-019-00811-5.

Fakher, S. et al., 2019. An experimental investigation of asphaltene stability in heavy crude oil during carbon dioxide injection. J Petrol Explor Prod Technol (2019) doi:10.1007/s13202-019-00782-7.

Fakher, S. et al., 2019. The Effect of Unconventional Oil Reservoirs; Nano Pore Size on the Stability of Asphaltene During Carbon Dioxide Injection. Carbon Management Technology Conference. doi:10.7122/CMTC-558486-MS.

Fakher, S. M., 2019. "Asphaltene stability in crude oil during carbon dioxide injection and its impact on oil recovery: A review, data analysis, and experimental study". Masters Theses. 7881.

Fakher, S. M., Imqam, A., & Bai, B. (2018, August 16). Enhancing Carbon Dioxide Flooding Sweep Efficiency in High Permeability Hydrocarbon Reservoirs Using Micro-Particle Gels. Society of Petroleum Engineers. doi:10.2118/192381-MS.

Fakher, S., 2019. Investigating Factors that May Impact the Success of Carbon Dioxide Enhanced Oil Recovery in Shale Reservoirs. Society of Petroleum Engineers. doi:10.2118/199781-STU.

Fakher, S., Bai, B., Imqam, A., & Wang, Y. (2017, October 9). Novel Mathematical Models to predict Preformed Particle Gel Placement and Propagation through Fractures. Society of Petroleum Engineers. doi:10.2118/187152-MS.

Fakher, S., Imqam, A., & Wanas, E. (2018, December 10). Investigating the Viscosity Reduction of Ultra-Heavy Crude Oil Using Hydrocarbon Soluble Low Molecular Weight Compounds to Improve Oil Production and Transportation. Society of Petroleum Engineers. doi:10.2118/193677-MS.

Gao, C. et al., 2013. Heavy Oil Production by Carbon Dioxide Injection, Green House Gasses Science and Technology, Society of Chemical Industry and John Wiley & Sons. doi:0.1002/ghg.1346.

Goual, L., 2012. Petroleum Asphaltenes, Crude Oil Emulsions- Composition Stability and Characterization, (Ed.), ISBN: 978-953-51-0220-5.

Hatzignatiou, D., and Lu, Y., 1994. Feasibility Study of CO2 Immiscible Displacement Process In Heavy Oil Reservoirs. Petroleum Society of Canada. doi:10.2118/94-90.

Holm and Josendal, 1974, Mechanisms of Oil Displacement By Carbon Dioxide. Society of Petroleum Engineers. doi:10.2118/4736-PA.

Holm, L.W. and Josendal, V.A., 1974. Mechanisms of Oil Displacement By Carbon Dioxide. Journal of Petroleum Technology, Society of Petroleum Engineers. doi:10.2118/4736-PA.

Jamaluddin, A.K.M. et al., 2000. Experimental and theoretical assessment of the asphaltene precipitation characteristics of the Sahil field under a proposed gas injection scheme. In: Paper SPE # 87292 presented at the SPE Conf. and Exh., 15–18October 2000, Abu Dhabi, UAE.

Jin, L. et al., 2017. Improving Oil Recovery by Use of Carbon Dioxide in the Bakken Unconventional System: A Laboratory Investigation. Society of Petroleum Engineers. doi:10.2118/178948-PA.

Kalantari-Dahagi, A. et al., 2006, Formation Damage due to Asphaltene Precipitation Resulting from CO2 Gas Injection in Iranian Carbonate Reservoirs. Society of Petroleum Engineers. doi:10.2118/99631-MS.

Kharrat, A. et al., 2013, Asphaltene Content Measurement Using an Optical Spectroscopy Technique, Energy & Fuels 2013 27 (5), 2452-2457. DOI: 10.1021/ef400050y.

Kim, S.T. et al., 1990. The role of asphaltene in wettability reversal. In: SPE Paper presented at the SPE Ann. Tech. Conf. and Exh., 1990, New Orleans, Louisiana.

Klins, M. and Ali, S.M., 1982. Heavy Oil Production by Carbon Dioxide Injection. Journal of Canadian Petroleum Technology, Society of Petroleum Engineers.

Maneeintr, K. et al., 2014. Analysis of Heavy Oil Emulsion-Carbon Dioxide Systems on Oil-Swelling Factor and Interfacial Tension by Using Pendant Drop Method for Enhanced Oil Recovery and Carbon Dioxide Storage. International Journal of Environmental Science and Development, **5** (2), 118- 123.

Mohammed, R. et al., 2017, Simulation Study of Asphaltene Deposition and Solubility of CO2 in the Brine During Cyclic CO2 Injection Process in Unconventional Tight Reservoirs, International Journal of Geological and Environmental Engineering, 11 **(6)** 485- 500.

Monger, T.G. and Fu, J.C., 1987. The nature of CO2-induced organic deposition. In: SPE Paper # 16713 presented at the SPE Ann. Tech. Conf. and Exh., Houston, TX.

Moradi, S. et al., 2012. Investigation of asphaltene precipitation in miscible gas injection processes: experimental study and modeling. Braz. J. Chem. Eng., São Paulo, v. 29, n. 3, p. 665-676.

Mullken, C. and Sandler, S., 1980. The Prediction of CO_2 Solubility and Swelling Factors for Enhanced Oil Recovery, Engineering Chemical Process Des. Development, American Chemical Society.

Nourozieh, H., Kariznovi, M., and Abedi, J., 2016. Measurement and Correlation of Solubility and Physical Properties for Gas-Saturated Athabasca Bitumen. SPE Production & Operations, Society of Petroleum Engineers. doi:10.2118/176016-PA.

Rassamdana, H.B. et al., 1996. Asphaltene flocculation and deposition: I. The onset of precipitation. AIChE J. 42 (1), 10–22.

Sasaki, K. et al., 2010. CO_2 Solubility Characteristics of Crude Oils Related to Carbon Capture and Utilization (CCU), Novel Carbon Resource Sciences Newsletter.

Shahriar M, The aggregation of asphaltene molecules as a function of carbon dioxide concentration (PhD Dissertation). Texas Tech University, 2014.

Shedid and Zekri, 2006, Formation Damage Caused by Simultaneous Sulfur and Asphaltene Deposition. Society of Petroleum Engineers. doi:10.2118/86553-PA.

Shen and Sheng, 2018, Experimental and numerical study of permeability reduction caused by asphaltene precipitation and deposition during CO2 huff and puff injection in Eagle Ford shale, Fuel, 211, 432-445, https://doi.org/10.1016/j.fuel.2017.09.047.

Silva, M.K. and Orr, F., 1987. Effect of Oil Composition on Minimum Miscibility Pressure-Part 1: Solubility of Hydrocarbons in Dense CO_2. SPE Reservoir Engineering, Society of Petroleum Engineers. doi:10.2118/14149-PA.

Soroush, S. et al., 2014. A Comparison of Asphaltene Deposition in Miscible and Immiscible Carbon Dioxide Flooding in Porous Media. Society of Petroleum Engineers. doi:10.2118/169657-MS.

Speight, J.G. et al., 1985. Molecular weight and association of asphaltenes: a critical review. Revue De L'Institut FrancaisDu Petrole 40 (1), 51–61.

Speight, J.G., 1999. The chemical and physical structure of petroleum: effect on recovery operations. J. Pet. Sci. Eng. 22,3–15.

Srivastava and Huang, 1997, Asphaltene Deposition During CO2 Flooding: A Laboratory Assessment. Society of Petroleum Engineers. doi:10.2118/37468-MS.

Sugai, Y., Babadagli, T. and Sasaki, K., 2013. Consideration of an Effect of Interfacial Area Between Oil and CO_2 on Oil Swelling, Journal of Petroleum Production Technology. **4** (2014), 105-112. doi:10.1007/s13202-013-0085-7.

Svrcek, W. and Mehrotra, A., 1982. Gas Solubility, Viscosity, and Density Measurements for Athabasca Bitumen. Journal of Canadian Petroleum Technology, Society of Petroleum Engineers.

Thawer, R. et al., 1990. Asphaltene Deposition in Production Facilities. Society of Petroleum Engineers. doi:10.2118/18473-PA.

Thomas, D. et al., 1995. Controlling Asphaltene Deposition in Oil Wells. Society of Petroleum Engineers. doi:10.2118/25483-PA.

Tran, T., 2014. Carbon Dioxide-Heavy Oil Systems: Thermodynamics, Transport and Interfacial Stability. Doctor of Philosophy Thesis Dissertation, Chemical Engineering, Missouri University of Science and Technology.

Vali, J. et al., 2011. A Fast and Simple Method for Modeling Oil Swelling in CO_2 Injection. Journal of Geope, **1** (2), 39-46.

Verma, M., 2015. Fundamentals of Carbon Dioxide Enhanced Oil Recovery (CO_2-EOR)- A Supporting Document of the Assessment Methodology for Hydrocarbon Recovery Using CO_2-EOR Associated with Carbon Sequestration. United States Geology Survey, United States Department of Interior.

Wang, C. et al., 2017, Effect of asphaltene precipitation on CO2-flooding performance in low-permeability sandstones: a nuclear magnetic resonance study, Royal Society of Chemistry, 61, 38367- 38376. 10.1039/C7RA06392J.

Wang, S. et al., 2016. Characterization of Produced and Residual Oils in the CO2 Flooding Process, Energy & Fuels 2016 30 (1), 54-62, DOI: 10.1021/acs.energyfuels.5b01828.

Yang, C. and Gu, Y., 2006. Diffusion Coefficients and Oil Swelling Factors of Carbon Dioxide, Methane, Ethane, Propane, and Their Mixtures in Heavy Oil, Journal of Fluid Phase Equilibria, El-Sevier. **243** (2006), 64-73.

Yen, A. et al., 2001. Evaluating asphaltene inhibitors: laboratory tests and field studies. In: Paper SPE #65376-MS presented at the SPE Int. Symp. Oilfield Chem. 2001,Houston, Texas.

Zendehboudi, S. et al., 2014. Asphaltene precipitation and deposition in oil reservoirs – Technical aspects, experimental and hybrid neural network predictive tools, Chemical Engineering Research and Design, 92 **(5)**, 857-875.

VI. A DATA ANALYSIS OF IMMISCIBLE CARBON DIOXIDE INJECTION APPLICATIONS FOR ENHANCED OIL RECOVERY BASED ON AN UPDATED DATABASE

ABSTRACT

Carbon Dioxide (CO_2) injection is an enhanced oil recovery technique used worldwide to increase oil recovery from hydrocarbon reservoirs. Immiscible CO_2 injection involves injecting the CO_2 into the reservoir at a pressure below which it will become miscible in the oil. Even though immiscible CO_2 injection has been applied extensively, very little research has been conducted to provide a comprehensive understanding of the mechanism and the applications of immiscible CO_2 injection. This research performs an in-depth data analysis is performed based on more than 200 experiments and 20 field tests from more than 40 researches to show the conditions at which immiscible CO_2 injection has been applied and the most frequent application conditions. Histograms and boxplots have been generated for temperature, CO_2 injection pressure, oil viscosity, molecular weight, and API gravity, CO_2 solubility, and finally oil swelling to show the ranges and frequency of application for all these parameters. Finally, crossplots have been generated from the data to show the relation of pressure and temperature to CO_2 solubility and oil swelling. The crossplots function to illustrate a relation between the variables and draws a conclusion as to what effect each parameter will have on the other.

1. INTRODUCTION

One of the most widely applied, and highly advantageous and productive enhanced oil recovery (EOR) methods is carbon dioxide injection. CO_2 can be injected into the reservoir as a miscible solvent, or an immiscible fluid [1-3]. The choice of whether the CO_2 should be miscible or immiscible is based on many factors mainly the reservoir fluid properties, including oil viscosity, molecular weight (MW), API gravity, and composition, and reservoir rock properties, including pay zone depth, thickness, and mineralogy. Generally, when miscibility is difficult to achieve, as is the case in moderately to heavily viscous oils, immiscible CO_2 becomes extremely valuable [4].

When the immiscible CO_2 is injected into the reservoir, one of the most significant interactions that occur between the gas and the oil is manifested in CO_2 solubility. During solubility, the CO_2 will diffuse into the oil and thus the oil will begin to swell [5-7]. Different crude oils will have different solubility based on their composition and properties, such as API gravity and Molecular Weight (MW) [8,9]. Another important parameter that has been shown to impact CO_2 solubility in crude oil is the thermodynamic conditions of the reservoir. Increasing the CO_2 injection pressure will result in a higher solubility, whereas increasing the temperature will result in a decrease in solubility due to the CO_2 molecules having a much higher activity of the CO_2 molecules at higher temperatures [10,11]. Solubility will occur in both miscible and immiscible solvent injection, with the main difference being that during miscible injection, the interfacial tension between the oil and the CO_2 will become zero [12,13]. Due to the high solubility of CO_2 in crude oil during immiscible CO_2 injection, this application can have a strong influence on increasing oil

recovery, even from heavy oil reservoirs [14,15]. Even though solubility has been proven to be an extremely important factor during immiscible CO_2 injection, no comprehensive data analysis has yet been performed to determine its overall impact on different crude oil from lab and field studies.

CO_2 solubility will result in the oil increasing in size or swelling. This swelling will help the crude oil acquire several beneficial characteristics, such as a lower viscosity, a higher relative permeability, and a larger volume. In order to measure the extent to which the crude oil has swollen, several experimental methods have been investigated. Most of the experiments conducted to evaluate oil swelling depended on transparent visualization experiments that can permit the ability to see the swelling phenomenon. Of these setups, the flow visualization experiments, and the pendant drop methods are the most widely utilized [6, 16,17]. Core flooding experiments have also been conducted to study the ability of immiscible CO_2 to increase oil recovery [18]. Immiscible CO_2 injection has also been coupled with other injection fluids such as water, and steam in hopes of increasing oil recovery [19-21]. Due to the abundance of methods by which oil swelling can be measured, and the many ways by which immiscible CO_2 injection can be applied, it is important to provide a guideline to these methods and their advantages and limitations.

Several mathematical and simulation modellings have also been used to study immiscible CO_2 injection. Several empirical correlations have been developed along the year to predict CO_2 solubility in crude oil and oil swelling [22-24]. CO_2-Oil interaction using reservoir simulation and computer modelling have been studied using basic black oil reservoir models, and also complex models that can distinguish the different phases and the interfacial tension [25-27]. Recently, a more complex computer modelling technique

referred to as Gene Expression Programming was used to develop a novel correlation used to determine CO_2 swelling in oil as a function of oil MW, oil specific gravity, reservoir temperature, bubble point pressure, and saturation pressure [28].

A plethora of researches and studies have been conducted using immiscible CO_2 injection in reservoirs and cores with light and intermediate crude oil. Immiscible CO_2 injection has been shown to be successful in producing from reservoirs with heavy oil as well. It is unclear at what conditions is immiscible CO_2 injection best applied. In order to be able to accurately and successfully apply immiscible CO_2 injection in both lab experiments and field studies, it is important to have a comprehensive understanding of the CO_2-oil interactions, and the extent to which they can alter different crude oil properties and characteristics. This research performs a data analysis based on more than 200 experiments and 20 field tests from more than 40 researches to show the conditions at which immiscible CO_2 injection has been applied and the most frequent application conditions. This will help determine the applicability range of immiscible CO_2 and improve on its application by illustrating where it can be applied most effectively. The data analysis includes both field and lab cases that involve immiscible CO_2 injection which makes this research applicable to an extremely wide range of both laboratory experiments involving CO_2 injection in immiscible conditions, and also to field projects with a nessacity of applying immisible CO_2 injection such as in heavy oil reservoirs, shallow oil reservoir, or in reservoirs with a low fracture pressure.

2. IMMISCIBLE CO₂ INJECTION DATA ANALYSIS

The data analysis was performed on more than fifty researches and field studies done on immiscible CO_2 injection in order to determine the ranges at which immiscible CO_2 injection was applied, and the most frequent application conditions. The data collected was from laboratory experiments, field tests, simulation models, review papers, and empirical researches using mathematical models. The percentage of data collected from each type of study is summarized in Figure 1. Almost half of the data was collected from experimental results, followed by simulation results which represented almost third of the data collected, and then finally the field, empirical and review data which represented close to a third of the data as well.
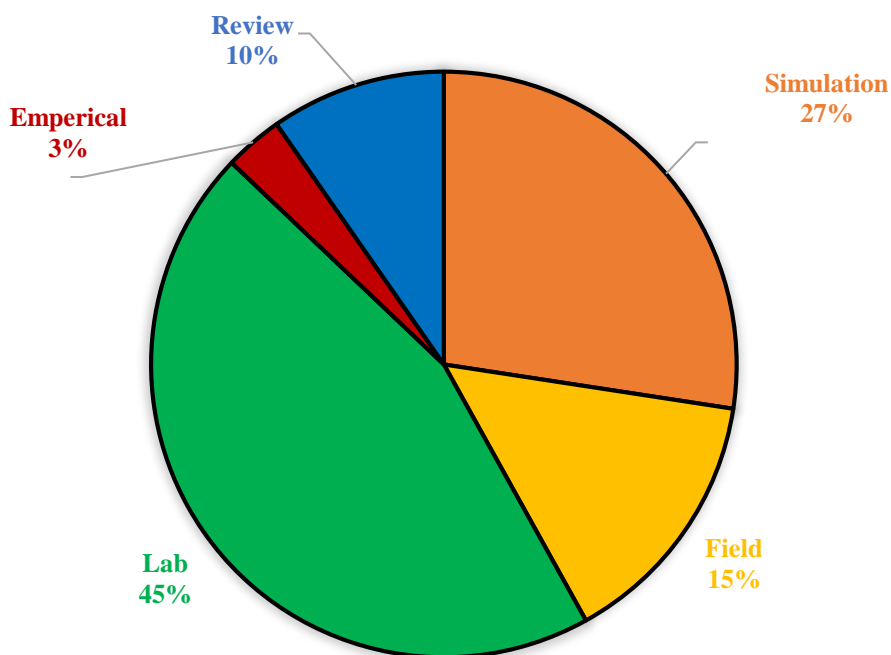
Figure 1. Types of Studies and Their Percentage

2.1. DATA PROCESSING METHODS

Histograms, also known as frequency plots, are usually depicted as column plots that represent different ranges of a variable and the frequency at which each range has been observed. Histograms are extremely important statistical analysis tools since they can easily show the most frequent range of application of a specific parameter or factor and thus determine the best applicability range based on previous studies and tests. Histograms are therefore essential when developing a new screening criterion for a specific application. The histograms developed in this research include Pressure and Temperature, Oil properties including oil MW, viscosity, and API Gravity, and finally the CO_2 impact on oil, which includes the CO_2 solubility, and oil swelling as a result of CO_2 interaction with the oil. An illustration of a typical histogram can be shown in Figure 2.
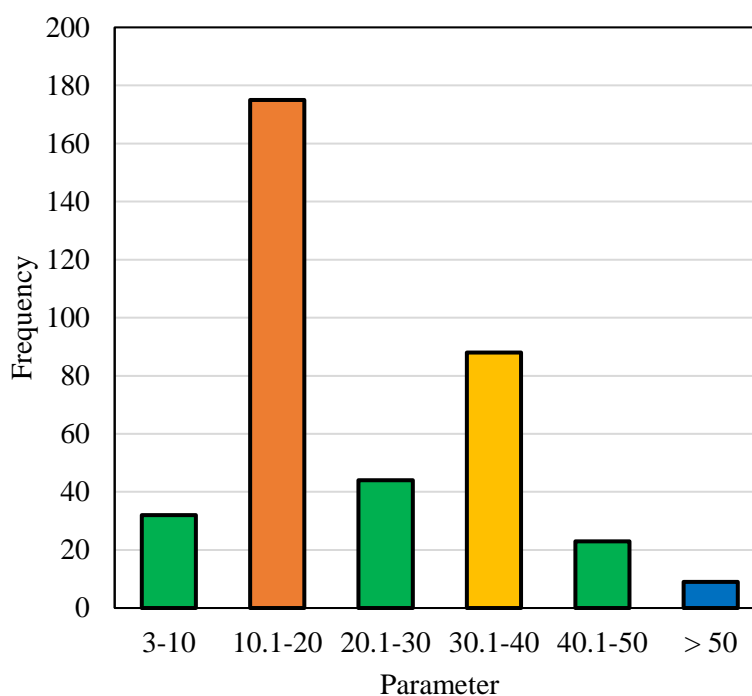
Figure 2. Histogram Example

Boxplots are important statistical analysis tools that can reveal much information about the data available. The boxplots can be used to determine how well the data is distributed. A common boxplot, such as the ones generated in this study, can be divided into five main components. The top part of the boxplot represents the maximum value found in all of the data points, whereas the bottom part represents the minimum value. The top box represents the third quartile range (75th percentile), while the bottom box represents the first quartile range (25th percentile). The middle line represents the median value, or the second quartile range (50th percentile). The cross mark points out the mean value of the data points. Boxplots for the CO_2 injection pressure, porous media temperature, oil properties, and CO_2 solubility and oil swelling have been generated in this research. Figure 3 shows an illustration of a boxplot and all the important sections within it.
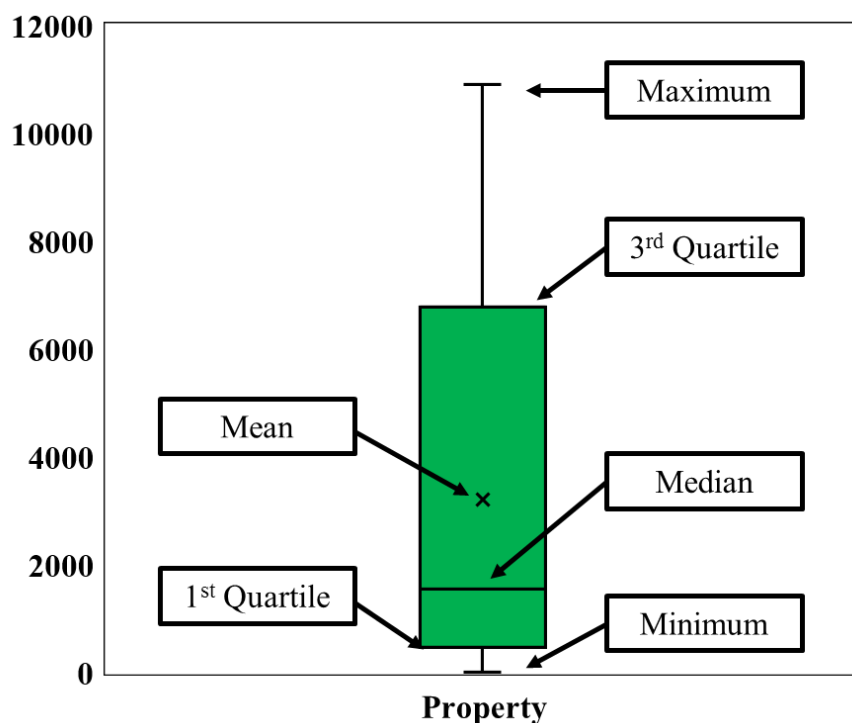
Figure 3. Boxplot Example

Crossplots are plots that relate one parameter to the other or attempts to illustrate or determine a relation between two, or more, parameters. A general trend can be observed in a crossplot, and sometimes a relation or mathematical model can be generated if enough data is utilized. This research generates four crossplots in an attempt to relate oil swelling and carbon dioxide solubility to both pressure and temperature.

2.2. METHODOLOGY

After the data was collected, a data set was created and then the data was processed by converting the units for all the values, determining and removing outliers, and plotting histograms, boxplots, and crossplots to reveal several relations between the variables. Table 1 summarizes all the histograms, and boxplots that were generated, and the units used for each studied factor.

Table 1. Summary of All Plots Generated

Factor	Units	Histogram	Boxplot
Pressure	psi	x	x
Temperature	^{0} C	x	x
Oil MW	g/mol	x	x
Oil Viscosity	cp	x	x
Oil API Gravity	^{0} API	x	x
CO$_2$ Solubility	mol fraction ($\frac{mol}{mol}$)	x	x
Oil Swelling	ml/ml	x	x

Four crossplots were also generated using the data; these include pressure and temperature vs both CO_2 solubility and oil swelling respectively. The histograms, boxplots, and crossplots will all be presented in this research and the significance of each plot will be explained.

3. RESULTS AND ANALYSIS

3.1. PRESSURE AND TEMPERATURE HISTOGRAMS

The CO_2 injection pressure and the reservoir temperature are two extremely important factors that will impact the CO_2 dissolution in the oil, and also the oil swelling, and thus will impact the productivity of the immiscible CO_2 injection process. As the reservoir temperature increases, the CO_2 solubility in the oil will decrease due to the increase in the activity of the gas molecules which will result in a tendency of the molecules to liberate from solution rather than become soluble in the oil [29,30]. This decrease in solubility will result in a lower oil swelling, which in turn will result in a decrease in oil recovery due to the decrease in the interaction of the CO_2 with the oil. Increasing the CO_2 injection pressure on the other hand will result in an increase in the CO_2 solubility, and thus an increase in the CO_2 interaction with the oil. This is due to the gas molecules being compressed into a smaller volume and thus will tend to solubilize in the oil. Increasing the pressure to an extremely high value will eventually result in the CO_2 becoming miscible in the oil [31,32]. Therefore, for immiscible CO_2 injection, a lower reservoir temperature, and a higher CO_2 injection pressure is more favorable, as long as the pressure remains beneath the miscibility pressure, and the formation fracture pressure.

The histograms for both the temperature and the pressure are shown in Figure 4. The highest frequency range is depicted in orange, the second highest is depicted in yellow, and the lowest frequency range is depicted in blue. The highest frequency range for the temperature histogram was between 20-30 ^{o}C, which is due to the higher CO_2 solubility at lower temperatures, as was explained before. The second highest was between 41-50 ^{o}C which is considered a medium temperature range; this range has a high frequency since CO_2 is usually preferred in its supercritical phase due to its advantageous properties at this phase. Supercritical CO_2 occurs at approximately 31.4 ^{o}C, and 1071 psi and thus this temperature range also had a high frequency. The highest frequency range of pressures occurred at pressures ranging from 10 to 500 psi and pressures between 501 and 1100 psi.
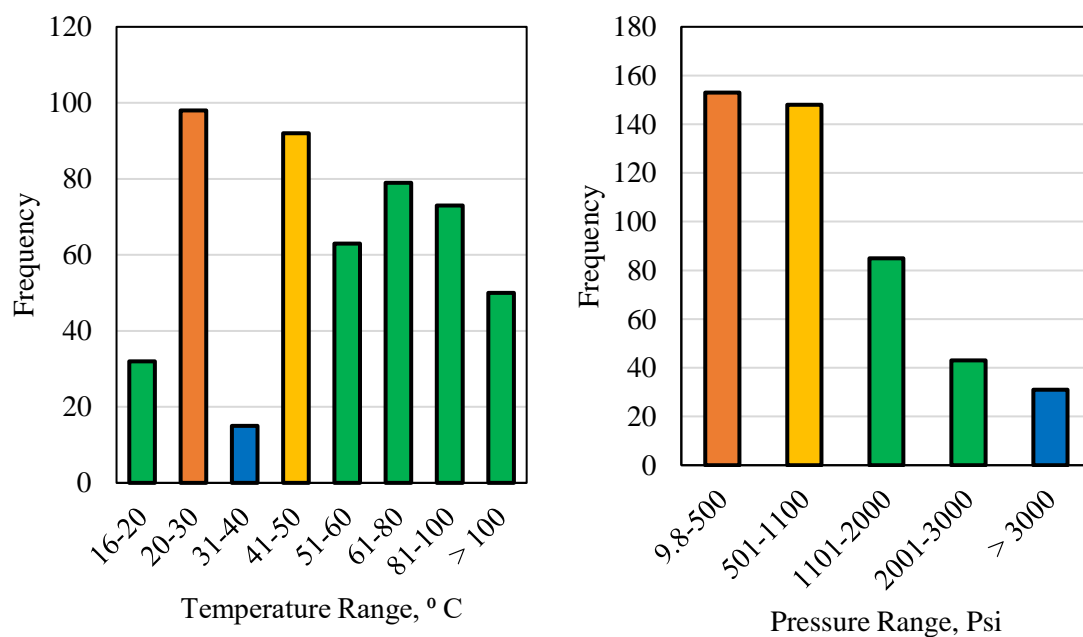
Figure 4. Temperature and Pressure Histograms

The majority of the values were near the 500 psi and 1100 psi, with most of the data coming from experimental results. The lower pressure ranges were tested more frequently due to most of the experiments testing immiscible CO_2 injection, and thus most of the researches tried to prevent the CO_2 from being miscible or partially miscible and thus lower pressures were preferred. The researches that used high pressures used crude oil with extremely high viscosity and thus miscibility was extremely difficult to reach. The range between 500 and 1100 psi was also very frequent, with most of the values in this range being close to the 1100 psi to ensure the CO_2 was in the supercritical state.

3.2. OIL PROPERTIES HISTOGRAMS

Histograms for three oil properties were generated in this research, including oil MW, oil viscosity, and oil API gravity. Figure 5 shows the histograms for both the oil MW and the oil viscosity. The highest oil MW frequency was found to be the oil MW above 500 g/mol. This is mainly due to the immiscible CO_2 injection becoming a common research direction and field implementation in heavy oil reservoirs due to its potential to increase oil recovery, and its lower cost and higher applications compared to thermal methods such as steam injection [33-35]. The highest frequency oil viscosity range was found to be between 100-500 cp, which complements the results for the oil MW since in this range the oil is classified as heavy oil, based on the definition of heavy oil provided by Gao, C. et al. [15] who defined heavy oil as having a viscosity greater than 100 cp. The definition of heavy crude oil can vary significantly from one reference to the other however and thus should be taken based on the conditions of the study and must be defined in each study to avoid confusion.
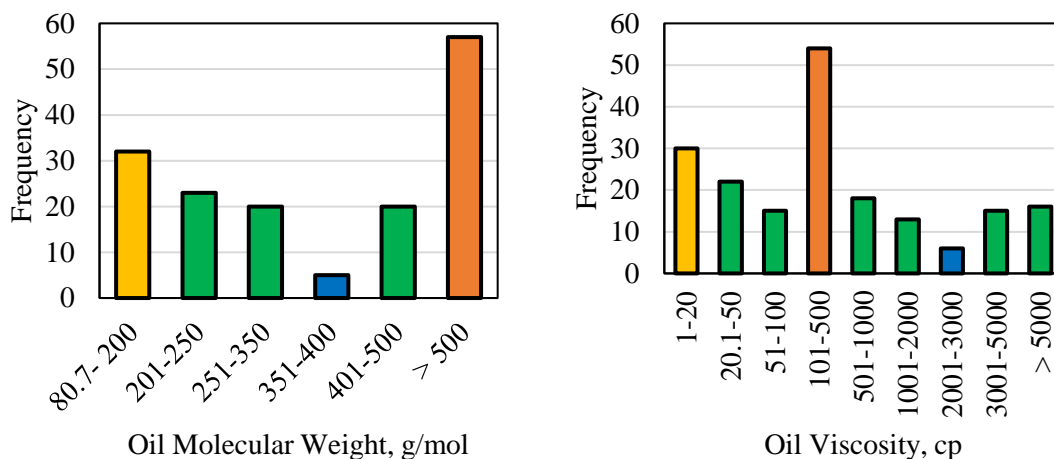
Figure 5. Oil MW and Oil Viscosity Histograms

The histogram showing the oil API gravity is represented in Figure 6. The highest frequency oil API gravity was in the range between 10.1-20 ⁰API, while the second highest frequency was between 30.1-40 ⁰API, both of which fall under the classification of heavy oil, above 10 ⁰API [15]. These results indicate that immiscible CO_2 injection has a high potential to produce from heavy oil reservoirs.
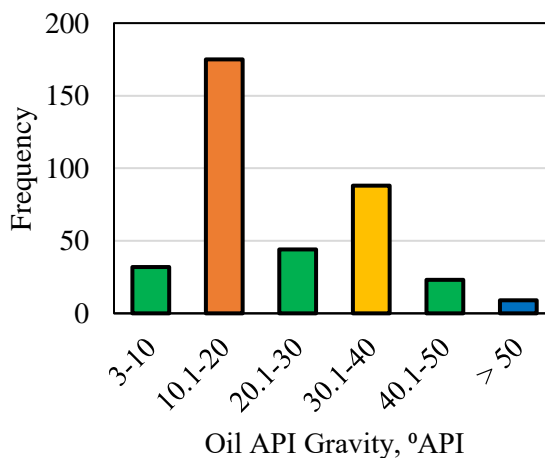
Figure 6. Oil API Gravity Histogram

3.3. SOLUBILITY AND SWELLING HISTOGRAMS

The interaction of CO_2 with the crude oil was also studied in this data analysis by generating histograms for both CO_2 solubility, and oil swelling, shown in Figure 7. The highest frequency for the CO_2 solubility was found to be the 0-0.1 mol/mol, while the highest frequency for the oil swelling was 1-1.1 ml/ml, both of which were the lowest ranges in the histograms. This can be explained through the CO_2 injection pressure histogram in Figure 4, where most of the application for immiscible CO_2 injections were found at the lowest pressure range, and since both CO_2 solubility and oil swelling are a strong function of injection pressure, the lowest ranges for both were found to be the ones with the highest frequency. This could be due to the researches being focused on immiscible CO_2 injection based on the results presented in Figure 5.
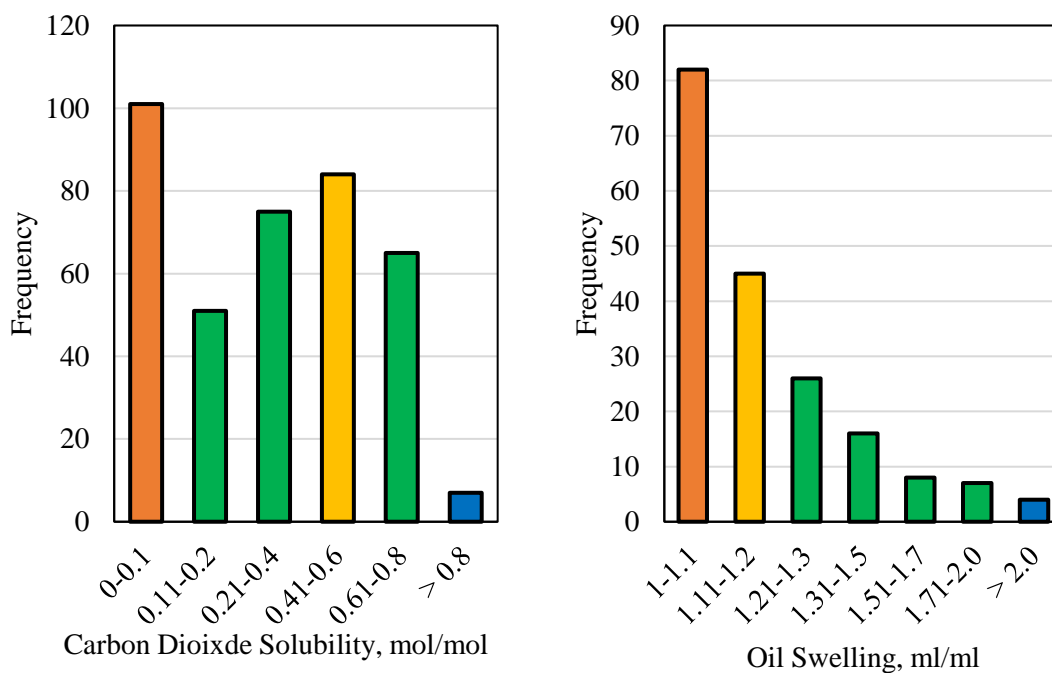
Figure 7. CO_2 Solubility and Oil Swelling Histograms

3.4. PRESSURE AND TEMPERATURE BOXPLOTS

The boxplots for both the CO_2 injection pressure and the temperature are shown in Figure 8. The maximum pressure used was 5000 psi, which is considered extremely high. This pressure was used for bitumen since, even at this high of a pressure, the CO_2 was not miscible. The lowest pressure used was close to 10 psig, equivalent to 24.7 psia. The highest temperature used was 315 ⁰C, whereas the lowest used was 16 ⁰C. For both boxplots, the distribution of the data in the first quartile range was much better than in the third quartile range, which is evident from the size of the rectangles within the boxplot. The median value was closer to the first quartile range which signifies than the majority of the data was closer to the lower values, which was the same conclusion observed from the histograms in Figure 4.
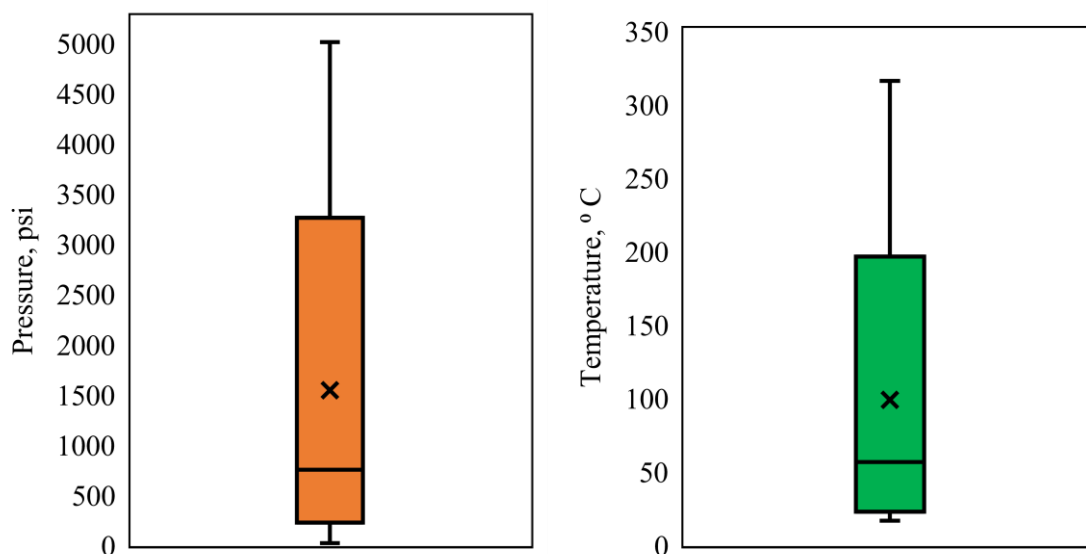
Figure 8. Pressure and Temperature Boxplots

3.5. OIL PROPERTIES BOXPLOTS

The boxplots for the oil MW and viscosity are shown in Figure 9. The boxplot for the oil MW shows no maximum value bar since the maximum value was integrated within the third quartile range due to the distribution of the data being extremely well. The minimum MW observed was 80 g/mol. The median value is much closer to the third quartile range since the majority of the data points were within this range, which is evident from the histogram shown in Figure 5. The oil viscosity boxplot shows an opposite trend with the median and the first quartile range being almost unnoticeable. This is due to the maximum frequency being extremely close to the median, with the majority of the data points closer to the first quartile range. The maximum viscosity observed was 23000 cp, which was for the bitumen. Figure 10 shows the boxplot for the oil API gravity. The maximum value recorded was close to 80 ºAPI, which signifies a very light oil, while the minimum was 3 ºAPI. The median value is closer to the first quartile range due to the highest frequency of data being close to that range.
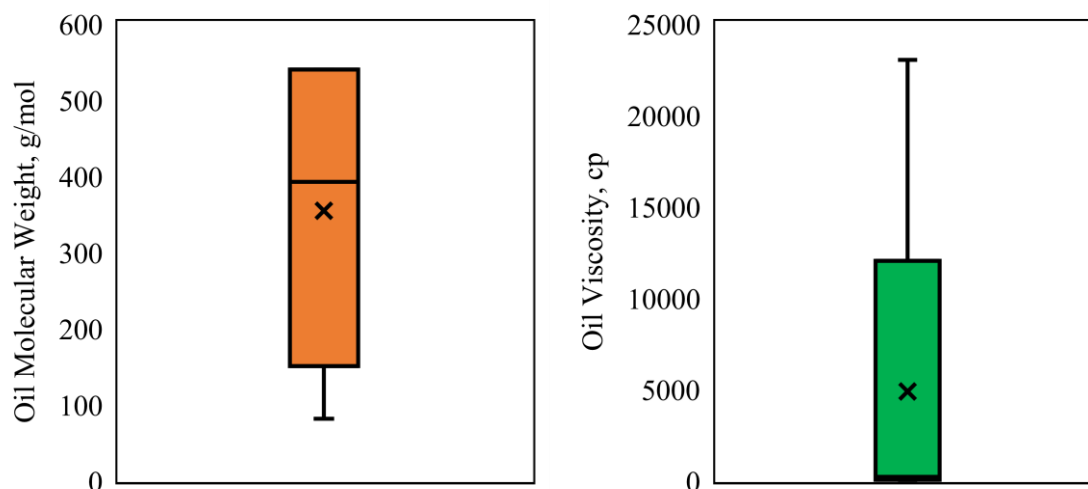
Figure 9. Oil Molecuar Weight and Oil Viscosity Boxplots
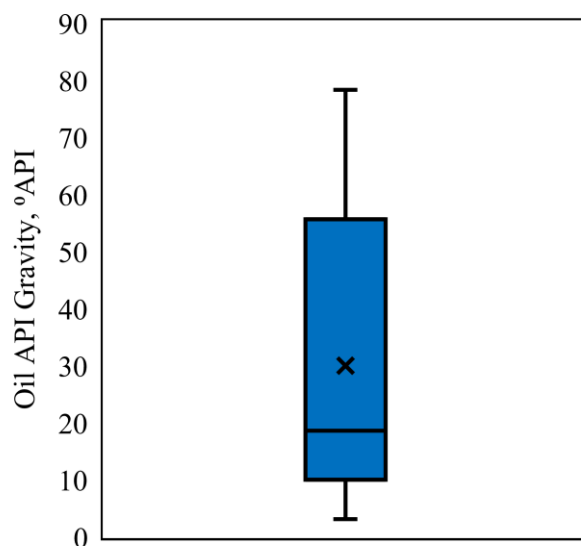
Figure 10. Oil API Gravity Boxplot

3.6. SOLUBILITY AND OIL SWELLING BOXPLOTS

The solubility and oil swelling boxplots are shown in Figure 11. The CO_2 solubility shows an almost symmetrical boxplot, which may signify that the data points are very closely distributed. This can be clearly seen in the CO_2 solubility histogram in Figure 7 where most of the peaks are extremely close in value. The highest solubility recorded was close to 1, which signifies that most of the CO_2 was soluble in the oil; this is a strong indication that miscibility was almost achieved at that point. The oil swelling boxplot shows a maximum swelling of 2.2, which is considered an extremely high value, and a minimum swelling of 1, which indicates no swelling. The median value is closer to the first quartile range since this is where the maximum frequency was observed in the histogram, Figure 7.
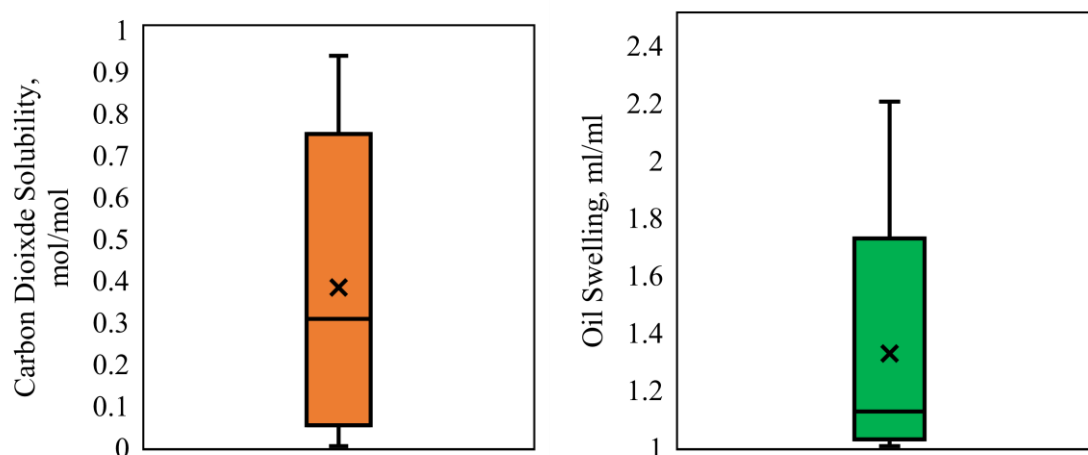
Figure 11. CO_2 Solubility and Oil Swelling Boxplots

3.7. CROSSPLOTS

Four crossplots were generated in this research to study the impact of CO_2 injection

pressure and porous media temperature on CO_2 solubility and oil swelling. Figure 12 shows

the effect of pressure and temperature on CO_2 solubility. The blue data points were found

to be outliers. For the CO_2 solubility versus pressure plot, the data points show a trend of

increasing solubility with pressure. This shows that as the CO_2 injection pressure increases,

the solubility of the CO_2 in the oil will also increase, which is the same conclusion reached

by most researchers. The plot showing CO_2 solubility versus temperature shows no obvious

trend, however, at the highest temperatures, almost all the data points show a very low CO_2

solubility, which is what most researchers also observed as the temperature increased. For

example, at 150, and 190 ºC, all of the data points show a solubility of less than 0.05

mol/mol. The effect of pressure and temperature on oil swelling is shown in Figure 13.

The blue data points represent outliers. As was stated eariler, as the CO_2 injection pressure

increases, the oil swelling will increase as well. This is the same trend that can be observed

in the plot showing oil swelling versus pressures. Regarding oil swelling versus temperature, the general trend shows a decrease in oil swelling with the increase in temperature, which is identical to what was explained previously.
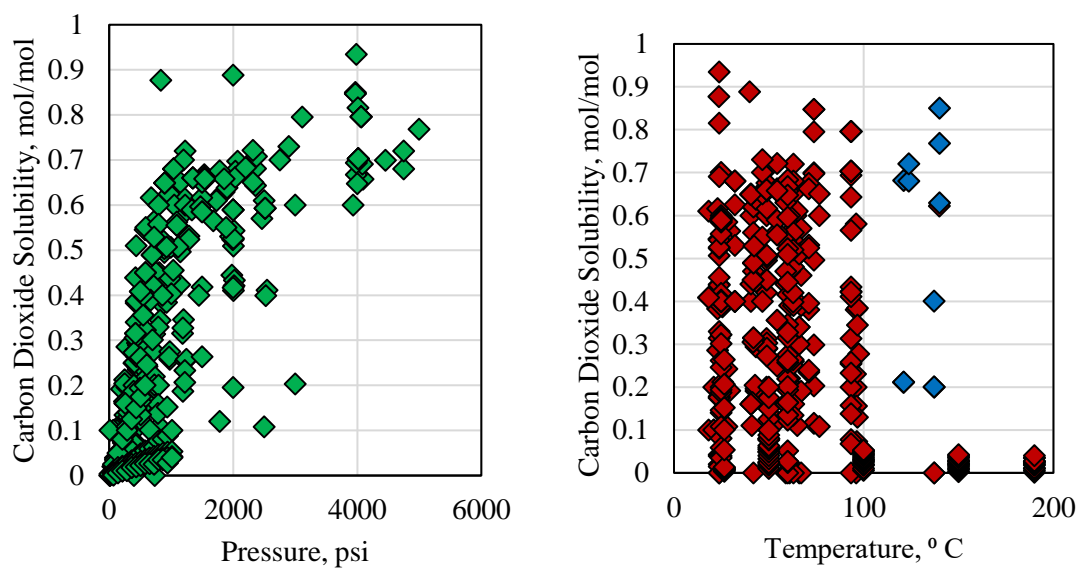
Figure 12. Effect of Pressure and Temperature on CO_2 Solubility
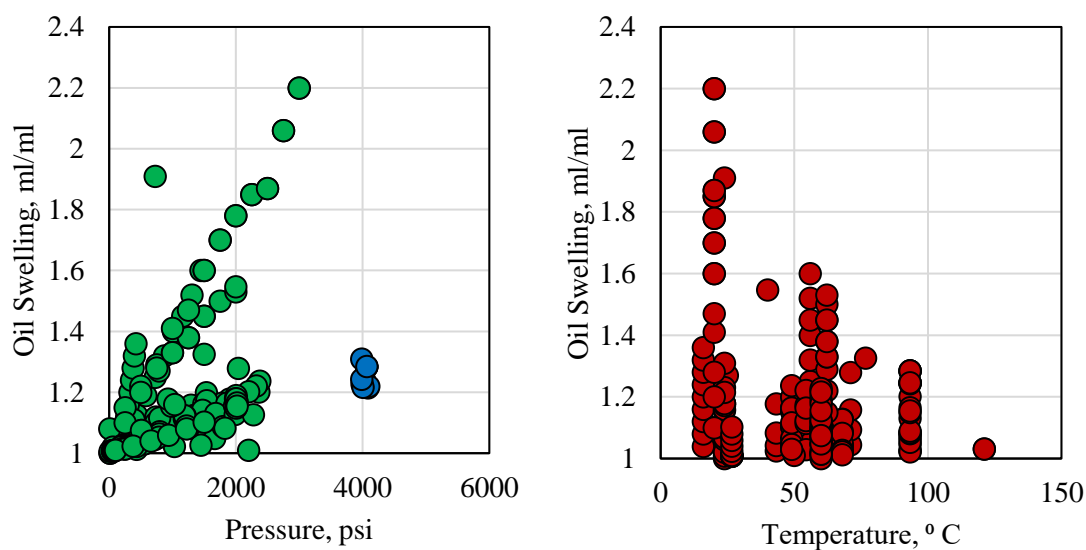
Figure 13. Effect of Pressure and Temperature on Oil Swelling

4. CONCLUSIONS

This research performs a data analysis based on hundreds of experimental, simulation, and field data to generate multiple histograms, boxplots, and crossplots in order to determine the data distribution and most frequent data range found for immiscible CO_2 injection. The main findings from this research are summarized as follows:

- Oil swelling is one of the main mechanisms that occurs during immiscible CO_2 injection, and is dependent on CO_2 solubility. Many factors will impact oil swelling including reservoir thermodynamic, rock, and fluid properties.

- Based on the data analysis performed, most of the data shows that lower pressures and low temperatures were used during immiscible CO_2 injection. This was to avoid miscibility of CO_2 since the main focus was immiscible CO_2.

- Based on the oil properties data analysis, immiscible CO_2 has been used to produce from heavy oil, since the histograms showed the highest frequencies in the heavy oil zone.

- Crossplots generated showed that CO_2 solubility, and oil swelling are highly dependent on the CO_2 injection pressure, and the reservoir temperature.

ACKNOWLEDGEMENTS

REFERENCES

Al-Jarba, M. and Al-anazi, B. D., 2009. A Comparison Study of the CO_2-Oil Physical properties Literature Correlations Accuracy Using Visual Basic Modelling Technique. NAFTA Journal. 287-291.

Al-Murayri, M. T. et al., 2011. Solubility Of Methane, Nitrogen, and Carbon Dioxide in Bitumen and Water for SAGD Modelling. Society of Petroleum Engineers. doi:10.2118/148630-PA.

Bahralolom, I. M. and Orr Jr, F. M., 1988. Solubility and Extraction in Multiple-Contact Miscible Displacements: Comparison of N2 and CO2 Flow Visualization Experiments. Society of Petroleum Engineers. doi:10.2118/15079-PA.

Barclay, T. H. and Mishra, S., 2016. New Correlations for CO_2-Oil Solubility and Viscosity Reduction for Light Oils. Journal of Petroleum Exploration Production Technology, Springer. 815-823.

Beeson, D. M. and Ortloff, G. D., 1959. Laboratory Investigation of the Water-Driven Carbon Dioxide Process for Oil Recovery. Society of Petroleum Engineers. doi:10.2118/1100-G.

DeRuiter, R. A. et al., 1994. Solubility and Displacement Behavior of a Viscous Crude With CO2 and Hydrocarbon Gases. Society of Petroleum Engineers. doi:10.2118/20523-PA.

Fakher, S. and Imqam, A., 2018a. Asphaltene Precipitation and Deposition during CO_2 Injection in Nano Shale Pore Structure and Its Impact on Oil Recovery. Fuel Journal, El-Sevier. 1029-1039. doi.org/10.1016/j.fuel.2018.10.039.

Fakher, S. and Imqam, A., 2018b. Investigating and Mitigating Asphaltene Precipitation and Deposition in Low Permeability Oil Reservoirs During Carbon Dioxide Flooding to Increase Oil Recovery. Society of Petroleum Engineers. doi:10.2118/192558-MS.

Farias, M. and Watson, R., 2007. Interaction of Nitrogen/CO_2 Mixtures with Crude Oil. Final Report to Department of Energy, Pennsylvania State University, Department of Energy and Geo-Environmental Engineering.

Gao, C. et al., 2013. Heavy Oil Production by Carbon Dioxide Injection. Greenhouse Gases Science and Technology Journal, Society of Chemical Industry and John Wiley & Sons. 185-195.

Hatzignatiou, D. G. and Lu, Y., 1994. Feasibility Study of CO2 Immiscible Displacement Process In Heavy Oil Reservoirs. Petroleum Society of Canada. doi:10.2118/94-90.

Henni, A. and Mather, A. E., 1999. Solubility of CO, NO, CH, And CH In Polar Solvents. Petroleum Society of Canada. doi:10.2118/99-13-25.

Holm, L. and Josendal, V. A., 1974. Mechanisms of Oil Displacement By Carbon Dioxide. Society of Petroleum Engineers. doi:10.2118/4736-PA.

Honarpour, M. M. et al., 2010. Rock-Fluid Characterization for Miscible CO2 Injection: Residual Oil Zone, Seminole Field, Permian Basin. Society of Petroleum Engineers. doi:10.2118/133089-MS.

Kang, S. et al., 2013. Scientific Research and Field Application of CO Immiscible Flooding in Heavy Oil Recovery. Society of Petroleum Engineers. doi:10.2118/165210-MS.

Klins, M.A. and Ali, S.M.F, 1982. Heavy Oil Production by Carbon Dioxide Injection. Society of Petroleum Engineers. Journal of Canadian Petroleum Technology 1982. doi:10.2118/82-05-06.

Martin, D. and Taber, J., 1992. Carbon Dioxide Flooding. Society of Petroleum Engineers. doi:10.2118/23564-PA.

Mullken, C.A. and Sandler, S.I. 1980. The Prediction of CO_2 Solubility and Swelling Factors for Enhanced Oil Recovery. Ind. Eng. Chem. Process Des. Dev. 19, 709-711.

Norouzi, H. et al., 2018. Analysis of Secondary and Tertiary High-Pressure Gas Injection at Different Miscibility Conditions: Mechanistic Study. Society of Petroleum Engineers. doi:10.2118/191119-PA.

Nourozieh, H. et al., 2016. Measurement and Correlation of Solubility and Physical Properties for Gas-Saturated Athabasca Bitumen. Society of Petroleum Engineers. doi:10.2118/176016-PA.

Pacheco-Roman, F. J. and Hejazi, S. H., 2015. Estimation of Solubility and Diffusivity of Gases in Heavy Oils by Use of Late-Time Pressure-Decay Data: An Analytical/Graphical Approach. Society of Petroleum Engineers. doi:10.2118/170957-PA.

Rostami, A. et al., 2017. Modeling of CO_2 Solubility in Crude Oil During Carbon Dioxide Enhanced Oil Recovery Using Gene Expression Programming. Fuel Journal, El Sevier. 768-782.

Sasaki, K. et al., 2013. CO_2 Solubility Characteristics of Crude Oils Related to Carbon Capture and utilization (CCU). Novel Carbon Resource Sciences Newsletter, 1-8.

Shokoya, O. et al., 2002. Evaluation of the Miscibility and Contribution of Flue Gas to Oil Recovery Under High Pressure Air Injection. Petroleum Society of Canada. doi:10.2118/02-10-03.

Silva, M. K. and Orr Jr, F. M., 1987. Effect of Oil Composition on Minimum Miscibility Pressure-Part 1: Solubility of Hydrocarbons in Dense CO2. Society of Petroleum Engineers. doi:10.2118/14149-PA.

Sugai, Y. et al., 2014. Consideration of an Effect of Interfacial Area between Oil and CO_2 on Oil Swelling. Journal of Petroleum Exploration Production Technology, Springer. 105-112.

Svrcek, W. Y. and Mehrotra, A. K., 1982. Gas Solubility, Viscosity And Density Measurements For Athabasca Bitumen. Petroleum Society of Canada. doi:10.2118/82-04-02.

Svrcek, W. Y. and Mehrotra, A. K., 1989. Properties Of Peace River Bitumen Saturated With Field Gas Mixtures. Petroleum Society of Canada. doi:10.2118/89-02-01.

Vali, J. et al., 2011. A Fast and Simple Method for Modeling of Oil Swelling in CO_2 Injection. JGeope Journal. 39-46.

Yang, C. and Gu, Y., 2004. Visualization of Interfacial Interactions of Crude Oil-CO2 Systems under Reservoir Conditions. Society of Petroleum Engineers. doi:10.2118/89366-MS.

Yang, C. and Gu, Y., 2006. Diffusion Coefficients and Oil Swelling Factors of Carbon Dioxide, Methane, Ethane, Propane, and Their Mixtures in Heavy Oil. Fluid Phase Equilibria Journal, El Sevier, 64-73.

Yang, C., and Gu, Y., 2007. A Novel Experimental Technique for Studying Solvent Mass Transfer and Oil-Swelling Effect in the Vapour Extraction (VAPEX) Process. Petroleum Society of Canada. doi:10.2118/07-09-04.

Yin, M., 2015. CO_2 Miscible Flooding Application and Screening Criteria. Masters Thesis, Petroleum Engineering Department, Missouri University of Science and Technology.

Yongmao, H. et al., 2004. Laboratory Investigation of CO2 Flooding. Society of Petroleum Engineers. doi:10.2118/88883-MS.

Zhang, Y. P. et al., 2006. Laboratory Investigation of Enhanced Light-Oil Recovery By CO_2/Flue Gas Huff-n-Puff Process. Petroleum Society of Canada. doi:10.2118/06-02-01.

VII. A SIMPLIFIED METHOD FOR EXPERIMENTALLY QUANTIFYING CRUDE OIL SWELLING DURING IMMISCIBLE CARBON DIOXIDE INJECTION

ABSTRACT

Immiscible carbon dioxide (CO_2) injection is one of the highly applied enhanced oil recovery (EOR) methods due to its high oil recovery potential and its ability to store CO_2 in the reservoir. The main mechanism of immiscible CO_2 injection is oil swelling. Generally, oil swelling is measured experimentally, or measured using modelling methods. This research conducts oil swelling experiments using a simplified method in order to easily and accurately measure oil swelling and determines some of the most significant factors that may impact oil swelling during CO_2 injection. The impact of varying CO_2 injection pressure, temperature, oil viscosity, and oil volume on oil swelling capacity was investigated. The simplified method managed to accurately determine the value of oil swelling for all the experiments. One of the factors that was found to impact the method significantly was the oil volume used. The oil volume in the experimental vessel was found to be extremely important since a large oil volume may result in a false oil swelling value. The oil swelling results were compared to other researches and showed that the method applied had an accuracy of over 90% for all the results obtained. This research introduces a simple method that can be used to measure oil swelling and applies this method to investigate some of the factors that may impact the oil swelling capacity during immiscible CO_2 injection.

1. INTRODUCTION

Carbon dioxide injection is currently one of many applied EOR techniques due to its multiple advantages, including its ability to increase oil recovery and its potential for carbon storage in the hydrocarbon reservoirs (Fakher, S. et al., 2017; 2018; 2019a; 2019b; Martin, F.D. and Taber, J.J., 1992; Verma, M., 2015; Perera, M. et al., 2016; Fakher, S., 2019). CO_2 can be either miscible or immiscible with the reservoir hydrocarbons based on the reservoir conditions and properties and the CO_2 properties and injection procedure (Fakher, S. and Imqam, A., 2018;2019;2020a;2020b). Immiscible CO_2 injection has currently gained much attention due to its ability to increase oil recovery from several types of oil reservoirs, including heavy oil reservoirs (Nourozieh, H. et al., 2016; Fakher, S.M., 2019). The main mechanism by which immiscible CO_2 injection can increase oil recovery is oil swelling (Fakher, S. et al., 2018;2019). During this interaction, the CO_2 partially dissolves in the crude oil and thus results in an increase in the volume of the crude oil due to CO_2 dissolution.

Multiple studies have conducted analytical, simulation, and computer modeling to investigate CO_2 injection's impact on oil swelling. Zhang, F. et al. (2019) underwent a numerical study to investigate the mechanism of CO_2 in unconventional reservoirs. Rostami, A. et al. (2017) utilized Gene Expression Programming to develop a novel correlation used to determine CO_2 swelling in oil as a function of oil MW, oil specific gravity, reservoir temperature, bubble point pressure, and saturation pressure. Richardson, W. et al (2019) and Ratnakar, R.R. and Dindoruk, B. (2020) studied the diffusivity of the gas in crude oil and its impact on oil recovery. Klins, M.A. and Ali, S.M.F. (1982)

performed a simulation study using a black oil model modified for CO_2 injection to investigate the impact of immiscible CO_2 injection on oil recovery. Barclay, T.H. and Mishra, S. (2016) developed novel empirical correlations for CO_2 solubility in crude oil and for oil viscosity reduction due to CO_2 saturation. Al-Jarba, M. and Al-Anazi, B.D. (2009) used a visual basic modelling technique to study the CO_2-oil physical properties. Mullken, C.A. and Sandler, S.I. attempted to develop an analytical equation of state based on the Peng-Robinson equation of state to characterize the oil and CO_2-oil binary interaction. Pacheco-Roman, F.J. and Hejazi, S.H. (2015) used a numerical method to predict the solubility and diffusivity of multiple gases in different heavy crude oils using a novel method based on delayed time and pressure decay data based on an analytical and graphical representation.

Several experiments have been conducted to study CO_2 interaction with oil and its ability to increase oil recovery during immiscible CO_2 injection (Tran, S. et al., 2019; Hao, H. et al., 2019; Alharthy, N. et al., 2018; Mahzari, P. et al., 2019; Sanaei, A. et al., 2018; Fakher, S. and Imqam, A., 2020c; 2020d; 2020e; Hoffman, B.T. and Rutledge, J.M., 2019). Svrcek, W.Y. and Mehrotra, A.K. (1982; 1989) performed experiments on extremely high molecular weight (MW) bitumen to investigate the impact of the CO_2 altering the bitumen's viscosity and density. Wang, M. et al (2019) introcuded new wettability modifiers in an attempt to increase oil recovery from low permeability reservoirs. Holm, L.W. and Josendal, V.A. (1974) provided an overview of the main differences between miscible and immiscible CO_2 injection. Yang, C. and Gu, Y. (2006) developed a modified experimental setup based on the Dynamic Pendant Drop Volume Analysis Method to measure the solvent diffusion coefficient and oil-swelling factor of a heavy oil using

propane as the solvent. Pourafshary, P. et al (2019) investigated the impact of the water to CO_2 ratio on the performance of CO_2 EOR in sandstone cores using both core flooding experiments and reservoir simulation. Sugai, Y. et al. (2014) studied the impact of surface interfacial area, capillary pressure, and grain size on oil swelling during CO_2 injection. They used a modified Pendant Drop Method setup, and an image analysis software to study the impact of these parameters. Ahmed, S. et al. (2018) underwent an advanced screening and optimization experimental study on the use of CO_2 Foam for EOR application. Silva, M.K. and Orr Jr., F.M. (1987) showed that as the MW of the oil increases, the CO_2 solubility decreases. Bahralolom, I. M. and Orr Jr., F.M. (1988) investigated the solubility of both CO_2 and nitrogen in crude oil using flow visualization experiments to assess the importance of solubility and extraction on the overall oil recovery. All the methods mentioned previously have been shown to have a good accuracy; however, a simpler method that requires less timely and tedious equipment can prove to be very useful when precise equipment is lacking or when a fast and accurate value for oil swelling is need.

Even though many researchers have conducted experiments to measure oil swelling, very little research has attempted to systematically investigate the factors that have a strong impact on oil swelling during CO_2 injection and then quantify the impact of these factors. Also, most of the methods used in the literature are dependent on the observation of the volume change using specific experimental setups. This research introduces a simple method to measure oil swelling experimentally without the use of complex equipment, compared to the more complex and commonplace methods used in the literature. The accuracy of the method applied in this research was verified by comparing the results obtained to results obtained from several studies that were conducted

on oil swelling. This research therefore introduces a simple method that can accurately measure oil swelling experimentally and investigates some of the main factors that may impact oil swelling during CO_2, injection including CO_2 injection pressure, temperature, crude oil viscosity, and oil volume in the experimental vessel.

2. BACKGROUND ON THE MECHANISM OF OIL SWELLING

Immiscible CO_2 injection differs from miscible CO_2 injection in terms of its interaction with crude oil. During immiscible CO_2 injection, the CO_2 will partially dissolve in the crude oil depending on the thermodynamic conditions, the oil properties, and the CO_2 properties. This dissolution will result in the oil volume increase, or oil swelling. Even though a volume of the CO_2 dissolves in the crude oil, there is still interfacial tension between the oil and the CO_2 that is hindering part of the CO_2 to dissolve. During miscible CO_2 injection, the interfacial tension between the CO_2 and the crude oil is eliminated (Norouzi, H. et al., 2019). The CO_2 will therefore completely dissolve in the crude oil regardless of either fluid's volume. Both fluids will therefore become one single phase. The single phase will have an overall larger volume than either phase alone, however, it cannot be defined as oil swelling in the same manner as immiscible CO_2 since the fluid is no longer oil phase, but a phase composed of both the oil and the CO_2 together.

When CO_2 is injected into the porous media bearing crude oil, the CO_2 will begin to interact with the oil. Based on the thermodynamic conditions, including pressure and temperature, and the oil properties, the CO_2 will begin to solubilize in the crude oil (Mullken, C.A. and Sandler, S.I., 1980). This solubility will result in an increase in the

volume of the oil, which is referred to as oil swelling. Oil swelling can affect oil recovery significantly through many mechanisms, including mobilizing the residual oil (Hatzignatiou, D.G. and Lu, Y., 1994), increasing the relative permeability of the oil by increasing the oil volume (Yang, C. and Gu, Y., 2006), and increasing the mobility of the oil through small capillaries (Tran, T.Q., 2014; Du, F., 2016). The main advantages that oil swelling will provide during oil recovery can be summarized as follows.

- **Crude Oil Viscosity Reduction:** When the CO_2 dissolves in the oil, the volume of the oil will increase. This will result in a significant reduction in oil viscosity (Gao, C. et al., 2013). The viscosity reduction potential will increase with the increase in CO_2 injection pressure and will decrease with the increase in temperature (Svrcek, W.Y. and Mehrotra, A.K., 1982; Mohtahhari, H. et al., 2013). A viscosity reduction of up to 90% has been reported in many cases during immiscible CO_2 injection (Kang, S. et al., 2013).

- **Interfacial Tension Reduction:** Immiscible CO_2 injection has been shown to reduce interfacial tension (IFT) between the CO_2 and water, and CO_2 and oil significantly in the reservoir (Gao, C. et al., 2013). The main IFT reduction mechanism is through CO_2 solubility in the oil, especially at elevated pressures, which creates a reduction in the IFT; however, it is not reduced to zero since the CO_2 is not miscible in the oil (Maneeintr, K. et al., 2014).

- **Blowdown Recovery:** After CO_2 injection is ceased and the CO_2 dissolves in the oil, production is resumed. During production, the CO_2 dissolved in the oil will begin to liberate or come out of solution. This mechanism can result in an increase

in oil recovery, reaching up to 18.6% in some cases (Klins, M.A. and Ali, S.M.F., 1982; Gao, C. et al., 2013).

- **Oil Relative Permeability Improvement:** Since oil swelling increases the volume of the oil phase in the reservoir, the relative permeability of the oil will also increase. This can help in the mobilization of the oil, and thus can improve oil recovery significantly.

- **Improved Oil Mobility:** By reducing the oil viscosity in the reservoir, the mobility of the oil is improved, since the mobility can be defined as the permeability of the oil phase divided by the oil viscosity.

3. EXPERIMENTAL MATERIAL

3.1. CRUDE OIL

Crude oil with viscosity ranging between 470 and 67 cp was used to conduct the experiments. The composition of the crude oil was determined using Gas Chromatography-Mass Spectrometry and is shown in Table 1.

Table 1. Crude Oil Composition and Asphaltene Concentration

Component	Weight Percentage, %
C1-C5	9.37
C6-C10	14.74
C11-C15	18.89
C16-C20	19.31
C21-C30	11.63
C30+	26.06

3.2. WATER BATH

A large volume water bath was used to heat up the vessels and to maintain isothermal conditions. The vessels were completely submerged in the water bath for the duration of each experiment.

3.3. HIGH PRECISION PRESSURE TRANSDUCERS

In order to record the pressure, a high precision transducer was used. The transducer was connected to the setup, and to a computer to log the pressure readings. Four pressure readings were logged every second.

3.4. THERMOMETER

A thermometer was suspended in the water bath to record the temperature of the vessels in the water bath to ensure that the temperature was constant. The experiment was repeated if a change of 0.3 ℃ or more was observed at any time during each experiment.

3.5. DISTILLED WATER

Distilled water was used both as the heating medium in the water bath and to pressurize the CO_2 in the accumulator before injection. The distilled water was displaced via the pump.

3.6. HIGH PRESSURE GAUGE

A pressure gauge was located at the outlet of the accumulator to record the injection pressure of the CO_2 for all experiments.

4. EXPERIMENTAL SETUP

An illustration of the experimental setup used to conduct all experiments is shown in Figure 1. The setup is composed of a syringe pump used to pressurize the CO_2. The CO_2 is housed in the accumulator, where water is injected via the pump to pressurize it. Two high pressure vessels are used to conduct the experiments. One of the vessels is used to heat up the CO_2 to the desired temperature before commencing the experiment. The other vessel houses the crude oil used for the oil swelling experiment.
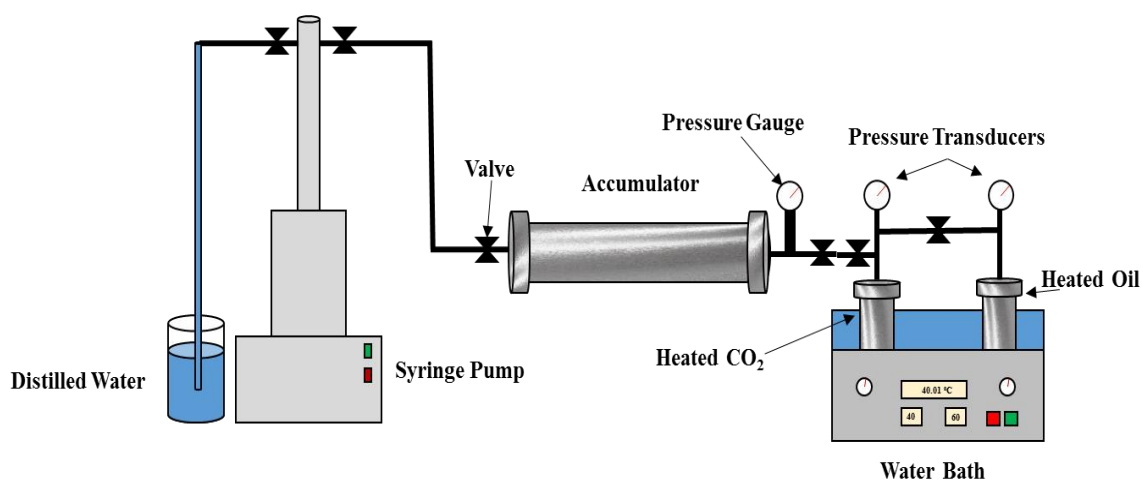
Figure 1. Oil Swelling Experimental Setup

Both vessels are placed in the water bath in order to heat up before beginning the experiment. Once the CO_2 and the oil are heated up, the CO_2 is injected in the oil bearing vessel and the experiment is then started. The pressure transducers are used to record the pressure in the vessels during CO_2 injection and during the oil swelling process. The pressure transducers record the data and digitize them on the computer via electrical cables.

This differs from the pressure gauge which represents the pressure reading via an analog indicator. The pressure transducers allow for the recording of the data for further analysis after the experiments were concluded while the pressure gauge was used mainly to ensure that there was no leakage and no sudden pressure change for the duration of the experiment.

5. EXPERIMENTAL PROCEDURES

The exact procedure followed to conduct all the experiments will be mentioned in this section. Each experiment was repeated at least three times in order to ensure repeatability and accuracy. The exact procedure is mentioned below.

1. Place a predefined volume of crude oil in one of the pressure vessels. Place both cells in the water bath.

2. Vacuum both cells for one hour. For the vessel bearing the crude oil, a mesh screen was placed to avoid the suction of the oil.

3. Pressurize the CO_2 in the accumulator to the design pressure. After pressurizing, inject the CO_2 into the empty pressure vessel and leave it to heat for 6 hours. The CO_2 was heated separately before injection into the crude oil to ensure that the temperature change was not impacting the overall experiment. The CO_2 has an extremely low temperature in the cylinder and thus it was imperative to equate its temperature to that of the experimental vessel before beginning the pressure recording.

4. Inject the CO_2 in the oil-bearing vessel and record the pressure change with time until no pressure change is observed.

5. Once the pressure becomes stable, the initial and final pressures are recorded, and then the experiment is terminated.

6. Perform the oil swelling calculations using the concept of change in volume due to CO_2 solubility in the crude oil. The oil swelling is calculated using the pressure values, and the properties of the oil and the CO_2 at the pressures and temperatures used.

7. Repeat each experiment at least three times and compare the results to ensure that the method used is repeatable and accurate.

6. OIL SWELLING CALCULATION METHODOLOGY

There are many methods by which oil swelling can be calculated. Some methods rely on empirical correlations, whereas others will rely on experimental results that are then analyzed and calculated using the principles of energy and matter conservation. Based on the experimental method implemented, the appropriate equation is applied. The majority of experiments that have been conducted to measure oil swelling relied on visual tests, where the oil can be seen through a transparent sight glass or vessel. However, the method used in this research relies on pressure change, which can then be translated to a volume change using the real gas equation of state. This method is highly advantageous since it requires no tedious calculations, and it also does not need sophisticated equipment in order to run the experiments. The only material needed is actually high pressure vessels and stainless steel connections and tube. The stainless steel material is needed to avoid corrosion which may occur due to the corrosive nature nature of CO_2.

Oil swelling can be simply defined as the ratio of the swelled oil volume to the original oil volume. Its most basic equation, based on the aforementioned definition, therefore becomes as follows:

$$S_o = \frac{V_{so}}{V_{uo}}$$

where S_o is the oil swelling in ml/ml, V_{so} is the volume of the swelled oil in ml, and V_{uo} is the volume of the unswelled oil or the original oil volume in ml.

The volume of the unswelled oil is extremely easy to determine, since it is usually predefined by the researcher before conducting the experiments. The more challenging volume to determine is that of the swelled oil. This experimental method relies on the change in pressure to determine the change in volume. In order to relate both the pressure and volume together, the real gas equation of state is used, as is shown:

$$PV = znRT$$

where P is the pressure of the CO_2, V is the CO_2 volume that occupies the experimental vessel, which is known by knowing the volume of the oil in the vessel and the compressibility of the CO_2, z is the compressibility factor of the CO_2 determined using empirical correlations or charts, n is the number of moles, R is the universal gas constant, and T is the temperature of the experiment.

The equation of state mentioned above must be included twice, both during the initial conditions and during the final conditions of the experiment. Pertaining to the initial conditions, all the variables in the equation of state are known since they are defined before conducting the experiment. Once the experiment is conducted, the final pressure can be recorded, and then by equating the initial and final conditions together, the final CO_2 volume can be determined. The initial and final conditions can be equated since this is a closed system with no losses, and thus by the definition of the first law of thermodynamics, energy cannot be created or destroyed. Therefore. by conservation of both energy and matter, the initial and final conditions can be equated. The equation then becomes:

$$\frac{P_1 V_1}{z_1 n_1 R T_1} = \frac{P_2 V_2}{z_2 n_2 R T_2}$$

where 1 and 2 represent the initial and final conditions for the CO_2 of the experiment, respectively.

The experiments were all conducted under isothermal conditions, and the number of moles does not change due the system being closed. This is especially true due to the extremely low oil volume used. If the oil volume is increased, then the mole change must be accounted for in the calculations. Also, the universal gas constant is a constant, and thus will not change during the experiment. Based on this, the equation can be reduced to the following:

$$\frac{P_1 V_1}{z_1} = \frac{P_2 V_2}{z_2}$$

The unknown variables in the equation are now P_2 and V_2. The pressure is identified using the experiment, and thus the only missing variable is now the V_2, which is the volume of CO_2 after swelling. It can be identified using the following equation:

$$V_2 = \frac{P_1 V_1 z_2}{P_2 z_1}$$

where P_1 is the initial pressure before gas expansion, V_1 is the initial volume of the CO_2, z_2 is the compressibility factor after swelling, which can be obtained from correlations or charts, P_2 is the equilibrium pressure after swelling ceases, and z_1 is the initial compressibility factor.

The above equations are all designed to measure the change in volume of the CO_2. The volume obtained from Equation (5) can then be used to calculate oil swelling using the initial oil swelling calculation shown in Equation (1). This is done by using the above equations and performing mathematical alterations to account for the change in the oil phase volume.

In order to calculate the oil phase volume from the above equations, the final CO_2 volume is used. By knowing the original oil volume, the original CO_2 volume, and the final CO_2 volume, the following equation can then be used to calculate the final oil volume.

$$V_{oil(f)} = \left(\frac{(V_1 + V_{oil(i)}) - (V_2)}{(V_1 + V_{oil(i)}) - (V_1)} \right) \times (V_{oil(i)})$$

where $V_{oil(f)}$ is the final oil volume which is the main unknown needed to calculate oil swelling, $V_{oil(i)}$ is the initial oil volume which is predetermined before undergoing the experiment, and V_1 and V_2 are the initial and final CO_2 volumes one of which is known, and the other is determined using the previous equations.

7. RESULTS AND ANALYSIS

This section will present and explain the results obtained from all the experiments conducted. The results will include the oil swelling values at different CO_2 injection pressures, including 500, 1000, and 1500 psi, temperature using 25, 40, and 60 ⁰C, oil viscosity using 470, 267, and 67 cp, and oil volume using 0.5, 1, and 2 ml. All experiments have been conducted at least three times in order to assess the applicability of the novel method and the repeatability of the results. The average difference between the results of each experiment was less than 10%.

7.1. CARBON DIOXIDE INJECTION PRESSURE EFFECT

The effect of CO_2 injection pressure on oil swelling was investigated using 500, 1000, and 1500 psi CO_2 injection pressures. By using all three pressures, two different phases of CO_2 were investigated, including gas and supercritical CO_2, respectively. The results for the oil swelling at the different CO_2 injection pressures can be seen in Figure 2. Experiments were conducted at 40 ⁰C using 1 ml of crude oil with 470 cp viscosity. Increasing the CO_2 injection pressure resulted in an increase in the oil swelling. This is due to the CO_2 being forced to dissolve in the oil with larger concentrations at higher pressures.

The difference between the oil swelling values, however, is not too large. Also, it was found that the overall oil swelling values are relatively low, with the zero value being 1. This is mainly due to the partial dissolution of the CO_2 in the oil due to the reduction in interfacial tension at the experimental conditions. If the pressure is increased, the oil swelling is expected to increase until a specific limit where the interfacial tension will reach zero. This is the point at which the injection is no longer immiscible, and the mechanism is no longer oil swelling. Rather, the CO_2 will become miscible since the minimum miscibility pressure has been reached. Based on this, the oil swelling values are usually considerably low to avoid reaching miscibility, thus focusing on immiscible CO_2 injection. The difference between the 1000 and 1500 psi is also observed to be lower than that between the 500 and the 1000 psi. This could be due to the closeness of the 1000 psi to the supercritical state and the 1500 psi being supercritical CO_2, which will have a larger overall dissolution compared to the 500 psi gaseous CO_2.
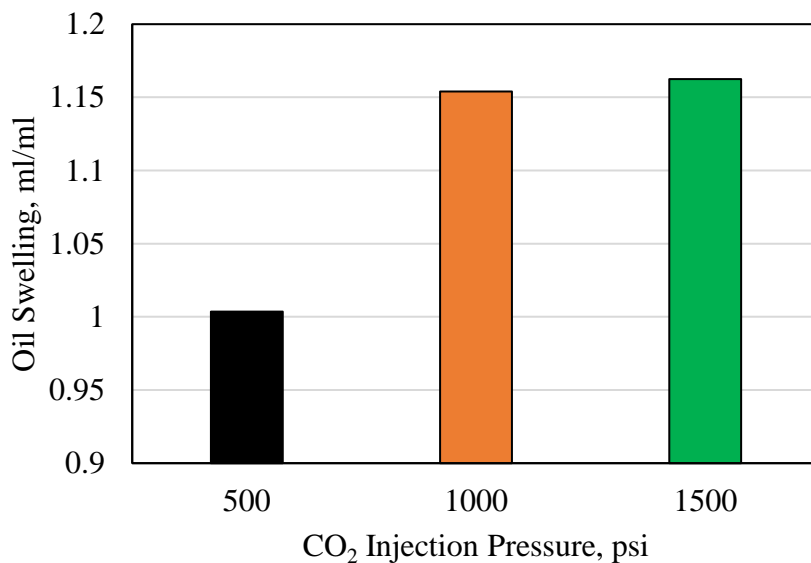
Figure 2. Effect of CO_2 Injection Pressure on Oil Swelling at 40 ⁰C, 1 ml of 460 cp Oil

7.2. TEMPERATURE EFFECT

Another significant parameter that was investigated was the temperature effect. The impact of varying the experimental vessel temperature on oil swelling was investigated using 25, 40, and 60 ⁰C. The results for oil swelling at all three temperatures are presented in Figure 3. The experiments were conducted using 1500 psi CO_2 injection pressure and 1 ml of crude oil with a viscosity of 470 cp at room temperature. At the 40 and 60 ⁰C the CO_2 was in the supercritical state, whereas at 25 ⁰C the CO_2 was not supercritical, since supercritical CO_2 will form at temperatures above 31.4 ⁰C only.
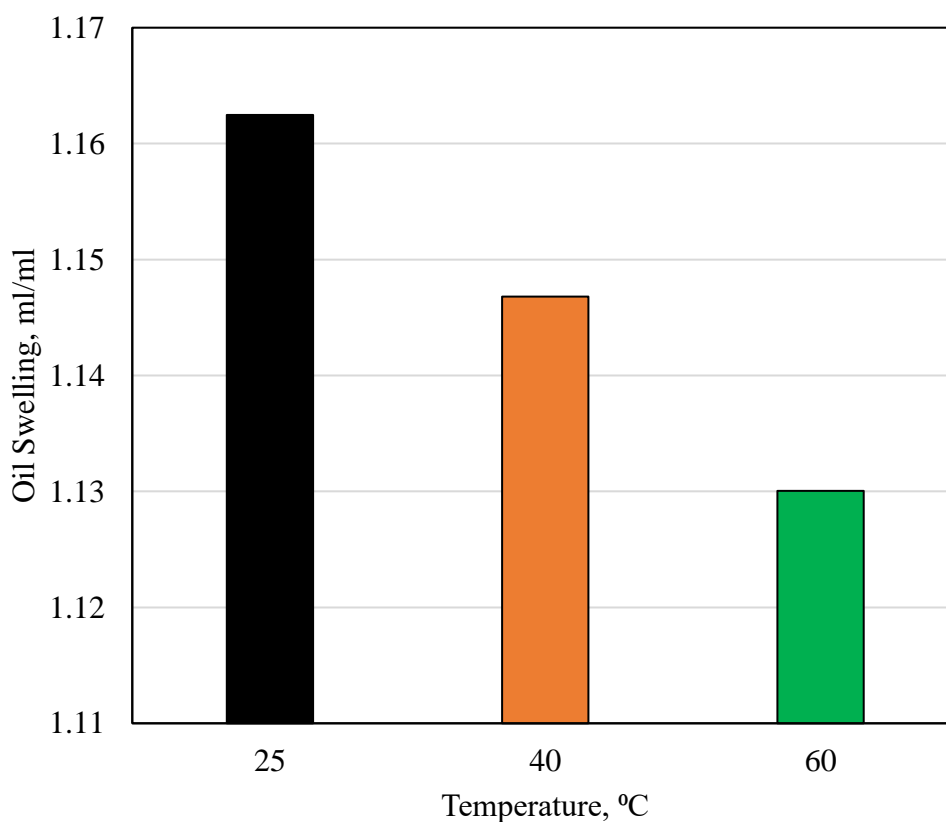
Figure 3. Effect of Temperature on Oil Swelling at 1500 psi Using 1 ml of 470 cp Oil

As the temperature increased, the oil swelling value decreased. This is mainly due to the increase in the activity of the CO_2 molecules at higher temperatures, which reduces its tendency to dissolve in the crude oil. This reduces the oil swelling potential significantly. It is therefore much more difficult for the CO_2 to become miscible in crude oil at higher temperature reservoirs. It is important to note that the temperature will have an impact on the oil viscosity as well, with the increase in temperature resulting in a decrease in oil viscosity. Since the crude oil used to conduct all the temperature experiments was the same, this viscosity reduction effect was negated. The effect of varying the oil viscosity was also studied in this research and will be explained in the following section to better illustrate the significance of both the temperature and viscosity effects.

7.3. CRUDE OIL VISCOSITY EFFECT

Different crude oils will interact differently with the CO_2 injected. It is therefore expected that crude oils with different viscosities will swell differently in the presence of CO_2. This is mainly due to the difference in interfacial tension between the CO_2 and crude oil containing a high percentage of lighter components compared to an oil with a prevalence of heavy components. The crude oil viscosity's effect on oil swelling was investigated using three different viscosity values, including 470, 267, and 67 cp. The oil swelling results for all the oil viscosity values are presented in Figure 4. All experiments were conducted using 1500 psi CO_2 injection pressure and 40 ºC, using 1 ml of crude oil. Increasing the oil viscosity resulted in a reduction in the oil swelling value. This is mainly due to the lighter oil having a lower IFT with the CO_2 at the same condition, which in turn

allowed for a larger swelling. The lighter oil will tend to reach miscibility with the CO_2 much faster than the heavier oil, and thus the IFT between the lighter oil and the CO_2 is much lower at the experimental conditions. It is important to note that the difference between the oil swelling values of the three viscosities is not very large. This is mainly because the difference in the viscosity is not very significant. Even the 470 cp oil is not considered extremely heavy oil, since some oils may reach a viscosity of more than 10,000 cp at reservoir conditions. The 10,000 cp crude oils are usually referred to as bitumen. They are extremely difficult to flow. The crude oil used in this study is much less viscous and thus was more ideal for running experiments. Also, the crude oil used in this research had a much larger swelling potential compared to the heavier and much more viscous 10,000 cp crude oil.
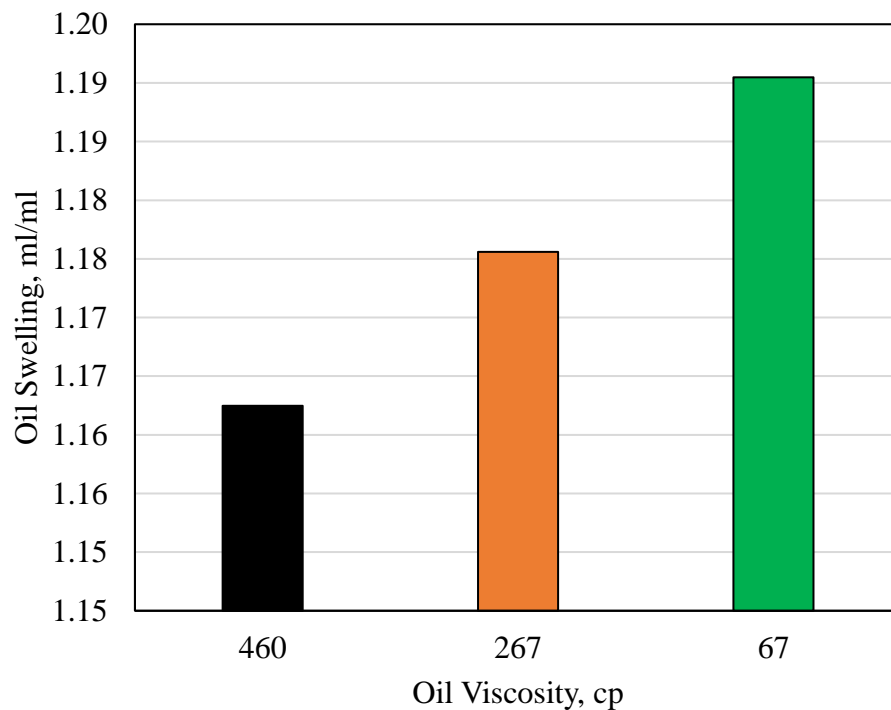
Figure 4. Effect of Oil Viscosity on Oil Swelling at 1500 psi and 40 ºC Using 1 ml Oil

7.4. CRUDE OIL VOLUME EFFECT

The volume of the oil in the experimental vessel can have a significant impact on the oil swelling value obtained. This is mainly due to the restriction that the experimental vessel volume may pose if the volume is too small to accommodate the volume of the fully swollen oil, and thus may result in a lower value than the actual potential for swelling. The impact of both decreasing and increasing the oil volume in the experimental vessel was therefore investigated using 0.5, 1, and 2 ml of crude oil. The oil swelling results using different volumes of oil can be seen in Figure 5. Experiments were conducted at 1500 psi CO_2 injection pressure, and also at 40 ºC, using crude oil with a viscosity of 470 cp. Decreasing the oil volume from 1 ml to 0.5 ml resulted in an increase in the oil swelling. However, this was extremely slight, which indicates that the 1 ml volume did not confine the oil in the vessel significantly and thus had very little impact on the swelling capacity of the crude oil at the experimental conditions used. Increasing the oil volume from 1 ml to 2 ml resulted in a noticeable decrease in the oil swelling capacity. This shows that if the volume of the crude oil is too large compared to the experimental vessel, this may result in erroneous results for the oil swelling. The oil may have much larger potential to swell than that observed in the results due to the confinement of the oil in the vessel that is housing it caused by the small volume of the vessel or the excess volume of the oil used to conduct the experiment.
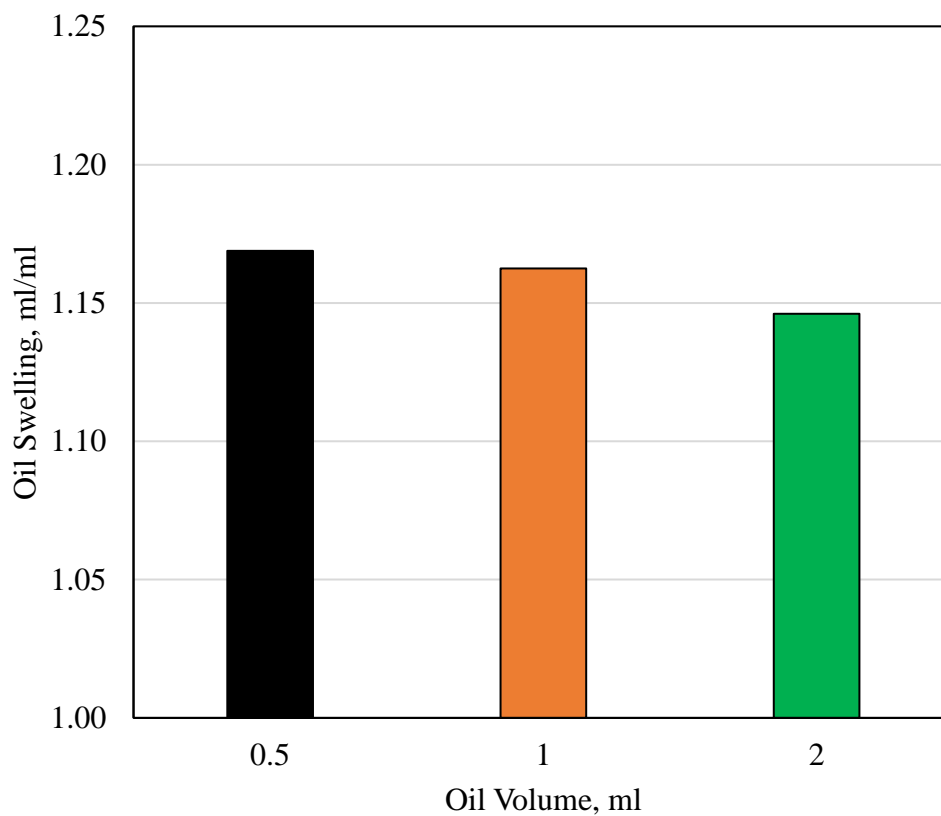
Figure 5. Effect of Oil Volume on Oil Swelling at 1500 psi and 40 ⁰C, 470 cp Oil

8. SIMPLE OIL SWELLING METHOD VALIDATION

The results obtained from the experiments conducted were compared to several oil swelling results obtained from more than thirty different studies that used different methods to measure oil swelling in order to test the accuracy of the results obtained using the method applied in this research. This section presents the comparison between the experimental results and the results from the literature, and also shows the degree of accuracy of the results obtained from the experiments compared to those obtained from the literature.

8.1. CARBON DIOXIDE INJECTION PRESSURE EFFECT

Oil swelling is a function of many parameters, and thus different oils will swell differently depending on their properties and the thermodynamic conditions under which they were subjected. The oil swelling values obtained using the three CO_2 injection pressures used in this research, including 500, 1000, and 1500 psi, were plotted with oil swelling values obtained from other research conducted in order to compare the values obtained to others. The comparison is shown in Figure 6. After the data was plotted, it was found that the values obtained from this research agreed with only a portion of the data points. A clear distinction can be made between the data points through the appearance of a separation. The majority of the data points that appear in the upper portion are oil swelling values associated with lighter crude oils, whereas the lower data points are associated with heavier crude oils, which have a lower swelling value at the same CO_2 injection pressure. Since the crude oil used to conduct the experiments has characteristics that are more closely related to heavy oils, the oil swelling values obtained followed the data points related to the heavy oil. This can be seen much more clearly when isolating the data points that are more closely related to the heavy oil, as can be seen in the plot on the right in Figure 6. A trend line was also incorporated in order to calculate the accuracy of the experimental results in comparison to the data points obtained from the literature. This was done in order to assess the accuracy of the results obtained using the experimental method to the results obtained using other methods presented in the literature. The accuracy percentages are shown in Table 2. The values obtained from the experiments had an extremely high accuracy compared to those obtained from the literature.
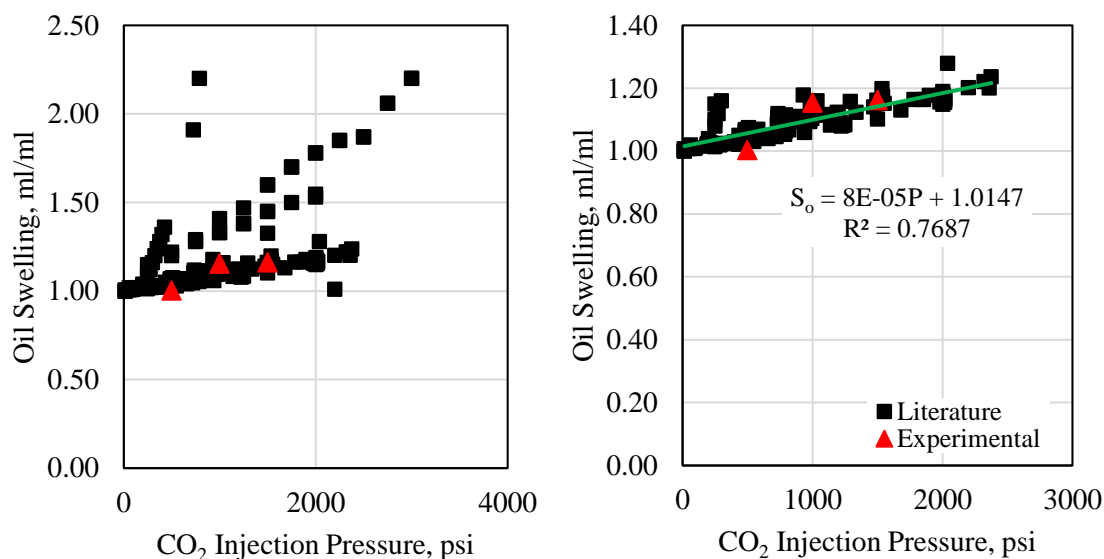
Figure 6. Experimental and Literature Oil Swelling Values at Different CO_2 Pressures

Table 2. Accuracy of CO_2 Injection Pressure Correlation

Pressure, psi	Experimental Oil Swelling, ml/ml	Correlation	Predicted Oil Swelling, ml/ml	Accuracy %
500	1.00358	$S_o = 0.00008P + 1.0147$	1.0547	94.9
1000	1.15399		1.0947	94.8
1500	1.16247		1.1347	97.6

8.2. TEMPERATURE EFFECT

A change in temperature of the reservoir can result in a change in the oil swelling capacity; however, a temperature change can also result in a change in other properties of the oil, most significantly the oil viscosity. It is therefore extremely important to compare the experimental results to those found in the literature. Figure 7 compares the results obtained from the experiments to those found in the literature. The initial observation from the plot will show that the data points do not follow a clear trend compared to the CO_2

injection pressure, shown in Figure 6. This is due to changes that occur to the crude oil properties when the temperature changes. Since different crude oils will have different characteristics, they will behave differently under different temperature conditions. The general trend for oil swelling is observed to be decreasing with the increase in temperature, as was also observed in the experiments conducted. After removing the data points that are irrelevant to the crude oil used in this research, as is shown in the plot on the right in Figure 7, a trend line was generated to evaluate the accuracy of the result obtained. Based on the accuracy results shown in Table 3, the experimental results had high accuracy, all above 90%, compared to the results from the literature.
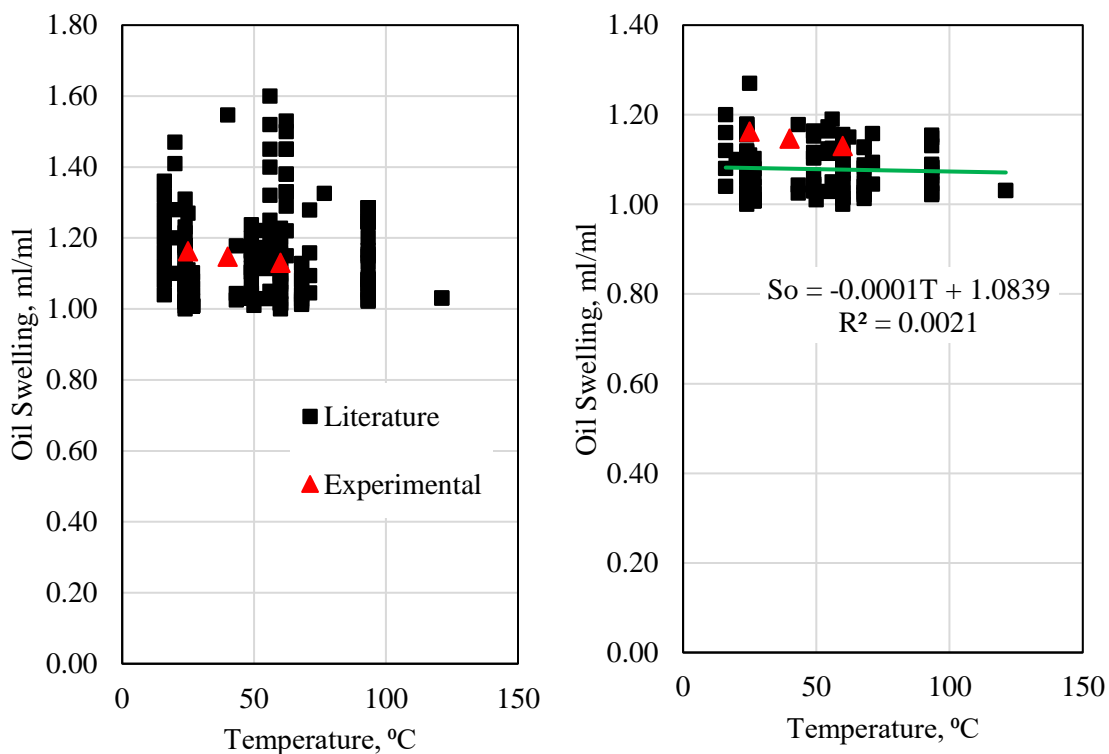
Figure 7. Experimental and Literature Oil Swelling Values at Different Temperatures

Table 3. Accuracy of Temperature Correlation

Temperature, ℃	Experimental Oil Swelling, ml/ml	Correlation	Predicted Oil Swelling, ml/ml	Accuracy %
25	1.16247	$S_o = -0.0001T + 1.0839$	1.0814	93.03
40	1.14681		1.0799	94.17
60	1.13005		1.0779	95.39

8.3. CRUDE OIL VISCOSITY EFFECT

Altering the crude oil viscosity will result in a change in the oil swelling capacity, as was shown in the experimental results. Figure 8 plots the oil swelling results from the experiments conducted and the results from the literature. The majority of the data obtained for viscosity is for oils with viscosity less than 500 cp, although some data points are higher in value. The general trend presented shows a decrease in oil swelling as the oil viscosity increases. The experimental results follow the general trend with high accuracy. from the accuracy results shown in Table 2.
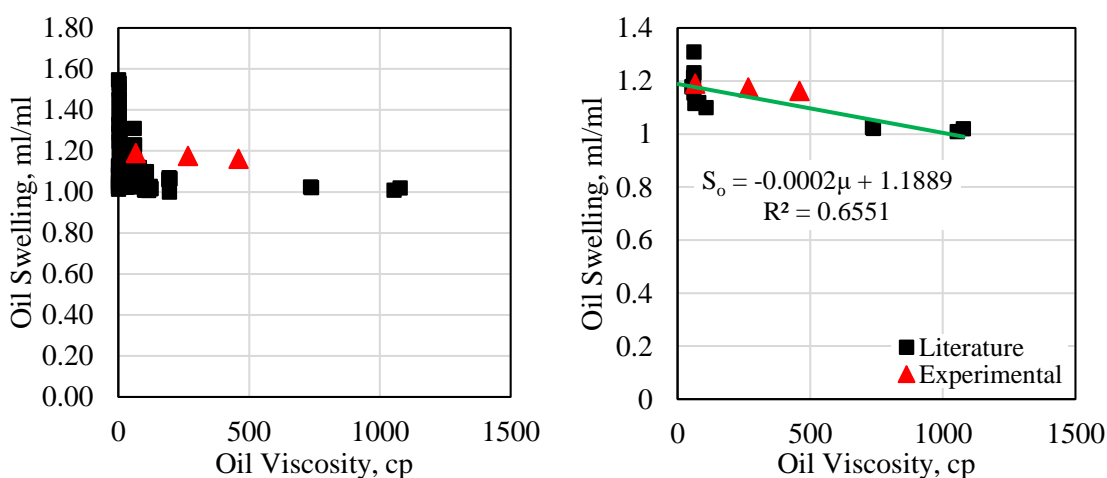
Figure 8. Experimental and Literature Oil Swelling Values for Different Oil Viscosities

Table 4. Accuracy of Oil Viscosity Correlation

Crude Oil Viscosity, cp	Experimental Oil Swelling, ml/ml	Correlation	Predicted Oil Swelling, ml/ml	Accuracy %
460	1.16247	$S_o = -0.0002\mu + 1.1889$	1.0969	94.36
267	1.17559		1.1355	96.59
67	1.19048		1.1755	98.74

9. CONCLUSIONS

This research investigates the extent to which the crude oil will swell under different conditions and the impact of different factors on oil swelling, including CO_2 injection pressure, experimental vessel temperature, crude oil viscosity, and crude oil volume in the experimental vessel using a simplified oil swelling measurement technique. The main conclusions obtained from this research are as follows.

- The oil swelling values that were obtained using the simplified method applied in this research were compared to several oil swelling values obtained from the literature and were found to follow the overall trend of the data points, which indicates that the method that was used had a high level of accuracy.

- Increasing the CO_2 injection pressure resulted in an increase in the oil swelling, due to a larger volume of CO_2 dissolving in the crude oil at the higher pressures.

- The oil swelling increased when the CO_2 was in the near-critical phase and the supercritical phase compared to the oil swelling in the gaseous phase.

- Increasing the temperature of the experimental vessel resulted in a decrease in the oil swelling capacity regardless of the phase of the CO_2. This is due to the increase

in the activity of the CO_2 molecules at elevated temperatures, which resulted in a lower tendency of the CO_2 molecules to dissolve in the crude oil.

- Reducing the oil viscosity resulted in an increase in the oil swelling at the same experimental conditions. This indicates that the lower viscosity crude oil has a larger overall potential. Also, this is an indication that the interfacial tension between the crude oil and the CO_2 decreases with the decrease in crude oil viscosity, therefore the swelling increases.

- The oil volume in the experimental vessel should be as low as possible to avoid having the oil confined due to the volume of the vessel, which may result in a lower oil swelling capacity.

- The novel method used in this research has been validated by comparing the results obtained from this research to those published in the literature. Based on the comparison, a high accuracy match was obtained between the results.

- The validation conducted was based on a variety of different crude oils obtained from multiple reservoirs worldwide. This helped increase the dependency and accuracy of the oil swelling method used.

ACKNOWLEDGEMENTS

REFERENCES

Ahmed, S. et al., 2018. Laboratory Study of CO2 Foam for Enhanced Oil Recovery: Advanced Screening, Optimization, and Evaluation. Society of Petroleum Engineers. doi:10.2118/192351-MS.

Alharthy, N. et al., 2018. Enhanced Oil Recovery in Liquid-Rich Shale Reservoirs: Laboratory to Field. Society of Petroleum Engineers. doi:10.2118/175034-PA.

Al-Jarba, M. and Al-Anazi, B. D., 2009. A Comparison Study of the CO_2-Oil Physical Properties Literature Correlation Accuracy Using Visual Basic Modelling Technique. NAFTA Journal, **60** (5), 287-291.

Al-Murayri, M. T., Harding, T. G., and Maini, B.B., 2011. Solubility of Methane, Nitrogen, and Carbon Dioxide in Bitumen and Water for SAGD Modelling. Journal of Canadian Petroleum Technology, Society of Petroleum Engineers. doi:10.2118/148630-PA.

Bahralolom, I. M., and Orr, F., 1988. Solubility and Extraction in Multiple Contact Miscible Displacements: Comparison of N_2 and CO_2 Flow Visualization Experiments. SPE Reservoir Engineering, Society of Petroleum Engineers. doi:10.2118/15079-PA.

Barclay, T., and Mishra, S., 2016. New Correlations for CO_2-Oil Solubility and Viscosity Reduction for Light Oils, Journal of Petroleum Production Technology, Springer. DOI 10.1007/s13202-016-0233-y.

DeRuiter, R.A., Nash, LJ., and Singletary, M.S., 1994. Solubility and Displacement Behavior of a Viscous Crude With CO_2 and Hydrocarbon Gases. SPE Reservoir Engineering, Society of Petroleum Engineers. doi:10.2118/20523-PA.

Du, F. An Experimental Study of Carbon Dioxide Dissolution Into a Light Crude Oil, 2016. Masters Thesis, Petroleum Systems Engineering, University of Regina.

Fakher, S. and Imqam, A. 2020c. A data analysis of immiscible carbon dioxide injection applications for enhanced oil recovery based on an updated database. SN Appl. Sci. 2, 448. https://doi.org/10.1007/s42452-020-2242-1.

Fakher, S. and Imqam, A., 2018. Investigating and Mitigating Asphaltene Precipitation and Deposition in Low Permeability Oil Reservoirs During Carbon Dioxide Flooding to Increase Oil Recovery. Society of Petroleum Engineers. doi:10.2118/192558-MS.

Fakher, S. and Imqam, A., 2019. Asphaltene precipitation and deposition during CO2 injection in nano shale pore structure and its impact on oil recovery. Fuel Journal, 273. 1029-1039. https://doi.org/10.1016/j.fuel.2018.10.039.

Fakher, S. and Imqam, A., 2020d. High pressure-high temperature carbon dioxide adsorption to shale rocks using a volumetric method. 95. https://doi.org/10.1016/j.ijggc.2020.102998.

Fakher, S. and Imqam, A., 2020e. Application of carbon dioxide injection in shale oil reservoirs for increasing oil recovery and carbon dioxide storage. 265. https://doi.org/10.1016/j.fuel.2019.116944.

Fakher, S. et al. 2019b. An experimental investigation of asphaltene stability in heavy crude oil during carbon dioxide injection. J Petrol Explor Prod Technol. https://doi.org/10.1007/s13202-019-00782-7.

Fakher, S. et al., 2017. Novel Mathematical Models to predict Preformed Particle Gel Placement and Propagation through Fractures. Society of Petroleum Engineers. doi:10.2118/187152-MS.

Fakher, S. et al., 2018. Investigating the Viscosity Reduction of Ultra-Heavy Crude Oil Using Hydrocarbon Soluble Low Molecular Weight Compounds to Improve Oil Production and Transportation. Society of Petroleum Engineers. doi:10.2118/193677-MS.

Fakher, S. et al., 2019. A Comprehensive Review on Gas Hydrate Reservoirs: Formation and Dissociation Thermodynamics and Rock and Fluid Properties. International Petroleum Technology Conference. doi:10.2523/19373-MS.

Fakher, S. et al., 2019a. A characterization of different alkali chemical agents for alkaline flooding enhanced oil recovery operations: an experimental investigation. SN Appl. Sci. 1, 1622. https://doi.org/10.1007/s42452-019-1662-2.

Fakher, S. et al., 2020. Hydrolyzed polyacrylamide – Fly ash reinforced polymer for chemical enhanced oil recovery: Part 1 – Injectivity experiments. 260. https://doi.org/10.1016/j.fuel.2019.116310.

Fakher, S. M. et al., 2018. Enhancing Carbon Dioxide Flooding Sweep Efficiency in High Permeability Hydrocarbon Reservoirs Using Micro-Particle Gels. Society of Petroleum Engineers. doi:10.2118/192381-MS.

Fakher, S. M., 2019. "Asphaltene stability in crude oil during carbon dioxide injection and its impact on oil recovery: A review, data analysis, and experimental study". Masters Theses. 7881.

Fakher, S., 2019a. Investigating Factors that May Impact the Success of Carbon Dioxide Enhanced Oil Recovery in Shale Reservoirs. Society of Petroleum Engineers. doi:10.2118/199781-STU.

Fakher, S., Imqam, A., 2020a A review of carbon dioxide adsorption to unconventional shale rocks methodology, measurement, and calculation. SN Appl. Sci. 2, 5 (2020). https://doi.org/10.1007/s42452-019-1810-8.

Gao, C. et al., 2013. Heavy Oil Production by Carbon Dioxide Injection, Green House Gasses Science and Technology, Society of Chemical Industry and John Wiley & Sons. doi:0.1002/ghg.1346.

Hao, H. et al., 2019. Feasibility Study of Gas-EOR Using CO2 and N2 Mixture in a Heavy Oil Reservoir: Experiments and Pilot Test. Carbon Management Technology Conference. doi:10.7122/CMTC-552521-MS.

Hatzignatiou, D., and Lu, Y., 1994. Feasibility Study of CO2 Immiscible Displacement Process In Heavy Oil Reservoirs. Petroleum Society of Canada. doi:10.2118/94-90.

Henni, A. and Mather, A.E., 1999. Solubility of CO_2, N_2O, CH_4, and C_2H_6 in Polar Solvents. Journal of Canadian Petroleum Technology, Society of Petroleum Engineers.

Hoffman, B. T. and Rutledge, J. M., 2019. Mechanisms for Huff-n-Puff Cyclic Gas Injection into Unconventional Reservoirs. Society of Petroleum Engineers. doi:10.2118/195223-MS.

Holm, L.W. and Josendal, V.A., 1974. Mechanisms of Oil Displacement By Carbon Dioxide. Journal of Petroleum Technology, Society of Petroleum Engineers. doi:10.2118/4736-PA.

Klins, M. and Ali, S.M., 1982. Heavy Oil Production by Carbon Dioxide Injection. Journal of Canadian Petroleum Technology, Society of Petroleum Engineers.

Mahzari, P. et al., 2019. An Improved Understanding About CO2 EOR and CO2 Storage in Liquid-Rich Shale Reservoirs. Society of Petroleum Engineers. doi:10.2118/195532-MS.

Maneeintr, K. et al., 2014. Analysis of Heavy Oil Emulsion-Carbon Dioxide Systems on Oil-Swelling Factor and Interfacial Tension by Using Pendant Drop Method for Enhanced Oil Recovery and Carbon Dioxide Storage. International Journal of Environmental Science and Development, **5** (2), 118- 123.

Martin, F.D., and Taber, J.J., 1992. Carbon Dioxide Flooding. Journal of Petroleum Technology, Society of Petroleum Engineers.

Mullken, C. and Sandler, S., 1980. The Prediction of CO_2 Solubility and Swelling Factors for Enhanced Oil Recovery, Engineering Chemical Process Des. Development, American Chemical Society.

Norouzi, H. et al., 2019. Analysis of Secondary and Tertiary High-Pressure Gas Injection at Different Miscibility Conditions: Mechanistic Study. Society of Petroleum Engineers. doi:10.2118/191119-PA.

Nourozieh, H., Kariznovi, M., and Abedi, J., 2016. Measurement and Correlation of Solubility and Physical Properties for Gas-Saturated Athabasca Bitumen. SPE Production & Operations, Society of Petroleum Engineers. doi:10.2118/176016-PA.

Pacheco-Roman, F. J., and Hejazi, S. H., 2015. Estimation of Solubility and Diffusivity of Gases in Heavy Oils by Use of Late-Time Pressure-Decay Data: An Analytical/Graphical Approach. SPE Journal, Society of Petroleum Engineers. doi:10.2118/170957-PA.

Perera, M. et al., 2016. A Review of CO_2-Enhanced Oil Recovery with a Simulated Sensitivity Analysis. Energies Journal. doi:10.3390/en9070481.

Pourafshary, P. et al., 2019. Effect of Water/CO Ratio on Performance of CO-Based EOR in a Sandstone Reservoir – Insights from Core Flood Tests and Simulations. Society of Petroleum Engineers. doi:10.2118/198624-MS.

Ratnakar, R. R., and Dindoruk, B., 2020. Effect of GOR on Gas Diffusivity in Reservoir-Fluid Systems. Society of Petroleum Engineers. doi:10.2118/191531-PA.

Richardson, W. et al., 2019. Diffusivity of Gas Into Bitumen: Part II; Data Set and Correlation. Society of Petroleum Engineers. doi:10.2118/195575-PA.

Rostami, A. et al., 2017. Modeling of CO_2 Solubility in Crude Oil During Carbon Dioxide Enhanced Oil Recovery Using Gene Expression Programming, Fuel Journal, El-Sevier.

Sanaei, A. et al., 2018. Comprehensive Study of Gas Cycling in the Bakken Shale. Unconventional Resources Technology Conference. doi:10.15530/URTEC-2018-2902940.

Sasaki, K. et al., 2010. CO_2 Solubility Characteristics of Crude Oils Related to Carbon Capture and Utilization (CCU), Novel Carbon Resource Sciences Newsletter.

Silva, M.K. and Orr, F., 1987. Effect of Oil Composition on Minimum Miscibility Pressure-Part 1: Solubility of Hydrocarbons in Dense CO_2. SPE Reservoir Engineering, Society of Petroleum Engineers. doi:10.2118/14149-PA.

Sugai, Y., Babadagli, T. and Sasaki, K., 2013. Consideration of an Effect of Interfacial Area Between Oil and CO_2 on Oil Swelling, Journal of Petroleum Production Technology. **4** (2014), 105-112. doi:10.1007/s13202-013-0085-7.

Svrcek, W. and Mehrotra, A., 1982. Gas Solubility, Viscosity, and Density Measurements for Athabasca Bitumen. Journal of Canadian Petroleum Technology, Society of Petroleum Engineers.

Svrcek, W. et al., 1989. Properties of Peace River Bitumen Saturated with Field Gas Mixtures. Journal of Canadian Petroleum Technology, Society of Petroleum Engineers.

Tran, S. et al., 2019. Studying Phase Behavior of Oil-Natural Gas Systems for Designing Gas Injection Operations: A Montney Case Study. Unconventional Resources Technology Conference. doi:10.15530/AP-URTEC-2019-198201.

Tran, T., 2014. Carbon Dioxide-Heavy Oil Systems: Thermodynamics, Transport and Interfacial Stability. Doctor of Philosophy Thesis Dissertation, Chemical Engineering, Missouri University of Science and Technology.

Vali, J. et al., 2011. A Fast and Simple Method for Modeling Oil Swelling in CO_2 Injection. Journal of Geope, **1** (2), 39-46.

Verma, M., 2015. Fundamentals of Carbon Dioxide Enhanced Oil Recovery (CO_2-EOR)-A Supporting Document of the Assessment Methodology for Hydrocarbon Recovery Using CO_2-EOR Associated with Carbon Sequestration. United States Geology Survey, United States Department of Interior.

Wang, M. et al., 2019. Novel Wettability Modifiers for Improved Oil Recovery in Tight Oil Reservoirs. Unconventional Resources Technology Conference. doi:10.15530/urtec-2019-1069.

Yang, C. and Gu, Y., 2006. Diffusion Coefficients and Oil Swelling Factors of Carbon Dioxide, Methane, Ethane, Propane, and Their Mixtures in Heavy Oil, Journal of Fluid Phase Equilibria, El-Sevier. **243** (2006), 64-73.

Zhang, F. et al., 2019. Numerical Investigation to Understand the Mechanisms of CO2 EOR in Unconventional Liquid Reservoirs. Society of Petroleum Engineers. doi:10.2118/196019-MS.

VIII. A REVIEW OF CARBON DIOXIDE ADSORPTION TO UNCONVENTIONAL SHALE ROCKS METHODOLOGY, MEASUREMENT AND CALCULATION

ABSTRACT

Carbon dioxide (CO_2) injection has been applied extensively in hydrocarbon reservoirs for both increasing oil recovery and CO_2 storage purposes. Recently, CO_2 injection has been proposed to increase oil recovery and for CO_2 storage in shale reservoirs. During CO_2 injection in shale reservoirs, adsorption will take place on the surface of the rock, which will impact both the oil recovery and the storage capacity. This research provides a roadmap to the different types of adsorption and the adsorption measurements and calculations with emphasis on the ones most applicable during CO_2 injection in shale reservoirs. The main two types of adsorption are initially explained including physisorption and chemisorption, and the major applicable adsorption isotherms are explained and their limitations are listed. The research then focusses on physisorption and its types, and hysteresis trends. The different methods used to measure adsorption are then illustrated and explained including volumetric, gravimetric, volumetric-gravimetric, oscillometry, and impedance spectroscopy. The different calculation methods for volumetric adsorption are then explained. Finally, the most common errors that have been observed during measurement and calculation of adsorption are listed and explained. This research provides a guideline to the proper and accurate measurement of CO_2 adsorption on shale rock during enhanced oil recovery applications and CO_2 storage operations in unconventional shale reservoirs to improve the productivity and applicability of this application.

1. INTRODUCTION

Carbon dioxide (CO_2) injection is currently one of the most applied enhanced oil recovery techniques in the oil industry due to several important reasons [1,2]. Firstly, CO_2 injection, either through flooding of cyclic huff-n-puff, can increase oil recovery significantly [3,4]. Secondly, CO_2 can be stored in several types of hydrocarbon reservoirs as part of the carbon storage initiative to reduce greenhouse emissions [5-8]. Recently, CO_2 injection in unconventional low permeability shale reservoirs has been investigated for both enhanced oil recovery from these reservoirs, and CO_2 storage [9]. In both applications, the CO_2 will adsorb to the shale rock surface, which will have an effect of oil recovery, and also CO_2 storage capacity [10-12].

The adsorption of CO_2 on the surface of shales, along with other rock, has been investigated using both computer simulation and modelling, and experimental work. Mohammad, S. [13] aimed to identify the most common sources of error associated with undergoing adsorption experiments. The errors investigated included the amount adsorbed through calculations, the void volume measured using helium, and the density of the injected gas which will affect the compressibility factor. Bahadori, A. and Vuthaluru, H. [14] developed a new correlation that can predict CO_2 adsorption isotherms for pressures up to 17.5 psi, and 196 ºC. The correlation was based on previously reported data, correlated as a function of CO_2 partial pressure for different temperatures. Clarkson, C. R. and Haghshenas, B. [15] used several models and tested their applicability in modeling CO_2 adsorption. They found that the simple Langmuir and Dubinin-Radushkevich models were the most adequate for modeling supercritical single component adsorption on coal

and shale as long as the density value is adjusted on the simulator for the CO_2 since it has a direct effect on the compressibility value. Yu, W. [16] used BET Isotherm rather than Langmuir Isotherm to model gas adsorption in Marcellus Shale. They observed that the Langmuir isotherm does not accurately model adsorption in all cases in the Marcellus shale, and hence a combination of BET and Langmuir isotherm should be applied. They also compared the results from both isotherms and evaluated long term adsorption. Psarras, P. [17] investigated CO_2 adsorption capacity in shale cores from the Eagle Ford basin using Molecular Simulation. The impact of increasing pressure and temperature, and also change in organic content and material was investigated. Le, T. D. [18] developed a new computational model to model flow of methane in fractured shale matrix based on averaging mass conservation equations. The model accounted for methane adsorption which had a strong effect on the flow of the gas and its relative permeability. They study did not use CO_2 however. Sudibandriyo, M. [19] illustrated the difference between the absolute adsorption, and Gibbs adsorption by measuring both values for the shale. They also showed that the helium compressibility can be obtained using correlation to measure the void space, whereas the CO_2 values should be obtained using other methods. Lafortune, S. [20] measured CO_2 adsorption on Mesozoic Marine Basin shale samples from France using magnetic suspension balance. The samples were crushed to powder size, and used for the adsorption experiments. As the temperature increased, the adsorption decreased, while increasing the pressure resulted in an increase in adsorption. The mineral composition of the shale also affect the adsorption capacity of CO_2. Luo, X. [21] investigated adsorption of several gases including methane, CO_2, and binary mixtures with different mole percentages of each gas using powdered shale samples of less than 0.5 mm

particle size. They measured adsorption based on a volumetric adsorption setup, and integrated a filter disk to prevent the particles from entering into the valves. Yuan, H. [22] attempted to use helium porosimeter to measure the volumetric adsorption capacity of Argillite rick shales. Since the volumetric based adsorption operates in the same manner as the helium porosimeter, the values they obtained were representative of the adsorption values on the shale. Lu, M. [23] developed a novel model fully based on a numerical producer combined with Artificial Neural-Network Technique to evaluate the lost gas volume, which includes the gas volume adsorbed to the surface of the coal, which occurs during production of coal. Perez, F. and Devegowda, D. [24] applied Monte Carlo Simulation to model methane and CO_2 adsorption. According to their results, having the rocks confined increased the adsorption capacity on the shale due to the increase in the attraction of the gas molecules which results in the density of the adsorbed phase being higher than that of the free phase.

Based on the previous work conducted on CO_2 adsorption to shales, it is clear that there are several methods present to measure adsorption experimentally and using computer simulation, and also, there are more than one method to calculate the adsorption value after conducting experiments. This research provides a detailed explanation of the different types of adsorption, and the one mostly related to CO_2 adsorption to shale rock. The research also mentions the most commonly used adsorption isotherms to model CO_2 adsorption to shale, and the advantages and disadvantages of each method. The research then explains the different types of physisorption, and then indicates the type that is most observed during CO_2 injection in shale reservoirs. The different types of experimental methods to measure adsorption are also explained in detail, and the advantages and

disadvantages of each method is mentioned. The two most common methods used to quantify CO_2 adsorption to shales are also shown, and the method by which they are applied is explained. By providing a comprehensive guideline to CO_2 adsorption on shale rocks, this research aims to function as a roadmap to the application of experimental studies on CO_2 adsorption in unconventional shale reservoirs for enhanced oil recovery and CO_2 storage purposes.

2. TYPES OF ADSORPTION

Adsorption is defined as the adhesion of atoms, ions, gas molecules, or liquids to the surface of an adsorbent **[**25]. There are two main constituents during any adsorption; these include the adsorbent, and the adsorbate [26,27]. The adsorbent is the surface on which adsorption will take place. The adsorbate is the substance which will adsorb on to the adsorbent's surface [28]. Adsorption occurs due to the adsorbent experiencing bond deficiency, which makes it thermodynamically favorable for the adsorbent to adsorb the adsorbate [29]. Desorption will occur once the adsorbate has enough energy to overcome the force holding it to the surface of the adsorbent and free itself from the surface. The general equation for adsorption is shown [30]. This equation is applicable for different fluids and adsorption surfaces and therefore it was referred to as a general equation. This is due to its definition including general terms, such as adsorbate and adsorbent.

$$Adsorbate + Adsorbent \underset{Desorption}{\overset{Adsorption}{\rightleftharpoons}} Adsorption$$
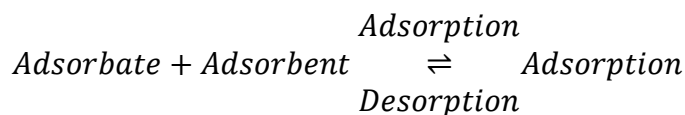
There are two main types of adsorption, including physisorption, and chemisorption. Several adsorption isotherms are also present to quantify adsorption for different adsorbents and adsorbates. The main types of adsorption, along with the adsorption isotherms and a subdivision of physisorption types are shown in Figure 1 below. Each of the parameters mentioned in the figure will be explained in detail later on. The main types that can be applied effectively and accurately to CO_2 adsorption on shale rocks will be pointed out as well.
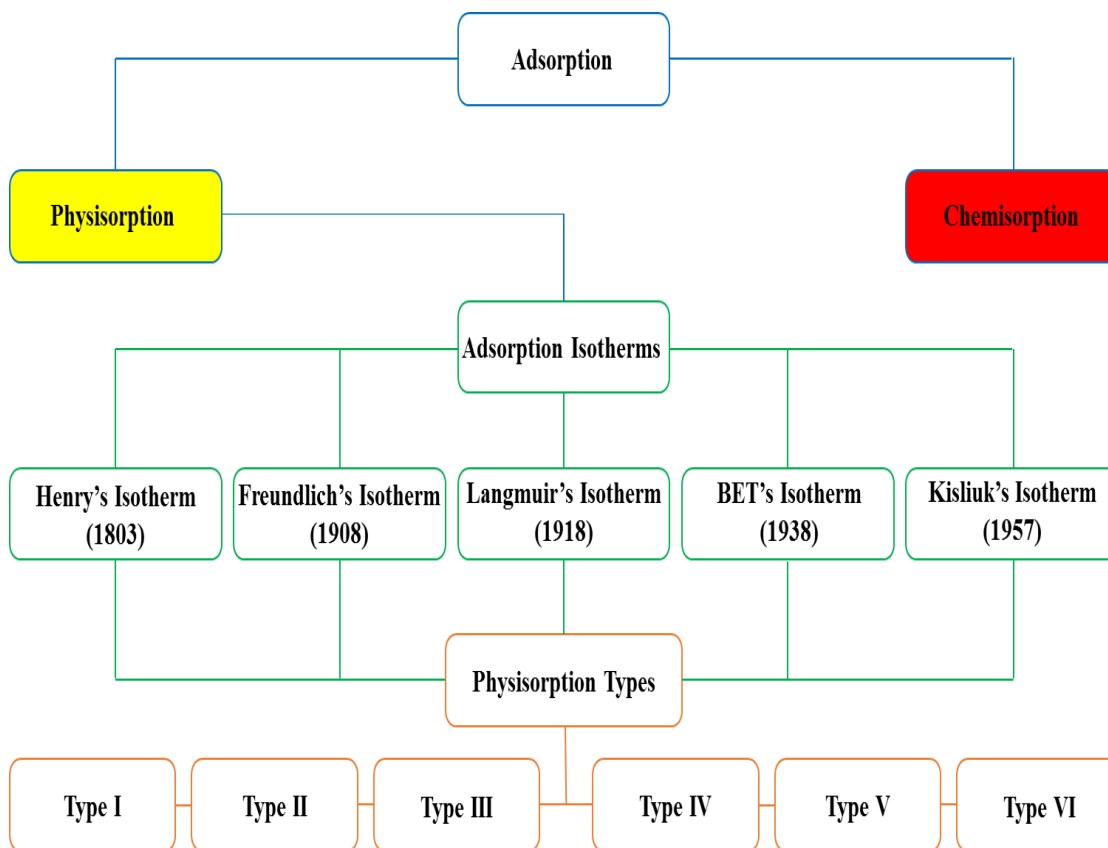
Figure 1. Flowchart of Main Types of Adsorption and Adsorption Isotherms

2.1. PHYSISORPTION

Physisorption, also referred to as physical adsorption, is the type of adsorption that takes place between CO_2 and shale during CO_2 injection in unconventional shale reservoirs [31-34]. It occurs at very low heats of adsorption, usually ranging between 20-40 kJ/mol. This is one of two main reasons why physisorption is a reversible or partially reversible process, meaning that desorption can occur after physisorption has taken place [35]. The second reason is that physisorption does not require any activation energy. It usually forms at low temperatures and decreases significantly with increasing temperature. During physisorption, the adsorbate will form multi-molecular layers on the adsorbent [30, 36]. The gas molecules of the CO_2 are held on the surface of the shale via Van Der Waals forces, which are considered weak forces [5, 37] The main characteristics of physisorption during CO_2 injection in shale reservoirs is shown in Figure 2.

Desorbed CO2; will occur in physisorption due to change in energy level which will severe the weak Van der Waals forces holding the gas molecules

Second CO2 Adsorbed Layer; Multiple Layer Adsorption will occur in physisorption which increases the adsorption capacity on the shale

First CO2 Adsorbed Layer; the initial gas layer will target the adsorption sites on the shale based on thermodynamic bond deficiency of the rock

Shale; Adsorption will occur on the surface of the shale rock

Figure 2. Main Characteristics of Physisorption

2.2. CHEMISORPTION

Chemisorption, also referred to as chemical adsorption, does not occur during CO_2 injection in shale reservoirs. It occurs at a high heat of adsorption, usually ranging from 30-400 kJ/mol. It requires a high activation energy to severe the bonds holding the adsorbate to the adsorbent. The adsorbate is held to the adsorbent via chemical bonds, which makes the process irreversible, unless extremely high energy is input into the system. Another main difference between physisorption and chemisorption is that during chemisorption, the adsorbate forms mono-molecular layers on the surface of the adsorbent, as opposed to the multi layers formed during physisorption [30, 38]. This is extremely advantageous for physisorption especially during CO_2 storage processes in shale reservoirs since the formation of multi-layers of the CO_2 on the shale surface will result in a higher volume of CO_2 adsorbed, and hence, a high CO_2 storage volume [39]. Figure 3 shows the main characteristics of chemisorption. The shale in Figure 3 is for explanation purposes only, since chemisorption will not form during CO_2 injection in unconventional shale reservoirs.

Desorbed CO_2; desorption will not occur in chemisorption unless tremendous energy is input to desorb the gas since the molecules are held via chemical bonds.

Second CO_2 Adsorbed Layer; Chemisorption is characterized by being mono-layered adsorption and hence only a single layer will be present on the adsorption sites
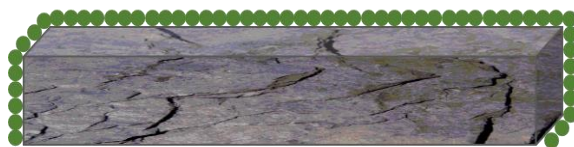
First CO_2 Adsorbed Layer; the initial gas layer will have a heat of adsorption ranging from 40-400 kJ/mol, which is considered very high compared to physisorption.

Shale; Gas adsorption on shales occurs as physisorption and not chemisorption

Figure 3. Main Characteristics of Chemisorption

3. ADSORPTION ISOTHERMS

Several adsorption isotherms have been developed along the years to model adsorption. Each of these isotherms has its own assumptions and limitations, which makes only a few of them applicable for accurate quantification of CO_2 adsorption on shale reservoirs. An adsorption isotherm predicts adsorption capacity of the adsorbate on the adsorbent at a specific temperature, hence the name isotherm, which comes from isothermal, measuring constant temperature. The main adsorption isotherms will be explained, with a main focus on those applicable to CO_2 adsorption in shale reservoirs.

3.1. HENRY'S ISOTHERM

Henry's Adsorption Isotherm was developed in 1803. It is the simplest form of adsorption isotherm and is usually referred to as the linear adsorption isotherm. The surface area of the adsorbate adsorbed onto the surface of the adsorbent is assumed to be proportional to the partial pressure of the injected gas. It is modeled using the equation.

$$X = K_H P_p$$

where X is the fraction of the surface of the adsorbent covered, P_p is the partial pressure, and K_H is Henry's adsorption constant, which is equal to:

$$K_H = \lim_{\delta \to 0} \frac{\delta_s}{\delta(z)}$$

where δ_s is the surface number density, which is the concentration of adsorbate molecules on the surface of the adsorbent, and $\delta(z)$ is the number density at free phase of adsorbate.

Henry's Isotherm is best used to describe the initial stage of the adsorption. It is not fully applicable however in complex adsorption processes, and thus is not the most suitable isotherm to use when modelling CO_2, or any other gas, adsorption to shale rock surface.

3.2. FREUNDLICH ISOTHERM

Freundlich and Kuster developed the first non-linear adsorption isotherm in 1906. It was an empirical formula developed for gas adsorbates. The formula is presented [41].

$$\frac{x}{m} = KP^{\frac{1}{n}}$$

where x is the mass of the adsorbate that is adsorbed, m is the total mass of the adsorbent, P is the pressure of the adsorbate, in this case CO_2 gas, and K and n are constants unique to each adsorbate at a specific temperature.

The Freundlich Isotherm has several drawbacks including that it is only applicable for gases, it is an empirical formula, and it does not function properly at high pressures. It can be used to model CO_2 adsorption on shales at very low pressures but deviates from the true value as the pressure increases, and thus it is not applicable in modeling real field applications since most of them are at relatively high pressures. It is important to note that the Freundlich Isotherm is not used almost at all to model CO_2 adsorption to shale due to its several assumptions and limitation to its application. Also, it is not used mainly due to the generation of more applicable isotherms that are currently being used.

3.3. LANGMUIR ISOTHERM

Langmuir developed the first scientifically based adsorption formula. The formula was developed in 1918 to model gas adsorption on solid surfaces. It was derived based on statistical thermodynamics. The formula is shown [42].

$$K_{ads} = \frac{[AS]}{[A][S]}$$

where K_{ads} is the adsorption equilibrium constant, [AS] represents the adsorbate molecules that have adsorbed to the surface of the adsorbent, [A] represents the adsorbate concentration, and [S] represents the surface of the adsorbent.

Langmuir defined the fraction of adsorption sites on the adsorbent that have been occupied by the adsorbate as θ. The sites that are not occupied can be represented as [1-θ]. By using these definitions, the following formula is reached [42].

$$\frac{[AS]}{[S]} = \frac{\theta}{1 - \theta}$$

Using the above formula, and the definition of K_{ads}, mentioned previously, the final form of the Langmuir Adsorption Isotherm can be reached. This is shown.

$$\theta = \frac{K_{ads}[A]}{1 + K_{ads}[A]}$$

The Langmuir Adsorption Isotherm has a wide range of applicability, especially that it can be used to model both physisorption and chemisorption. It is one of the most applied isotherms to model CO_2 adsorption to shale rocks. The isotherm does have some drawbacks however, which are manifested in the assumptions made during its development. These assumptions include that the adsorbent has a specific number of sites where the adsorbate can get adsorbed, the adsorption will occur in only one layer, hence the isotherm can only model monolayer adsorption, and the adsorption sites are energetically equivalent, and the adsorbed molecules do not interact [43].

3.4. BRUNAUER – EMMETT – TELLER ISOTHERM

The Langmuir isotherm assumes monolayer adsorption, which maybe applicable in chemisorption, however, it will deviate from the true solution in physisorption, which takes place between CO_2 and shale, since physisorption involves multi-layer adsorption. The BET Adsorption Isotherm was developed in 1938 and is an improved version of the Langmuir Adsorption Isotherm. BET can account for multi-layer adsorption, which in turn can properly model physisorption. It has been applied by many researchers to model CO_2 adsorption in shale reservoirs and has proven to be superior to the Langmuir isotherm in many cases. The BET isotherm formula is shown [44]. The BET isotherm is highly accurate in determining CO_2 adsorption capacity, however it is important to note that it is also more complicated compared to the Langmiur Isotherm and thus requires more time when used to model adsorption.

$$\frac{P_e}{v(P_o - P_e)} = \frac{1}{v_m c} + \frac{c - 1}{v_m c}\frac{P_e}{P_o}$$

where P_e and P_o are the equilibrium and saturation pressures of the adsorbate at the temperature of adsorption, v is the adsorbed gas quantity, v_m is the monolayer adsorbed gas quantity, c is the BET constant equal to:

$$c = \exp\left(\frac{E_1 - E_2}{RT}\right)$$

where E_1 is the heat of adsorption for the first layer, E_2 is the heat of adsorption for the second and higher layers and is equal to the heat of liquefaction.
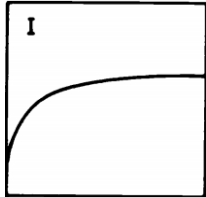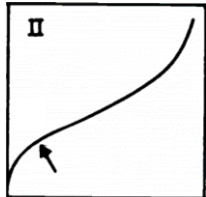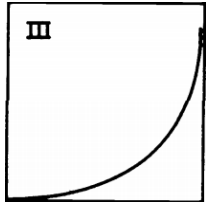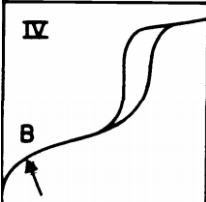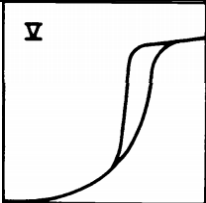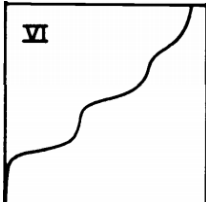
The BET isotherm essentially applies the Langmuir isotherm to multiple layers while taking into consideration the difference in adsorption between each layer. The BET is one of the most suited isotherms that can model physisorption, and thus can accurately model CO_2 adsorption to shale. It has two drawbacks however, which include that it assumes that the gas molecules only interact with the adjacent layers, above and beneath it, and it is considered complex to use, compared to the other isotherms [44].

4. PHYSISORPTION TYPES

Since physisorption is more complex than chemisorption in terms of forming multi-layers of adsorbate on the adsorbent, several physisorption types have been observed. These types can be grouped into six major divisions based on the behavior of the adsorption quantity at different partial pressures. Relative pressure is defined as the sample pressure divided by the saturation vapor pressure [45].

Table 1. Physisorption Isotherm Types [49]

Physisorption Isotherm Type	Description	Chart
Type I	Type I isotherms are usually observed in solids with micro-pores, with relatively small external surfaces, activated carbons, and zeolites.	
Type II	Type II isotherm represents both mono and multi-layer adsorption. The arrow in the plot points to the pressure at which multi-layer adsorption will commence.	
Type III	Type III is most noticeable for its convex shape which makes it difficult to determine the transition between mono and multi-layer adsorption.	
Type IV	Type IV is mostly characterized by its hysteresis loop which occurs due to the adsorbate condensation.	
Type V	Type V is another form of Type III which is only observed for a very limited number of adsorbents.	
Type VI	Type VI represents stepwise multi-layer adsorption, where the steepness of the steps depends on the temperature of the experiment.	

Using relative pressure allows for the removal of the effect of temperature on the sample change in pressure and thus allows for the creation of an isotherm [46]. Different isotherms will depend on the saturation vapor pressure. The relative pressure ranges from 0-1, where a relative pressure of 1 represents a complete saturation, meaning that all adsorption sites available have been occupied by the CO_2 [47, 48]. Based on the properties of the fluid and the rock, the relation between the relative pressure and the adsorption will change. The six main types of physisorption isotherms are shown in Table 1. Many other types of adsorption isotherms can also exist. An isotherm is obtained for different material and at isothermal conditions while varying other parmaters, most notably pressure. For each material, a different isotherm could be observed. The isotherms mentioned in the table are general isotherms that multiple trends have been observed around. Even though many materials may deviate from these isotherms, if the general isotherm trend is observed with caution, it may be noticed that the trend follows one of the isotherms mentioned in the table. This is based on the method by which the isotherm was obtained and the accuracy of the isotherm measurements and illustration for the different samples.

5. ADSORPTION HYSTERISIS

Adsorption hysteresis is the process of adsorption then desorption of the adsorbate on the adsorbent, usually during multi-layer physisorption, due to the capillary condensation in mesopores structures [49]. The four most commonly observed hysteresis loops are shown in Figure 5. The four loops are usually observed as a sequence of extremity, beginning from H1, which is considered the least extreme, up to H4, which is

the most extreme. H2 and H3 are considered intermediates. The desorption branch of the hysteresis loop will take one of the four shales seen in Figure 5 and is a strong function of the adsorbate rather than the adsorbent, and so in CO_2 adsorption on shale, the desorption will be a strong function of the CO_2 conditions such as temperature, and partial pressure rather than the shale adsorption sites. Type H4 is the most commonly seen in shale since it is associated with narrow slit-like pores, indicated by micro-porosity [50].
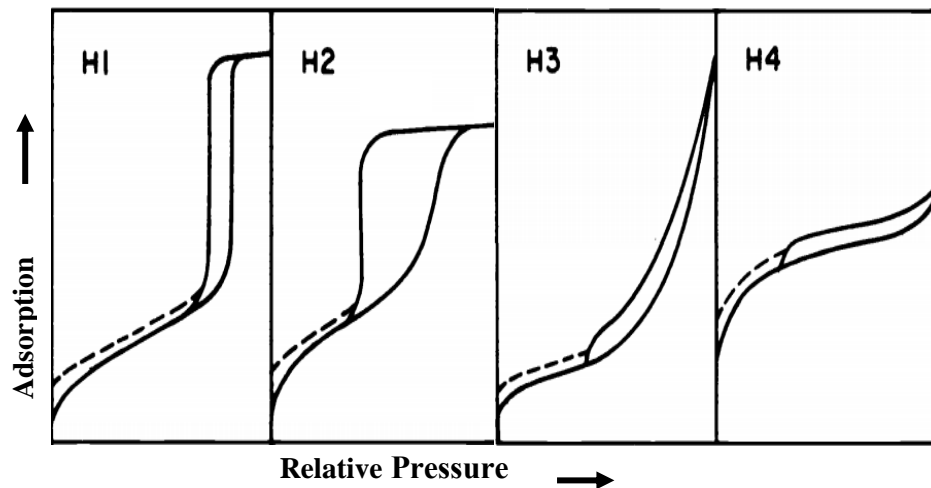
Figure 5. Types of Physisorption Hysteresis Behavior [49]

6. ADSORPTION MEASUREMENT

Several methods have been applied to measure the adsorption value [51, 52]. The main methods applied include volumetric, gravimetric, volumetric-gravimetric, oscillometry, and impedance spectroscopy. Each of these methods will be explained, and the main advantages and disadvantages of each will be pointed out.

6.1. VOLUMETRIC MEASUREMENT

      The volumetric method of measuring adsorption is considered one of the simplest, yet effective methods of measuring adsorption in terms of the mechanism [53]. The mechanism is based on Boyles Volumetric Gas Expansion law [54]. An illustration of the setup for volumetric adsorption measurement is shown in Figure 6.

Pressure Transducers

Reference Cell   **Sample Cell**
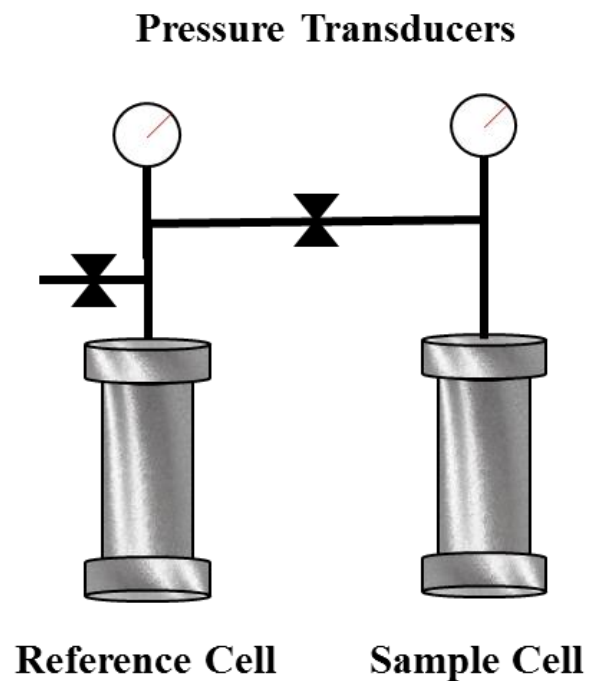
Figure 6. Illustration of Volumetric Adsorption Apparatus

      The volumetric adsorption apparatus is composed of a reference cell, where the adsorbate, CO_2, is initially pressurized, and heated to the design conditions. The sample cell contains the adsorbate sample, shale, and is connected to the reference cell and separated via a high pressure valve. The reference cell should be smaller in volume than the sample cell to allow sufficient gas expansion to be observed; this will help reduce the

difficulty in observing the equilibrium pressure. Once both cells are ready, and the CO_2 in the reference cell is pressurized and heated, the valve is opened, and the gas is allowed to expand. Once the equilibrium pressure is reached, the adsorption value can be calculated. The volumetric method has several advantages that make it a widely used method, however, it also has some major disadvantages that must be noted and accounted for when using this method to avoid error in the adsorption value. The main advantages and disadvantages of the volumetric method are presented in Table 2. Even though the advantages and disadvantages mentioned in the table are highly observed when using the volumetric adsorption method, it should be noted that some of these advantages may not be observed while conducting the experiment, and also some of the disadvantages may not occur or be observed as well. This is highly dependent on the exact setup used since there are multiple setups observed from the volumetric adsorption method. Each of these setups works under the same concept of volume measurement through pressure expansion, however the mechanism by which each separate setup is operated and constructed will determine the accuracy of the obtained experimental results and also will determine the advantages and disadvantages of the experimental setup accordingly. The calculations of the adsorption using the volumetric method remain universal, however. One of the advantages mentioned is the fact that the method has a relatively simple concept. It is important to clarify that simple concept does not undermine the importance of extreme accuracy requirement when undergoing this method. The simple concept refers to the overall method and ability to use it and understand its concept within a short duration. The actual experiments however require extreme accuracy and in some cases also require a long duration to ensure correct equilibrium values.

Table 2. Volumetric Adsorption Method Advantages and Disadvantages

Advantages	Disadvantages
Simple Concept: Volumetric gas adsorption setups are very simple compared to the other methods and do not require complex equipment to give accurate results.	**Volume of Adsorbent**: The volume of shale needed to conduct the adsorption experiments using the volumetric method is much larger than that needed in the other measurement methods. At least several grams are needed for accurate measurements to be obtained.
Apparatus and Measurement: As long as the pressure transducers are calibrated accurately, the measurements become very simple to conduct.	**Equilibrium Indication**: CO_2 adsorption can last for seconds, minutes, hours, or even days in some cases. The pressure equilibrium can sometimes be very difficult to observe and can sometimes be misleading.
	Cell Wall Adsorption: The CO_2 may adsorb to the wall of the reference cell or the sample cell which may result in some errors in the adsorption value. This may be overcome however during the adsorption calculation.

6.2. GRAVIMETRIC MEASUREMENT

The gravimetric method to measure adsorption is based on mass rather than pressure. Using the microbalance, the difference in mass can indicate the amount of gas that has adsorbed to the shale [55]. The setup is nearly identical to the volumetric setup, with the only difference being that the pressure transducers are replaced with the microbalance. An illustration of the gravimetric adsorption measurement setup is shown in Figure 7. The setup includes a microbalance. This balance can measure very slight changes in the weight which is imperative for the overall calculation of the adsorption using the gravimeteric adsorption method.
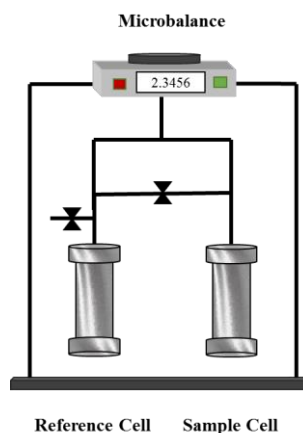
Figure 7. Illustration of Gravimetric Adsorption Apparatus

The gravimetric adsorption measurement method has many advantages [56,57], and also has some major drawbacks both of which should be known before conducting the experiment to avoid errors. The advantages and disadvantages of the gravimetric adsorption method are presented in Table 3.

Table 3. Gravimetric Adsorption Method Advantages and Disadvantages

Advantages	Disadvantages
Accuracy: The microbalances used for the gravimetric adsorption measurements are usually extremely accurate.	**Complexity**: Microbalances are much more complex in terms of usage compared to the volumetric setup.
Volume of Adsorbent: A few milligrams of shale can be used to obtain extremely accurate results using the gravimetric method.	
Cell Wall Adsorption: Wall adsorption does not pose a problem during gravimetric adsorption measurement since mass balance of the gas is not part of the calculation.	**Measurement**: The setup requires recording of many parameters such as pressure, temperature, concentration, and also several calibrations are needed which adds to the complexity.

6.3. VOLUMETRIC – GRAVIMETRIC MEASUREMENT

Since both the volumetric and the gravimetric adsorption measurement methods have some advantages and disadvantages, combining both to measure adsorption was performed in order to overcome some of the disadvantages. This was referred to as the volumetric-gravimetric method [56]. An illustration of the setup used to conduct the volumetric-gravimetric adsorption measurements is shown in Figure 8.
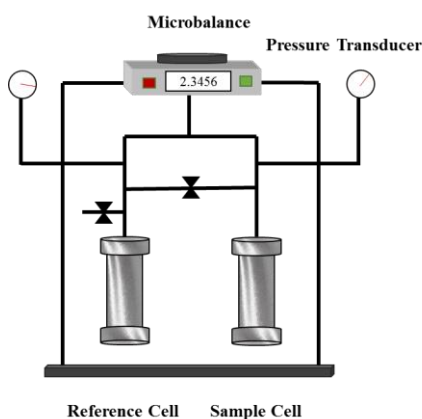
Figure 8. Illustration of Volumetric-Gravimetric Adsorption Apparatus

The setup is a combination of both the volumetric and the gravimetric adsorption setups, explained previously. The volumetric adsorption setup is connected to a microbalance, and hence both the pressure difference and the weight change can be recorded. The main advantage of this setup is the extremely high accuracy since both the pressure change and weight change results can be compared. The disadvantages of the setup are the high complexity of the new setup due to the presence of both the pressure transducers and the microbalance, and the large volume of adsorbent, shale, needed since the volumetric measurement of the setup will be inaccurate without a large volume [56].

6.4. OSCILLOMETRY MEASUREMENT

Oscillometry adsorption measurement is based on the oscillation of the sample cell, which results is a beam distortion which can be used to measure adsorption. An illustration of the setup is shown in Figure 9. The setup consists of an oscillating disk filled with the adsorbent, shale. The disk is fixed to a torsional wire and is stabilized by a steam beneath it. At the bottom of the stem, a small mirror is fixed. A laser beam is directed to the mirror as the oscillating disk is rotating. The beam is reflected via the mirror, and based on the angle of the oscillating disk, the reflection of the laser beam will create two angles, referred to as α_1 and α_2. The reflected beams are received by the diodes which produce electric signals of opposite signs, and hence the time when the reflected beam is crossing the area between the two diodes can be detected very accurately. The oscillation of the pendulum will produce several time signals which will be used to calculate angular frequency and logarithmic decrement, using a Gaussian Minimization procedure. This can then be used to measure the adsorption value [56].
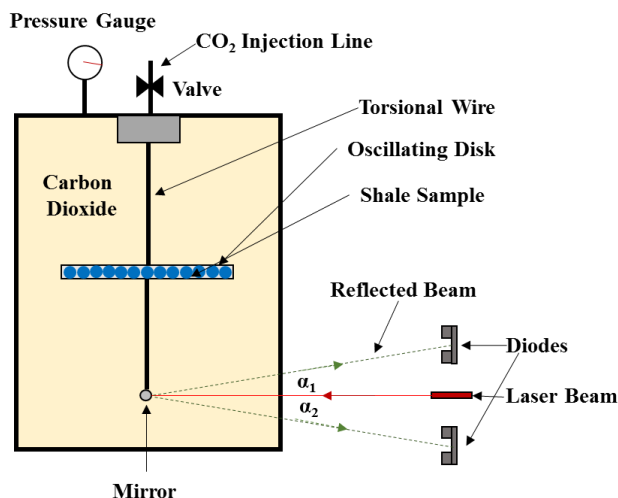
Figure 9. Illustration of Oscillometry Adsorption Apparatus

The main advantage of using the oscillometry method to measure adsorption is the measuring apparatus since it allows for the determination of both the total mass of the adsorbent and the adsorbate without using helium method. The oscillometry does have some disadvantages as well. The advantages and disadvantages of the oscillometry adsorption method are summarized in Table 4.

Table 4. Oscillometry Adsorption Method Advantages and Disadvantages

Advantages	Disadvantages
Measuring Apparatus: Allows for accurate the determination of both the total mass of the adsorbent and the adsorbate without using helium method.	**Calibration**: The torsional wire is severely affected by temperature and thus should be calibrated constantly to avoid errors in the reading, or the material should be heat resistant.
	Pendulum Material: The pendulum must be made of high durability material that will not be affected or affect the laser beam.
	Pressure Limitation: The oscillometry method is not accurate at low pressures and thus should not be used at these conditions. Low pressures are usually based on the application however and thus the exact values are highly dependent on the material used for adsorption measurement and the adsorption fluid as well.
	Duration of Experiment: The experiment will sometimes take a few weeks to undergo, which makes it extremely time consuming compared to the few hours, or at most few days needed using the volumetric or gravimetric methods.

6.5. IMPEDANCE SPECTROSCOPY

When a weakly electric material, such as shale, is exposed to a static or alternating electric field, the molecular state of the material is changed. The nuclei of the atoms or the molecules are shifted in the direction of the electric field, whereas the electrons are moved in the opposite direction, hence dipole moments are created. The sum of the dipole moments in the material are referred to as the dielectric polarization of the material and can measured using impedance [56]. By applying oscillating-electric field, specific impedance curves can be obtained, which are unique to different materials. A molecular interpretation of the curves can be used to quantify the adsorption value. An illustration of the setup is shown in Figure 10.
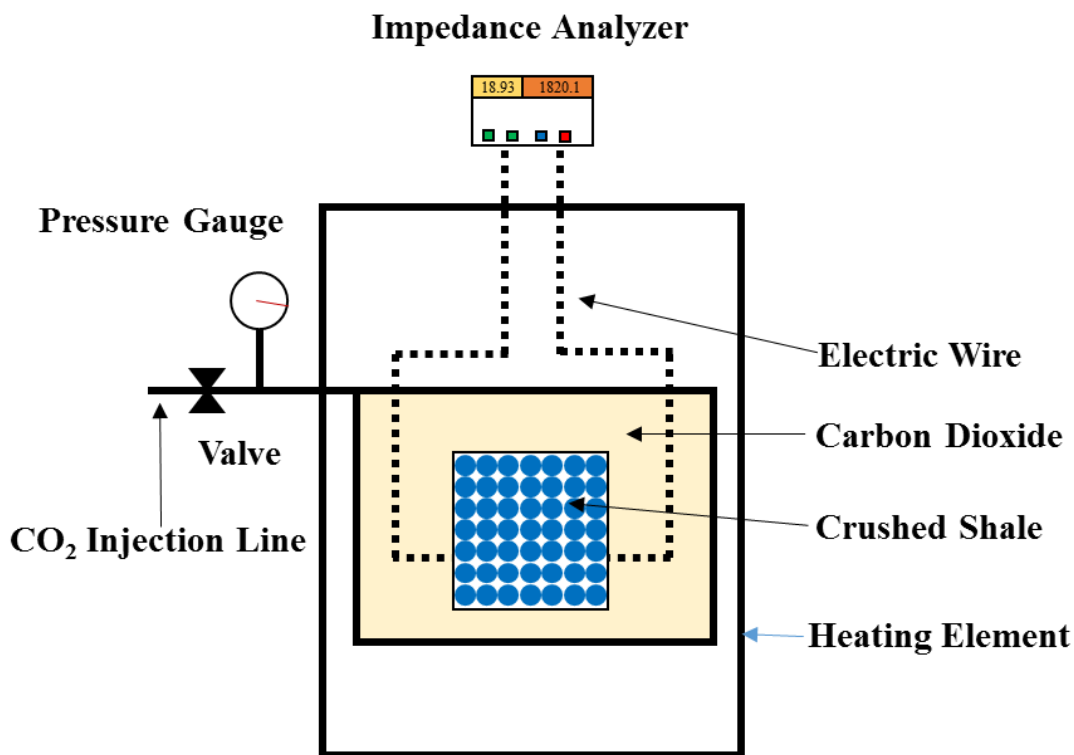
Figure 10. Illustration of Impedance Adsorption Apparatus

The main advantages of using the impedance spectroscopy adsorption measurements and the main disadvantages of using this method are presented in Table 5 in order to avoid error when measuring adsorption using this method.

Table 5. Impedance Spectroscopy Method Advantages and Disadvantages

Advantages	Disadvantages
Measuring Apparatus: Dielectric impedance measurements are very easily performed and can yield accurate results even under extreme pressure and temperature conditions.	**Adsorbent Material**: Only dielectric or weakly electric conducting material can be used since materials that can conduct electricity easily will heat up, which may cause problems.
Kinetics Observation: Impedance measurements can detect internal changes and chemical processes which cannot be observed using volumetric or gravimetric methods.	**Frequency Spectrum**: A broad range of frequency is needed, which results in longer durations and more complex measurements.
Versatility: In addition to measuring adsorption, impedance can be used to characterize the adsorbent material.	**Molecular Interpretation**: Interpretation of the impedance measurements and curves can be extremely tedious and thus the other methods are usually preferred over it.

7. VOLUMETRIC ADSORPTION CALCULATIONS

Calculation of the adsorption value takes place after the experiment has been conducted. Since there are several methods to conduct the adsorption experiments as shown above, there are multiple equations that are applied based on the results obtained using the experimental method. For example, if the volumetric method is used, the equilibrium value obtained will be a pressure reading and so the input to the equations must be a pressure reading in order to obtain the adsorption value, however, if the impedance spectroscopy

experimental method is used, an impedance value will be input to a different equation to obtain the adsorption value. Since this research is focused on CO_2 adsorption to shale rocks, the equations explained will be related to the volumetric method, since this is the most widely used adsorption measurement technique for CO_2 adsorption to shale [58-60]. There are two main methods used to perform the adsorption calculation for the volumetric experimental method including the absolute adsorption calculation, and the Gibbs adsorption calculation, both of which will be explained [61].

Generally, adsorption is a function of the adsorbent, which is the shale, the adsorbate, which is the CO_2, and the volume of the CO_2 adsorbed. The general adsorption equation is shown.

$$V_{total} = V_{solid} + V_{gas} + V_{ads}$$

where V_{total} is the total volume of the system, V_{solid} is the volume of the shale in the sample cell, V_{gas} is the volume of the CO_2 injected, and V_{ads} is the volume of the CO_2 adsorbed.

When the shale sample is placed in the sample cell, the shale grains will not fill up the whole cell since some voids will remain between the grains. The general definition of the void space is given as:

$$V_{void} = V_{gas} + V_{ads} = V_{total} - V_{solid}$$

where V_{void} is the void space volume. The void space is usually measured before the adsorption experiment and a gas with very low adsorption potential is used, usually helium.

The void space is calculated based on the pressure, temperature, compressibility, and volume of the gas in the pump and the cell. The equation for the void space is shown [61].

$$V_{void} = \frac{\left(\frac{P_h \Delta V}{zT}\right)_{pump}}{\left(\frac{P_2}{z_2 T} - \frac{P_1}{z_1 T}\right)_{cell}}$$

where P_h is the pressure of the helium in the pump, ΔV is the change in volume of the helium between the pump and the cells, P_2 and P_1 are the pressure of the helium after and before expansion respectively, z_1 and z_2 are the compressibility of the helium before and after expansion, and T is the temperature of the cells.

After calculating the void space, the CO_2 adsorption can be calculated based on the total volume injected and the total volume unadsorbed based on the number of moles using the following equation.

$$n_{ads} = n_{inj} - n_{unads}$$

where n_{ads} is the number of moles of CO_2 adsorbed to the shale, n_{inj} is the total number of moles of CO_2 injected, and n_{undas} is the number of moles of CO_2 that were not adsorbed.

For both the absolute and the Gibbs calculation methods, the number of moles of CO_2 injected is agreed upon and is calculated as follows.

$$n_{inj} = \left(\frac{P \Delta V}{zRT}\right)_{pump}$$

The difference between the absolute and the Gibbs adsorption value is mainly in the number of moles of CO_2 that are unadsorbed. This difference will be indicated when explaining each calculation method and its principles.

7.1. GIBBS ADSORPTION

Gibbs adsorption calculation neglects the volume occupied by the adsorbed phase when calculating the volume of unadsorbed gas. The adsorbed CO_2 on the shale rock will occupy some volume in the sample cell, and thus will affect the value of the unadsorbed CO_2 volume calculated. The Gibbs calculation assumes that the volume occupied by the adsorbed CO_2 is not occupied. This will result in some error in the adsorption capacity calculation. The equation for the Gibbs adsorption is shown [19].

$$n_{ads}^{Gibbs} = n_{total} - V_{void}\rho_{gas}$$

7.2. ABSOLUTE ADSORPTION

Absolute adsorption takes into consideration the volume occupied by the adsorbed phase when the unadsorbed volume is calculated. The volume occupied by the adsorbed CO_2 on the shale surface will affect the remaining volume that can be occupied by the unadsorbed CO_2 [61]. The number of moles of CO_2 adsorbed therefore becomes as follows.

$$n_{ads}^{abs} = n_{total} - V_{gas}\rho_{gas}$$

8. MAIN SOURCES OF ERROR IN VOLUMETRIC ADSORPTION DETERMINATION

When measuring and calculating the adsorption value, several common errors have been made which will affect the adsorption quantity severely. These errors are extremely commonplace and have been noticed amongst many researchers. In this section, this research summarizes the main errors that are associated with the adsorption calculation using the volumetric adsorption method, shown in Table 6 [13,56,62,63].

Table 6. Main Sources of Error in Volumetric Adsorption Determination

Source of Error	Explanation
Volume Adsorbed	Some calculations assume no helium adsorption, which could result in an error if the application requires accounting for this adsorption, and thus, if helium adsorption will impact the application.
Volume Injected	The volume of CO_2 injected should be calculated based on the volumes of the cells and the compressibility values, rather than depending on the injected volume.
Density of Adsorbate	The density of the adsorbate is affected by many conditions including temperature, pressure, and compressibility. It is easy to obtain the density.
Temperature Change	Changing the temperature will affect both the overall adsorption, and the gas itself. The gas will begin to expand which will make it extremely difficult to observe the equilibrium value.
Cell's Volume	Both the reference cell and the sample cell volumes must be known since they are imperative in the calculations. Any dead volume must be accounted for in the calculations.

9. CONCLUSIONS

During the application of CO_2 injection in unconventional shale reservoirs, CO_2 adsorption is an imperative factor that will impact enhanced oil recovery potential, and CO_2 storage capacity. This research provides a roadmap to the different types of adsorption and adsorption isotherms and measurement techniques to function as a guideline for the accurate application of experimental CO_2 adsorption in shale reservoirs. The main conclusions obtained from this research are summarized below.

- Adsorption is a function of both the adsorbate and the adsorbent. This shows that in order to properly study CO_2 adsorption to shale, both the CO_2 and shale properties should be considered.

- The most applicable isotherm to model CO_2 adsorption to shale is the BET since it overcomes the limitations of the Langmuir isotherm.

- Adsorption hysteresis is extremely important since it can give an indication of the adsorption-desorption cycle and thus can hint to the actual capacity of CO_2 that can be stored.

- The most common experimental methods used to measure adsorption are the volumetric and the gravimetric methods due to their simplicity and high accuracy as long as they are conducted properly.

- Different adsorption methods will have different sources of error. Each method must therefore be studied thoroughly in order to avoid conducting errors that may impact the accuracy of the results.

ACKNOWLEDGEMENTS

REFERENCES

Al Ismail, M. I. et al., 2014. The Effect of CO_2 Adsorption on Permeability Anisotropy in the Eagle Ford Shale. Unconventional Resources Technology Conference. doi:10.15530/URTEC-2014-1921520.

Aljamaan, H., et al., 2017. Multiscale Imaging of Gas Adsorption in Shales. Society of Petroleum Engineers. doi:10.2118/185054-MS.

Al-Mutarreb, A.M. et al., 2018. The Influence of shales characteristics on CO2 adsorption behaviour under sub-critical conditions. IOP Conference Series: Earth and Environmental Science. doi :10.1088/1755-1315/164/1/012031.

Bahadori, A., and Vuthaluru, H., 2010. Rapid Prediction of Carbon Dioxide Adsorption Isotherms for Molecular Sieves Using Simple Correlation. Society of Petroleum Engineers. doi:10.2118/122882-PA.

Bouzgarrou, S. et al., 2015. Experimental Adsorption and Modelisation of CO_2 on Adsorbents Collected from Elborma Field in South Tunisia. *Journal of Surface Engineered Materials and Advanced Technology*, **5**, 52-63. doi: 10.4236/jsemat.2015.51006.

Brown, T. et al., 2019. Pressure-varying Langmuir parameters and stepped nitrogen adsorption on alumina and silica. Physical Chemistry Journal, Royal Society of Chemistry.

Brunauer, S. et al., 1938. Adsorption of Gases in Multimolecular Layer. Journal of the American Chemical Society. 60, 2, 309-319. doi: 10.1021/ja01269a023.

Chareonsuppanimit, P. et al., 2012. High-Pressure Adsorption Of Gases On Shales: Measurements And Modeling, International Journal of Coal Geology, 95, https://doi.org/10.1016/j.coal.2012.02.005.

Charoensuppanimit, P. et al., 2016. Measurement and Modeling of Gas Adsorption on Shales. Energy & Fuels Journal, **30** (3), 2309-2319, https://doi.org/10.1021/acs.energyfuels.5b02751.

Chen, G. et al., 2016. Research of CO_2 and N_2 Adsorption Behavior in K-Illite Slit Pores by GCMC Method. Journal of Scientific Reports, **6**, https://doi.org/10.1038/srep37579.

Clarkson, C. R., 2003. Application of a New Multicomponent Gas Adsorption Model to Coal Gas Adsorption Systems. Society of Petroleum Engineers. doi:10.2118/78146-PA.

Clarkson, C. R., and Haghshenas, B., 2013. Modeling of Supercritical Fluid Adsorption on Organic-Rich Shales and Coal. Society of Petroleum Engineers. doi:10.2118/164532-MS.

Cook, M. and Douglas, H., 1949. Extrapolation of Adsorption Isotherms to High Relative Pressures and the Determination of the Surface Pressure of Adsorbed Films on Solids. J. Am. Chem. Soc. 1949, 71, 3, 791-797. https://doi.org/10.1021/ja01171a009.

Czepirski, L. et al., 2000. Some Generalization of Langmuir Adsorption Isotherm. Internet Journal of Chemistry, 3, 14.

Ehrburger-Dolle, F., 1999. A New Way to Analyze Adsorption Isotherms. Langmuir 1999, 15, 18, 6004-6015. https://doi.org/10.1021/la981349r.

Eliebid, M. et al., 2017. Adsorption Role in Shale Gas Recovery and the Feasibility of CO_2 in Shale Enhanced Gas Recovery: A Study on Shale Gas from Saudi Arabia. Society of Petroleum Engineers. doi:10.2118/187667-MS.

Foo, K. Y. and Hameed, B. H. 2010. Insights into the Modeling of Adsorption Isotherm Systems. Chemical Engineering Journal. 156. 2-10. https://doi.org/10.1016/j.cej.2009.09.013.

Fuji, T., et al., 2015. Evaluation Of CO_2 Sorption Capacity Of Rocks Using A Gravimetric Method For CO2 Geological Sequestration, Energy Procedia, **1,** (1), 3723- 3730, https://doi.org/10.1016/j.egypro.2009.02.

Gasparik, M. et al., 2015. High-Pressure/High-Temperature Methane-Sorption Measurements on Carbonaceous Shales by the Manometric Method: Experimental and Data-Evaluation Considerations for Improved Accuracy. Society of Petroleum Engineers. doi:10.2118/174543-PA.

Golshahi, N. et al., 2019. Asphaltene Structural Changes Induced by Carbon Dioxide Injection. Offshore Technology Conference. doi:10.4043/29730-MS.

Hall, F. E. et al., 1994. Adsorption of Pure Methane, Nitrogen, and Carbon Dioxide and Their Binary Mixtures on Wet Fruitland Coal. Society of Petroleum Engineers. doi:10.2118/29194-MS.

Heller, R. and Zoback, M., 2014. Adsorption of Methane and Carbon Dioxide on Gas Shale and Pure Mineral Samples. Journal of Unconventional Oil and Gas Resources, **8**, 14-24. https://doi.org/10.1016/j.juogr.2014.06.001.

Henry, W. 1803. Experiments on the Quantity of Gases Absorbed by Water, at Different Temperature and Under Different Pressures. Philosophical Transactions of the Royal Society of London, 93, 29-42.

Ibrahim, A. F. and Nasr-El-Din, H. A., 2015. Carbon Dioxide Sequestration in Coal Formations. International Petroleum Technology Conference. doi:10.2523/IPTC-18278-MS.

Jedli, H. et al., 2017. Carbon Dioxide Adsorption Isotherm Study On Various Cap Rocks In A Batch Reactor For CO2 Sequestration Processes, Applied Clay Science, **136**, 199-207, *0169- 1317,* https://doi.org/10.1016/j.clay.2016.11.022.

Jin, Z., and Firoozabadi, A., 2016. Thermodynamic Modeling of Phase Behavior in Shale Media. Society of Petroleum Engineers. doi:10.2118/176015-PA.

Kang, S. M. et al., 2011. Carbon Dioxide Storage Capacity of Organic-Rich Shales. Society of Petroleum Engineers. doi:10.2118/134583-PA.

Kazemi, M., and Takbiri-Borujeni, A., 2016. Molecular Dynamics Study of Carbon Dioxide Storage in Carbon-Based Organic Nanopores. Society of Petroleum Engineers. doi:10.2118/181705-MS.

Kecheng, Z. et al., 2019. Molecular Simulation of Carbon Dioxide and Methane Adsorption in Shale Organic Nanopores. Energy & Fuels 2019 33 (3), 1785-1796.DOI:10.1021/acs.energyfuels.8b02851.

Keller, J. and Staudt, R. 2005. Gas Adsorption Equilibria, Experimental Methods and Adsorptive Isotherms, Springer Science.

Khaleel, M. et al., 2018. Amine-Functionalized Hierarchical Zeolites for Carbon Dioxide Capture. Society of Exploration Geophysicists.

Lafortune, S. et al., 2014. Assessing CO2 Adsorption Capacities onto Shales through Gravimetric Experiments: A First Step in the Feasibility Study of Coupling "Fracking" with Carbon Storage, Energy Procedia, **63**, 5933-5937, *1876-6102*, https://doi.org/10.1016/j.egypro.2014.11.629.

Langmuir, I. 1918, The Adsorption of Gases on Plane Surfaces of Glass, Mica, and Platinum. Journal of the American Chemical Society. 40, 9, 1361-1403. doi: 10.1021/ja02242a004.

Le, T. D. et al., 2017. A New Matrix/Fracture Multiscale Coupled Model for Flow in Shale-Gas Reservoirs. Society of Petroleum Engineers. doi:10.2118/181750-PA.

Liu, Q. et al., 2018. Macroscale Mechanical and Microscale Structural Changes in Chinese Wufeng Shale With Supercritical Carbon Dioxide Fracturing. Society of Petroleum Engineers. doi:10.2118/181369-PA.

Lu, M., et al., 2017. A New Method for the Estimation of Lost Gas During the Measurement of the Gas Content of Coal. Society of Petroleum Engineers. doi:10.2118/176976-PA.

Luo, X. et al., 2015. Adsorption Of Methane, Carbon Dioxide And Their Binary Mixtures On Jurassic Shale From The Qaidam Basin In China, International Journal of Coal Geology, 150–151, 210-223, https://doi.org/10.1016/j.coal.2015.09.004.

Lutynski, M. et al., 2017. CO2 sorption of Pomeranian gas bearing shales – the effect of clay minerals, Energy Procedia, 125, 457-466. https://doi.org/10.1016/j.egypro.2017.08.153.

Manju, M and Joewondo, P., 2014. CO2 Sorption Capacity in Clay-Rich Shales with Moisture Content. 14th Greenhouse Gas Control Technologies Conference Melbourne 21-26 October (GHGT-14) . Available at SSRN: https://ssrn.com/abstract=3365692.

Meng, X. et al., 2017. Experimental and Numerical Study of Enhanced Condensate Recovery by Gas Injection in Shale Gas-Condensate Reservoirs. Society of Petroleum Engineers. doi:10.2118/183645-PA.

Mohagheghian, E. et al., 2015. Carbon Dioxide Compressibility Factor Determination Using a Robust Intelligent Method, The Journal of Supercritical Fluids, **101**, 140- 149, *0896- 8446*, https://doi.org/10.1016/j.supflu.2015.03.014.

Mohammad, S. et al., 2009. Experimental Uncertainties in Volumetric Methods for Measuring Equilibrium Adsorption. Energy & Fuels, **23**, 2810-2820. https://doi.org/10.1021/ef8011257.

Ngo, T., 2015. Reservoir Capacity Estimates in Shale Plays Based on Experimental Adsorption Data. Masters Thesis.

Orr, F. M., 2004. Storage of Carbon Dioxide in Geologic Formations. Society of Petroleum Engineers. doi:10.2118/88842-JPT.

Perez, F. and Devegowda, D., 2017. Methane and Carbon Dioxide Adsorption in Kerogen Models Using Molecular Simulations, Mewbourne School of Petroleum and Geological Engineering, The University of Oklahoma.

Psarras, P. et al., 2017. Methane and CO_2 Adsorption Capacities of Kerogen in the Eagle Ford Shale from Molecular Simulation. Accounts of Chemical Research, https://doi.org/10.1021/acs.accounts.7b00003.

Rani, S. et al., 2015. Comparison of Void Volume for Volumetric Adsorption Studies on Shale from India. Journal of Natural Gas Science and Engineering. **26**, 725-729. https://doi.org/10.1016/j.jngse.2015.07.012.

Reynolds, M. M. and Buendia, J., 2017. Permanently Sequester Anthropogenic Carbon Dioxide - Through Hydraulic Fracturing. Society of Petroleum Engineers. doi:10.2118/185033-MS.

Santos, J. M., and Akkutlu, I. Y., 2013. Laboratory Measurement of Sorption Isotherm under Confining Stress with Pore-Volume Effects. Society of Petroleum Engineers. doi:10.2118/162595-PA.

Sathre, R and Masanet, E. 2013. Prospective Life-Cycle Modeling of a Carbon Capture and Storage System Using Metal-Organic Frameworks for CO_2 Capture. RSC Advances. 3, 4964-4975.

Shi, J. et al., 2019. Competitive adsorption phenomenon in shale gas displacement processes. RSC Adv., 2019, 9, 25326-25335. DOI: 10.1039/C9RA04963K.

Sing, K., 1984. Reporting Physisorption Data for Gas/Solid Systems with Special Reference to the Determination of Surface Area and Porosity. International Union of Pure and Applied Chemistry, Physical Chemistry Division, Commission on Colloid and Surface Chemistry Including Catalysis.

Smit, B. et al., 2014. Introduction to Carbon Capture and Sequestration. Imperial College Press.

Sudibandriyo, M. et al., 2003. Adsorption of Methane, Nitrogen, Carbon Dioxide, and Their Binary Mixtures on Dry Activated Carbon at 318.2 K and Pressures up to 13.6 MPa. *Langmuir* **2003** *19* (13), 5323-5331. https://doi.org/10.1021/la020976k.

Tajnik, T. et al., 2013. Investigation of adsorption properties of geological materials for CO_2 storage. Int. J. Energy Res., 37: 952-958. doi:10.1002/er.2901.

Thommes, M. et al., 2015. Physisorption of Gases, with Special Reference to the Evaluation of Surface Area and Pore Size Distribution (IUPAC Technical Report), Journal of Pure Applied Chemistry, 1-19.

Van Dongen, R.H. et al., 1971. Physical adsorption at high relative pressures. Surface Science, 28 (1), 237-257. https://doi.org/10.1016/0039-6028(71)90097-5.

Yang, S. et al., 2016. Effects of Multicomponent Adsorption on Enhanced Shale Reservoir Recovery by CO2 Injection Coupled with Reservoir Geomechanics. Society of Petroleum Engineers. doi:10.2118/180208-MS.

Yanian, Z. et al., 2015. Study on Controlling Factors of Shale Gas Adsorption. ACTA Geologica Sinica, **89**, 300- 301.

Yu, W. et al., 2016. Modeling Gas Adsorption in Marcellus Shale With Langmuir and BET Isotherms. Society of Petroleum Engineers. doi:10.2118/170801-PA.

Yuan, H. et al., 2017. Investigation on Gas-Adsorption-Induced Swelling and Permeability Evolutions of Cox Argillite, Fresh Journal of Mechanics.

Zhang, P. 2016. Adsoprtion and Desorption Isotherms. Kere-Search Group.

Zhao, H. et al., 2017. Sorption Hysteresis of Light Hydrocarbons and Carbon Dioxide in Shale and Kerogen. Scientific Research. https://doi.org/10.1038/s41598-017-13123-7.

IX. HIGH PRESSURE – HIGH TEMPERATURE CARBON DIOXIDE ADSORPTION TO SHALE ROCKS USING A VOLUMETRIC METHOD

ABSTRACT

With the current increase in hydrocarbon production from shale reservoirs, several methods have been applied to improve recovery from these unconventional oil and gas sources. Carbon dioxide (CO_2) injection is one of the methods that can be used to increase oil recovery and store the CO_2 in the reservoir via adsorption. This research investigates the CO_2 storage applicability in the North East Oklahoma shale, which is part of the southern section of the Kansas Basin for CO_2 storage, as well as the factors impacting the storage capacity. The shale mineralogy was initially identified using X-Ray Diffraction (XRD) analysis. CO_2 adsorption on shale was measured using a volumetric-based adsorption apparatus. The effect of varying the CO_2 phase, injection pressure, temperature, shale particle size, and shale volume in the sample cell was studied. Increasing the pressure resulted in an increase in adsorption, whereas increasing the temperature showed an opposite trend. No trend can be observed when decreasing the shale volume, since decreasing the volume using the volumetric adsorption apparatus will result in erroneous results. This research investigates and highlights the main factors that will impact CO_2 adsorption to North East Oklahoma shale during CO_2 injection in order to assess the applicability of CO_2 injection storage purposes.

1. INTRODUCTION

CO_2 injection is a method applied in the hydrocarbon industry to increase oil recovery (Fakher, S. and Imqam, A., 2018; 2019; 2020a; 2020b; 2020c; Fakher, S. et al., 2017; 2018; 2019a; 2019b; Fakher, S.M., 2019). During its propagation through the formation, CO_2 can adsorb to the grains and remain inside the reservoir (Perez, F. and Devegowda, D., 2017; Al-Mutarreb, A.M. et al., 2018; Miedzinska, D. and Lutynski, M., 2017). This can significantly aid the CO_2 storage initiative and thus decrease the environmental impact from the hydrocarbon production (Le, T.D. et al., 2017; Carey, J.W. et al., 2015; Yang, Z. et al., 2018; Fakher, S., 2019). It is important to understand and analyze the impact of different factors on CO_2 adsorption in the reservoir, since this will affect the volume of CO_2 that can be stored.

The reservoir thermodynamic conditions, rock and fluid properties, and injected fluid characteristics and properties will greatly impact the adsorption capacity (Singh, H. and Cai, J., 2018; Khosrokhavar, R. et al., 2014). Many studies have investigated the impact of pressure on adsorption (Psarras, P. et al., 2017; Kang, S.M. et al., 2011; Jin, Z. and Firoozabadi, 2016; Yang, S. et al., 2016; Aljamaan, H. et al., 2017; Clarkson, C.R., 2003; Lafortune, S. et al., 2014; Al Ismail, M. I. et al., 2014; Santos, J.M. and Akkutlu, I.Y., 2013). It was found that increasing the CO_2 injection pressure resulted in an increase in the adsorption capacity; however, there was a maximum limit to which this increase occurred (Bouzgarrou, S. et al., 2015; Luo, X. et al., 2015; Bahadori, A. and Vuthaluru, H.B., 2010; Yu, W. et al., 2016; Heller, R. and Zoback, M., 2014; Chen, G. et al., 2016; Eliebid, M. et al., 2017; Yuan, H. et al., 2017). Beyond the maximum limit, it was reported

that any increase in the pressure would result in a decrease in adsorption due to the CO_2 molecules repelling each other at extremely high pressures (Gasparik, M. et al., 2015; Chareonsuppanimint, P. et al., 2012; 2016; Clarkson, C.R. and Hagheshenas, B., 2013; Lu, M. et al., 2017; Sing, K., 1984; Sudibandriyo, M. et al., 2002). Most of the researchers mentioned above have researched the effect of pressure on CO_2 adsorption, however, very little research has focused on the impact of the CO_2 phase on adsorption and storage capacity in shale.

The reservoir temperature was found to have a controversial effect on CO_2 adsorption, with some researchers mentioning an increase in adsorption with the increase in temperature (Bouzgarrou, S. et al., 2015; Psarras, P. et al., 2017; Chareonsuppanimint, P. et al., 2012; Heller, R. and Zoback, M., 2014; Fujii,T. et al.; Yanian, Z. et al., 2015), while others reported the opposite (Gasparik, M. et al., 2015; Jedli, H. et al., 2017; Jin, Z. and Firoozabadi, A., 2016; Luo, X. et al., 2015; Chen, G. et al., 2016; Bahadori, A. and Vuthaluru, H.B., 2010; Lafortune, S. et al., 2014). This is mainly due to the temperature having an impact on several other parameters, including the pressure and the shale properties. Increasing the temperature will result in an increase in pressure as well, which may impact the adsorption capacity. It is therefore advised to undergo temperature experiments at isobaric conditions. The temperature may also affect the properties and structures of different clays in the shale, which in turn may impact adsorption (Psarras, P. et al., 2017; Yu, W. et al., 2016). Since different shale samples will have different mineralogy, temperature may result in a contrasting effect on adsorption when tested on different samples. It is therefore important to study the impact of temperature for the North East Oklahoma shale since it has not yet been investigated.

The rock properties have also been reported to greatly affect CO_2 adsorption capacity (Yang, Z. et al., 2016; Yue, N. et al., 2018; Murugesu, M. et al., 2019). Shale will have different clay contents and different clay types. Many researchers have reported that clay type and concentration will influence adsorption significantly (Lui, Q. et al., 2018; Aljamaan, H. et al., 2017; Jedli, H. et al., 2017; Jin, Z. and Firoozabadi, 2016; Ngo, T., 2015). As the clay content in the shale increases, adsorption will also increase (Aljamaan, H. et al., 2017; Bouzgarrou, S. et al., 2015; Jin, Z. and Firoozabadi, 2016). Based on this, shale with high clay content is more favorable for CO_2 storage operations. In addition, the presence of carbonate minerals will also influence adsorption since they react with the CO_2 (Luo, X. et al., 2015; Mohammad, S. et al., 2009; Tajinik, T. et al., 2012; Aljamaan, H. et al., 2017). It is important to determine the mineralogy of the shale before undergoing adsorption experiments to understand the adsorption capacity of the shale samples.

This research aims to investigate a new type of shale from North East Oklahoma which is a part of the Kansas Basin for CO_2 storage (USGS-CO_2 Sequestration, 2019) that may have a large potential for CO_2 storage due to its high clay content. To the authors' knowledge, no research has been conducted to study CO_2 storage in this shale. The research studies the impact of CO_2 phases. In addition, the research studies the impact of reservoir temperature on CO_2 adsorption capacity. This will help determine if the North East Oklahoma shale is a suitable reservoir for CO_2 storage and the conditions at which the maximum capacity of CO_2 can be stored in the formation.

2. ADSORPTION GOVERNING EQUATIONS

Generally, adsorption can be defined as the tendency of an adsorbent to adsorb to an adsorbate due to a bond deficiency between the adsorbent and the adsorbate. The general adsorption equation is shown in Equation (1):

$$V_{total} = V_{solid} + V_{gas} + V_{ads}$$

where V_{total} is the total volume of the system, V_{solid} is the volume of the shale in the sample cell, V_{gas} is the volume of the CO_2 in the bulk phase or free gas, and V_{ads} is the volume of the CO_2 adsorbed.

When the shale sample is placed in the sample cell, the shale grains will not fill up the whole cell, since some voids will remain between the grains. It is crucial that these void spaces are measured, since the total volume of the adsorbent and the adsorbate will be incorrect if the void space is not measured. The general definition of the void space is shown in Equation (2):

$$V_{void} = V_{gas} + V_{ads} = V_{total} - V_{solid}$$

where V_{void} is the void space volume. The void space is usually measured before the adsorption experiment and a gas with very low adsorption potential is used, usually helium. The void space is calculated based on the pressure, temperature, compressibility, and

volume of the gas in the pump and the cell. The equation for the void space is shown in Equation (3):

$$V_{void} = \frac{\left(\frac{P_h \Delta V}{zT}\right)_{pump}}{\left(\frac{P_2}{z_2 T} - \frac{P_1}{z_1 T}\right)_{cell}}$$

where P_h is the pressure of the helium in the pump, ΔV is the change in volume of the helium between the pump and the cells, P_2 and P_1 are the pressure of the helium after and before the expansion, respectively, z_1 and z_2 are the compressibility of the helium before and after the expansion, and T is the temperature of the cells.

After calculating the void space, the CO_2 adsorption can be calculated based on the total volume injected and the total volume unadsorbed based on the number of moles using Equation (4).

$$n_{ads} = n_{inj} - n_{unads}$$

where n_{ads} is the number of moles of CO_2 adsorbed to the shale, n_{inj} is the total number of moles of CO_2 injected, and n_{undas} is the number of moles of CO_2 that were not adsorbed.

$$n_{inj} = \left(\frac{P\Delta V}{zRT}\right)_{pump}$$

For both the absolute and the Gibbs calculation methods, the number of moles of CO_2 injected is agreed upon and is calculated in Equation (5).

Both the absolute and the Gibbs adsorption were calculated in this research. The main difference between the absolute and the Gibbs adsorption is the method by which the unadsorbed CO_2 is calculated. The Gibbs adsorption neglects the volume occupied by the adsorbed phase when calculating the volume of the unadsorbed gas. In other words, the Gibbs calculation underestimates the adsorbed CO_2, and hence the adsorption value will be less than that of the absolute. Equation (6) is shown below (Sudibandriyo, M. et al., 2003).

$$n_{ads}^{Gibbs} = n_{total} - V_{void}\rho_{gas}$$

The Absolute Adsorption takes into consideration the volume occupied by the adsorbed phase when calculating the unadsorbed volume. Thus, the value is not underestimated. This in turn results in a larger value compared to the Gibbs adsorption. Equation (7) is shown below (Charoensuppanimit, P. et al., 2016).

$$n_{ads}^{Abs} = n_{total} - V_{gc}\rho_{gas}$$

In Equation (7), the V_{gc} term includes the total volume of the gas in the cells, including the adsorbed and the unadsorbed phases, and thus accounts for all the gas in the cells. This ensures that the adsorption value is not underestimated. In Equation (6) however, the V_{gas} term is replaced by the V_{void}, which is the void volume in the cells. This

does not account for the unadsorbed phase, since it only takes into consideration the void space within the cells and thus underestimates the calculated adsorption value.

The volume of unadsorbed CO_2 can be calculated for the Gibbs adsorption using Equation (8): (Charoensuppanimit, P. et al., 2012)

$$n_{unads}^{Gibbs} = \frac{P_{af}V_{void}}{z_{af}RT}$$

By knowing the Gibbs unadsorbed CO_2 volume, the Gibbs adsorption can then be calculated using Eq. (4). The absolute adsorption can then be calculated using the value of the Gibbs adsorption by relating both values using Equation (9): (Sudibandriyo, M. et al., 2002)

$$n_{ads}^{Abs} = n_{ads}^{Gibbs}\left(\frac{\rho_{ads}}{\rho_{ads} - \rho_{gas}}\right)$$

where ρ is the density. The value that is not easy to obtain is the density of the adsorbed gas, ρ_{ads}, and this volume is usually obtained using the liquid density at the atmospheric pressure boiling point (Sudibandriyo, M. et al., 2002; Arri, L. E. and Yee, D., 1992).

3. EXPERIMENTAL MATERIAL

The experimental materials used to conduct the experiments are explained in this section, as follows. All the material was obtained prior to conducting the experiments.

3.1. SPECIALLY DESIGNED ADSORPTION SETUP

A specially designed apparatus was developed based on gas volumetric expansion to measure both helium void space and CO_2 volumetric adsorption.

3.2. WATER BATH

A temperature-adjustable water bath was used to adjust the temperature of the setup. The setup was fully submerged in the water bath for the duration of the experiments.

3.3. HIGH ACCURACY THERMOMETER

The thermometer was used to measure the temperature of the water bath during the duration of the experiments. If the temperature change was more than 0.5 ℃, the experiment was repeated.

3.4. PRESSURE TRANSDUCERS

Two pressure transducers with a pressure limit of 3000 psi (20.684 mPa) were used to record the pressure during the duration of the experiments.

3.5. CERAMIC MORTAR AND PESTLE

A ceramic mortar and pestle were used to crush the shale samples with the least amount of heat generation to avoid altering the properties of the shale.

3.6. CRUSHED SHALE SAMPLES

A shale sample, obtained from North East Oklahoma, USA, was used to conduct all the experiments. The shale was crushed to three different sizes: 590, 140, and 53µm. The sample sizes were based on the final sieve size through which the shale particles passed through after using more than 10 sieves.

3.7. VACUUM PUMP

The vacuum pump was used to vacuum both the sample cell and the reference cell before running any experiment. The vacuum pump used vacuum oil which was changes after every several runs to ensure that the pump was working efficiently.

3.8. GAS PYCNOMETER

The density of the shale was measured using a gas pycnometer. Six values were averaged, and the result was used as the shale density. The difference between each value was less than 0.001 g/cm^3. The pycnometer utilizes an extruding noneacting gas to propagate through the pores and measures the overall density. The gas used in this research with the pyconometer was helium. This was mainly due to the ability of helium to extrude through the small pores of the shale and also since the helium does not react with the shale or the clays in the shale matrix.

4. EXPERIMENTAL SETUP

The setup used to conduct the experiments is shown in Figure 1. A syringe pump is used to pressurize the CO_2 using distilled water. The pump injects the water into an accumulator with a piston inside, which separates the water from the CO_2. A CO_2 source is connected to the accumulator from the other side to fill up the accumulator. A pressure gauge is used to show the pressure of the CO_2 in the accumulator. Once the required pressure is reached, a valve is opened to inject the CO_2. The specially designed adsorption setup is composed of a reference cell and a sample cell. The reference cell is much smaller in volume than the sample cell in order to be able to accurately record the pressure drop. Both the sample cell and the reference cell have a pressure transducer connected to them to record the pressure.
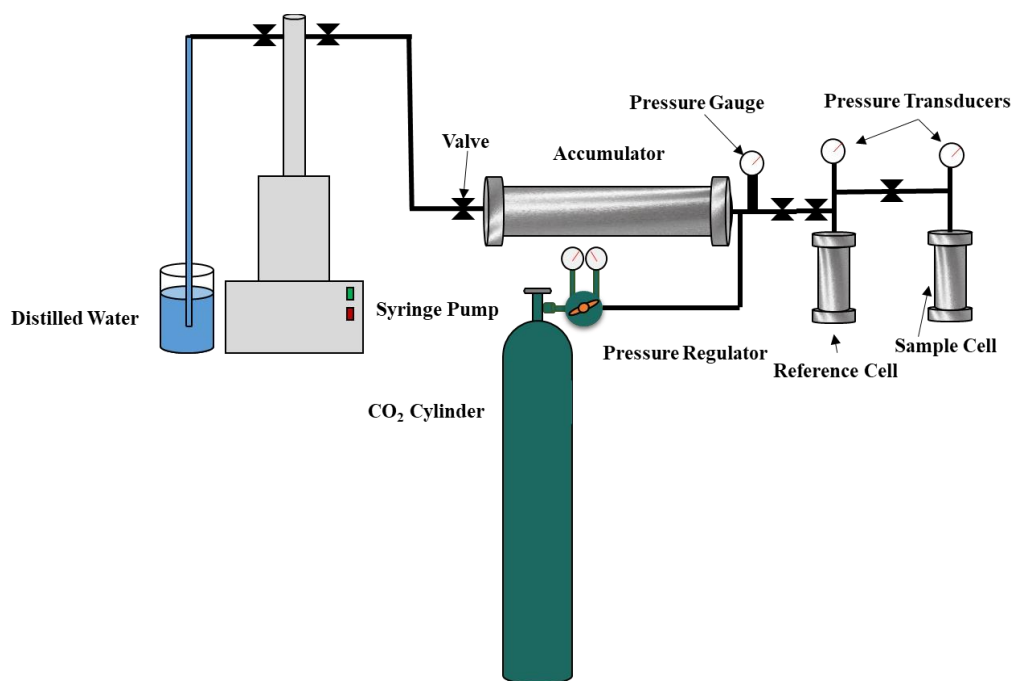

Figure 1. Illustration of Experimental Setup

5. EXPERIMENTAL PROCEDURE

A specially designed procedure was developed and followed to conduct all the experiments in order for all the results obtained to be both repeatable and comparable. The exact procedure is mentioned below.

1. The shale samples are crushed to the desired particle sizes using a mortar and pestle. The mortar and pestle are used instead of an electrical device to reduce the amount of heat generated during the crushing to avoid altering the properties of the clays in the shale. After the samples are crushed, they are sieved using a stack of sieves starting with 20 mesh and reaching up to 350 mesh.

2. After the shale samples are sorted, the sample cell is filled with a specific volume using the shale size needed for the experiment. The volume of the shale sample is determined using the weight and the density of the sample in order to account for the pores present between the crushed shale particles. The density of the shale is determined using a Gas Pycnometer.

3. A mesh screen with a pore size smaller than the shale particle size is placed on top of the sample cell before it is sealed to avoid movement of the shale sample outside of the sample cell during pressurizing or depressurization.

4. The sample cell is then connected to the sealed reference cell with a valve in between both cells to regulate the flow of the gas from the reference cell to the sample cell. The reference cell is much smaller in volume than the sample cell in order for the transducers to accurately record the pressure expansion of the helium and the CO_2.

5. Both cells are then connected to a vacuum pump and vacuumed for 12 hours. All valves are then sealed to avoid any air going inside the cells. The pressure within the cells, which is negative due to the vacuum pump, is then recorded.

6. The vacuumed cells are then placed in a water bath and are left to heat to the required temperature overnight. The pressure is then recorded again to observe any difference in pressure, which could indicate leakages.

7. Before measuring the adsorption, the void space is measured. This indicates the volume that is not occupied by shale. Helium is injected into the reference cell after it is pressurized to the design pressure. It is then left to heat in the reference cell for 6 hours to reach the design temperature.

8. The valve connecting the reference cell to the sample cell is then opened, and the helium is left to expand in both cells. The pressure recording commences as soon as the valve is opened.

9. The experiment is run until the pressure equalizes in both cells and becomes stable. This could take up to 12 hours.

10. Steps 7, 8, and 9 are then repeated using CO_2 as the injection gas to measure CO_2 adsorption. The main difference between helium void space and CO_2 adsorption is the equations used to calculate the values for the void space and the adsorption, as explained previously.

6. RESULTS AND DISCUSSION

The results obtained from this research include the shale mineralogy obtained using XRD, and finally, the CO_2 adsorption capacity under different phases, pressure and temperature conditions for different shale particle sizes and shale volumes.

6.1. SHALE MINERALOGY

Shale mineralogy was identified using XRD analysis. The shale was pulverized into a size of 350 mesh. Next, the shale was placed in distilled water and mixed vigorously. The suspended clays were then left for 10 hours to ensure that they remained suspended in the water. Since the clays did not remain suspended, nine drops of clagon were added to help the clays remain suspended. The suspension was left overnight, and then the suspended clay sample was taken and dried. Three samples were made and run during XRD analysis in order to ensure accuracy and repeatability. After the XRD was done on the samples, they were put in a furnace at 600 ⁰C for 12 hours. This was done to decisively determine the presence of kaolinite peaks since they disappear after heat treatment at this temperature.

The results of the XRD and its analysis for both the untreated and the heat treated sample are shown in Figure 2. The mineral equivalent for each peak was determined based on the 2θ value and the intensity; each mineral has a specific fingerprint that will define it during XRD. Since some minerals can be confused with others, the heat treated XRD is conducted to differentiate between them, as is the case for chlorite and kaolinite.
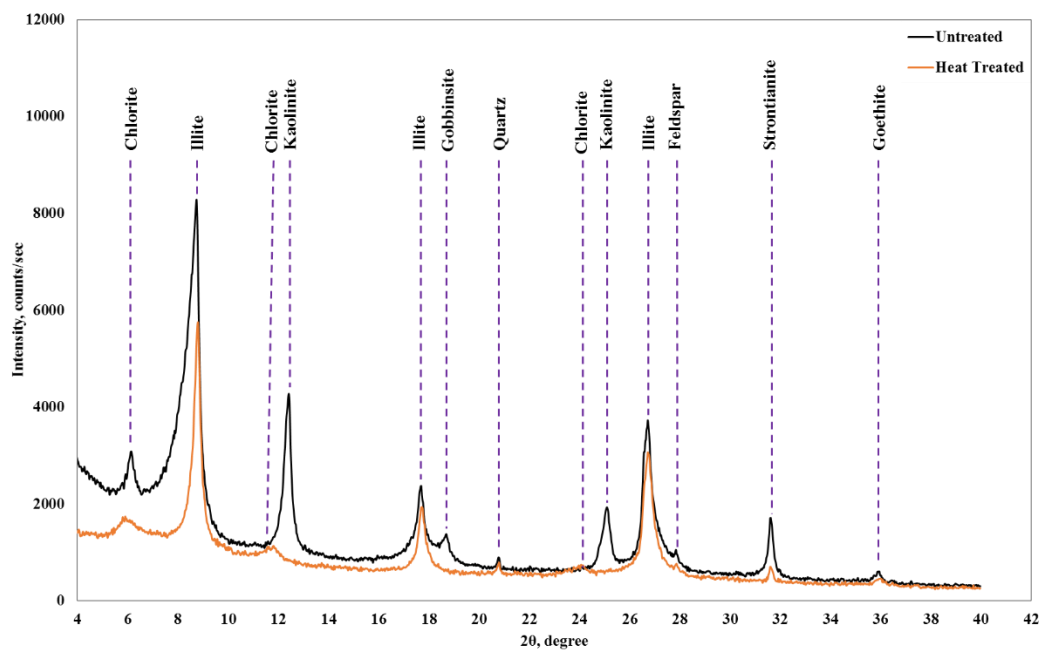
Figure 2. XRD Result for Northeast Oklahoma Shale

Based on the XRD analysis, the shale has a large clay content. This high clay content can affect the adsorption capacity; an increase in clay mineral content usually results in an increase in the shale adsorption capacity (Chareonsuppanimit, P. et al., 2016; Chen, G. et al., 2016; Heller, R. and Zoback, M., 2014; Sudibandriyo, M. et al., 2003; Yuan, H. et al., 2017); this will be shown when presenting the adsorption results. The kaolinite clay does not show in the heat treated XRD run since it is destroyed at 500-550 ⁰C. Another mineral, goethite, was also determined by comparing the heat treated run to the normal run, since goethite will form a dome-like structure in the heat treated XRD run. In order to determine the correct minerals and clays using the XRD, a match between the Intensity and the location of the degree had to be conducted for each of the minerals and

clays defined. It was also important to ensure that the determined mineral did not coincide with another one.

Based on the XRD results, the shale used in this study has a high percentage of clay (30-40%). This high percentage of clay can affect the CO_2 adsorption in two main ways, mainly based on the structure of the clay and the water content of the shale itself. The two effects are as follows:

- **Clay Structure Impact:** Gas adsorption will primarily occur on active sites in the shale containing organic carbons, and thus adsorption will increase with the increase in clay content in the shale (Chareonsuppanimit, P., et al., 2016). Since clay minerals have larger surface areas compared to other minerals in the shale structure, they tend to increase the total porosity of the rock and also increase the available sites for adsorption, which in turn result in a larger gas storage capacity and a larger adsorption potential (Zhang, C. et al., 2017). Based on this, research conducted on several types of shale showed that shale with a higher clay content will result in a larger adsorption capacity (Heller, R. and Zoback, M., 2014).

- **Water Saturation Impact:** Since clays have a high affinity for water, if the water concentration or the humidity level in the shale is high, the clays will begin to absorb the water and swell. This will result in a decrease in the total porosity and a decrease in the adsorption sites, since the water will occupy some of these sites (Zhang, C. et al., 2017). The water saturation impact was not studied in this research since the shale particles were pulverized and then added in the sample cell. No water was used in the experimental sample cell.

6.2. VOID SPACE

When the shale particles are placed in the reference cell, some small spaces will exist between the particles. This volume is referred to as the void volume and must be accounted for during each experiment, since this is considered excess volume that will be occupied by the CO_2 and will not contribute to the adsorption. The void space therefore signifies the pores present between the grains and is thus similar to the total porosity of the system. The void volume is also an essential factor in the adsorption calculations, as was shown previously. The void volume is usually measured using a gas with extremely low adsorption; the gas used in this study to measure void volume is helium, which is the most widely used gas to measure adsorption. Helium has many advantages that make it extremely suitable to use when measuring the void space. These advantages include (Torsaeter, O., and Abtahi, M., 2000):

- Helium is a noble gas and thus is non-reactive, which reduces the risk of altering the shale matrix during void space measurement.

- Helium can be modeled as an ideal gas at most pressure and temperature conditions.

- Since helium has small molecules, it has a high diffusivity coefficient and thus can penetrate into extremely small pore sizes.

- Helium has extremely low adsorptivity to shales and thus will not affect the shale matrix, and helium will provide void space values with the least error possible (Torsaeter, O., and Abtahi, M., 2000).

The effect of varying the helium injection pressure, temperature, shale particle size, and shale volume on the void volume was studied, and the results are explained below.

6.3. CARBON DIOXIDE ADSORPTION

After measuring the void volume for each experiment, the CO_2 adsorption was measured and calculated. The effect of varying CO_2 phase, injection pressure, temperature, shale particle size, and shale volume on the void volume was studied. The results obtained from this study are also compared to other CO_2 adsorption studies that used shale rocks from different sources to illustrate how the adsorption will vary based on the shale type.

At different phases, the CO_2 will have different properties and will also sorb differently. It is therefore important to determine if the CO_2 phase will impact the adsorption of the North East Oklahoma shale. Figure 3 shows the adsorption values for gaseous, liquid, and supercritical CO_2 phases. The gaseous phase resulted in the lowest adsorption capacity.
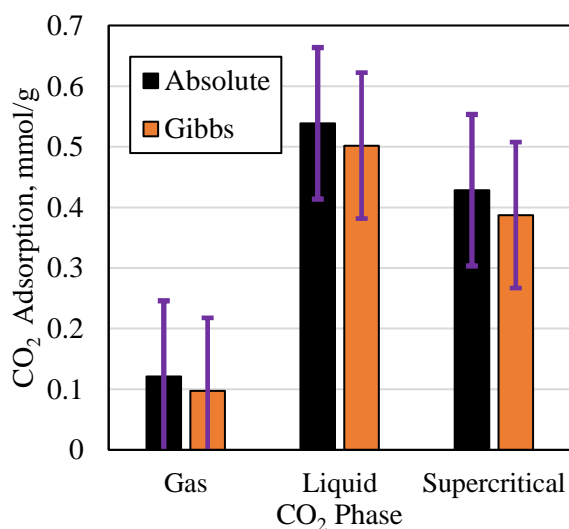

Figure 3. CO_2 Adsorption in mmol/g for Different CO_2 Phases

When the CO_2 was in the liquid phase, the highest adsorption value was observed. For the supercritical CO_2, the adsorption was higher than the gas, but slightly lower than the liquid. This could be due to the difference in density of the CO_2 at the different phases. Increasing the density will allow for a larger volume to be adsorbed to the shale. When the density of the CO_2 was obtained, the values were 0.192, 0.823, and 0.651 g/cm^3 for the gas, liquid, and supercritical CO_2, respectively.

The CO_2 injection pressures that were evaluated include 500 (3.447), 1000 (6.895), 1500 (10.342), and 2000 (13.790) psi (mPa) using the 53 micron shale particle size, shale volume of 3.8 cm^3, and 40 ºC. The results for the absolute and the Gibbs adsorptions are shown in Figure 4. Increasing the pressure from 500 to 1500 psi resulted in a significant increase in the CO_2 adsorption. This is mainly due to the increased compression of the gas molecules as the pressure is increased, which increases the CO_2 adsorption on the shale rock. However, when the pressure is increased from 1500 psi (10.342 mPa) to 2000 psi (13.790 mPa), the adsorption value increases very little. This is due to the repulsion forces between the gas molecules increasingly rising higher at 2000 psi (13.790 mPa); in fact, many researchers observed a decrease in CO_2 adsorption capacity at extremely high pressures (Sudibandriyo, M. et al., 2003; Nog, T., 2010; Chareonsuppanimit, P. et al., 2012; Lafortune, S. et al., 2014), which is similar to the trend seen in Figure 3, although the pressure at which the decrease happens was not reached. The pressure decrease was not observed in this research due to the pressure limitation. The highest pressure value studied in this research was 2000 psi. The pressure could not be increased further due to several limitation. The main limitation was the valves which had a maximum operating pressure of 2500 psi and thus the pressure could not be increased to ensure a safety margin. The

second main limitation was the capacity of the accumulator used from pressurization. The limited capacity of the acculator allowed only for a specific volume of CO_2 or helium to be injected in the accumulator and thus limited the pressurization process.
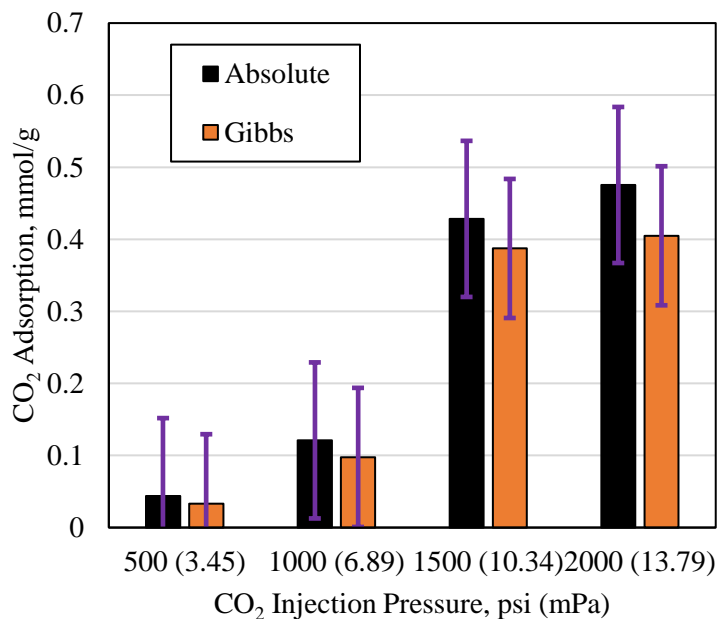
Figure 4. CO_2 Adsorption in mmol/g at Different Pressures Using 3.8 cm^3 of 53μ, 40 °C

The effect of both decreasing and increasing the temperature on CO_2 adsorption capacity was investigated using three different temperatures, including 25, 40, and 60 °C. The experiments were conducted using 3.8 cm^3 of shale, the 53 micron shale particle size, and 1500 psi (10.342 mPa) CO_2 injection pressure. The results of the CO_2 adsorption at different temperatures is shown in Figure 5. Decreasing the temperature from 40 to 25 °C resulted in an increase in the CO_2 adsorption capacity. This is due to the lower energy of the gas molecules at lower temperatures, which increases their adsorption to the shale rock. Increasing the temperature from 40 to 60 °C resulted in the opposite trend, where the

adsorption decreased due to the increase in energy of the gas molecules, which results in their increased movement and subsequently a decrease in CO_2 adsorption (Psarras, P. et al., 2017; Sing, K., 1984).
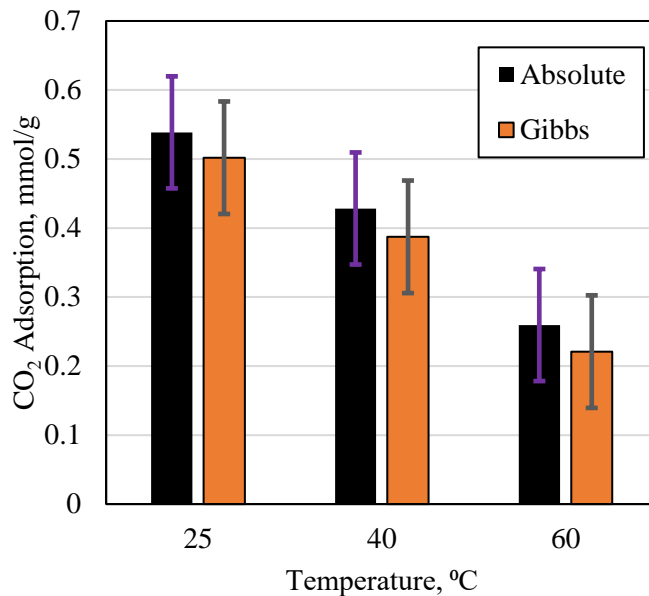
Figure 5. CO_2 Adsorption in mmol/g at Different Temperatures Using 3.8 cm^3 of 53 micron Shale at 1500 psi (10.342 mPa)

The experiments conducted in this research used shale particles that were pulverized to a very small mesh size. An important factor to consider in this case is whether these small particle sizes are representative of a shale core or not. Based on this, the effect of changing the shale particle size on CO_2 adsorption capacity was studied using three different shale particle sizes, including 53, 149, and 590 microns. All experiments were conducted using 3.8 cm^3 of shale, 1500 psi (10.342 mPa) CO_2 injection pressure, and 40 °C. Figure 6 shows the results of CO_2 adsorption using different shale particle sizes. The shale particle size had almost no impact on the CO_2 adsorption value. This indicates that

the shale particles can be used to accurately model adsorption, regardless of their size. This will also help in being able to compare the results obtained from this research to other research that did not use the same particle size used in this research.
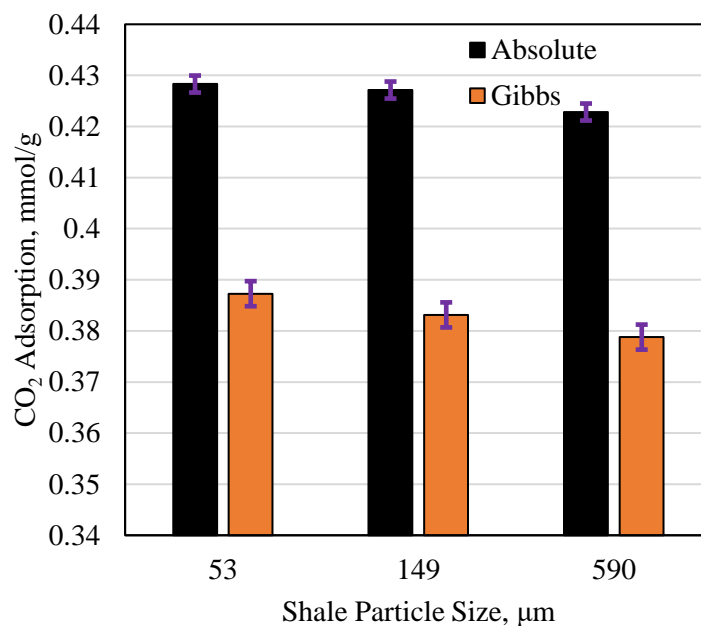
Figure 6. CO_2 Gibbs and Absolute Adsorption in mmol/g Using Different Shale Particle Sizes using 3.8 cm^3 Shale Volume at 1500 psi (10.342 mPa) and 40 ⁰C

Reducing the shale volume in the sample cell when measuring CO_2 adsorption using the volumetric adsorption apparatus will yield highly erroneous results, with the error increasing as the volume of the shale in the reference cell decreases (Santos, J. M., and Akkutlu, I. Y., 2013; Mohammad, S. et al., 2009). This is partially due to the adsorption of the CO_2 onto part of the sample cell wall, which results in a confused adsorption value (Mohammad, S. et al., 2009). Three experiments were conducted with a gradual decrease in the shale volume to both verify and emphasize this high error phenomenon. Shale volumes of 3.80, 3.42, and 2.66 cm^3 in the sample cell were studied using the 53 micron

shale particle size, 1500 psi (10.342 mPa) CO_2 injection pressure, and 40 ºC temperature. The CO_2 adsorption results are shown in Table 1. No obvious trend could be noticed, even when repeating the experiments, which both validates and emphasizes the claim that when using the Volumetric based adsorption measurement, the sample cell should be filled up with the minimum amount of dead volume.

Table 1. Effect of Shale Volume on CO_2 Adsorption

Shale Volume, cm³	Void Space Volume, cm³	Absolute Adsorption, mmol/g	Gibbs Adsorption, mmol/g
2.66	4.45	0.42833	0.38399
3.42	4.43	0.42835	0.38462
3.80	4.33	0.42830	0.38728

The CO_2 adsorption values obtained in this research were compared to the adsorption capacities of other shale plays, including Woodford shale in USA, Upper Toarcian shale in France, and New Albany shale in USA in order to evaluate the CO_2 adsorption capacity of the shale used in this research compared to other shale plays. The adsorption capacity was also compared to pure activated carbon and pure zeolite to show the adsorption capacity of pure material compared to normal shales. The comparison is shown in Table 2. The activated carbon and pure zeolite have an extremely high adsorption capacity compared to the shales. This is an indication that some minerals other than clays also have an extremely high adsorption capacity and thus will impact the overall adsorption if they are present in the shale.

Table 2. Comparing Adsorption Experimental Results to Other Shale Samples

Reference	Adsorbent	Temp, ºC	Pressure, psi (mPa)	Adsorption, mmol/g
Sudibandriyo, M. et al. 2003	Activated Carbon	45	478.62 (3.3)	7.106
			1016.714 (7.01)	8.434
			1604.12 (11.06)	8.781
			1937.703 (13.36)	8.924
Nog, T. 2010	Pure Zeolite	25	500 (3.447)	5.800
			-	-
			-	-
			-	-
Chareonsuppanimit, P. et al., 2012	Woodford Shale	55	401.75 (2.77)	0.093
			1003.66 (6.92)	0.144
			1409.77(9.72)	0.157
			1802.82 (12.43)	0.150
Lafortune, S. et al. 2014	Upper Toarcian Shale	25	435.11 (3)	0.280
			580.15 (4)	0.330
			725.19 (5)	0.380
			-	-
Lafortune, S. et al. 2014	Upper Toarcian Shale	40	435.11 (3)	0.200
			580.15 (4)	0.240
			725.19 (5)	0.280
			-	-
Chareonsuppanimit, P. 2016	New Albany Shale	55	443.82 (3.054)	0.072
			1009.46 (7)	0.109
			1615.72 (11.14)	0.115
			1827.48 (12.6)	0.100
Current Study	NE Shale	40	500 (3.447)	0.044
			1000 (6.895)	0.121
			1500 (10.342)	0.428
			2000 (13.790)	0.475
Current Study	NE Shale	25	1500 (10.342)	0.539
Current Study	NE Shale	60	1500 (10.342)	0.259

The results obtained from the shale used in this study are very close to the other shales. This helps in validating the experimental results obtained from this research and also gives an indication of the range for the expected adsorption values in different types of shales. The experiments conducted in this research were done at 25, 40, and 60 ⁰C, and 500 (3.447), 1000 (6.895), 1500 (10.342), and 2000 (13.790) psi (mPa), which are extremely close to those conducted by other researchers mentioned in the table. This makes it possible to compare their results to those from the North East Oklahoma Shale that is used in this study. Based on the absolute adsorption values of all the shales including the Northeast Oklahoma Shale, it can be observed that the Northeast Oklahoma shale had a higher adsorption capacity at the same thermodynamic conditions compared to all the other shales. This is a strong indication that it can be a better CO_2 storage site compared to many other shale plays.

7. CONCLUSIONS

This research investigated the effect of temperature, pressure, shale particle size, and shale particle volume on CO_2 adsorption to North East Oklahoma Shale using a specially designed volumetric adsorption apparatus that is based on the volumetric expansion of gas. The main conclusions obtained from this research are shown below.

- The North East Oklahoma Shale was found to have a higher adsorption capacity than the Woodford, Upper Toarcian, and New Albany shale at the same thermodynamic conditions based on the experimental results obtained.

- Increasing the temperature resulted in a decrease in the CO_2 adsorption capacity for the North East Oklahoma Shale. This agrees with some of the other shale types.

- The liquid CO_2 phase was found to have a higher adsorption capacity compared to the gas and the supercritical CO_2. This shows that the CO_2 phase may be an important factor to be considered for CO_2 storage applications in shale, or unconventional reservoirs.

- Based on the XRD results, the North East Oklahoma shale was found to have a considerable concentration of different types of clay, mainly including Illite and Kaolinite.

- Decreasing the volume of shale in the sample cell resulted in a change in adsorption value; therefore, it is recommended to use the same volume in all experiments and to occupy the sample cell completely to reduce the dead volume.

- Altering the shale particle size resulted in a very small impact on adsorption equilibrium. This shows that the small particles can be used to model adsorption accurately.

ACKNOWLEDGEMENTS

REFERENCES

Al Ismail, M. I. et al., 2014. The Effect of CO_2 Adsorption on Permeability Anisotropy in the Eagle Ford Shale. Unconventional Resources Technology Conference. doi:10.15530/URTEC-2014-1921520.

Aljamaan, H., et al., 2017. Multiscale Imaging of Gas Adsorption in Shales. Society of Petroleum Engineers. doi:10.2118/185054-MS.

Al-Mutarreb, A.M. et al., 2018. The Influence Of Shales Characteristics On CO2 Adsorption Behaviour Under Sub-Critical Conditions. 2nd International Conference on Energy and Environmental Science. Earth and Environmental Science 164 (2018) 012031 doi :10.1088/1755-1315/164/1/012031.

Arri, L. E. and Yee, D., 1992. Modeling Coalbed Methane Production with Binary Gas Sorption, SPE Paper 24363. Presented at the SPE Rocky Mountain Regional Meeting, Casper, WY, May 18-21.

Bahadori, A., and Vuthaluru, H., 2010. Rapid Prediction of Carbon Dioxide Adsorption Isotherms for Molecular Sieves Using Simple Correlation. Society of Petroleum Engineers. doi:10.2118/122882-PA.

Bouzgarrou, S. et al., 2015. Experimental Adsorption and Modelisation of CO_2 on Adsorbents Collected from Elborma Field in South Tunisia. *Journal of Surface Engineered Materials and Advanced Technology*, **5**, 52-63. doi: 10.4236/jsemat.2015.51006.

Carey, J.W. et al., 2015. Leakage Processes in Damaged Shale: In Situ Measurements of Permeability, CO_2-Sorption Behavior and Acoustic Properties. AGU monograph "Caprock Integrity in Geological Storage".

Chareonsuppanimit, P. et al., 2012. High-Pressure Adsorption Of Gases On Shales: Measurements And Modeling, International Journal of Coal Geology, 95, https://doi.org/10.1016/j.coal.2012.02.005.

Chareonsuppanimit, P. et al., 2016. Measurement and Modeling of Gas Adsorption on Shales. Energy & Fuels Journal, **30** (3), 2309-2319, https://doi.org/10.1021/acs.energyfuels.5b02751.

Chen, G. et al., 2016. Research of CO_2 and N_2 Adsorption Behavior in K-Illite Slit Pores by GCMC Method. Journal of Scientific Reports, **6**, https://doi.org/10.1038/srep37579.

Clarkson, C. R., 2003. Application of a New Multicomponent Gas Adsorption Model to Coal Gas Adsorption Systems. Society of Petroleum Engineers. doi:10.2118/78146-PA.

Clarkson, C. R., and Haghshenas, B., 2013. Modeling of Supercritical Fluid Adsorption on Organic-Rich Shales and Coal. Society of Petroleum Engineers. doi:10.2118/164532-MS.

Eliebid, M. et al., 2017. Adsorption Role in Shale Gas Recovery and the Feasibility of CO_2 in Shale Enhanced Gas Recovery: A Study on Shale Gas from Saudi Arabia. Society of Petroleum Engineers. doi:10.2118/187667-MS.

Fakher, S. (2019, September 23). Investigating Factors that May Impact the Success of Carbon Dioxide Enhanced Oil Recovery in Shale Reservoirs. Society of Petroleum Engineers. doi:10.2118/199781-STU.

Fakher, S. and Imqam, A. 2020b. Application of carbon dioxide injection in shale oil reservoirs for increasing oil recovery and carbon dioxide storage, Fuel, 265, 116944, ISSN 0016-2361. https://doi.org/10.1016/j.fuel.2019.116944.

Fakher, S. and Imqam, A., 2018. Investigating and Mitigating Asphaltene Precipitation and Deposition in Low Permeability Oil Reservoirs During Carbon Dioxide Flooding to Increase Oil Recovery. Society of Petroleum Engineers. doi:10.2118/192558-MS.

Fakher, S. and Imqam, A., 2019. Asphaltene precipitation and deposition during CO2 injection in nano shale pore structure and its impact on oil recovery. Fuel Journal, 273. (1029-1039. https://doi.org/10.1016/j.fuel.2018.10.039.

Fakher, S. and Imqam, A., 2020a. An Experimental Investigation of Immiscible Carbon Dioxide Interactions with Crude Oil: Oil Swelling and Asphaltene Agitation. Fuel.

Fakher, S. et al., 2018. Investigating the Viscosity Reduction of Ultra-Heavy Crude Oil Using Hydrocarbon Soluble Low Molecular Weight Compounds to Improve Oil Production and Transportation. Society of Petroleum Engineers. doi:10.2118/193677-MS.

Fakher, S. et al., 2019. A Comprehensive Review on Gas Hydrate Reservoirs: Formation and Dissociation Thermodynamics and Rock and Fluid Properties. International Petroleum Technology Conference. doi:10.2523/19373-MS.

Fakher, S. M., 2019. "Asphaltene stability in crude oil during carbon dioxide injection and its impact on oil recovery: A review, data analysis, and experimental study". Masters Theses. 7881.

Fakher, S., Abdelaal, H., Elgahawy, Y. et al. A characterization of different alkali chemical agents for alkaline flooding enhanced oil recovery operations: an experimental investigation. SN Ap. Sci. 1, 1622 (2019). https://doi.org/10.1007/s42452-019-1662-2.

Fakher, S., and Imqam, A. A review of carbon dioxide adsorption to unconventional shale rocks methodology, measurement, and calculation. SN Appl. Sci. 2, 5 (2020). https://doi.org/10.1007/s42452-019-1810-8.

Fakher, S., Bai, B., Imqam, A., & Wang, Y. (2017, October 9). Novel Mathematical Models to predict Preformed Particle Gel Placement and Propagation through Fractures. Society of Petroleum Engineers. doi:10.2118/187152-MS.

Fujii, T., et al., 2015. Evaluation Of CO_2 Sorption Capacity Of Rocks Using A Gravimetric Method For CO2 Geological Sequestration, Energy Procedia, **1,** (1), 3723- 3730, https://doi.org/10.1016/j.egypro.2009.02.

Gasparik, M. et al., 2015. High-Pressure/High-Temperature Methane-Sorption Measurements on Carbonaceous Shales by the Manometric Method: Experimental and Data-Evaluation Considerations for Improved Accuracy. Society of Petroleum Engineers. doi:10.2118/174543-PA.

Heller, R. and Zoback, M., 2014. Adsorption of Methane and Carbon Dioxide on Gas Shale and Pure Mineral Samples. Journal of Unconventional Oil and Gas Resources, **8**, 14-24. https://doi.org/10.1016/j.juogr.2014.06.001.

Jedli, H. et al., 2017. Carbon Dioxide Adsorption Isotherm Study On Various Cap Rocks In A Batch Reactor For CO2 Sequestration Processes, Applied Clay Science, **136**, 199-207, *0169- 1317,* https://doi.org/10.1016/j.clay.2016.11.022.

Jin, Z., and Firoozabadi, A., 2016. Thermodynamic Modeling of Phase Behavior in Shale Media. Society of Petroleum Engineers. doi:10.2118/176015-PA.

Kang, S. M. et al., 2011. Carbon Dioxide Storage Capacity of Organic-Rich Shales. Society of Petroleum Engineers. doi:10.2118/134583-PA.

Khosrokhavar, R. et al., 2014. Sorption of CH_4 and CO_2 on a Carboniferous Shale from Belgium Using a Manometric Setup. International Journal of Coal Geology 128–129 (2014) 153–161.

Lafortune, S. et al., 2014. Assessing CO2 Adsorption Capacities onto Shales through Gravimetric Experiments: A First Step in the Feasibility Study of Coupling "Fracking" with Carbon Storage, Energy Procedia, **63**, 5933-5937, *1876-6102*, https://doi.org/10.1016/j.egypro.2014.11.629.

Le, T. D. et al., 2017. A New Matrix/Fracture Multiscale Coupled Model for Flow in Shale-Gas Reservoirs. Society of Petroleum Engineers. doi:10.2118/181750-PA.

Liu, Q. et al., 2018. Macroscale Mechanical and Microscale Structural Changes in Chinese Wufeng Shale With Supercritical Carbon Dioxide Fracturing. Society of Petroleum Engineers. doi:10.2118/181369-PA.

Lu, M., et al., 2017. A New Method for the Estimation of Lost Gas During the Measurement of the Gas Content of Coal. Society of Petroleum Engineers. doi:10.2118/176976-PA.

Luo, X. et al., 2015. Adsorption Of Methane, Carbon Dioxide And Their Binary Mixtures On Jurassic Shale From The Qaidam Basin In China, International Journal of Coal Geology, 150–151, 210-223, https://doi.org/10.1016/j.coal.2015.09.004.

Miedzinska, D. and Lutynski, M. 2017. CO2 - CH4 sorption induced swelling of gas shales: An experimental study on the Silurian shales from the Baltic Basin, Poland. Physicochemical Problems of Mineral Processing. 54(2), 2018, 415-427.

Mohammad, S. et al., 2009. Experimental Uncertainties in Volumetric Methods for Measuring Equilibrium Adsorption. Energy & Fuels, **23**, 2810-2820. , https://doi.org/10.1021/ef8011257.

Murugesu, Manju Pharkavi and Joewondo, Nerine and Prasad, Manika, CO2 Sorption Capacity in Clay-Rich Shales with Moisture Content. 14th Greenhouse Gas Control Technologies Conference Melbourne 21-26 October (GHGT-14). Available at SSRN: https://ssrn.com/abstract=3365692.

Ngo, T., 2015. Reservoir Capacity Estimates in Shale Plays Based on Experimental Adsorption Data. Masters Thesis.

Perez, F. and Devegowda, D., 2017. Methane and Carbon Dioxide Adsorption in Kerogen Models Using Molecular Simulations, Mewbourne School of Petroleum and Geological Engineering, The University of Oklahoma.

Psarras, P. et al., 2017. Methane and CO_2 Adsorption Capacities of Kerogen in the Eagle Ford Shale from Molecular Simulation. Accounts of Chemical Research, https://doi.org/10.1021/acs.accounts.7b00003.

Rani, S. et al., 2015. Comparison of Void Volume for Volumetric Adsorption Studies on Shale from India. Journal of Natural Gas Science and Engineering. **26**, 725-729. https://doi.org/10.1016/j.jngse.2015.07.012.

Santos, J. M., and Akkutlu, I. Y., 2013. Laboratory Measurement of Sorption Isotherm under Confining Stress with Pore-Volume Effects. Society of Petroleum Engineers. doi:10.2118/162595-PA.

Sing, K., 1984. Reporting Physisorption Data for Gas/Solid Systems with Special Reference to the Determination of Surface Area and Porosity. International Union of Pure and Applied Chemistry, Physical Chemistry Division, Commission on Colloid and Surface Chemistry Including Catalysis.

Sudibandriyo, M. et al., 2003. Adsorption of Methane, Nitrogen, Carbon Dioxide, and Their Binary Mixtures on Dry Activated Carbon at 318.2 K and Pressures up to 13.6 MPa. *Langmuir* **2003** *19* (13), 5323-5331. https://doi.org/10.1021/la020976k.

Tajnik, T. et al., 2013. Investigation of adsorption properties of geological materials for CO_2 storage. Int. J. Energy Res., 37: 952-958. doi:10.1002/er.2901.

Torsaeter, O., and Abtahi, M., 2000. Experimental Reservoir Engineering Laboratory Workbook, Department of Petroleum Engineering and Applied Geophysics, Norwegian University of Science and Technology.

USGS-CO_2 Sequestration, 2019. Geologic CO_2 Sequestration Map, United States Geological Survey. https://co2public.er.usgs.gov/viewer/.

Yang, S. et al., 2016. Effects of Multicomponent Adsorption on Enhanced Shale Reservoir Recovery by CO2 Injection Coupled with Reservoir Geomechanics. Society of Petroleum Engineers. doi:10.2118/180208-MS.

Yang, Z. et al., 2018. Experimental Study on Selective Adsorption/Desorption of CO2 and CH4 Behaviors on Shale under a High-Pressure Condition. Energy & Fuels 2018 32 (9), 9255-9262. DOI: 10.1021/acs.energyfuels.8b02068.

Yanian, Z. et al., 2015. Study on Controlling Factors of Shale Gas Adsorption. ACTA Geologica Sinica, **89**, 300- 301.

Yu, W. et al., 2016. Modeling Gas Adsorption in Marcellus Shale With Langmuir and BET Isotherms. Society of Petroleum Engineers. doi:10.2118/170801-PA.

Yuan, H. et al., 2017. Investigation on Gas-Adsorption-Induced Swelling and Permeability Evolutions of Cox Argillite, Fresh Journal of Mechanics.

Yue, N. et al., 2018. Influencing Factors and Selection of CH4 and CO2 Adsorption on Silurian Shale in Yibin, Sichuan Province of China. Energy & fuels 2018 v.32 no.3 pp. 3202-3210.

Zhang, C. et al., 2017. Characteristics of Clay-Abundant Shale Formations: Use of CO_2 for Production Enhancement. Energies Journal.

X. APPICATION OF CARBON DIOXIDE INJECTION IN SHALE OIL RESERVOIRS FOR INCREASING OIL RECOVERY AND CARBON DIOXIDE STORAGE

ABSTRACT

Carbon dioxide (CO_2) injection is an enhanced oil recovery method that has the potential to increase oil recovery from unconventional shale reservoirs while also storing a portion of the injected CO_2 into the reservoir thus reducing the CO_2 environmental impact. This research studies the ability of cyclic CO_2 injection to increase oil recovery from shale cores and the impact of different factors on the oil recovery potential. The research then studies the ability to store the injected CO_2 in the shale through adsorption and the storage capacity at different reservoir thermodynamic conditions. Oil recovery was impacted significantly by the CO_2 injection pressure. The CO_2 phase was also found to be a factor related to the CO_2 injection pressure and also had a strong impact on oil recovery. Increasing the soaking time of the CO_2 increased the oil recovery due to the increase in the interaction time between the CO_2 and the crude oil. The storage potential of the CO_2 in the shale was influenced significantly by the pressure and temperature. Increasing the CO_2 injection pressure increased the CO_2 adsorption, while increasing the temperature decreased the adsorption capacity. Based on the experiments conducted, it was found that cyclic CO_2 injection could be a means of both increasing oil recovery from shale reservoirs and also for CO_2 storage operations to reduce CO_2 environmental impact.

1. INTRODUCTION

CO_2 injection is a well established enhanced oil recovery technique that has been used in many hydrocarbon reservoirs for decades [1]. Recently, CO_2 injection has also been applied to increase oil recovery from unconventional shale reservoirs [2-6]. During its interaction with the shale, the CO_2 has also been found to adsorb to the shale rock [7-11]. This is extremely useful for CO_2 storage operations. Understanding the factors that impact oil recovery and adsorption is therefore important in order to increase oil recovery from unconventional shale reservoirs and also increase the CO_2 storage capacity in shale during CO_2 injection in this unconventional hydrocarbon reservoir type.

CO_2 can be injected into the reservoir by flooding or using cyclic CO_2 injection. Cyclic CO_2 injection, also referred to as huff-n-puff, has been reported to have a higher recovery in shale reservoirs compared to flooding [3-6]. During cyclic CO_2, one well is used for injection and production. The CO_2 interacts with the crude oil, mainly reducing its viscosity and thus improving the oil's mobility [12-13]. Different factors will impact the productivity of cyclic CO_2 injection. These include the pressure and temperature conditions, CO_2 soaking time, and number of productive CO_2 soaking cycles [1-6, 12-14]. Due to the novelty of cyclic CO_2 injection in shale reservoirs, few studies have conducted extensive experiments to investigate the factors impacting cyclic CO_2 productivity from shale. Also, very little research has attempted to combine both oil recovery and CO_2 storage in shale.

Many factors may impact the adsorption capacity of the CO_2 in the shale reservoir. These factors can be grouped into reservoir properties, shale properties, and injected fluid properties [25-26]. The reservoir pressure and temperature will have an extremely strong impact on CO_2 adsorption capacity [8-19]. For the shale properties, the shale mineralogy will impact adsorption since some minerals and clays have a larger adsorption capacity compared to others [20-22]. The total organic content of the shale will also play an important role in its adsorption capacity [20-25]. Different fluids will have different adsorption capacities based on their properties and interactions with the shale itself [7-9, 24]. Although these properties have all been investigated, very little research has attempted to connect it to oil recovery using cyclic CO_2 injection in shale cores.

Cyclic CO_2 injection has a large potential to increase oil recovery from both stimulated and unstimulated shale reservoirs. The CO_2 can also be stored in the shale thus reducing the environmental impact of the oil recovery operation. This research studies the factors impacting the oil recovery from shale reservoirs and the CO_2 storage capacity in shale during cyclic CO_2 injection to assess the applicability of using this method in different shale plays and quantifies the impact of different factors. This can help increase oil recovery from unconventional shale reservoir and also help store large volumes of CO_2 in these reservoirs.

2. EXPERIMENTAL MATERIAL

The material used to conduct the CO_2 injection experiments and the CO_2 adsorption experiments are as follows.

2.1. CRUDE OIL

Crude oil was used to conduct all the cyclic CO_2 injection experiments. The oil had an average composition: 9.7% C_1-C_5, 14.74% C_6-C_{10}, 38.2% C_{11}-C_{20}, and 37.36% C_{20+}.

2.2. SHALE CORES

The shale cores used were outcrops obtained from Oklahoma. The cores were one inch in diameter, and an average of 2 inch in length.

2.3. CARBON DIOXIDE

CO_2 was supplied using a high pressure CO_2 cylinder with a purity of 99.99%. The cylinder is commercially available.

2.4. HELIUM

Helium was supplied using a high pressure Helium cylinder with a purity of 99.99%. The cylinder is commercially available.

2.5. HIGH PRESSURE GAUGES

Gauges with a maximum pressure of 3000 psi were used in all experiments. The gauges can operate in high temperature conditions.

2.6. HIGH PRESSURE VALVES

The valves used had a maximum operating pressure of 2500 psi. Since the highest pressure experiment was at 2000 psi, the valves could be used safely.

2.7. MORTAR AND PESTLE

A mortar and pestle were used to crush the shale samples for the CO_2 adsorption experiments.

2.8. WATER BATH

The water bath was used to maintain the temperature during the experiments. If the temperature changed by 0.2 ℃ or more, the experiment was repeated.

2.9. THERMOMETER

A high accuracy thermometer was used to measure the temperature for the duration of the experiments.

3. EXPERIMENTAL SETUPS

Two experimental setups will be explained in this section. First, the setup used to conduct the cyclic CO_2 injection experiments will be illustrated and explained. Following this, the setup used to conduct the adsorption experiments will be explained.

An illustration of the setup used to conduct the cyclic CO_2 injection experiments is shown in Figure 1. The setup was designed to mimic the field procedure of the cyclic injection operation. It is composed of a syringe pump used for pressurizing the CO_2 present in the accumulator. The accumulator is attached to the main vessel which houses the shale core. This vessel was specially designed to have a valve for CO_2 injection and crude oil production.
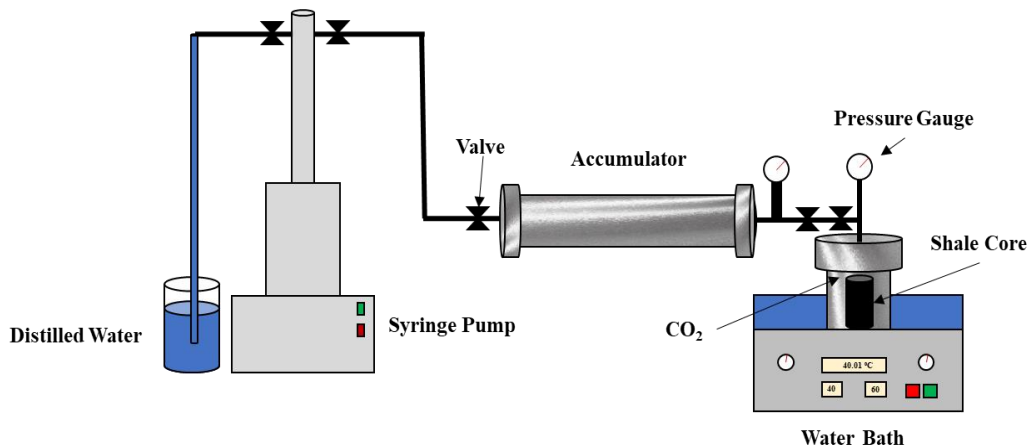
Figure 1. Cyclic CO$_2$ Injection Setup

An illustration of the setup used to conduct the CO$_2$ adsorption experiments is shown in Figure 2. The setup is based on the volumetric method of measuring adsorption. A syringe pump is used to pressurize the CO$_2$. Two cells are used to measure the CO$_2$ adsorption. The reference cell is occupied by the pressurized CO$_2$, and the sample cell houses the shale. The main aim of the reference cell is to contain the CO$_2$ at a reference pressure that is needed for the adsorption calculation.
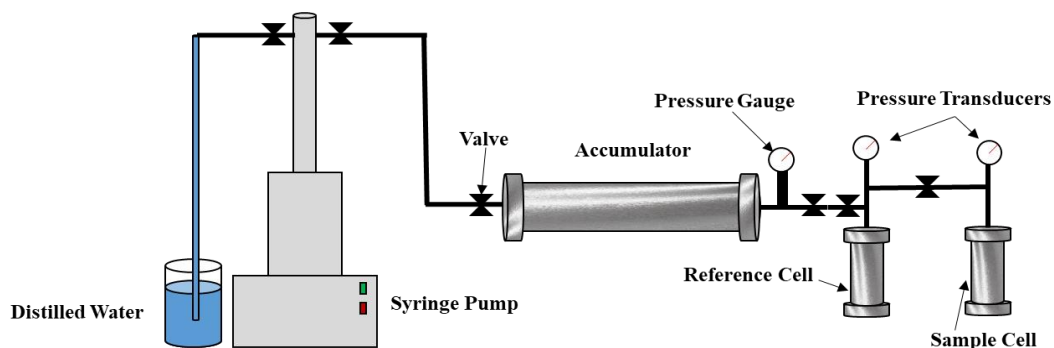

Figure 2. CO$_2$ Adsorption Setup

4. EXPERIMENTAL PROCEDURES

The procedure followed to conduct the cyclic CO_2 injection and the CO_2 adsorption experiments is explained in this section.

The cyclic CO_2 injection procedure was designed to mimic the actual field procedure. All experiments were conduct using the same procedure in order to be able to compare the results. The procedure is as follows:

1. The shale cores were saturated with the crude oil by placing the cores in a high pressure vessel filled with crude oil. The vessel was then placed in an oven at high temperature and kept for seven continuous months. The cores were weighed before and after saturation to determine the pore volume.

2. To begin the cyclic CO_2 experiment, a saturated shale core is placed in the high pressure vessel. The vessel is then sealed, placed in the water bath, and vacuumed for 12 hours.

3. The CO_2 is then injected into the pressure vessel and left to soak at the design pressure and temperature for a designed soaking time.

4. After the soaking time is completed, the vessel is depressurized, and the shale core is retrieved. The oil recovery is measured using the change in weight of the core.

5. After the oil recovery is measured, a new cycle is commenced. For each new cycle, the cell was vacuumed to ensure that there is no air in the cell which could alter the results of the experiments. The cycles are stopped when the incremental oil recovery was less than 0.5%. The shale core is then analyzed for fractures.

The procedure followed to conduct the CO_2 adsorption experiments is based on the volumetric adsorption measurement principle. The exact procedure is as follows:

1. The shale sample was initially pulverized to micron sized particles using a mortar and pestle. This was done to reduce the time required for the CO_2 to diffusive into the shale matrix and adsorb. A mortar and pestle were used instead of an electric blender in order to avoid the generation of excessive heat that may alter the clays in the shale.

2. The sample cell was then filled with the shale particles. Both the sample cell and the reference cell were then vacuumed for 12 hours. A mesh screen was placed in the sample cell to prevent the suction of the shale particles during vacuum.

3. The void space between the shale particles was then measured using helium. The void space value was used during the adsorption calculations.

4. CO_2 was injected into the reference cell to the predetermined pressure. The reference cell was then sealed, and the pressure was expanded to the sample cell.

5. The pressure was recorded until the pressure value in both the sample cell and the reference cell reached equilibrium. This usually occurred after three to ten days. The adsorption capacity was then calculated based on the equilibrium pressure value. This large variation in equilibrium pressure time is due to the difference in interaction between CO_2 and shale at different conditions and to ensure that the correct equilibrium time has been recorded.

5. RESULTS AND ANALYSIS

The results for the cyclic CO_2 injection experiments, and the CO_2 adsorption experiments will be discussed in this section. The effect of each studied factor will be quantified and explained.

5.1. CYCLIC CARBON DIOXIDE INJECTION

The results obtained from the cyclic gas injection experiments will be presented and explained in this section. The effect of varying the CO_2 injection pressure, CO_2 phase, experimental vessel temperature, CO_2 soaking time, shale core fracture, and number of injection cycles on the oil recovery was studied.

The impact of increasing the CO_2 pressure on oil recovery was studied using 500, 1000, and 1350 psi CO_2 soaking pressure. The oil recovery results for all three pressures are shown in Figure 3. All three experiments were conducted at 40 ⁰C using 6 hours CO_2 soaking time. Increasing the CO_2 injection pressure resulted in an increase in the oil recovery. It was also observed that increasing the pressure resulted in the increase in the number of productive CO_2 cycles. Increasing the pressure from 500 psi to 1000 psi resulted in a slight increase in oil recovery, however increasing the pressure from 1000 to 1350 psi resulted in a significant increase in oil recovery. This could be associated with two significant factors including the CO_2 phase, which will be explained in detail in a separate section, and the stimulation of natural fractures within the shale core.
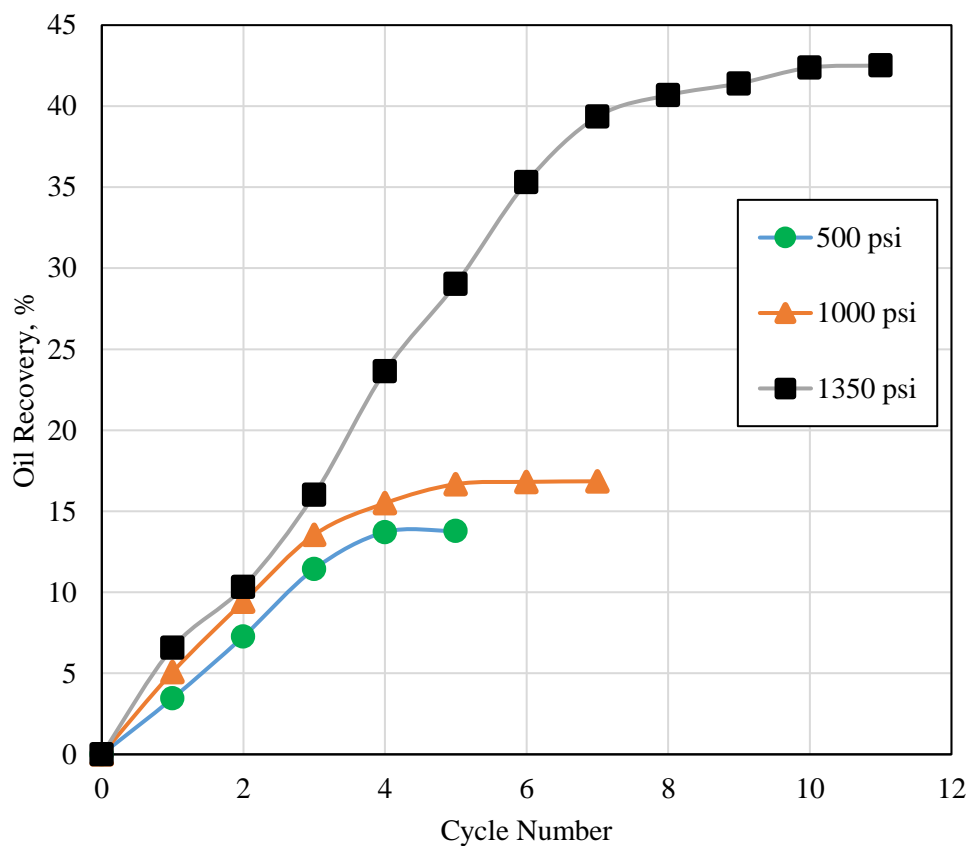
Figure 3. Effect of CO_2 Injection Pressure on Oil Recovery

The 1350 psi experiment resulted in an excessive stimulation of the natural fractures within the shale cores, which in turn increased oil recovery significantly. Figure 4 shows a comparison between the same shale core after the third CO_2 injection cycle and the final CO_2 injection cycle for the 1350 psi experiment. After the final experiment, it can be observed that the shale core had more than ten fractures within it. These were induced sequentially as the cycles progressed and became extremely severe after the ninth cycles. By stimulating the natural fractures, the CO_2 had a larger contact surface area with the shale, which resulted in a higher oil recovery.

| **Third Cycle** | **Final Cycle** |

Figure 4. Shale Core Sample for 1350 psi Experiment at 40 ⁰C and 6 hrs Soaking Time

Based on the observations made during the study of the CO_2 injection pressure effect, it was found that the CO_2 phase may have a strong impact on the oil recovery potential during injection in shale cores. Figure 5 shows the oil recovery results for gas, liquid, and supercritical CO_2. All three experiments were conducted using 6 hours CO_2 soaking time at 40 °C and using 500, 1000, and 1350 psi pressure for the gas, liquid, and supercritical CO_2 respectively. Based on the results, altering CO_2 phase impacted the oil significantly. Supercritical CO_2 resulted in the highest oil recovery, reaching up to 42%. Liquid CO_2 managed to recover more oil compared to the gas CO_2. This shows that increasing the CO_2 injection pressure may not be the only contributing factor to oil recovery increase; the CO_2 phase may also play a strong role in the oil recovery increase as well. The reason behind this could be due to the properties of the CO_2 at its different phases. In its gaseous phase, the CO_2 density is considerably low however it is more

difficult to extrude through the pores due to the low pressure. When in liquid phase, the CO_2 becomes denser and thus a larger volume is mobilized into the pores however a large volume also remains in the nanopores and thus oil recovery reduces gradually. In supercritical CO_2, the pressure is higher, however the CO_2 density actually becomes lower than that of the liquid. This aids in the CO_2 extrusion in the nanopores and thus more oil can be recovered. This could be the main reason behind the liquid CO_2 having a higher initial oil recovery compared to the supercritical CO_2.
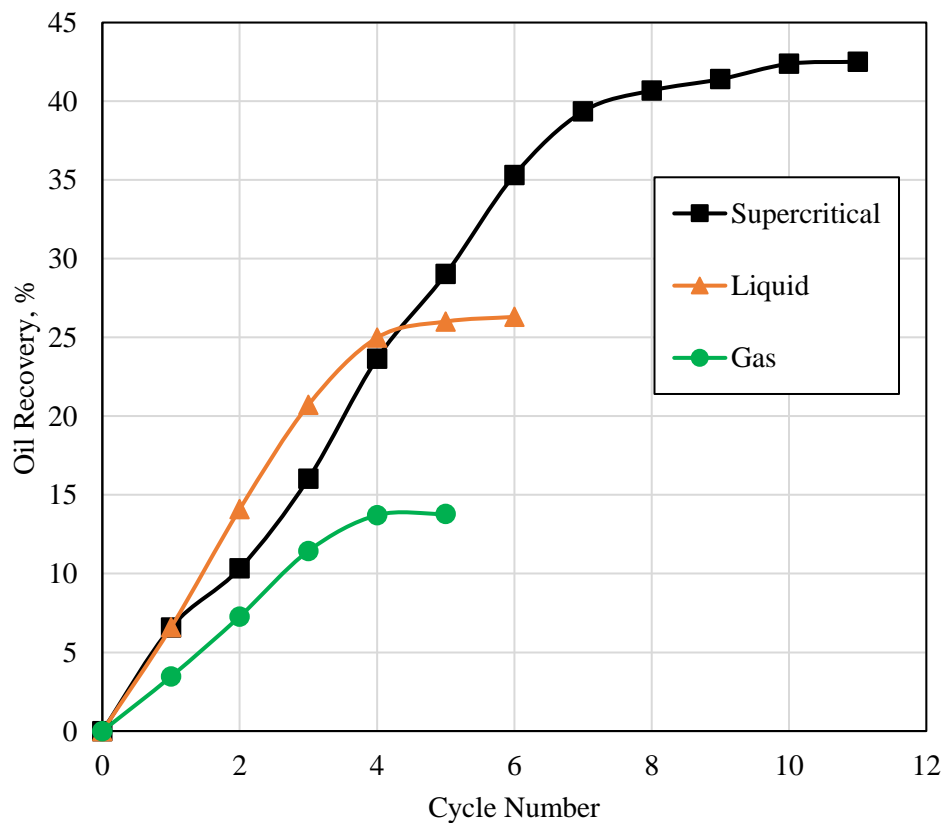

Figure 5. Effect of CO_2 Phase on Oil Recovery

Reservoir temperature is one of the factors that cannot be controlled since it is an innate property of the reservoir. It is important to investigate if and how temperature will impact oil recovery to understand the oil recovery potential from different shale plays with different temperatures. Figure 6 shows the results for three temperatures including 25, 40 and 60 ⁰C. All experiments were conducted using 1350 psi, and 6 hours soaking time. Increasing the temperature resulted in an increase in oil recovery. This could be due to the expansion of the pores at high temperature, and the reduction in viscosity of the crude oil. As the temperature increases, the pores will begin to increase in size due to the shale-rock grains slightly expanding. The grains' consolidation begins decreasing due to weakening in their cementing material at high temperatures and thus are more prone to cracking at their weakest point which creates the natural fractures. The number of productive CO_2 cycles shows no specific trend. The highest oil recovery achieved was 49% using 60 ⁰C. The oil recovery may have been larger for the 25 °C initially due to the change in viscosity and pore expansion having little effect in the initial stages. As the cycles progressed, their effect became more prominent and thus the 40 °C experiment began producing more. The 25 °C experiment may have produced more initially due to a slight difference in the average pore size of the core, or due to the presence of different natural fractures in the core attributed to experimental error. This was overcome by the viscosity reduction and pore expansion effects with the cycle progression, however. The temperature effect can vary from one shale reservoir to the other based on the shale properties including mineralogy, clay content, total organic content, and ductility or brittleness. Also, some reservoir fluids may impact the overall temperature effect.
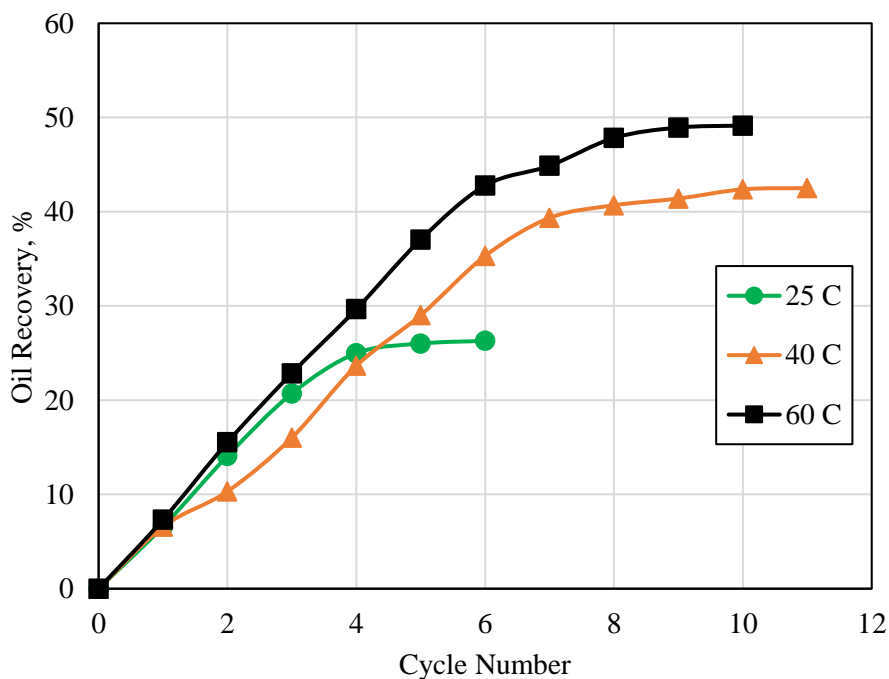
Figure 6. Effect of Temperature on Oil Recovery

After multiple CO_2 injection cycles using the 25 ⁰C experiment, a clear color change was observed. This color change was due to the production of the crude oil. Figure 7 shows a comparison between the third and the final injection cycle for the core. As can be observed, the shale core color changed due to the mobilization and production of the crude oil. This shows that the CO_2 can actually diffuse into the nanopores of the shale core and mobilize the crude oil within. This is also a good indication that the CO_2 will extrude through the pores, and thus can be stored within the matrix since it has the ability to diffuse into it. The mobilization of the crude oil from the matrix is evident from the change in color which indicates that oil recovery has occurred. This is also supported by the oil recovery results which shows that as the CO_2 injection cycles progress, the oil recovery increases until a point where no, or very little, oil recovery increment is observed.

| Third Cycle | Final Cycle |

Figure 7. Shale Core Sample at 25 ºC Using 1350 psi CO_2 Pressure and 6 hrs Soaking

Soaking time is defined as the time that the CO_2 is allowed to interact with the formation fluids and rock before production is resumed. Increasing the soaking time between the CO_2 and the oil is expected to increase the oil recovery. Figure 8 shows the oil recovery results using 1, 6, 12, and 24 hours CO_2 soaking time. All experiments were conducted at 40 ºC using 1350 psi. Increasing the CO_2 soaking time increased the oil recovery, as was expected. When the CO_2 soaking time was increased from 12 hours to 24 hours, the oil recovery increased was extremely small. This indicates that there will be a point where the increase in CO_2 soaking time will not be beneficial. This is extremely important for field application since soaking time is considered non-producing time, and thus it is costly to increase it, especially if the oil recovery increase is extremely small, as was the case in the 12 and 24 hour experiments.
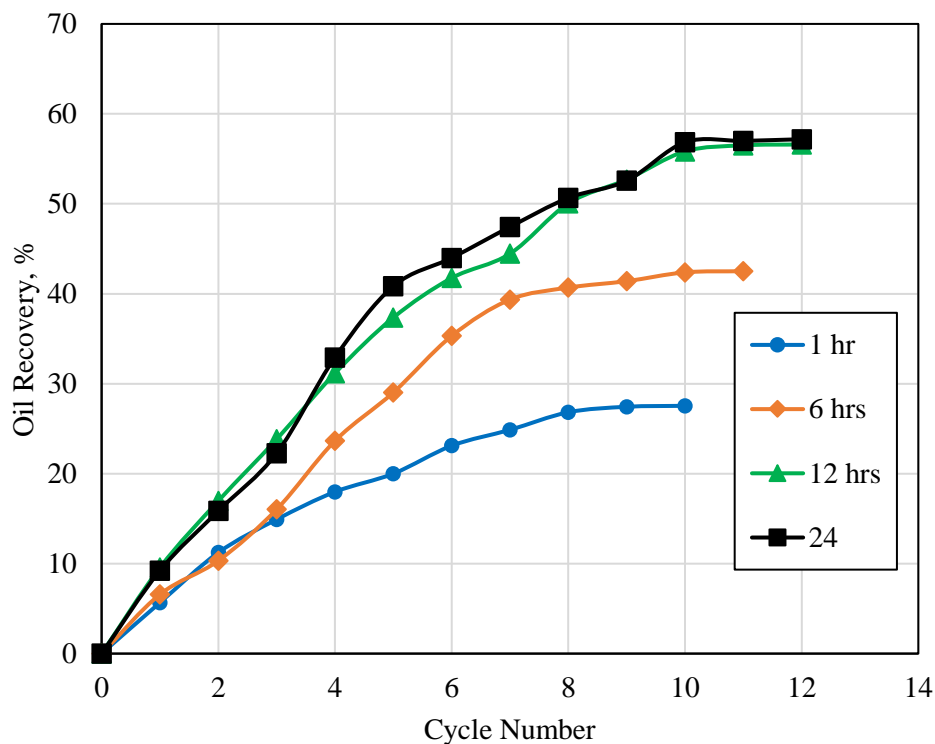
Figure 8. Effect of CO_2 Soaking Time on Oil Recovery

The shale core used to conduct the 12 hour soaking time experiment was visually analyzed by comparing it before the CO_2 soaking to its state after the third and final cycles. The comparison is shown in Figure 9. Before beginning the cycles, the core was completely saturated with the crude oil. After the third cycle, the color began to fade due to the recovery of 22% of the crude oil from the core. Also, some fractures began to appear in the core due to the CO_2 injection. When the final cycle was concluded, the color of the core faded even more due to more than 50% of the oil being produced. Also, the fractures became more prominent, as is shown in the images.
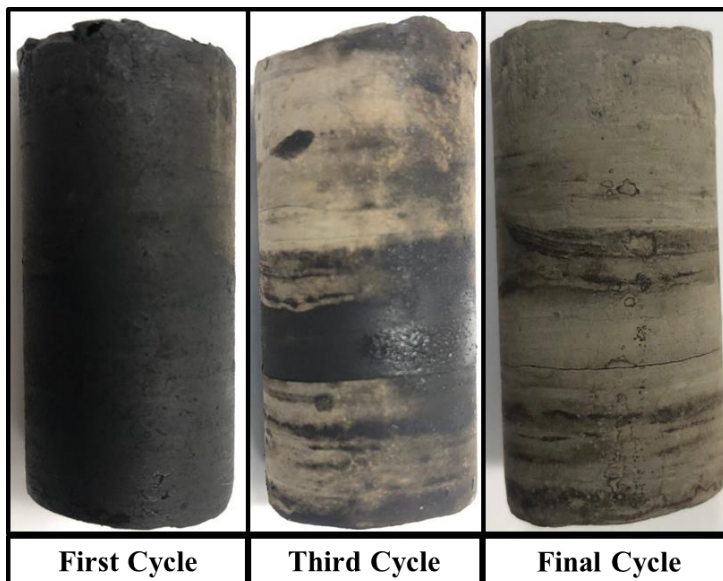
| First Cycle | Third Cycle | Final Cycle |

Figure 9. Shale Core Sample for 12 hrs Soaking Time Using 1350 psi Pressure and 40 ⁰C

It is important to investigate the applicability of cyclic CO_2 injection in both stimulated and unstimulated shale cores in order to assess if CO_2 will increase oil recovery from both. This can help in accessing previously fractured wells to recover more oil and also for CO_2 storage. Figure 10 compares the oil recovery from a fractured and an unfractured core. All experiments were conducted using 1350 psi CO_2 injection pressure, 40 ⁰C, and 67 cp crude oil using a 6 hr period CO_2 soaking time. Initially, it could be observed that the unstimulated shale core resulted in a higher oil recovery compared to the stimulated. However, before discussing the result it is important to note that fractured shale core broke several times during the injection cycle, and some small chunks of the shale core were being lost which resulted in a large error during the quantification of the oil produced. This resulted in the experiment being terminated before reaching the maximum oil recovery potential. When looking at the oil recovery results, it can be seen that the oil recovery for the stimulated shale core increased at a much faster rate compared to that of

the unstimulated core. This gives an indication that the stimulated shale core may have produced a larger volume of oil if more injection cycles were performed. It is therefore difficult to reach a conclusive answer as to which will produce the highest oil recovery, however, based on the results, cyclic CO_2 injection can increase oil recovery from both stimulated and unstimulated shale plays.
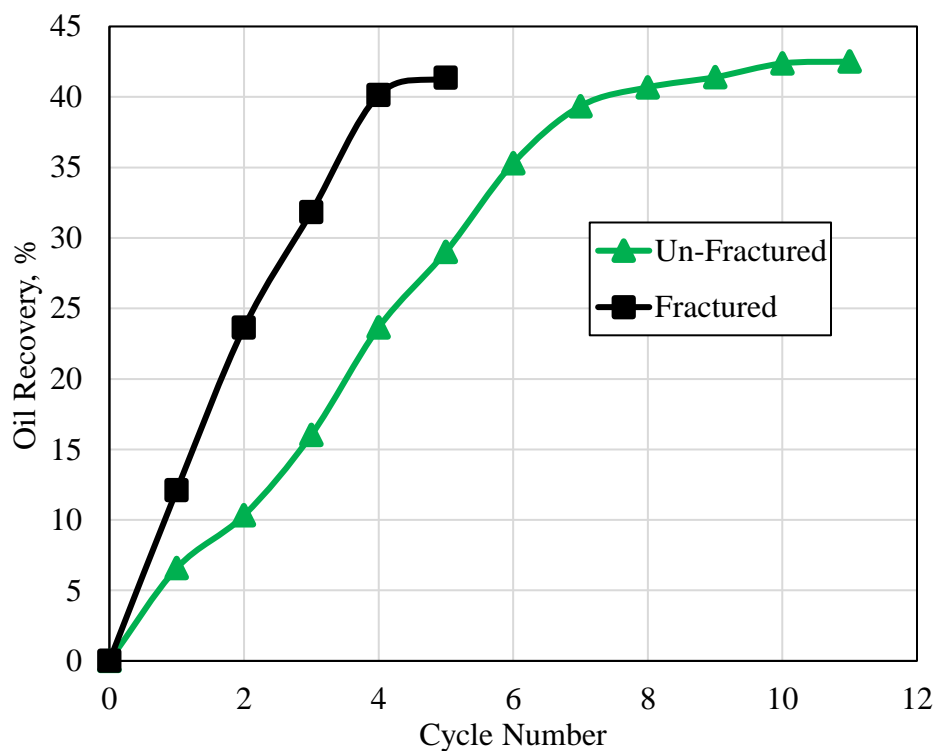

Figure 10. Effect of Induced Fracture on Oil Recovery at 1350 psi, 40 °C and 6 hrs

The fractured core was initially saturated with crude oil along with all the other cores and then fractured into three pieces. A picture of the fractured core is presented in Figure 11. When the pieces of the fractured core were analyzed, it was emphasized that the cores were fully saturated with crude oil from the inside color of the core. After the final

cycle was complete, the core was analyzed from different angles. Based on the images some natural fractures were stimulated, and a large part of the core was broken. This was due to the excessive pressure applied by the CO_2, and also the initial state of the core.
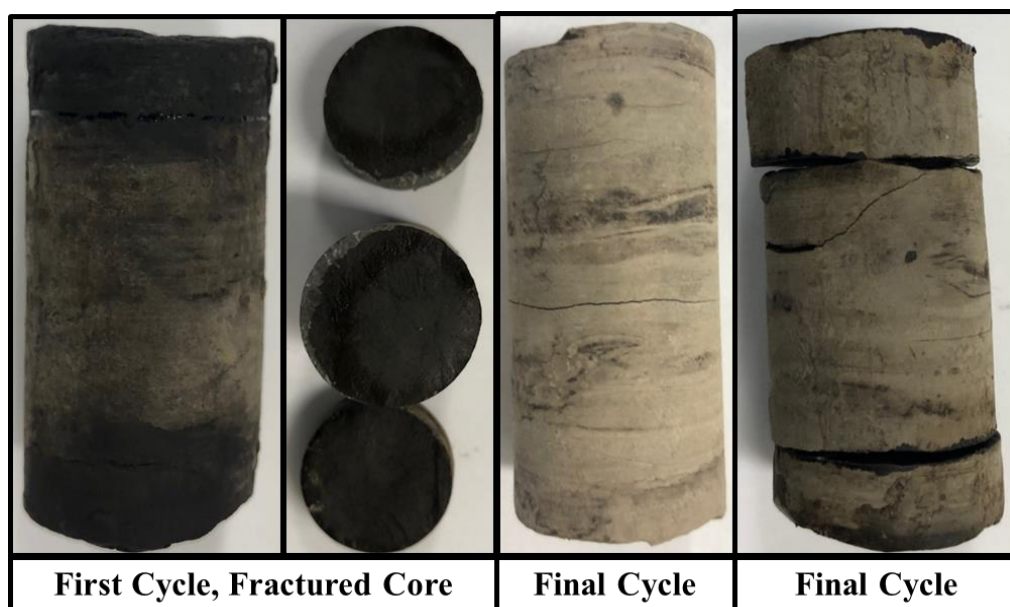

Figure 11. Fractured Shale Core Sample

An important factor to consider during CO_2 huff-n-puff is the number of CO_2 injection cycles required, and at what point will CO_2 injection be non-productive. In this research, the number of CO_2 injection and production cycles was not controlled but was rather determined based on oil recovery. When it was observed that no more oil recovery was obtained from the shale core, no incremental cycles were performed. Table 1 presents the number of cycles for all the experiments conducted in this research. Based on the results, it can be seen that increasing the CO_2 injection pressure resulted in an increase in the number of soaking cycles. Altering the temperature showed no clear trend in terms of

the number of soaking cycles. Increasing the CO_2 soaking time resulted in an increase in the number of CO_2 soaking cycles, although when the CO_2 soaking time increased from 12 to 24 hrs the number of soaking cycles did not change. This was also reflected in the small change in oil recovery as well.

Table 1. Number of CO_2 Soaking Cycles for Cyclic CO_2 Injection Experiments

Pressure, psi	Temperature, ⁰C	Soaking Time, hrs	Soaking Cycles
500	40	6	5
1000	40	6	7
1350	40	6	11
1350	25	6	6
1350	60	6	10
1350	40	1	10
1350	40	12	12
1350	40	24	12

5.2. CARBON DIOXIDE STORAGE

The CO_2 storage capacity was measured through the volume of CO_2 that can be adsorbed to the shale rock sample. The effect of varying the shale particle size, CO_2 injection pressure, and the temperature on the CO_2 adsorption capacity was investigated. The adsorption isotherm for the shale cores used in this study is presented in Figure 12. The adsorption isotherm was generated at 40 ⁰C using the 53 μm particle size. All adsorption values are reported in scf/ton. The adsorption isotherm provides insight on the

adsorption behavior of the shale sample used, and thus can aid in determining the adsorption capacity at the temperature at which the isotherm was generated.
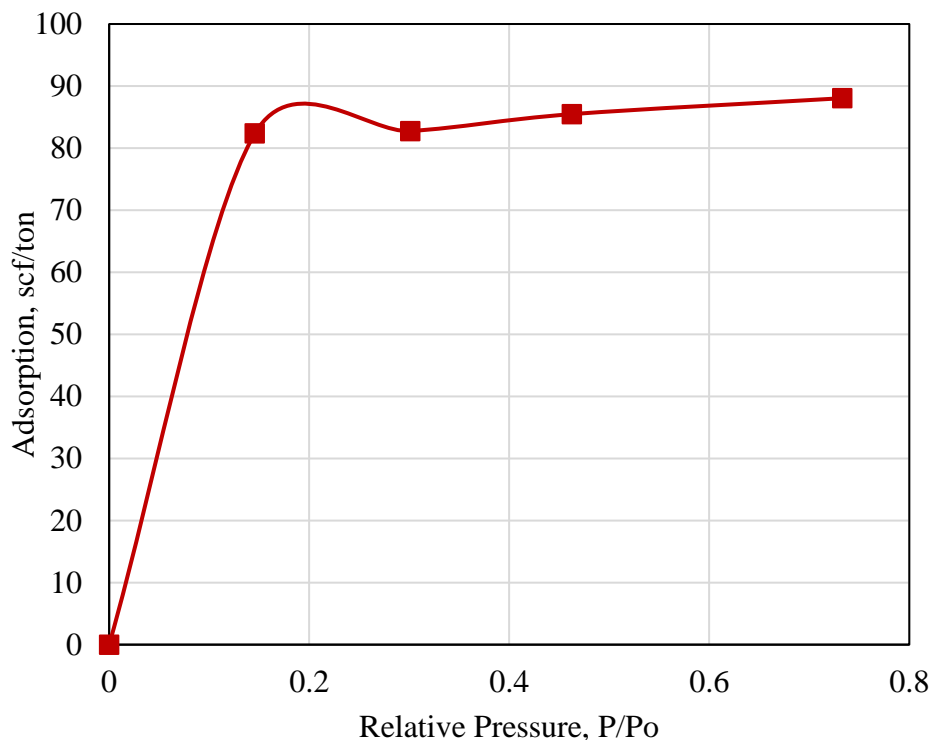

Figure 12. CO_2 Adsorption Isotherm

The experiments conducted in this research used shale particles that were pulverized to a very small mesh size. An important factor to consider in this case is whether these small particle sizes are representative of a shale core, since the cyclic CO_2 injection experiments were conducted using shale cores. Based on this, the effect of changing the shale particle size on CO_2 adsorption capacity was studied using three different shale particle sizes including 53, 149, and 590 microns. Figure 13 shows the CO_2 adsorption capacity in scf/ton for all three shale particle sizes. All experiments were conducting using

1500 psi CO_2 injection pressure, and 40 ⁰C. Altering the shale particle size was found to have an extremely small impact on shale adsorption; this is evident from the change in adsorption value being less than 0.1 scf/ton. This indicates that the shale particles can be used to accurately model CO_2 adsorption to shale and are representative of actual shale cores. The main advantage of pulverizing the shale is to reduce the time for the CO_2 equilibrium pressure between the reference and sample cell to be reached.
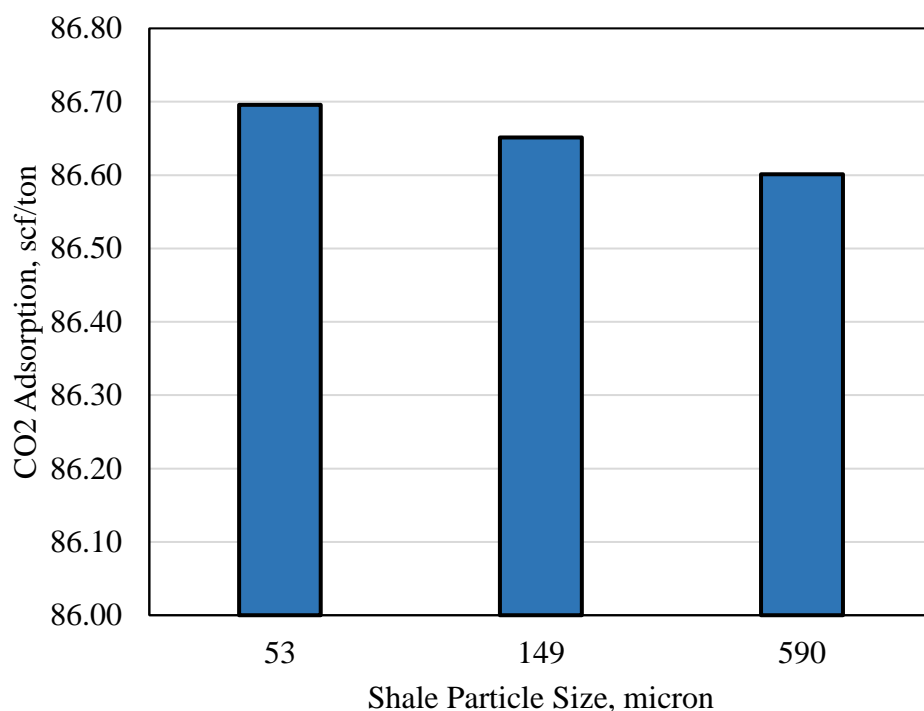

Figure 13. Shale Particle Size Effect on CO_2 Adsorption at 1500 psi and 40 ⁰C

The impact of increasing the CO_2 injection pressure on the CO_2 storage capacity in the shale was studied using 500, 1000, 1500, and 2000 psi pressures. The CO_2 adsorption results for all pressures are shown in Figure 14. All experiments were conducted at 40 ⁰C

using 53 μm shale particle size. Increasing the CO_2 injection pressure resulted in an increase in the adsorption volume. The highest adsorption capacity reached was 92 scf/ton using the 2000 psi injection pressure. Even though increasing the pressure resulted in an increase in the CO_2 storage capacity, it is important to note that an excessive increase in pressure in field applications may result in uncontrolled fractures which increase the reservoir heterogeneity and thus decrease to productivity of the cyclic CO_2 injection. This shows that in order to both increase oil recovery and increase storage, the factors impacting both operations should be analyzed together.
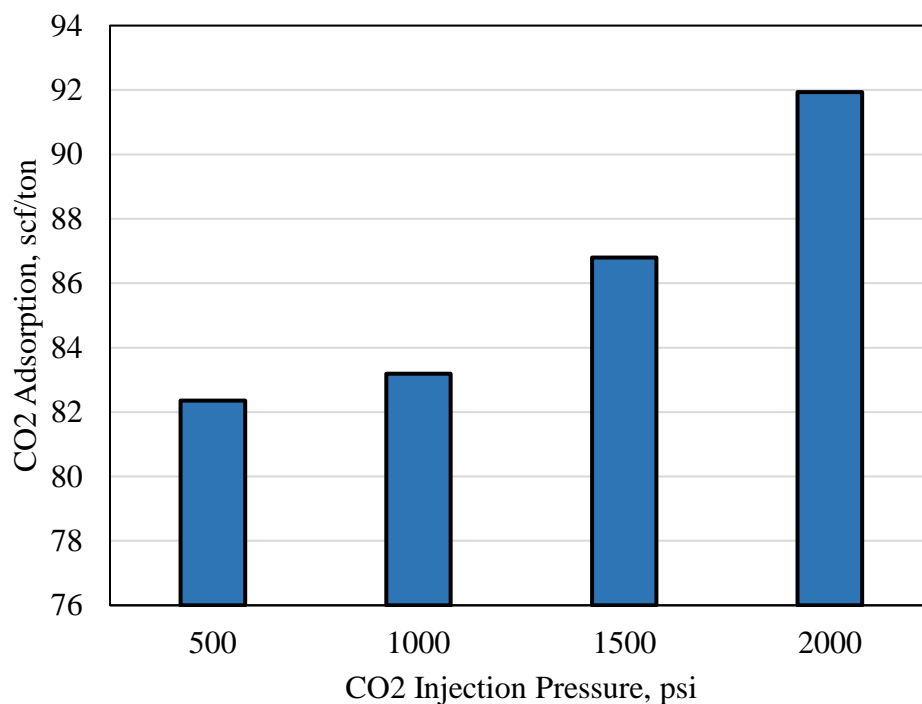

Figure 14. CO_2 Injection Pressure Effect on CO_2 Adsorption Using 40 ⁰C and 53 μm

The impact of temperature on the CO_2 storage capacity was also studied in order to relate it to the oil recovery and to determine the applicability of CO_2 storage in a wide range of shale plays with different reservoir temperatures. The impact of temperature on the CO_2 storage capacity is shown in Figure 15. All experiments were conducted using 1500 psi and 53 μm shale particle size. Three temperatures were investigated, including 25, 40, and 60 °C. Increasing the temperature resulted in a decrease in the CO_2 storage capacity. The opposite trend was observed when investigating the impact of temperature on oil recovery. This is very significant since oil recovery and CO_2 storage were impacted oppositely by temperature. It is therefore important to evaluate the shale play CO_2 storage capacity even if it is seen as a good candidate for oil recovery, especially if CO_2 storage is part of the injection project.
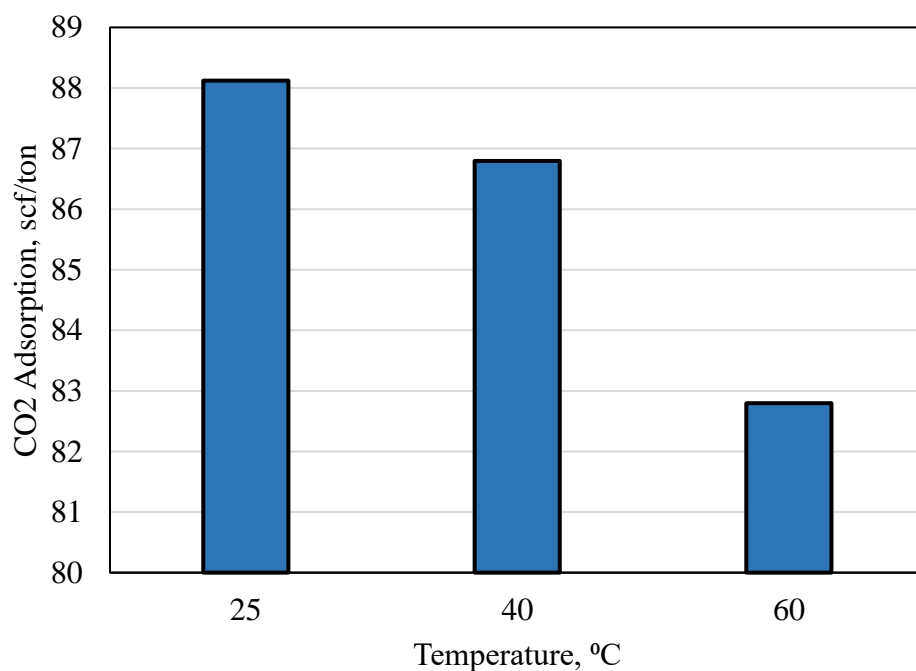
Figure 15. Effect of Temperature on CO_2 Adsorption Using 1500 psi and 53 μm

5.3. IMPACT OF DIFFERENT FACTORS ON RECOVERY AND ADSORPTION

Based on the experiments conducted, it was found that multiple factors will impact the ability of CO_2 injection to increase oil recovery from shale and also to store a volume of the injected CO_2 in the reservoir via adsorption. Although some factors showed the same trend in terms of improving oil recovery and increasing CO_2 adsorption, other showed an opposite trend. Table 2 provides a summary of the impact of different factors that have been studied in this research on increasing oil recovery and CO_2 adsorption. The only factor that showed a common trend was the CO_2 injection pressure, while all other factors either showed an opposite trend, or had no significant impact on one of the studied parameters. Understanding the impact of these factors is extremely important in determining the optimum conditions at which CO_2 injection can both increase oil recovery and also reduce the environmental impact by storing a portion of the injection CO_2 in the reservoir.

Table 2. Impact of Different Factors on Oil Recovery and CO_2 Adsorption

Factor Increase	Impact on Oil Recovery	Impact on CO_2 Adsorption
CO_2 Injection Pressure	Increased	Increased
CO_2 Phase	Changed	Changed
CO_2 Soaking Time	Increased to a Limit	No Impact (Equilibrium Pressure)
Temperature	Increased	Decreased
Number of Cycles	Increased to A Limit	-
Stimulated vs Unstimulated	Altered Based on Fractures	-
Particle Size	-	No Significant Effect

6. CONCLUSIONS

This research investigates the ability of CO_2 injection to increase oil recovery from shale reservoirs, and the ability to store part of the injected CO_2 in the shale during the injection process. The main findings obtained from this research are as follows:

- Cyclic CO_2 injection was found to have a strong potential in increasing oil recovery from both fractured and unfractured shale cores.

- The shale samples had a large CO_2 adsorption capacity at different conditions, which indicates the ability to store a large volume of CO_2 in the shale.

- Pulverizing the shale into micron sized particles had very little effect on the adsorption capacity. This indicates that the small shale particles could be used to model shale cores effectively.

- For the unfractured core experiments, increasing CO_2 pressure resulted in an increase in oil recovery. Natural fractures were also observed when the pressure was increased. This eventually led to several of the unfractured cores to break into multiple pieces.

- Increasing the temperature increased the oil recovery, but it also decreased the CO_2 adsorption capacity. This indicates that temperature is one of the critical factors since it has the potential to increase oil recovery but will also result in a reduction in CO_2 storage.

ACKNOWLEDGEMENTS

REFERENCES

Aljamaan, H., et al., 2017. Multiscale Imaging of Gas Adsorption in Shales. Society of Petroleum Engineers. doi:10.2118/185054-MS.

Bahadori, A., and Vuthaluru, H., 2010. Rapid Prediction of Carbon Dioxide Adsorption Isotherms for Molecular Sieves Using Simple Correlation. Society of Petroleum Engineers. doi:10.2118/122882-PA.

Bouzgarrou, S. et al., 2015. Experimental Adsorption and Modelisation of CO_2 on Adsorbents Collected from Elborma Field in South Tunisia. Journal of Surface Engineered Materials and Advanced Technology, 5, 52-63. doi: 10.4236/jsemat.2015.51006.

Chen, G. et al., 2016. Research of CO_2 and N_2 Adsorption Behavior in K-Illite Slit Pores by GCMC Method. Journal of Scientific Reports, 6, https://doi.org/10.1038/srep37579.

Eliebid, M. et al., 2017. Adsorption Role in Shale Gas Recovery and the Feasibility of CO_2 in Shale Enhanced Gas Recovery: A Study on Shale Gas from Saudi Arabia. Society of Petroleum Engineers. doi:10.2118/187667-MS.

Fakher, S. and Imqam, A., 2019. A review of carbon dioxide adsorption to unconventional shale rocks methodology, measurement, and calculation. https://doi.org/10.1007/s42452-019-1810-8.

Fakher, S. and Imqam, A., 2019. Asphaltene precipitation and deposition during CO_2 injection in nano shale pore structure and its impact on oil recovery, Fuel, 237, 1029-1039, ISSN 0016-2361, https://doi.org/10.1016/j.fuel.2018.10.039.

Fakher, S. et al., 2019a. Roadmap to Asphaltene Characteristics, Properties, and Presence in Crude Oils Based on an Updated Database From Laboratory Studies. Carbon Management Technology Conference. doi:10.7122/CMTC-558560-MS.

Fakher, S. et al., 2019b. The Effect of Unconventional Oil Reservoirs Nano Pore Size on the Stability of Asphaltene During Carbon Dioxide Injection. Carbon Management Technology Conference. doi:10.7122/CMTC-558486-MS.

Gamadi, T. D. et al., 2014. An Experimental Study of Cyclic CO2 Injection to Improve Shale Oil Recovery. Society of Petroleum Engineers. doi:10.2118/169142-MS.

Hawthorne, S. B. et al., 2013. Hydrocarbon Mobilization Mechanisms from Upper, Middle, and Lower Bakken Reservoir Rocks Exposed to CO. Society of Petroleum Engineers. doi:10.2118/167200-MS.

Heller, R. and Zoback, M., 2014. Adsorption of Methane and Carbon Dioxide on Gas Shale and Pure Mineral Samples. Journal of Unconventional Oil and Gas Resources, 8, 14-24. https://doi.org/10.1016/j.juogr.2014.06.001.

Jedli, H. et al., 2017. Carbon Dioxide Adsorption Isotherm Study On Various Cap Rocks In A Batch Reactor For CO2 Sequestration Processes, Applied Clay Science, 136, 199-207, 0169- 1317, https://doi.org/10.1016/j.clay.2016.11.022.

Jin, Z., and Firoozabadi, A., 2016. Thermodynamic Modeling of Phase Behavior in Shale Media. Society of Petroleum Engineers. doi:10.2118/176015-PA.

Luo, X. et al., 2015. Adsorption Of Methane, Carbon Dioxide And Their Binary Mixtures On Jurassic Shale From The Qaidam Basin In China, International Journal of Coal Geology, 150–151, 210-223, https://doi.org/10.1016/j.coal.2015.09.004.

Murugesu, Manju Pharkavi and Joewondo, Nerine and Prasad, Manika, CO2 Sorption Capacity in Clay-Rich Shales with Moisture Content. 14th Greenhouse Gas Control Technologies Conference Melbourne 21-26 October (GHGT-14) . Available at SSRN: https://ssrn.com/abstract=3365692.

Ngo, T., 2015. Reservoir Capacity Estimates in Shale Plays Based on Experimental Adsorption Data. Masters Thesis.

Sheng, J., 2017. Optimization of Huff-n-Puff Gas Injection in Shale Oil Reservoirs. Petroleum, 3, 431-437.

Shoaib, S., and Hoffman, B. T., 2009. CO_2 Flooding the Elm Coulee Field. Society of Petroleum Engineers. doi:10.2118/123176-MS.

Vega, B. et al., 2010. Experimental Investigation of Oil Recovery From Siliceous Shale by Miscible CO2 Injection. Society of Petroleum Engineers. doi:10.2118/135627-MS.

Yang, S. et al., 2016. Effects of Multicomponent Adsorption on Enhanced Shale Reservoir Recovery by CO2 Injection Coupled with Reservoir Geomechanics. Society of Petroleum Engineers. doi:10.2118/180208-MS.

Yang, S. et al., 2016. Effects of Multicomponent Adsorption on Enhanced Shale Reservoir Recovery by CO2 Injection Coupled with Reservoir Geomechanics. Society of Petroleum Engineers. doi:10.2118/180208-MS.

Yu, W. et al., 2014. Simulation Study of CO2 Huff-n-Puff Process in Bakken Tight Oil Reservoirs. Society of Petroleum Engineers. doi:10.2118/169575-MS.

Yu, W. et al., 2016. Modeling Gas Adsorption in Marcellus Shale With Langmuir and BET Isotherms. Society of Petroleum Engineers. doi:10.2118/170801-PA.

Yuan, H. et al., 2017. Investigation on Gas-Adsorption-Induced Swelling and Permeability Evolutions of Cox Argillite, Fresh Journal of Mechanics.

Yue, N. et al., 2018. Influencing Factors and Selection of CH4 and CO2 Adsorption on Silurian Shale in Yibin, Sichuan Province of China. Energy & fuels 2018 v.32 no.3 pp. 3202-3210.

SECTION

2. CONCLUSIONS AND RECOMMENDATIONS

2.1. CONCLUSIONS

This research performs several experimental studies in order to provide a holistic view on the factors that may impact immiscible CO_2 injection in shale reservoir in an attempt to determine the domain at which this technology is best applied. The main conclusions obtained from this research will be provided in this section.

- Based on the data analysis performed, it was found that several factors need to be considered when undergoing immiscible CO_2 injection operations. These factors include, but are not limited to, pressure and temperature, crude oil properties, and CO_2 solubility and swelling.

- A clear trend was observed when plotting CO_2 solubility and oil swelling with pressure and temperature. As the pressure increased, the CO_2 solubility and oil swelling increased, while decreasing temperature showed an opposite trend.

- After plotting the flow regime maps, it was found that specific flow regimes will be observed in different pore sizes based on the thermodynamic conditions used to generate the maps. This helps reveal the correct method to model CO_2 flow in a specific pore size in the shale reservoirs.

- When using the volumetric method to measure adsorption, there are many things that must be taken into consideration, including the volume of the shale sample in

the sample cell and the accuracy by which the void space between the particles is measured.

- When the CO_2 injection pressure increased, the adsorption also increased to a specific volume beyond which no further adsorption will be observed. Increasing the temperature resulted in an opposite trend however.

- Several factors impacted asphaltene stability in the crude oil. These factors may include reservoir properties such as the oil properties, and reservoir thermodynamics, and operational properties such as CO_2 injection pressure and production drawdown. These factors must be taken into consideration to avoid having severe asphaltene damage.

- The extent to which oil swells during interaction with the CO_2 is impacted by several factors including CO_2 injection pressure, temperature, oil viscosity, and oil volume. Increasing the CO_2 injection pressure resulted in an increase in oil swelling, while increasing temperature reduced oil swelling. Lower oil viscosity resulted in a higher swelling as well.

- Cyclic CO_2 injection was found to be extremely effective in producing from shale cores, including both stimulated and unstimulated. Several factors will have a strong impact on oil recovery however, including CO_2 injection pressure, soaking time, temperature, and the number of soaking cycles used.

- When undergoing cyclic CO_2 injection, it is important to know the appropriate soaking time to use, since at some point, increasing the soaking time will actually bring no, or very little, benefit and thus will be considered a waste of time.

- Reservoir simulation showed that the experimental data could be accurately modeled, and future prediction can be therefore made with a high level of confidence in the data and results produced.

2.2. FUTURE WORK RECOMMENDATIONS

This research aimed to investigate a specific aspect of GEOR in unconventional shale reservoirs. As is any other work however, many other parameters and aspects still need to be investigated furthermore in this topic. Based on this, below are some recommendations for future work that can be conducted pertaining to GEOR in shale reservoirs.

- Investigate miscible CO_2 injection in shale reservoirs and its interactions and recovery potential compared to immiscible CO_2.

- Study the use of a different gas other than CO_2, such as nitrogen or methane, or a mixture of gases for GEOR application in unconventional shale.

- Study the dissolution of some components of the rock during CO_2 injection, and the factors impacting this dissolution, especially in shales with a high concentration of calcites.

- Compare the performance of different shale rocks under the same conditions in order to obtain a more generalized understanding of CO_2 GEOR in shale.

- Generate mathematical correlations and models that can accurately predict different gases' interactions and productivity from shale reservoirs as a function of the thermodynamic conditions of the reservoir, and the operational conditions used to undergo the CO_2 EOR operation.

VITA

Sherif Fakher was born in Richmond Virginia, USA. He received his bachelor's degree from the American University In Cairo, Cairo, Egypt, in 2016 in Petroleum and Energy Engineering. He was admitted as a PhD student at Missouri University of Science and Technology, in the department of Petroleum Engineering, under the Chancellor's Distinguished Fellowship in 2016. His research interest included reservoir engineering, with a focus on Gas Enhanced Oil Recovery, especially in unconventional shale reservoirs. He authored many papers on the topic of Enhanced Oil Recovery and gave presentations in various conferences worldwide. He obtained his Master of science degree in Petroleum Engineering from Missouri University of Science and Technology in May 2019 under the title of "Asphaltene Stability in Crude Oil During Carbon Dioxide Injection and Its Impact on Oil Recovery: A Review, Data Analysis, and Experimental Study". He completed his PhD in Petroleum Engineering from Missouri University of Science and Technology in May 2020.